frontiers | Research Topics

Nature-based solutions for urban water management

Edited by
Junguo Liu, Zhan Tian, Qinghua Ye,
Laixiang Sun and Shiqiang Wu

Published in
Frontiers in Environmental Science
Frontiers in Earth Scienc

ISSN 1664-8714
ISBN 978-2-8325-4516-4
DOI 10.3389/978-2-8325-4516-4

About Frontiers

Frontiers is more than just an open access publisher of scholarly articles: it is a pioneering approach to the world of academia, radically improving the way scholarly research is managed. The grand vision of Frontiers is a world where all people have an equal opportunity to seek, share and generate knowledge. Frontiers provides immediate and permanent online open access to all its publications, but this alone is not enough to realize our grand goals.

Frontiers journal series

The Frontiers journal series is a multi-tier and interdisciplinary set of open-access, online journals, promising a paradigm shift from the current review, selection and dissemination processes in academic publishing. All Frontiers journals are driven by researchers for researchers; therefore, they constitute a service to the scholarly community. At the same time, the *Frontiers journal series* operates on a revolutionary invention, the tiered publishing system, initially addressing specific communities of scholars, and gradually climbing up to broader public understanding, thus serving the interests of the lay society, too.

Dedication to quality

Each Frontiers article is a landmark of the highest quality, thanks to genuinely collaborative interactions between authors and review editors, who include some of the world's best academicians. Research must be certified by peers before entering a stream of knowledge that may eventually reach the public - and shape society; therefore, Frontiers only applies the most rigorous and unbiased reviews. Frontiers revolutionizes research publishing by freely delivering the most outstanding research, evaluated with no bias from both the academic and social point of view. By applying the most advanced information technologies, Frontiers is catapulting scholarly publishing into a new generation.

What are Frontiers Research Topics?

Frontiers Research Topics are very popular trademarks of the *Frontiers journals series*: they are collections of at least ten articles, all centered on a particular subject. With their unique mix of varied contributions from Original Research to Review Articles, Frontiers Research Topics unify the most influential researchers, the latest key findings and historical advances in a hot research area.

Find out more on how to host your own Frontiers Research Topic or contribute to one as an author by contacting the Frontiers editorial office: frontiersin.org/about/contact

Nature-based solutions for urban water management

Topic editors

Junguo Liu – Southern University of Science and Technology, China
Zhan Tian – Southern University of Science and Technology, China
Qinghua Ye – Deltares, Netherlands
Laixiang Sun – University of Maryland, United States
Shiqiang Wu – Nanjing Hydraulic Research Institute, China

Citation

Liu, J., Tian, Z., Ye, Q., Sun, L., Wu, S., eds. (2024). *Nature-based solutions for urban water management*. Lausanne: Frontiers Media SA.
doi: 10.3389/978-2-8325-4516-4

Table of contents

frontiers | Frontiers in Environmental Science

TYPE Editorial
PUBLISHED 05 July 2023
DOI 10.3389/fenvs.2023.1228154

OPEN ACCESS

EDITED AND REVIEWED BY
Michael Nones,
Institute of Geophysics, Poland

*CORRESPONDENCE
Junguo Liu,
junguo.liu@gmail.com

RECEIVED 24 May 2023
ACCEPTED 31 May 2023
PUBLISHED 05 July 2023

CITATION
Liu J, Sun L, Tian Z, Ye Q, Wu S and Zhang S (2023), Editorial: Nature-based solutions for urban water management. *Front. Environ. Sci.* 11:1228154. doi: 10.3389/fenvs.2023.1228154

Editorial: Nature-based solutions for urban water management

Junguo Liu[1,2]*, Laixiang Sun[3], Zhan Tian[1], Qinghua Ye[4], Shiqiang Wu[5] and Shuyu Zhang[1]

[1]School of Environmental Science and Engineering, Southern University of Science and Technology, Shenzhen, China, [2]North China University of Water Resources and Electric Power, Zhengzhou, China, [3]Department of Geographical Sciences, University of Maryland, College Park, MD, United States, [4]Deltares, Software Centre, Delft, Netherlands, [5]State Key Laboratory of Hydrology-Water Resources and Hydraulic Engineering, Nanjing Hydraulic Research Institute, Nanjing, China

KEYWORDS

green infrastructure, rainwater, water resources, human-natural systems, urban water

Editorial on the Research Topic
Nature-based solutions for urban water management

Water, serving as a vital resource for urban development, imparts both advantages and complications, particularly concerning urban pluvial flooding. Consequently, there is a growing recognition of the necessity to incorporate nature-based solutions (NBS) into urban water management system. These integrated solutions leverage natural processes and ecosystem services in tandem with the traditional "grey infrastructures" that predominantly depend on engineering interventions (Palmer et al, 2015). The aim is to foster resilient communities and cities adept at managing water-related hazards effectively.

To advance this mission, it is imperative to bridge the existing gap between urban hydrodynamic research and the deployment of NBS. Additionally, there is a need to expand the prevailing cost-benefit analysis methodology and develop innovative approaches that consider multiple criteria and the synergistic integration of both grey and green measures. By encouraging further exploration in this field, we propose a Research Topic focusing on *Nature-based solutions for urban water management*. The intention of this Research Topic is to provide a devoted platform for researchers to probe various Research Topic, thereby facilitating advancements in the understanding and implementation of NBS in urban water management.

Through the publication of research articles and discussions within this Research Topic, we seek to promote knowledge exchange, interdisciplinary collaboration, and the development of effective strategies and tools to address the complex challenges associated with urban water management. Integrating nature-based solutions into our urban planning and engineering practices presents a pathway towards fostering cities that are more sustainable and resilient.

We invite researchers from various disciplines to contribute their expertise and insights to this Research Topic, ultimately fostering a collective effort to enhance the management of urban water resources and mitigate the impacts of flooding events.

Liu et al. have proposed a comprehensive urban utilization model that integrates blue, green, and gray water infrastructure (Figure 1). Their study entails a quantitative analysis and simulation of the intricate relationship between rainwater infiltration, stagnation, storage, use, and drainage at the community scale. Furthermore, the authors provide in-depth discussions on the abundance and quality of rainfall water resources within blue-green-gray

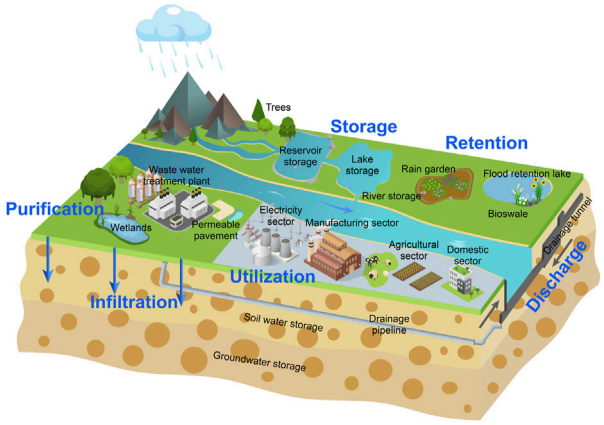

FIGURE 1
The framework of the rainwater utilization model integrated with blue, green, and gray water infrastructure (Liu et al.).

infrastructures, taking into account various urban hydrological processes, including storage, use, and drainage.

The simulation results have enabled the evaluation of rainwater management's impact on urban watersheds, as well as the assessment of utilization efficiency and the delicate balance between supply and demand. As a result, the model allows for the strategic spatial arrangement of infrastructures to maximize rainwater Research Topic and significantly enhance rainwater utilization efficiency, providing valuable support to municipal planning endeavors.

The integration of green, blue, and gray infrastructure within individual buildings and across urban network systems has demonstrated remarkable improvements in rainwater utilization capacity. When synergistically combined with other essential infrastructures such as transportation, water, energy, and telecommunications, the planning, design, and development of urban rainwater resource utilization not only effectively address challenges in water environment management but also contribute to the creation of a livable and healthful urban environment.

The articles featured in this Research Topic serve as a valuable resource, offering both technological and theoretical support for this innovative framework, while also playing a crucial role in the advancement of rainwater utilization practices.

Since the inception of the Sponge City initiative in China, substantial advancements have been made in the realm of urban rainwater resource utilization. However, the achieved outcomes have fallen short of the anticipated scale, with utilization rates remaining considerably low.

Chen et al. outlined the current Sponge City approach from the perspectives of planning content and planning process to fill the gap in the existing guidelines of the Sponge City Programme. Key missing elements that could promote the development of current Sponge City planning were identified. The study delved into and optimized the targets for pluvial flood protection, strategies for planning interventions, and instruments for interdisciplinary cooperation in the planning process. The refined approach was successfully applied in the Sponge City planning for Qinhuai District, Nanjing City.

Liu et al. conducted a review of regions and cities in China where Sponge City projects have been implemented. Their findings highlight that southern China devotes more attention to hydrological processes related to water storage, whereas northern China emphasizes processes connected to the infiltration of stormwater.

Jin et al. proposed individual criteria for mapping high-absorbance areas at the regional and local scales. Water table dynamics after large infiltration events from rainfall were simulated via numerical analysis with the consideration of different hydraulic characteristics.

Xu et al. reviewed the evolution of rainwater utilization management modes in advanced countries, classified urban rainwater utilization measures into three categories, including source control, medium transmission, and terminal treatment, and summarized the advantages, disadvantages, and scope of the application of these measures.

Jia et al. proposed a framework for blue-green-gray infrastructure classification based on machine learning algorithms and unmanned aerial vehicle (UAV) images. This framework was applied at the Southern University of Science and Technology campus, Shenzhen, China. This study demonstrated the feasibility of using UAV images in the urban blue-green-gray infrastructure classification.

Harnessing urban rainwater resources to alleviate water shortage also requires the adoption of economically efficient techniques to improve and control water quality.

Tian et al. proposed a data-driven approach to quantify the effects of rainfall on river pollution and applied it to the Shiyan River in Shenzhen, China. They found that the most important factor affecting river pollution is the dry period, followed by average rainfall intensity, maximum rainfall in 10-min interval, total rainfall, and initial runoff intensity. By employing a newly proposed artificial neural network model, they predicted that the event-mean concentration of the Chemical Oxygen Demand would be much lower during heavy rains compared to light rainfall.

Zhang et al. proposed a novel waterlogging depth prediction model that only uses rainfall data as input. A "rainfall-waterlogging amplification factor" based on the geographical features of monitoring stations is constructed to quantify the mapping relationship between rainfall and waterlogging depths at different locations. This method effectively overcomes the limited coverage of monitoring stations and historical waterlogging data.

Zhang et al. developed a three-module methodological options framework based on the combination of hydrological modeling, statistical analysis, and conceptual approaches, to guide the selection of attribution methods. The effectiveness framework was evaluated by applying it to China's Upper Yangtze River Basin. The SWAT-based method was found to be the best approach to quantify the influences of climate change and human activities on streamflow. It was also found that climate change dominates the changes in streamflow.

Dai et al. proposed a method for selecting sensitive monitoring parameters and optimizing the distribution of monitoring sites in lakes. This method was applied to the large-scale river-to-lake water diversion project, i.e., Water Diversion from the Yangtze River to Lake Taihu in China.

Seven physicochemical parameters, sensitive to seasonal water diversion, were identifies and employed to optimize the site distribution and daily water quality monitoring. It was found that the introduction of allochthonous pollutants and biological species through water diversion projects could have significant ecological effects on the urban drinking water quality.

Sun et al. unfolded the mass exchange mechanism of water and soil on the soil surface in the rainfall splash erosion process. The splash erosion was found to be proportional to the rainfall kinetic energy and has a linear relation to the infiltration amount. The single raindrop kinetic energy and the splash erosion have a quadratic parabola relation, and the splash velocity is about 1/3 of the single raindrop terminal velocity.

Author contributions

JL–conceptualization, writing, review and editing
LS–conceptualization, writing, review and editing
ZT–methodology, investigation, visualization, review
QY–methodology, investigation, visualization, review
SW–methodology, investigation, visualization, review
SZ–conceptualization, writing, editing. All authors contributed to the article and approved the submitted version.

References

Palmer, M. A., Liu, J., Matthews, J. H., Mumba, M., and D'Odorico, P. (2015). Manage water in a green way. *Science* 349, 584–585. doi:10.1126/science.aac7778

Acknowledgments

We gratefully acknowledge the support received for this study from the Shenzhen Science and Technology Program (Grant No. KCXFZ20201221173601003), the National Key Research and Development Program of China (Grant No. 2018YFE0206200), and the Henan Provincial Key Laboratory of Hydrosphere and Watershed Water Security.

Conflict of interest

The authors declare that the research was conducted in the absence of any commercial or financial relationships that could be construed as a potential conflict of interest.

Publisher's note

frontiers in Environmental Science

ORIGINAL RESEARCH
published: 02 July 2021
doi: 10.3389/fenvs.2021.700463

Hydrogeological Criteria to Improve the Sponge City Strategy of China

Mengxiao Jin[1,2†], *Michele Lancia*[2,3*†], *Yong Tian*[2,3], *Stefano Viaroli*[4], *Charles Andrews*[5], *Junguo Liu*[2,3] *and Chunmiao Zheng*[2,3*]

[1]School of Environment, Harbin Institute of Technology, Harbin, China, [2]Guangdong Provincial Key Laboratory of Soil and Groundwater Pollution Control, School of Environmental Science and Engineering, Southern University of Science and Technology, Shenzhen, China, [3]State Environmental Protection Key Laboratory of Integrated Surface Water-Groundwater Pollution Control, School of Environmental Science and Engineering, Southern University of Science and Technology, Shenzhen, China, [4]Department of Sciences, University of Roma Tre, Rome, Italy, [5]S.S. Papadopulos and Associates, Inc., Rockville, MD, United States

China is facing frequent waterlogging and an increasing water scarcity that mirrors the fast urban and economic expansion of the last 4 decades. To mitigate these issues, the government promulgated the "Sponge City" strategy; a concept rooted in practices in western countries aimed at collecting and reusing 65–90% of urban rainfall. The application consists of absorbent infrastructures such as green roofs and rain gardens combined with the pre-existing urban environment. However, due to climate heterogeneities and the different urbanization contexts in China, these goals may seem overly ambitious in many areas of the country. Compact urbanization, together with heavy rainfall concentrated in short events, puts dramatic stresses on these infrastructures. At the same time, overdesigned infrastructures are expensive and may not be practical to retrofit in existing urban areas. In this paper, the role of urban aquifers as natural Sponge City elements are investigated throughout China. The method of implementation is inexpensive and easy to apply, favoring the direct infiltration to the subsoil after the conversion of the urban surfaces from impervious to permeable. Infiltration to urban aquifers alleviates the pressure on sewers, urban streams, as well as waste-water treatment plants. Considering urban aquifers with different hydraulic characteristics, water table dynamics after large infiltration events from rainfall are simulated via numerical analysis. Hydrogeological and geomorphological analyses are carried out to individuate criteria for the mapping of high absorbance areas at the regional and local scales. A Sponge City approach involving the urban aquifers can represent a winning formula for the success of this ambitious but compelling plan.

Keywords: geomorphology, groundwater, hydrogeology, urban aquifers, waterlogging

OPEN ACCESS

Edited by:
Prosun Bhattacharya, Royal Institute of Technology, Sweden

Reviewed by:
Trista McKenzie, University of Hawaii at Manoa, United States
Kangning Xu, Beijing Forestry University, China

***Correspondence:**
Michele Lancia
lancia@sustech.edu.cn
Chunmiao Zheng
zhengcm@sustech.edu.cn

†These authors have contributed equally to this work

Specialty section:
This article was submitted to Water and Wastewater Management, a section of the journal Frontiers in Environmental Science

Received: *26 April 2021*
Accepted: *14 June 2021*
Published: *02 July 2021*

Citation:
Jin M, Lancia M, Tian Y, Viaroli S, Andrews C, Liu J and Zheng C (2021) Hydrogeological Criteria to Improve the Sponge City Strategy of China. Front. Environ. Sci. 9:700463. doi: 10.3389/fenvs.2021.700463

INTRODUCTION

Waterlogging and water scarcity are severe issues as highlighted in the 2020 World Water Development Report (WWDR, 2020). Climate change projections indicate with high confidence that extreme precipitation events and heatwaves will become globally more intense and frequent, increasing flood and drought risks (Polade et al., 2014). Adaptation and mitigation are two complementary strategies for managing and reducing the risks of climate change on water

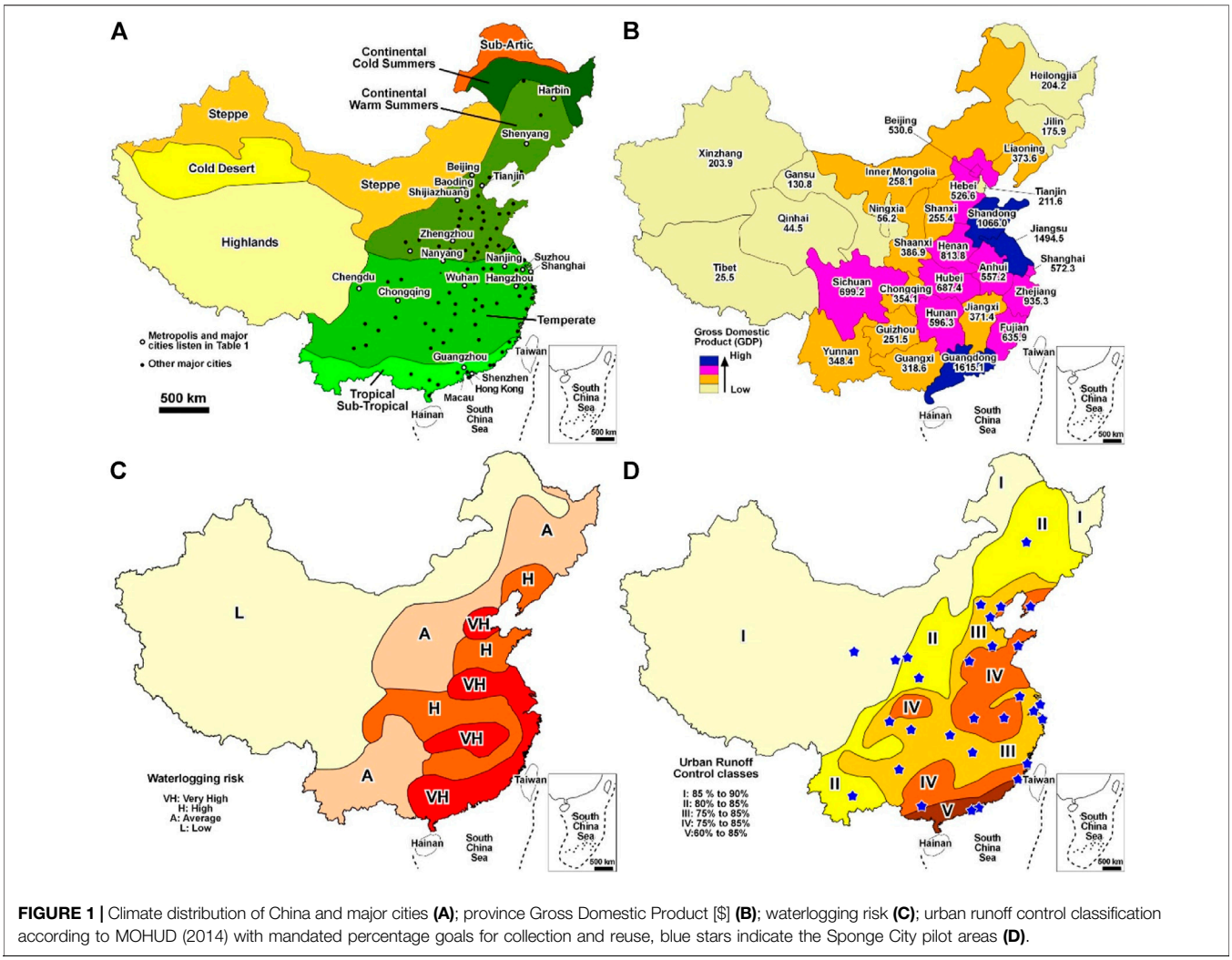

FIGURE 1 | Climate distribution of China and major cities **(A)**; province Gross Domestic Product [$] **(B)**; waterlogging risk **(C)**; urban runoff control classification according to MOHUD (2014) with mandated percentage goals for collection and reuse, blue stars indicate the Sponge City pilot areas **(D)**.

resources. Engineering and technological options, as well as social and institutional measures, can transform the climate change from risk to opportunity (WWDR, 2020).

In China, the fast urbanization of the last decades is a concurrent cause to the serious water problems the country is facing (Zheng et al., 2010; Liu et al., 2013; Zheng and Gorelick, 2015, Hua et al., 2020). Megacities are distributed along the eastern coastline and the main river valleys (**Figure 1A**); due to the dry climate and related water scarcity, internal sectors are less populated. Climate is also responsible for the different water management practices between the northern and the southern parts of China. Temperate to tropical areas in the south mitigate the dry periods by collecting the copious summer rainfall *via* an extended system of dams and artificial basins (Chen et al., 2016); the drier plains in the north rely on the exploitation of the decreasing groundwater resources (Liu et al., 2008; Wang et al., 2018). Differences in water management strategies also reflect the distribution of the Gross Domestic Product (GDP) that varies considerably among the provinces (**Figure 1B**). Despite the climate and economic diversities, a significant amount of water is concentrated in Chinese cities and megacities as a result of impervious areas and external sources of water (Liu et al., 2013; Zhao et al., 2015). Pristine resources from outside satisfy the water demand and later flow to sewers, WWTPs (Waste-Water Treatment Plants), and urban channels. Flow from rainfalls and storms represent a transient but significant increment of the urban runoff as buildings, roads and other urban surfaces are impervious. In fact, more than climate, the waterlogging risk (**Figure 1C**) reflects the concentration of urban centers.

To mitigate the waterlogging risk and simultaneously tackle the water scarcity, the Chinese government promulged the Sponge City concept. Sponge City is based on the western strategies and practice known as Low Impact Development (in United.States and Canada), Best Management Practices, Sustainable Drainage System (United Kingdom), or Water Sensitive City (Australia) (Fletcher et al., 2015; Huang et al., 2020). All these practices slow and attenuate the flow of storm water from buildings and infrastructures. Sponge City is ambitious (Randall et al., 2019); current guidelines (MOHURD-Ministry of Housing and Urban Rural Development, 2014) mandate the collection and reuse of a

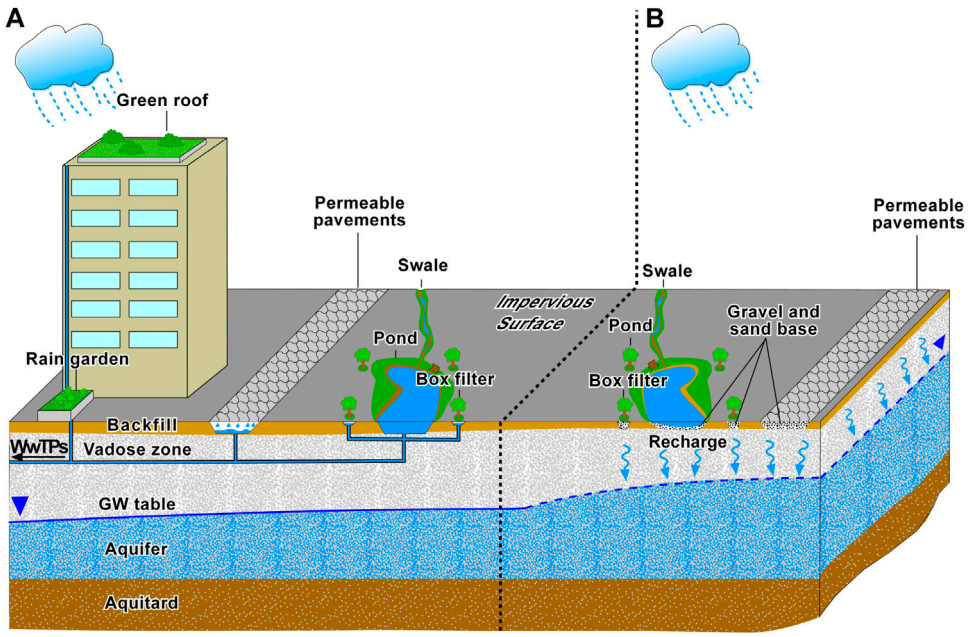

FIGURE 2 | Classic Sponge City design with water collected via pipes and tanks **(A)**; infiltration-based installations, backfill continuity is interrupted by a base of gravel and sand favoring infiltration **(B)**.

significant amount of the urban rainfall according to the climate characteristics (**Figure 1D**). Sponge City projects have already been started in 30 cities and megacities with several pilot sites and an enlargement to other cities from 2020 to 2030 (SC-State Council, 2015; Xia et al., 2017). The concept consists of a combination of facilities collecting stormwater, connected to pipes and tanks (**Figure 2A**), that is later reused after treatment at theWWTPs. Facilities also aim to restore the ecological functions of urban rivers and streams, modernize the urban architecture, and provide economic advantages (Nguyen et al., 2019). Sponge City can represent a cure-all strategy but requires huge investments, especially at the long-term scale. Beside the installation costs, the treatment of collected water, gardening and pipe maintenance is expensive and Sponge City retrofitting with pipes and tanks is challenging in urban areas.

For an improvement of the Sponge City concept, it is proposed that urban aquifers be used as natural Sponge City tanks where there is sufficient infiltration potential (**Figure 2B**). In fact, the impervious coverage from pavements and infrastructures blocks the natural infiltration and recharge to urban aquifers, which are typically only recharged via leakage of pipes and tanks, irrigation excess or rainfall infiltration from gardens and flowerbeds (Lerner, 2002). Infiltration-based installations are cheaper as the installation and setup of subterranean pipes and tanks, infrastructures monitoring, and the treatment of collected water can be avoided. Only a layer of sand and gravel in contact with the vadose zone is required to by-pass the less permeable backfill (**Figure 2B**).

The absorbance capacity of aquifers is heterogeneous and depends on the local hydrogeological features that are influenced by geology and geomorphology. However, the impacts of the spatial heterogeneity on the development of Sponge City are poorly understood.

The objectives of this paper are 1) investigate in the urban context the water table dynamics via numerical methods (Niswonger et al., 2011) after a copious rainfall; 2) perform a regional scale analyses to classify the urban aquifers of China; 3) point out the most profitable infiltration-based approach that can be used to improve the cost-benefit ratio of Sponge City, with examples from the most populous cities of China.

MATERIALS AND METHODS

Infiltration Criteria and Investigations

Infiltration-based installations are efficacious in areas with great absorbance capacity. Silty to clayey soils can absorb a limited quantity of water while greater amounts run off to streams and channels. On the contrary, average to high permeability soils, such as silty sands and gravels, have the capacity to infiltrate a large amount of rain, transferring the water to the aquifers, via the vadose zone (**Figure 2B**). Hydraulic conductivity of shallow soils is a parameter easy to characterize, even in the urban areas where local heterogeneities can locally block the infiltration process. The storage capacity and groundwater dynamics of urban aquifers are more complicated. The location of the groundwater table is the second fundamental parameter for assessing the storage capacity of an urban aquifer. Infiltration triggers a rise of the groundwater table, inversely proportional to the specific yield (**Figure 2B**).

High permeability soils with a deep groundwater table are not ubiquitous. The bedrock in the mountainous and hilly terrains is

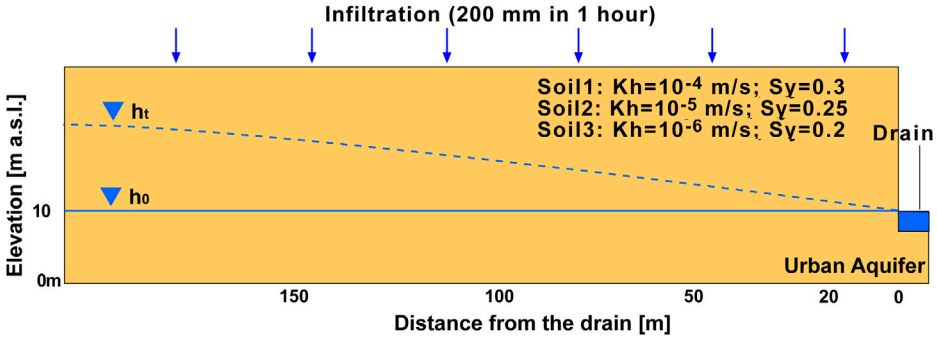

FIGURE 3 | Schematic of the numerical model; h0 indicates the water table in steady-state conditions, ht the water table during the seepage.

generally impervious, favoring runoff and soil erosion due to low rainfall infiltration on the bedrock outcrops. At the regional scale, alluvial sequences have a fining sequence of sediments and hydraulic conductivity decreases moving downstream, as rivers and streams progressively lose their capacity to transport the eroded material (Freeze and Cherry, 1979). However, alluvial plains and coastal areas generally have a shallow groundwater table near the ground surface. Mapping suitable areas at regional scale is not trivial. The classical approach consists of field investigations and modelling (Brassington, 2007). Hydrogeological maps and three-dimensional models characterize the volume and hydraulic conductivity of soils; water wells and piezometers monitor the groundwater table; and numerical modelling can simulate the groundwater table under different conditions (Anderson et al., 2015). Analysis of satellite images record the urban expansion providing an overview of the hydrogeological zones converted from rural to urban. A great amount of data and long-term observations are required.

At regional scale, the classical investigation approach is not practical, because of the huge amount of data required A numerical analysis of an urban aquifer connected to a drain is used to understand water-table dynamics as a function of specific yield and the hydraulic conductivity following a large infiltration event. Considering the numerical results, the hydrogeological complexes of China are reinterpreted as a function of their infiltration and storage capacity. The resulting conceptual model is applied and discussed for the seventeen most populous megacities of China, highlighting their absorbance capacity at the regional scale. Major cities suitable for infiltration-based installations (**Figure 2B**) are identified.

Flow Model Construction

A two-dimensional numerical model was constructed using MODFLOW-NWT code (Niswonger et al., 2011) with the GMS® graphical interface to investigate water-table dynamics following an infiltration event. The model domain is discretized with square cells, with a size of 2 m. The model represents a homogeneous aquifer with a base of 200 m, discharging the groundwater flow in a stream or drain located at 10 m a.s.l. Drain is introduced *via* the Drain Package (DRN), with a hydraulic conductance of 0.001 m^2/s. First stress period, in steady-state conditions, has a null infiltration and simulates dry periods. Second stress period simulates a huge rainstorm with a length of 1 h and an infiltration from the top layer of 200 mm (CMA, China Metereological Administration, 2013), *via* Recharge Package (RCH). Remaining 14 stress periods have a length of 1 day and null infiltration. Unsaturated Zone Flow Package (UZF) is used to simulate the water table rise through the dry cells located above the water table. Three soils with decreasing horizontal hydraulic conductivity and specific yield are considered: soil 1 (Kh = $1 \bullet 10^{-4}$ m/s and Sy = 0.3); soil 2 (Kh = $1 \bullet 10^{-5}$ m/s and Sy = 0.25); soil 3, (Kh = $1 \bullet 10^{-6}$ m/s and Sy = 0.2). Soil range represents aquifers from coarse sand to a silty sand. **Figure 3** schematizes the numerical model. Vertical hydraulic conductivity is set equal to $1 \bullet 10^{-4}$ m/s to simulate the rise of the water table in undrained conditions. This condition is precautionary as is assumed that all the water is absorbed by the soil before the seepage processes start.

Hydrogeology of China

The hydrogeology of China reflects the complex geological evolution of the area. Pre-Cambrian to Mesozoic bedrock sequences, outcropping throughout the mountain chains, alternate with Tertiary to Quaternary basins filled with unconsolidated sediment (Yin, 2006; Li et al., 2014; Zhang et al., 2020). For the sake of simplicity, eight hydrogeological units are used to describe the hydrogeology of China as shown on **Figure 4** and as described below:

- The alluvial sequence unit (1) fills the Neogene-Quaternary basins and consists in alternation of fine and coarse soils, deposited in a fluvial to lacustrine environment. From a hydrogeological point of view, the unit is a multi-layer aquifer with a high hydraulic conductivity and high specific yield.
- The piedmont unit (2) lies between the alluvial sequence and bedrock units and consists in a thick accumulation of coarse sediments, mainly from rivers. It is considered as a single aquifer, with a high hydraulic conductivity and high specific yield.
- The delta unit (3) consists of an accumulation of fine Quaternary sediments, mainly silt and clay, arranged in a

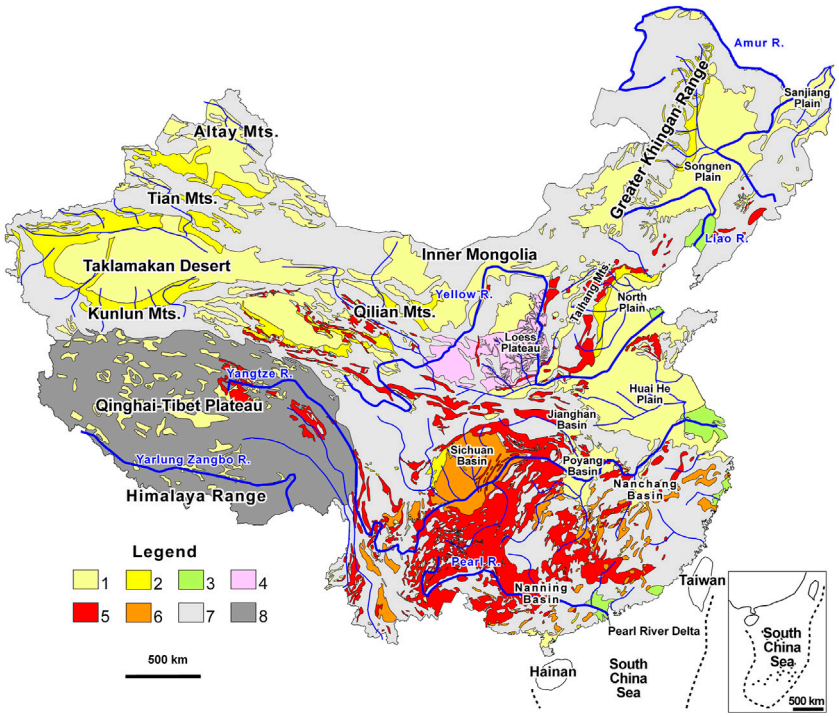

FIGURE 4 | Hydrogeological map of China. Key to the Legend: 1) Alluvial sequence; 2) Piedmont bands; 3) Delta 4) Loess; 5) Fissured Bedrock; 6) Karstified carbonate sequence; 7) Impervious bedrock; 8) Permafrost. Redrawn and simplified from CGS (1979).

multi-layer aquifer. Because of the high content of clay, the hydraulic conductivity and high specific yield is average to low.

- The loess unit (4) is a thick accumulation of Quaternary eolian deposits, forming an extended plateau in the central sector of the Yellow River. Sequence has a dominant silty and loamy texture that confers an average hydraulic conductivity and an average specific yield.
- The karst unit (5) consists in thick carbonate sequences from Pre-Cambrian to Mesozoic. Tropical to sub-tropical areas show mature karst landforms with large water-level responses to seasonal recharge. In cold and dry climates, karst processes are not well-developed because of the low precipitation and, secondarily, because carbonate sequences are generally overlain by less permeable Paleozoic shales or Quaternary sediments. Hydraulic conductivity is variable from average to very high.
- The fractured bedrock unit (6) and impervious bedrock unit (7) characterize the mountain sectors. Hydraulic conductivity depends on the fracture density that is related to the tectonic activity. Slopes are covered by weathering blankets representing a shallow aquifer. Thickness and hydraulic conductivity of these aquifers vary according to climate, lithology and morphology. Warm-humid tropical areas have weathered blankets tens of meter thick consisting of clayey sands. In cold and dry areas, the weathered blanket is typically only a few meters thick with sandy gravel, detritus and bedrock blocks.
- The permafrost unit (8) is constituted by bedrock with a very low to low hydraulic conductivity because of the frozen terrains. Unit extensively outcrops throughout the Qinghai-Tibet Plateau.

RESULTS AND DISCUSSION

Numerical Results

The model simulates the water table dynamics of an urban aquifer connected to a drain. Parameter of the urban aquifer vary among the three soils. Due to the undrained conditions, the water table instantly rises in the first hour of the simulation (**Figure 5**). In soil 1 the simulated water-table rise is 0.67 m; in soil 2 is 0.79 m; in soil 3 is 1 m.

Following the peak water-table rise, the water table slowly declines. The simulated water levels at 20, 50, 100, and 150 m from the drain are shown on **Figure 5**. After 14 days and at 20 m from the drain, soil 1 dissipates 46.3% of the initial increment; at 50 m from the dissipation is 30.2%, at 100 m is 12.3% and at 150 m is 3.5% (**Figure 5A**). Hydraulic characteristics of soil 1 correspond to a coarse medium sand. Soil 1 the piedmont unit (2) and the paleochannels of the alluvial sequence unit (1). If gravel is present, soil becomes more conductive and seepage processes are quicker. At 20 m from the drain, soil 2 dissipates 36.3 % of the initial increment and at 50 m 7.8 %. At 100 m and 150 m from the drain, dissipation is null at the end of the simulation (**Figure 5B**). Hydraulic characteristics of soil 2 correspond to fine sand to silty

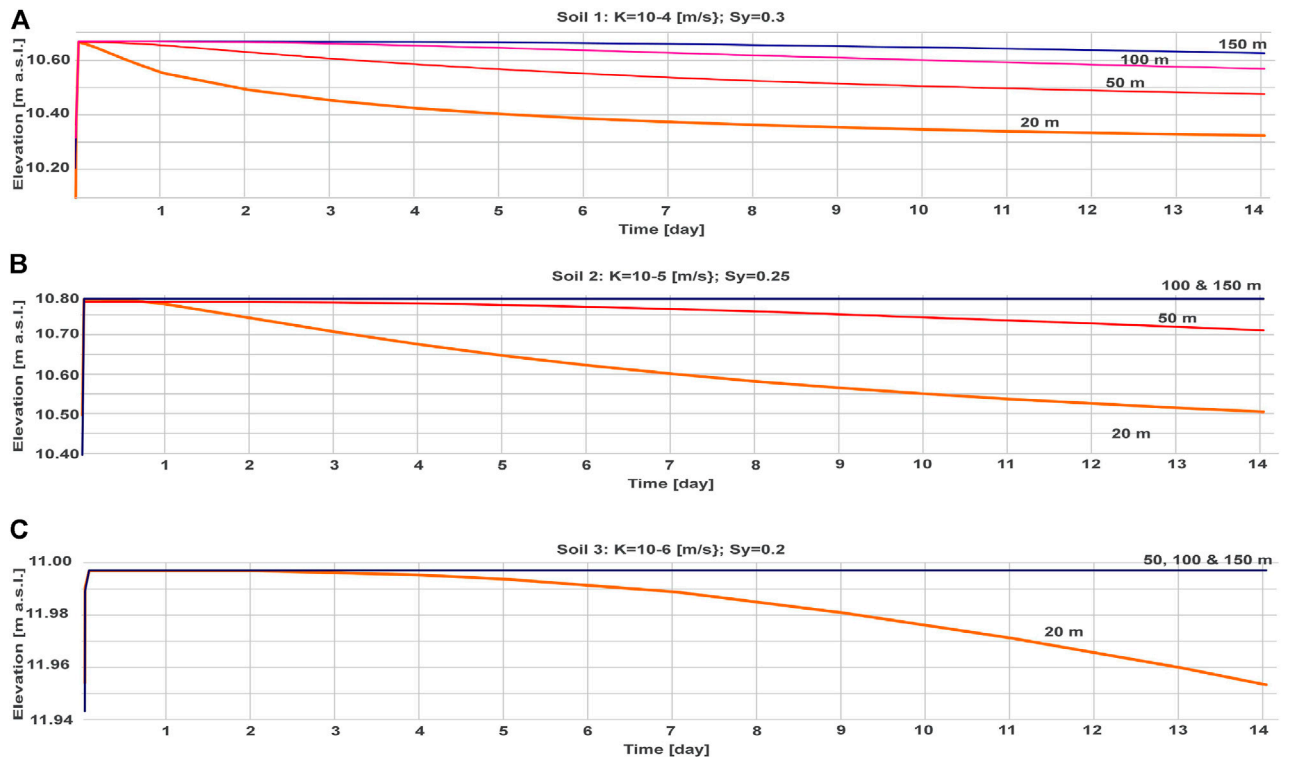

FIGURE 5 | Water-level declines in Soil 1 **(A)** Soil 2 **(B)**, and Soil 3 **(C)** in the two weeks after the recharge of 200 mm in 1 hour caused by a rainstorm. Water-level hydrographs are presented at 20, 50, 100, and 150 m from the drain.

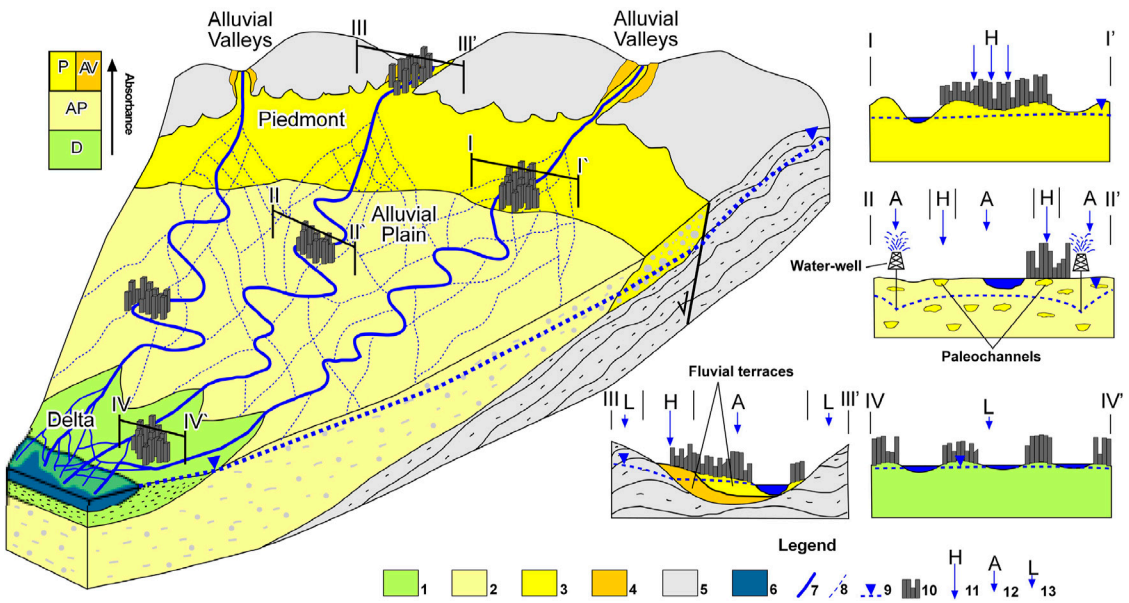

FIGURE 6 | Conceptual zonation for rainfall potential at the catchment scale. Key to the legend: Deltaic sequence (1); Alluvial plain sequence (2); Piedmont and recent terrace sequences (3); older terrace sequence (4); bedrock (5); seawater (6); river (7); paleochannels (8); groundwater table (9); urban areas (10); High (11), Average (12) and Low (13) potential absorbance.

sand; investigated soil is representative of the alluvial sequence unit (1). Soil 3 dissipates 0.4 % of the initial increment at 20 m from the drain. At 50, 100 and 150 m from the drain, water table remains steady after 14 days (**Figure 5C**). Hydraulic characteristics of soil 3 correspond to sandy silt or a mixture of sand, silt and clay. It is representative of the lacustrine sequence of the delta unit (3) and the alluvial sequence unit (1). In case of a higher content of clay, these units present a lower conductivity and less capacity to dissipate the infiltrated water.

Proposed Conceptual Model

Urbanized aquifers are located throughout the Quaternary alluvial sequence. In these large systems tectonically triggered, a remarkable decrease in hydraulic conductivity and sediment size occurs moving downstream as transport capacity of the rivers decreases as the morphology flattens. In accordance with the geomorphological features, characteristics of urban aquifers are reinterpreted according to their absorbance capacity (**Figure 6**). Absorbance capacity of urbanized fractured and karst sequence is also evaluated.

The Piedmont

The piedmont connects mountain terrains and plains (**Figure 6**). It consists of a thick sequence of highly porous and permeable sediments, mainly sand and gravel, accumulated by alluvial and gravitative processes (Bowman, 2017). The sediments on the Piedmont are the product of slope readjustment triggered by changes in the base level of rivers and the sea, induced by tectonic or climate factors at the geologic time scale. The width of the Piedmont can be large and interconnected with alluvial fans. Thickness and width of the piedmont depends on the accumulation space created by tectonics.

In the Songnen, the Huai He, the North Plains, the Sichuan Basin, and the endorheic basins in the northwest the piedmonts are several kilometers wide (**Figure 4**), hosting numerous cities and megacities (CGS, 1979). Rivers and streams are incised, and their base level is tens of meters lower than the ground level of the cities (Zhang and Fei, 2008). In combination with the highly permeable soils with a small hydraulic gradient throughout the aquifers, these areas are characterized by a high absorbance capacity. Basins and valleys of southern China are smaller because the reduced tectonic activity and sediments are less permeable due to the higher clay content, favored by the warmer weather. However, in tropical climates, flow landslides intersect the weathered blankets increasing the thickness of the piedmont bodies (Lancia et al., 2020b). Compared to the northern basins triggered by tectonics, piedmont bands are less thick, smaller and less permeable but able to absorb the copious runoff of the tropical areas. Lancia et al. (2020a) pointed out the great absorbance capacity of a thin piedmont located in Shenzhen in southern China, under sub-tropical conditions (**Figure 1A**); Water-level fluctuations on the piedmont indicate a water table that responds rapidly to precipitation, able to absorb the runoff during the storms and transmit water to downstream aquifers. Performed numerical analysis (**Figure 5A**) confirm the capacity of this unit to dissipate the overpressure after remarkable infiltration. This zone is strategic for managing storm water runoff. Because of the higher costs of construction and management, the piedmont is generally urbanized only at the end of the expansion process, when flat alluvial plains and valleys are completely developed.

Alluvial Plains and Valleys

The alluvial plains originated from sediments eroded throughout the mountain sectors, and subsequently transported and deposited by fluvial activity (Freeze and Cherry, 1979). Riverbeds and paleochannels consist of permeable deposits, coarse sand, and gravel, with variable thickness and width. A mixture of less permeable sediments, silty sands to clay and silt, was deposited during the flood events among the riverbeds. Despite the soil heterogeneity, the groundwater table is generally shallow and near ground surface, due to the flat morphology. As observed in the numerical analysis (**Figure 5B**), to dissipate infiltrated water a consistent number of drains are required, increasing the costs of the infiltration-based installations. As a result, these areas have a reduced absorbance potential. The main basins of southern China are traversed by major rivers that contribute to keep the groundwater levels steady.

Anthropogenic activities of the last decades depleted the local groundwater resources, depressing the groundwater table. In northern China, the groundwater table is located tens meter from the ground level (Zheng et al., 2010; Cao et al., 2013). Because of the depressed groundwater table, most of the rivers and streams are seasonally dry and act as natural Sponge City installations, with storm runoff rapidly infiltrating into the aquifer (**Figure 6**). During urbanization, rivers were deviated, and permeable riverbeds urbanized. The detection and reconversion of those areas via infiltration-based installations would provide substantial benefits. The drainage network naturally changes at the geological time scales, leaving numerous channels buried at different depth throughout the alluvial plain. Paleochannels represent the most important absorbance elements and are developed along old drainage directions. Analysis of satellite images and aerial photos can be used to detect and map the paleochannel, considering the tone, color, and pattern of the image. Paleochannels are subsequently verifiable via direct investigations. Despite their lower resolution, older image datasets are useful as areas are less urbanized. Wu et al. (1996) mapped five series of paleochannels in the North Plain, arranged in 20 paleochannels zones, several of them exceeding 100 km in length.

Delta Regions

Deltas are in proximity of river outlets, consisting of clayey to silty dominated sequences. In China, numerous metropolitan areas, including Shanghai and Guangzhou, are built on these sequences, thanks to the flat morphology and the proximity to the coastline. In wet climates, the water demand typically is satisfied by upstream reservoirs and basins; in dry climates deeper aquifers located several hundred meters below the ground surface are utilized for water supply. Because of the abundant impervious layers and lenses characterizing the sequence, the groundwater table is shallow and near the ground surface. Shallow surface

TABLE 1 | Hydrogeological characteristics and absorbance capacity of the 17 most populous Chinese cities.

Name	Population (million) NBSC-National Bureau of Statistics of China (2019)[a]	Climate	Rainfall rate [mm/y] CMA, China Metereological Administration (2020)	Hydrogeologic Zones and Potential Infiltration	References (Geological and hydrogeological data)
Shanghai	24.23	Temperate	1,166	Quaternary deltaic sequence of silty sand alternate to clay and silty clay, arranged in a multilayer aquifer. Groundwater table on average located between 0.5 and 1.5 m below the ground surface. Low to very low infiltration potential	Xu et al. (2009)
Beijing	21.54	Continental	585	Thick quaternary alluvial fan and alluvial plain sequence. Aquifers have a high hydraulic conductivity, from 2.3×10^{-5} m/s to 2×10^{-3} m/s. Groundwater table located tens of meter below the ground level, because of the exploitation via water-wells. High potential infiltration in the city center, very high in the suburbs surrounding the taihang mountains	Zheng et al. (2010), Zhou et al. (2016), Zhang and Fei (2008)
Chongqing	20.32	Temperate	1,130	Folded mesozoic bedrock incised by Yangtze River and its tributaries. Terrigenous sedimentary strata have an average to low infiltration potential; Yangtze River alluvial terrace, karstified strata, and the small but continuous piedmont bands of the anticline reliefs have high to very potential infiltration.	Chen et al. (2017)
Guangzhou	14.90	Sub-Tropical	1845	Low permeability quaternary deltaic sequence in contact with Paleozoic to mesozoic hilly terrains with varied hydraulic characteristics. Shallow groundwater table almost coincident with the ground level throughout the delta sequence, with low potential infiltration. High potential infiltration on the piedmont in the suburbs	Lancia et al. (2020b)
Shenzhen	13.02	Sub-Tropical	1936	Paleozoic to tertiary hilly terrains alternating with quaternary fluvial to coastal sediments. Hydraulic conductivity and water table depth varied. High potential infiltration throughout the piedmont bands	Lancia et al. (2020a), Lancia et al. (2020b)
Chengdu	8.99	Temperate	904	Thick and permeable alluvial fan sequence mainly constituted by gravel. Groundwater table has declined in the last decades because of the groundwater abstraction, currently deeper than 6 m from the ground. Potential infiltration is average to high	Rong et al. (2019)
Wuhan	8.90	Temperate	1,256	Recent clayey lacustrine deposits about 10–20 m thick cover the sandy and more permeable quaternary sandy sequence. Groundwater table aligned with the main river stages, averaging 5–10 m below land surface. Potential Infiltration is average to low	Private Report
Suzhou	8.15	Temperate	1,076	Quaternary sequence of fluvial, lagoon and marine deposits, 200 m thick, constituting a multilayer aquifer. Shallow deposits are constituted by 5–7 m of clay and silt, with a hydraulic conductivity from 1×10^{-7} m/s to 1×10^{-8} m/s. Potential infiltration is low to very low.	Chen et al. (2003)
Tianjin	7.60	Continental	544	Quaternary sequence of sand, silt and clay constituting a multilayer aquifer. Phreatic aquifer is silty with a hydraulic conductivity from 1×10^{-5} m/s to 1×10^{-7} m/s. Groundwater table is steady and located less than 2 m from the ground level also thanks to the seawater intrusion from Bohai Bay. Low potential infiltration.	Wu et al. (2018), Ha et al. (2020)
Hangzhou	7.59	Temperate	1,420	Clayey marine sequences about 20 m thick, with deltaic characteristics, cover the alluvial sediments throughout the urban center. City has a low absorbance capacity except for piedmonts along the mountains and the small bedrock hills that interrupt the morphology of the plain	Li et al. (2006)
Zhengzhou	7.44	Continental	636	Quaternary multi-layer aquifer, located at the right side of Yellow River. Consistent regional water table decline with extensive groundwater exploitation and shallow water-wells dry. Absorbance capacity high to very high	Sun et al. (2009)

(Continued on following page)

TABLE 1 | (*Continued*) Hydrogeological characteristics and absorbance capacity of the 17 most populous Chinese cities.

Name	Population (million) NBSC-National Bureau of Statistics of China (2019)[a]	Climate	Rainfall rate [mm/y] CMA, China Metereological Administration (2020)	Hydrogeologic Zones and Potential Infiltration	References (Geological and hydrogeological data)
Nanjing	6.96	Temperate	1,091	Alluvial sequence of the Yangtze River characterized by clayey deposits, alternating with sandy paleochannels. Urban center has a shallow groundwater table located between 1 and 2 m. below land surface. Low to very low absorbance capacity	Private Report
Shenyang	6.74	Continental	716	Thick sequence of gravel and sand with hydraulic conductivity between 1×10^{-3} m/s and 1×10^{-4} m/s located between the piedmont and the alluvial valley of liao River. Cones of depression induced by water pumping significantly increases the absorbance capacity. High to very high absorbance capacity	Zhou et al. (2011)
Harbin	5.51	Continental	519	Thick and heterogeneous alluvial sequence arranged with paleochannels and alluvial terraces and groundwater table located 30–50 m below the ground level. Potential infiltration average to high	Dai et al. (2011)
Shijiazhuang	5.06	Continental	483	Thick and permeable alluvial sequence arranged with channels and with a hydraulic conductivity from 1×10^{-3} m/s and 1×10^{-4} m/s. Groundwater table located tens of meter from the ground level, with a constant drawdown of 1.5 m/y because of anthropic withdraw. High potential infiltration	Shen et al. (2005), Zhang and Fei (2008)
Baoding	5.01	Continental	550	Thick and permeable alluvial fan and plain sequence with hydraulic conductivity from 5×10^{-4} m/s to 2×10^{-3} m/s. Groundwater table located 30–40 m from the ground level because of the exploitation via water-wells. High potential infiltration	Zhang and Fei (2008)
Nanyang	4.63	Temperate	765	Thick quaternary sequence of sand and gravel, interbedded with silty clay layers. Shallow aquifer is interconnected with rivers and streams. Groundwater table averages about 4 m from the ground level, but cones of depression due to the heavy abstraction from the shallow aquifer (71.4 million of m^3 per year) increase the infiltration potential. Average to high potential infiltration	Han et al. (2004)

[a]*Based on residence permit statistics.*

waters and seawater intrusions offset the local groundwater table drawdown triggered by shallow wells. Therefore, absorbance capacity is low at the regional scale (**Figure 6**). Numerical analysis (**Figure 5C**) suggest that the dissipation of infiltrated water occurs only in proximity of the drains within two weeks of an infiltration event.

Fractured and Karstified Carbonate Bedrock

Karst and fractured bedrock aquifers are natural sponge city facilities. These systems are characterized by an optimal absorbance capacity. These aquifers occur throughout China (**Figure 4**) and villages and major cities rely on these for water supply (Daoxian, 1991). Fracturing ratio, mainly related to the tectonic stresses, influences the hydraulic conductivity. Fractured bands are distributed along the main tectonic stresses.

Karst processes have a regional impact on groundwater circulation in the urban environment. In northern China, karst processes coincide with rural mountain reliefs, often interbedded with less permeable soils and naturally preserved from pollution. On the contrary, extensive and continuous karst fields characterize wide portion of southern China, with villages and urban centers built on it. Because most of the rainfall is concentrated in the summer months, episodes of drought in the mountain villages alternate with river floods in the valleys. With a regional groundwater table located even hundreds of meters below the ground surface, cities and villages are built in correspondence of dolinen, polje or other karst features able to retain the storm water for a longer period like a Sponge City facility, thanks to impermeable deposits as terre rosse or bauxite levels (Daoxian, 1991). Thus, even if the absorbance rate and the regional water availability are high, smaller communities can suffer water scarcity and the introduction of above the ground Sponge City facilities is recommended to store a strategic amount of water for exceptional drought events.

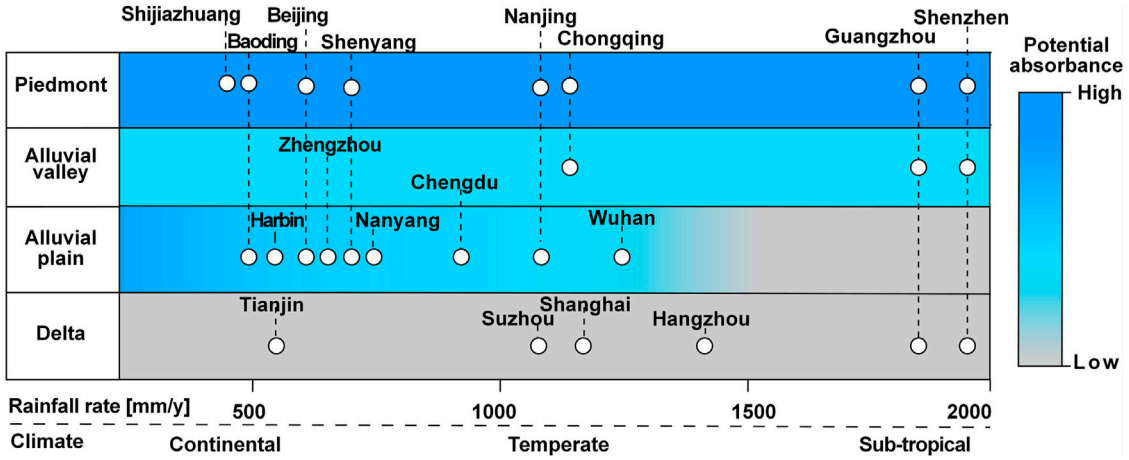

FIGURE 7 | Subsoil characteristics and rainfall rate define the absorbance potential at the regional scale. Alluvial valleys fractured to karst bedrock and piedmont have a good potential absorbance at any rainfall rate. The recent exploitation of urban aquifers has increased absorbance potential on the alluvial plains and in the Sichuan Basin at Chengdu. A low potential absorbance characterizes the delta areas in all climatic regimes.

Absorbance Capacity of Chinese Megacities

The hydrogeological setting and absorbance capacity of the 17 most populous megacities of China are summarized in **Table 1**. During the latest urban expansion, Chinese megacities expanded in areas with high hydraulic conductivity soils. In Beijing, the piedmont bands of Taihang Mts. were continuously urbanized and in a minor way in Shijiazhuang and Baoding; in Chonqing, Guangzhou and Shenzhen, the hilly and mountain sectors are the only areas preserved from urbanization. Bounded by morphological barriers, these cities expanded to the piedmonts and later urbanization intensified in the nearby valleys. The recent impermeabilization of high absorbance areas at the megacity scale is a triggering factor for both waterlogging as well as water scarcity. Infiltration-based installations applied at large scale can provide immediate benefits.

In the wide alluvial plains and valleys (**Figure 6**), exploitation of the urban aquifers for water supply to meet the insatiable water demand of the megacities amplifies the absorbance capacity. The regional groundwater table of alluvial plains in the megacities of Harbin, Beijing, and Baoding has been significantly depressed and absorbance is high in correspondence of the high permeability terrain. In the recent years, the groundwater table in the southern cities of Chengdu and Nanyang has declined to several meters (Han et al., 2004; Rong et al., 2019) below ground surface because of the increasing water demand; a worrying trend. According to our analysis, only the sub-tropical alluvial plains characterized by a good system of dams and reservoirs have a low absorbance potential.

Megacities built on deltaic deposits have a low absorbance potential because the groundwater table is at or near the ground surface (**Figure 7**). The absorbance capacity remains low regardless of rainfall rate. Rainfall varies significantly from north to south and is 1,500 mm/y greater at Shenzhen in the south than in Tianjin in the north. The low hydraulic conductivity of the shallower layers and the frequent saline intrusions result in limited exploitation of the urban aquifers. The exploitation of deeper aquifers, related to different paleo-environment, do not have any impact on the absorbance capacity on the shallow aquifer.

Aquifer Management Optimization

Conductive aquifers are able to dissipate infiltrated water in a reasonable amount of time and the application of infiltration-based installations are profitable (e.g., soil 1, **Figure 5A**). In less permeable deposits, a denser network of drains can be introduced to favor the dissipation of the infiltrated water, increasing the costs. Recharge with undrained conditions is conservative as it simulates the maximum water table increment associated with a single rainstorm. In fact, it is assumed that all the water infiltrates from the top level to the water table through the vadose zone during the rainstorm. In the practice, soil can absorb the stormwater in a slower amount of time, temporarily flooding the infiltration-based installations. Natural infiltration rates in gravelly to silty loam is estimated by Johnson (1963) between 126.0 and 12.7 cm per hour. If expected infiltration from storms are higher than soil infiltration rate and these installations cannot be flooded, a thicker base of gravel and sand can increase the collection of the water storm. A thicker base, though, would increases the installation and setup cost. Therefore, the thickness of the installation base must be designed according to the climate and the groundwater characteristics.

Hydrogeological analyses, supported by numerical evidence, have identified the infiltration potential in major urban areas in China, according to the hydrogeological and climate feature and the anthropogenic activities (**Table 1**). These analyses, following the procedures outlined in this study, could be easily expanded to cover other urban areas in China. As absorbance capacity sensibly varies along the catchment (**Figure 6**), Sponge City plans are optimized if realized at the regional scale. As the infiltration-

based installations are inexpensive relative to other Sponge City components, urban areas characterized by a high infiltration capacity should be exploited to their fullest (Lancia et al., 2020a). In small catchments with high rate of urbanization, large use of infiltration-based features also can mitigate the flood risk.

Benefits include the larger available storage capacity that could be economically convenient as it increases the baseflow of streams and rivers in urban areas supported by groundwater. This will result in aesthetic and ecological improvements of the urban environment (Nguyen et al., 2019). The major risk associated with infiltration is that groundwater may become polluted if the storm water is polluted. Although subsoils have the capacity to attenuate pollutants, infiltration should be limited to clean water from roofs, parks, and residential streets. The risks of pollution and chemical spills in major roads and industrial areas is high and connection with aquifers should be avoided (Lancia et al., 2020a).

Increased aquifer recharge can also reduce the contaminant load from sewers. Sewer pipes, located above the groundwater table, tend to exfiltrate pollutants via cracks and fractures. If infiltration-based installations increase the groundwater table over the sewer pipes, flow is inverted and groundwater infiltrates into the sewer preventing the pollutant leakage (Chisala and Lerner, 2008; Su et al., 2020). This beneficial effect is transitory and efficacious just after the rain before the water table declines as groundwater flows to river and streams. However, in megacities with a tropical climate the effect can be long lasting. At the same time, a water table higher than the pressurized pipes also reduces the water loss from the water-supply system, mitigating to an extent water scarcity (Lerner, 2002). According to MOHURD-Ministry of Housing and Urban Rural Development (2014), the water supply systems of China have a water loss rate between 15 and 25%.

CONCLUSION

The application of the Sponge City concept is an excellent opportunity to address water scarcity and mitigate the waterlogging risk in the urban areas of China. Together with the classic Sponge City elements, numerical and hydrogeological analysis suggest that infiltration-based installations have great potential in many areas of the country. Infiltration-based installations can provide both considerable economic and environment benefits and should be the preferred Sponge City strategy in less developed areas of China, due to the minor costs. Because of the varied lithological, climatic and hydrogeological setting of Chinese urban areas, guidelines developed at the provincial scale, rather than the national scale, can be more efficacious. With the implementation of the suggested methods, based on both climate and infiltration capacity, a more precise definition of the runoff control classes is possible. Performed hydrogeological analysis assess the potential infiltration of the Chinese megacities. The potential infiltration is high along the piedmont or along the alluvial valleys characterized by permeable soils; megacities settled on less permeable delta sequence have a low potential infiltration. The drawdown of the water level, due to anthropic or climate factors, can increment the potential infiltration.

Infiltration-based installations require detailed characterization of the urban aquifers. Preliminary studies, including monitoring of the water table and incremented infiltration scenarios after retrofitting, are essential to optimize the Sponge City plan. According to the outlined criteria, it is possible that the capital and operating costs of the Sponge City facilities can be kept within a manageable range, while at the same time an additional source of water can be provided to reduce water scarcity. The proposed conceptual model also highlights new policies for urban expansions. New urban developments should be prioritized in the low infiltration areas. Urbanization on high infiltration zones should be limited or prohibited.

DATA AVAILABILITY STATEMENT

The original contributions presented in the study are included in the article/supplementary material, further inquiries can be directed to the corresponding authors.

AUTHOR CONTRIBUTIONS

All authors listed have made a substantial, direct, and intellectual contribution to the work and approved it for publication

FUNDING

The study was supported by the National Key R&D Program of China (project numbers 2016YFC0402806, and 2018YFE0206200), National Natural Science Foundation of China (Grant No. 41861124003); and the High-level Special Funding of the Southern University of Science and Technology (Grant Nos. G02296302, G02296402).

REFERENCES

Anderson, M. P., Woessner, W. W., and Hunt, R. J. (2015). *Applied Groundwater Modelling – Simulation of Flow and Advective Transport*. 2nd Ed. Amsterdam: Academic Press, Inc. Elsevier, 535.

Bowman, D. (2017). *Principles of Alluvial Fan Morphology*. Berlin: Springer-Verlag, 151.

Brassington, R. (2007). *Field Hydrogeology*. West Sussex, England: Wiley, 265.

Cao, G., Zheng, C., Scanlon, B. R., Liu, J., and Li, W. (2013). Use of Flow Modeling to Assess Sustainability of Groundwater Resources in the North China Plain. *Water Resour. Res.* 49, 159–175. doi:10.1029/2012WR011899

CGS (1979). *Chinese Geological Survey*, 1. Beijing: Hydrogeological map of People`s Republic of China, scale.

Chen, C., Pei, S., and Jiao, J. (2003). Land Subsidence Caused by Groundwater Exploitation in Suzhou City, China. *Hydrogeology J.* 11, 275–287. doi:10.1007/s10040-002-0225-5

Chen, J., Shi, H., Sivakumar, B., and Peart, M. R. (2016). Population, Water, Food, Energy and Dams. *Renew. Sustain. Energ. Rev.* 56, 18–28. doi:10.1016/j.rser.2015.11.043

Chen, K.-L., Wu, H.-N., Cheng, W.-C., Zhang, Z., and Chen, J. (2017). Geological Characteristics of Strata in Chongqing, China, and Mitigation of the Environmental Impacts of Tunneling-Induced Geo-Hazards. *Environ. Earth Sci.* 76, 10. doi:10.1007/s12665-016-6325-7

Chisala, B. N., and Lerner, D. N. (2008). Distribution of Sewer Exfiltration to Urban Groundwater. *Proc. Inst. Civil Eng. - Water Manage.* 161 (6), 333–341. doi:10.1680/wama.2008.161.6.333

CMA, China Metereological Administration (2013). Classification Standard of Precipitation Intensity. [in Chinese] Retrieved from http://www.cma.gov.cn/2011xzt/2013zhuant/20130620_3/2013062002/201308/t20130816_223400.html (Accessed June 2020).

CMA, China Metereological Administration (2020). Climate Bulletins of Chinese Cities. [in Chinese] Retrieved from http://www.cma.gov.cn (Accessed June 2020).

Dai, C. L., Li, Z. J., Du, S. M., and Liu, C. H. (2011). Evaluation of Shallow Groundwater Quantity in Harbin by Numerical Modeling. *Adv. Mater. Research.* 255-260, 2745–2750. doi:10.4028/www.scientific.net/amr.255-260.2745

Daoxian, Y. (1991). *Karst of China*. Beijing: Geological Publishing House, 224pp.

Fletcher, T. D., Shuster, W., Hunt, W. F., Ashley, R., Butler, D., Arthur, S., et al. (2015). SUDS, LID, BMPs, WSUD and More - the Evolution and Application of Terminology Surrounding Urban Drainage. *Urban Water J.* 12 (7), 525–542. doi:10.1007/s12665-016-6325-710.1080/1573062x.2014.916314

Freeze, R. A., and Cherry, J. A. (1979). *Groundwater*. Englewood Cliff, NJ: Prentice-Hall, 606.

Ha, D., Zheng, G., Loáiciga, H. A., Guo, W., Zhou, H., and Chai, J. (2020). Long-term Groundwater Level Changes and Land Subsidence in Tianjin, China. *Acta Geotech.* 16, 1303–1314. doi:10.1007/s11440-020-01097-2

Han, J., Wang, B., and Cao, B. (2004). *Division of Groundwater Systems and Significance of Water Supply in Nanyang City*, 26. China: Ground Water, 14–16.1 [in Chinese.

Hua, S., Jing, H., Yao, Y., Guo, Z., Lerner, D. N., Andrews, C. B., et al. (2020). Can Groundwater Be Protected from the Pressure of china's Urban Growth? *Environ. Int.* 143, 105911. doi:10.1016/j.envint.2020.105911

Huang, Y., Tian, Z., Ke, Q., Liu, J., Irannezhad, M., Fan, D., et al. (2020). Nature-based Solutions for Urban Pluvial Flood Risk Management. *WIREs Water* 7, e1421. doi:10.1002/wat2.1421

Johnson, A. I. (1963). *A Field Method for Measurement of Infiltration. General Ground-Water Techniques*. Denver: U.S. Geological Survey Water-Supply Paper.

Lancia, M., Su, H., Tian, Y., Xu, J., Andrews, C., Lerner, D. N., et al. (2020b). Hydrogeology of the Pearl River Delta, Southern China. *J. Maps* 16 (2), 388–395. doi:10.1080/17445647.2020.1761903

Lancia, M., Zheng, C., He, X., Lerner, D. N., Andrews, C., and Tian, Y. (2020a). Hydrogeological Constraints and Opportunities for "Sponge City" Development: Shenzhen, Southern China. *J. Hydrol. Reg. Stud.* 28, 100679. doi:10.1016/j.ejrh.2020.100679

Lerner, D. N. (2002). Identifying and Quantifying Urban Recharge: a Review. *Hydrogeology J.* 10, 143–152. doi:10.1007/s10040-001-0177-1

Li, C., Tang, X., and Ma, T. (2006). Land Subsidence Caused by Groundwater Exploitation in the Hangzhou-Jiaxing-Huzhou Plain, China. *Hydrogeol J.* 14, 1652–1665. doi:10.1007/s10040-006-0092-6

Li, J., Zhang, Y., Dong, S., and Johnston, S. T. (2014). Cretaceous Tectonic Evolution of South China: A Preliminary Synthesis. *Earth-Science Rev.* 134, 98–136. doi:10.1016/j.earscirev.2014.03.008

Liu, J., Zang, C., Tian, S., Liu, J., Yang, H., Jia, S., et al. (2013). Water Conservancy Projects in China: Achievements, Challenges and Way Forward. *Glob. Environ. Change* 23 (3), 633–643. doi:10.1016/j.gloenvcha.2013.02.002

Liu, J., Zheng, C., Zheng, L., and Lei, Y. (2008). Ground Water Sustainability: Methodology and Application to the North China Plain. *Groundwater* 46 (6), 897–909. doi:10.1111/j.1745-6584.2008.00486.x

MOHURD-Ministry of Housing and Urban Rural Development (2014). *Technical Guidelines of the Sponge City Development—Low Impact Development Systems for Storm Water*. Beijing: Beijing University of Civil Engineering and Architecture, 86. [in Chinese] Retrieved from http://www.mohurd.gov.cn/wjfb/201411/W020141102041225.pdf

NBSC-National Bureau of Statistics of China (2019). Statistical Bulletin on National Economic and Social Development. [in Chinese] Year 2018. Online report. Available at: http://www.stats.gov.cn/tjsj/ndsj/2019/indexch.htm (Accessed June 2020).

Nguyen, T. T., Ngo, H. H., Guo, W., Wang, X. C., Ren, N., Li, G., et al. (2019). *Implementation of Specific Urban Water Management-Sponge City*, 652. Science of the Total Environment, 147–162. doi:10.1016/j.scitotenv.2018.10.168

Niswonger, R. G., Panday, S., and Ibaraki, M. (2011). *MODFLOW-NWT, A Newton Formulation for MODFLOW-2005*. U.S Geological Survey Techniques and Methods, 6-A37.

Polade, S. D., Pierce, D. W., Cayan, D. R., Gershunov, A., and Dettinger, M. D. (2014). The Key Role of Dry Days in Changing Regional Climate and Precipitation Regimes. *Scientific Rep.* 4, 1–8. doi:10.1038/srep04364

Randall, M., Sun, F., Zhang, Y., and Jensen, M. B. (2019). Evaluating Sponge City Volume Capture Ratio at the Catchment Scale Using SWMM. *J. Environ. Manage.* 246, 745–757. doi:10.1016/j.jenvman.2019.05.134

Rong, X., Lu, H., Wang, M., Wen, Z., and Rong, X. (2019). Cutter Wear Evaluation from Operational Parameters in EPB Tunneling of Chengdu Metro. *Tunnelling Underground Space Tech.* 93, 103043. doi:10.1016/j.tust.2019.103043

SC-State Council (2015). *The General Office of the State council Advice on Promoting Construction of Sponge Cities*. Beijing: GOSCThe State Council, 75. Available at: http://www.gov.cn/zhengce/content/2015-10/16/content_10228.htm.

Shen, Y., Tang, C., Xiao, J., Oki, T., and Kanae, S. (2005). "Effects of Urbanization on Water Resource Development and its Problems in Shijiazhuang, China. Sustainable Water Management Solutions for Large Cities" in Proceedings of Symposium S2 Held during the Seventh IAHS Scientific Assembly at Foz do Iguaçu, Brazil, April 2005. Editors D. A. Savic, M. A. Marino, H. H. Savenije, and J. C. Bertoni (Brazil: IAHS Publ).

Su, X., Liu, T., Beheshti, M., and Prigiobbe, V. (2020). Relationship between Infiltration, Sewer Rehabilitation, and Groundwater Flooding in Coastal Urban Areas. *Environ. Sci. Pollut. Res.* 27, 14288–14298. doi:10.1007/s11356-019-06513-z

Sun, R., Jin, M., Giordano, M., and Villholth, K. G. (2009). Urban and Rural Groundwater Use in Zhengzhou, China: Challenges in Joint Management. *Hydrogeol J.* 17 (17), 1495–1506. doi:10.1007/s10040-009-0452-0

Wang, Y., Zheng, C., and Ma, R. (2018). Review: Safe and Sustainable Groundwater Supply in China. *Hydrogeol J.* 26, 1301–1324. doi:10.1007/s10040-018-1795-1

Wu, C., Xu, Q., Zhang, X., and Ma, Y. (1996). Paleochannels on the North China Plain: Types and Distributions. *Geomorphology* 18, 5–14.

Wu, Y.-X., Lyu, H.-M., Shen, J. S., and Arulrajah, A. (2018). Geological and Hydrogeological Environment in Tianjin with Potential Geohazards and Groundwater Control during Excavation. *Environ. Earth Sci.* 77, 1–17. doi:10.1007/s12665-018-7555-7

WWDR (2020). *World Water Development Report 2020 – Water and Climate Change*. Paris: UNESCO, 219.

Xia, J., Zhang, Y., Xiong, L., He, S., Wang, L., and Yu, Z. (2017). Opportunities and Challenges of the Sponge City Construction Related to Urban Water Issues in China. *Sci. China Earth Sci.* 60, 652–658. doi:10.1007/s11430-016-0111-8

Xu, Y.-S., Shen, S.-L., and Du, Y.-J. (2009). Geological and Hydrogeological Environment in Shanghai with Geohazards to Construction and Maintenance of Infrastructures. *Eng. Geology.* 109, 241–254. doi:10.1016/j.enggeo.2009.08.009

Yin, A. (2006). Cenozoic Tectonic Evolution of the Himalayan Orogen as Constrained by Along-Strike Variation of Structural Geometry, Exhumation History, and Foreland Sedimentation. *Earth-Science Rev.* 76 (1-2), 1–131. doi:10.1016/j.earscirev.2005.05.004

Zhang, Z.-K., Ling, M.-X., Lin, W., Sun, M., and Sun, W. (2020). "Yanshanian Movement" Induced by the Westward Subduction of the Paleo-Pacific Plate. *Solid Earth Sci.* 5 (2), 103–114. doi:10.1016/j.sesci.2020.04.002

Zhang, Z., and Fei, Y. (2008). *Atlas of Groundwater Sustainable Utilization in North China Plain*. Beijing: China Map Publishing House, 185. [in Chinese].

Zhao, X., Liu, J., Liu, Q., Tillotson, M. R., Guan, D., and Hubacek, K. (2015). Physical and Virtual Water Transfers for Regional Water Stress Alleviation in China. *Proc. Natl. Acad. Sci. USA* 112 (4), 1031–1035. doi:10.1073/pnas.1404130112

Zheng, C., and Gorelick, S. (2015). Global Change and the Groundwater Management challenge. *Water Resource Res.* 51, 1–21. doi:10.1002/2014WR016825

Zheng, C., Liu, J., Cao, G., Kendy, E., Wang, H., and Jia, Y. (2010). Can China Cope with its Water Crisis?-Perspectives from the North China Plain. *Groundwater* 48 (3), 350–354. doi:10.1111/j.1745-6584.2010.00695_3.x

Zhou, H., Wang, D., Sun, C., Tian, W., Yang, P., and Teng, F. (2011). Simulation Study on the Recovery and Storage of the Funnel of the Water Source in the central City of Shenyang. *J. China Hydrol.* 31 (5), 47–51. [in Chinese].

Zhou, Y., Xiao, W., Wang, J., Zhao, Y., Huang, Y., Tian, J., et al. (2016). Evaluating Spatiotemporal Variation of Groundwater Depth/Level in Beijing Plain, a Groundwater-Fed Area from 2001 to 2010. *Adv. Meteorology* 2016, 1–11. doi:10.1155/2016/8714209

Conflict of Interest: Author CA was employed by the company S.S. Papadopulos and Associates, Inc.

The remaining authors declare that the research was conducted in the absence of any commercial or financial relationships that could be construed as a potential conflict of interest.

frontiers in Environmental Science

ORIGINAL RESEARCH
published: 28 September 2021
doi: 10.3389/fenvs.2021.748231

Revisiting China's Sponge City Planning Approach: Lessons From a Case Study on Qinhuai District, Nanjing

Shiyang Chen[1,2], Frans H. M. van de Ven[1,2]*, Chris Zevenbergen[3,4], Simon Verbeeck[5], Qinghua Ye[2,3], Weijun Zhang[6] and Liang Wei[7]*

[1]Department of Water Management, Faculty of Civil Engineering and Geosciences, Delft University of Technology, Delft, Netherlands, [2]Deltares, Delft, Netherlands, [3]Department of Hydraulic Engineering, Faculty of Civil Engineering and Geosciences, Delft University of Technology, Delft, Netherlands, [4]IHE Delft Institute for Water Education, Delft, Netherlands, [5]LOLA Landscape Architects, Rotterdam, Netherlands, [6]Ewaters, Shanghai, China, [7]Achterboschzantman International, Leeuwarden, Netherlands

OPEN ACCESS

Edited by:
Ahmed El Nemr, National Institute of Oceanography and Fisheries (NIOF), Egypt

Reviewed by:
James Andrew Griffiths, National Institute of Water and Atmospheric Research (NIWA), New Zealand
Jiahong Liu, China Institute of Water Resources and Hydropower Research, China

***Correspondence:**
Shiyang Chen
shiyang.chen07@gmail.com
Frans H. M. van de Ven
f.h.m.vandeven@tudelft.nl

Specialty section:
This article was submitted to Water and Wastewater Management, a section of the journal Frontiers in Environmental Science

Received: *27 July 2021*
Accepted: *13 September 2021*
Published: *28 September 2021*

Citation:
Chen S, van de Ven FHM, Zevenbergen C, Verbeeck S, Ye Q, Zhang W and Wei L (2021) Revisiting China's Sponge City Planning Approach: Lessons From a Case Study on Qinhuai District, Nanjing. Front. Environ. Sci. 9:748231. doi: 10.3389/fenvs.2021.748231

Integrating sustainable urban water management into the urban planning process is essential for developing water-resilient cities. To this end, the central government of the People's Republic of China initiated the "Sponge City" programme. However, challenges and gaps exist in current urban planning practice. The operationalizable planning approach to realise the multiple objectives of Sponge City is missing in the existing guidelines. Using a local example of Sponge City planning in Nanjing City as a case study, this paper outlines the current Sponge City approach from the perspectives of planning content and planning process. A qualitative comparative analysis between Nanjing's Sponge City planning and Auckland Water Sensitive Design, as well as an evaluation of the Sponge City approach through the lens of Dutch urban water management, identified key missing elements that would enhance the current Sponge City planning approach. Examples include targets for pluvial flood protection, a strategy for planning interventions, and tools for interdisciplinary cooperation in the planning process. This enhanced approach was successfully applied in the Sponge City planning for Qinhuai District, Nanjing City. Nevertheless, challenges on data availability and the decision-makers' mindsets called for more efforts on the interface of research and policy development for upscaling the Sponge City approach.

Keywords: Sponge City, water management, urban planning, comprehensive approach, co-design

INTRODUCTION

In order to comply with the concept of sustainability, many countries issued policies to support urban development with a minimum impact on the environment. The European Green Deal provides a roadmap for making the EU's economy sustainable by turning climate and environmental challenges into opportunities across all policy areas and making the transition just and inclusive for all (European Commission, 2019). Similarly, the ecological civilization (or eco-civilization) endorsed by the Chinese government calls for prioritizing resource conservation, ecosystem protection, and rehabilitation through a green, circular, and low-carbon development approach (State Council, 2015).

TABLE 1 | Challenges in planning content and process of current Sponge City.

Category	Challenges	References	Implication
Planning content	"[. . .] a national standard is critically needed for planning and organising SCD [Sponge City development] at the city or basin level to bridge the onsite engineering design of individual LID practices and the functional goals of sponge cities. **The importance and necessity of such a holistic systematic approach** is further justified by the complexity and interlinkage of the multiple urban water issues [. . .]projects under SCD should function **not only to tackle flooding and other water issues but also to take the opportunity to improve urban liveability and development sustainability**."	Ma et al. (2020)	The need of holistic thinking of urban water systems with multiple objectives and co-benefits
	"the GB50014-2006 code [*Code for design of outdoor wastewater engineering*] of practice **does not indicate** how drainage design should be undertaken in older towns or districts, or indicate **how current practices should be integrated with new, more sustainable drainage practice**."	Chan et al. (2018)	
	"They [guidelines] are, by large, merely the translation and combination of similar the guidelines widely used in the US and **do not consider variations in regional and local conditions** such as soil, climate and topography variances. Lack of design standards and codes has limited the ability of local communities to implement sponge city projects based on local conditions."	Li et al. (2017)	
	"**Need of integrated urban water system theory.**[. . .]Although the construction guideline of Sponge City was proposed, the widely-used control rate of annual average runoff amount only focused on the storage and infiltration measures of source controls with deficient capacities.**"**	Xia et al. (2017)	
Planning process	"**the competing priorities of stakeholders and their reluctance to make trade-offs**, which obstruct future investment in the SCP [Sponge City Program]"	Qi et al. (2020)	The need of stimulating efficient and effective stakeholder engagement (co-design) process
	"[. . .] the **inter-agency cooperation and working across functions has not always been easy** in China due to the difficulty of working across divisions, agencies, and political boundaries with diverse groups and diverse interests."	Li et al. (2017)	
	"[. . .] sponge city systems are mostly built above ground and scattered in large regions; some located in private land interfering with public life. Therefore, **public opinion and acceptance of sponge city construction** can easily hinder its success."	Li et al. (2017)	
	"**Complexity of hydrological models impedes the multi-disciplinary collaboration.**"	Cai, (2016)	

Water is increasingly recognized by urban planners as an essential steering element to realize urban sustainability goals (Hooimeijer, 2014; Stead, 2014; Hurlimann and Wilson, 2018). The international trend of urban water management is to develop "water sensitive cities" (Brown et al., 2009). To this end, new planning and design concepts emerged, such as Low Impact Development, Sustainable Urban Drainage Systems, and Water Sensitive Urban Design. These planning and design concepts embrace interlinking nature-based solutions (NBS) with grey infrastructures to increase urban resilience via peak flow reduction, water quality improvement, and by developing new ecosystem services within the limitedly available urban space. One of the crucial challenges hindering the implementation of such concepts is how to value and design hybridized blue-green-gray systems with a variety of stakeholders (Kumar et al., 2020).

The rapid increase of impervious surfaces and removal of natural water storage such as natural wetlands and lakes due to urbanization has increased the occurrence of urban flooding in China (Wang et al., 2012). According to an investigation carried out by the Ministry of Housing and Urban-Rural Development (MHURD) in 2010, 137 of 351 Chinese cities suffered more than three flooding events from 2008 to 2010 (Che and Zhang, 2019). In addition, more than 400 cities are short of water supply; 110 cities face severe water shortage situations (Li et al., 2016). Moreover, polluted water discharged into surface water and groundwater has severely impacted public health and the local ecology (He and Xing, 2006; Sun et al., 2016). Faced with issues of flooding, drought, aquatic habitat degradation, and groundwater depletion, China needed an integrated and comprehensive solution involving not one single department but multiple departments (Yu et al., 2015). For these reasons, the Sponge City Programme was initiated in 2014 by the Chinese central government (MHURD, 2014).

Since then, the Sponge City concept has been tested and become increasingly developed. According to the definition given in the evaluation standard of 2018, the concept has expanded on 2014s guidelines to become an integrated urban water management strategy incorporated in urban planning and design. The Sponge City concept now including objectives of water ecology, water resource, water environment, water safety, and water culture (MHURD, 2018).

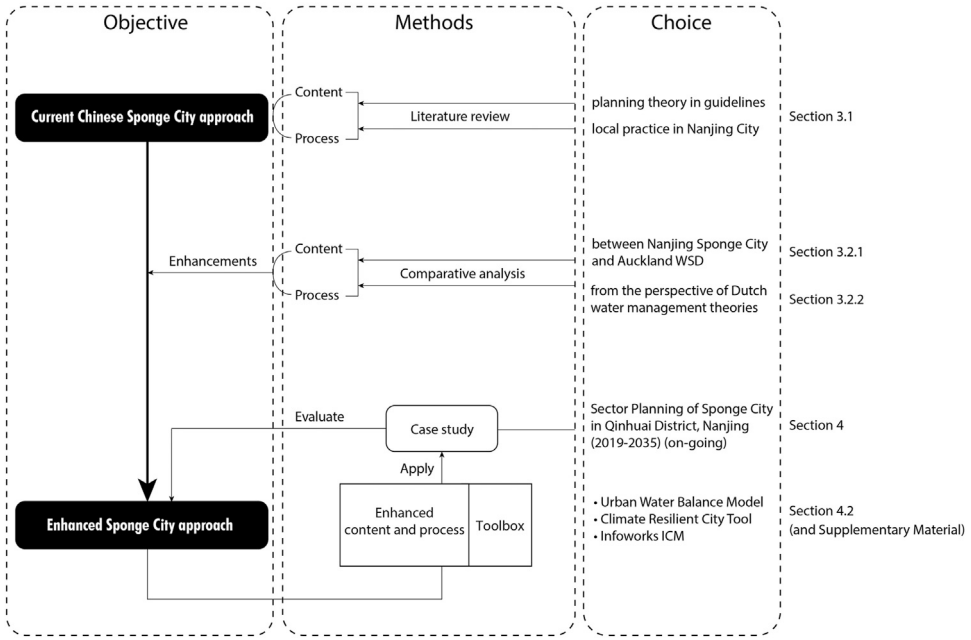

FIGURE 1 | Methodological scheme of this paper.

However, scholars reported difficulties regarding its implementation in practice. Practitioners, such as water planners/managers/engineers, struggle with both contents of the Sponge City concept and the organization of an effective and efficient planning process. Key challenges in Sponge City planning fall into two dimensions, i.e., planning content—what is being addressed—and planning process—how these issues are being addressed (see **Table 1**). The lack of an operationalizable and justifiable approach considering both holistic urban water systems and stakeholder engagement is a crucial factor impeding the local implementation of the Sponge City concept.

This article aims to evaluate the current Sponge City planning practice in Nanjing, identify challenges and gaps, in which an enhanced planning approach can be formulated, and to demonstrate the enhanced planning applicability using Qinhuai District in Nanjing as a case study.

METHODOLOGY

Enhancing the Planning Approach

In order to enhance the current Sponge City planning practice in Nanjing and reveal challenges and gaps in the application of this enhanced approach, we first present the latest developments in existing Sponge City planning, based on studies of both national governmental policy documents and documents on local policy implementation in Nanjing. Current Sponge City local implementation is analysed in two dimensions, i.e., planning content—*what* is being addressed—and planning process—*how* these issues are being addressed. To identify options to improve this current Sponge City planning approach, we use qualitative methods, including literature review and comparative analysis, as illustrated in **Figure 1**.

The differences between China's Sponge City and other approaches to urban water management can be found by comparing their overarching guiding principles and concepts (see **Supplementary Material SA**). Since Water Sensitive Urban Design (WSD) and Sponge City share the strategy of incorporating stormwater management in the urban planning process, the guidelines of Nanjing Sponge City planning are compared with those of Auckland's Water Sensitive Design. WSD also includes approaches like Low Impact Development and Sustainable Urban Drainage Systems and is considered comprehensive. Both the Sponge City approach and the WSD approach are typically customized for the local conditions in a specific city. That is why a comparison at the local level is appropriate. In addition, to test the robustness of the underlying principles in the Sponge City planning approach, the approach is evaluated through the lens of the principles in water management practices of the Netherlands. The Dutch principles are used as evaluation criteria since the well-developed Dutch water management practices may provide inspiring experiences to other countries with similar situations.

Differences between the approaches—in terms of both planning content and planning process—allowed us to reflect on the Sponge City approach and identify potential improvements in the planning content and the process. Based on the results, an adapted Sponge City planning approach is proposed and, as a hypothesis, is considered to be an enhanced version. This enhanced version of Sponge City planning approach is evaluated by its application in an ongoing

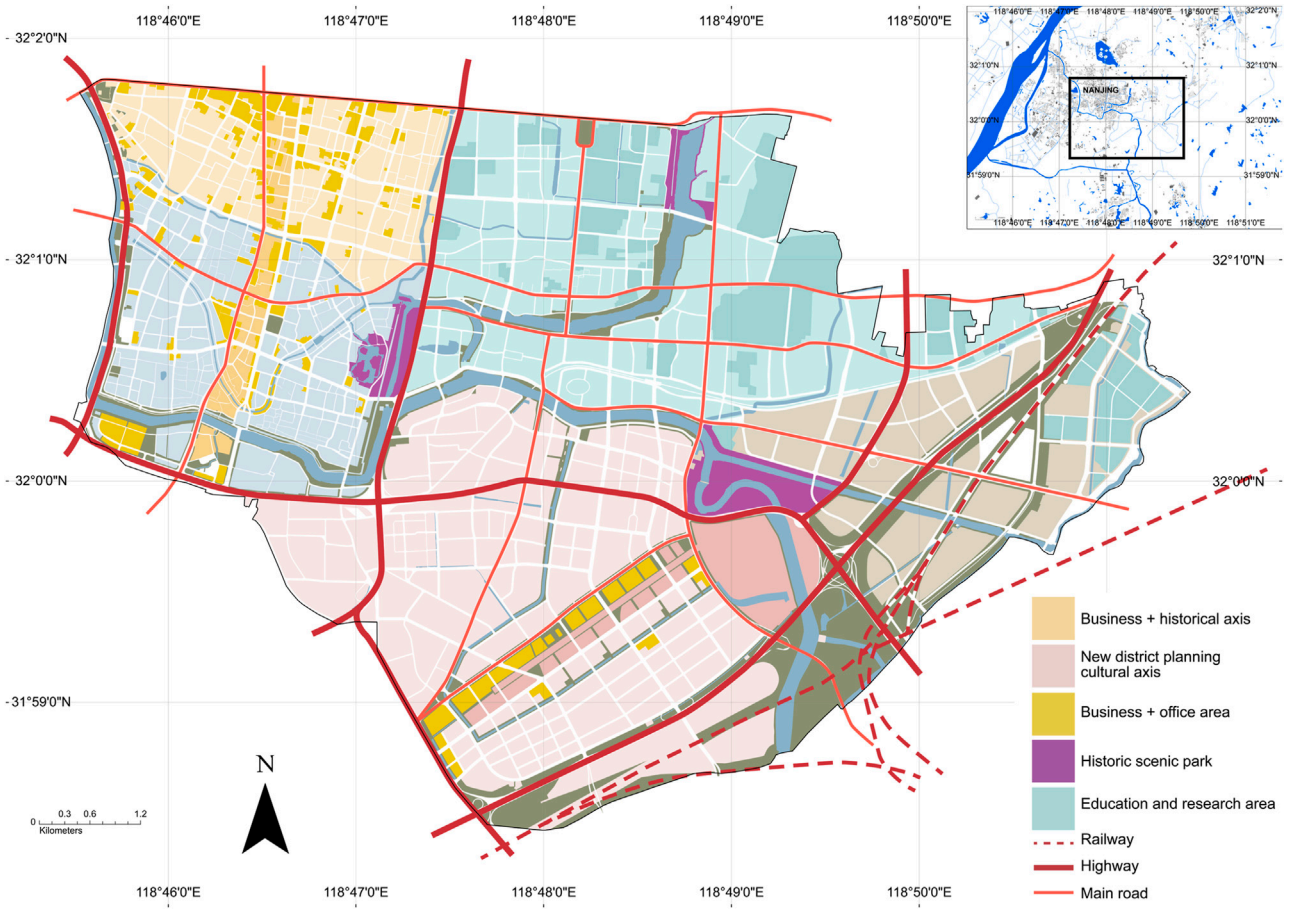

FIGURE 2 | The land use map of Qinhuai District.

Sponge City planning project of Qinhuai District, Nanjing City.

Case Study Description

Development and application of the enhanced Sponge City approach was part of a project to implement the national Sponge City policy at the local level of Nanjing City. The objective was to deliver a Sponge City plan for Qinhuai District, including sponge measures to mitigate pluvial flooding and improve surface water quality while obtaining co-benefits such as mitigation of the urban heat island effect, strengthening water culture, etc. The enhanced Sponge City planning approach was applied (including spatial analysis, sponge size calculation, hydraulic modelling, suggested sponge measures, etc.), and its results were incorporated in the project outcomes. The case study is used to demonstrate how the enhanced approach can be applied in practice with an evaluation to determine the added value of the newly created measures.

Several tools were applied to provide insights into both the potentials and the challenges of the proposed sponge measures. Tools used for this research include the Urban Water Balance Model (Brolsma and Vergroesen, 2020), InfoWorks ICM (Costa et al., 2021), and Climate City Resilient Tool (CRCT) (van de Ven et al., 2016; McEvoy et al., 2018; McEvoy, 2019).

Site Description

Nanjing City is situated at the Yangtze River Delta, which has a humid subtropical climate influenced by the East Asian monsoon (Mao et al., 2012). Between 1949 and 1978, in need of land, the government filled canals and ponds without realizing their hydrological, historical, ecological, landscape, and other values (Liu and Han, 2014). Consequently, intense precipitation in the rainy season with other factors such as urban landcover change, low topography, etc., has resulted in frequent flooding hazards in recent decades.

Qinhuai District is located at the heart of Nanjing City with a total area of 49 km^2, south of the city's downtown, with the old royal palace clustered in the northwest and old canal networks interweaved in the urban landscape (see **Figure 2**).

Qinhuai District contains 19% green spaces and 6.8% water surfaces. These blue and green spaces are scattered and have not yet been planned to systematically contribute to eco-system protection, flood defence, recreation, and other co-benefits. Stormwater runoff in Qinhuai District is conveyed by a separate system of pipes and local canals, pumped into the Qinhuai River, and further discharged to the Yangtze River. The current strategy for pluvial flood protection is "discharge",

without consideration of "retain" and "store" in urban planning. Moreover, poor water quality in the canal systems not only endangers the aquatic ecosystem but also hinders local heritage protection. Sponge City planning can be a trigger to smooth the confrontation between historical cultural heritage and urban development, especially in the north-western area of the district.

COMPARATIVE ANALYSIS OF THE CURRENT SPONGE CITY PLANNING APPROACH

Sponge City Planning Approaches and Its Local Application in Nanjing

After the first official debut at the Central Urbanization Conference in 2013, the Sponge City concept was formulated and supported by a series of documents from the central government. MHURD released the first technical guideline of Sponge City construction (MHURD, 2014), which outlines the technical framework of Sponge City construction. The approach integrates the Sponge City concept in the urban planning processes, including land development, greenery planning, water system planning, transport planning, etc., The first version of governmental documents formulated performance indicators on six aspects, i.e., water ecology, water environment, water resources, water safety, institutional system building and implementation, demonstration effects (MHURD, 2015). The request of making local Sponge City planning, published by MHURD in March 2016, sets general principles of downscaling Sponge City indicators to city level (MHURD, 2016). In 2018 the official national standard was released for evaluating sponge effects (MHURD, 2018).

It can be concluded from those guiding documents that Sponge City seeks a comprehensive approach to solve urban water related issues; Stormwater is to be managed by at-source measures, en route conveyance, and end-of-pipe measures. Water retention is required as part of the ecological indicators. The size of this "sponge" is determined by an indicator called VCRa (Volume Capture Ratio of annual rainfall).

Driven by the central government's policy, the Sponge City concept, and the planning approach cascaded down to local levels, with more detailed local interpretations and planning procedures. Such local applications are, e.g., found in the Sponge City plans of multiple administrative levels in Nanjing City. Our analysis of these plans gave detailed insights into the local implementation/interpretation process (NPNRB 2018a; 2018b; Wei, personal communication, December 4, 2019). The Nanjing Sponge City planning content and process are illustrated in **Figure 3** and **Figure 4**, respectively.

As shown in **Figure 3**, Nanjing's Sponge City approach covers five topics, each of which has different sub-topics in the next ring. The main topics are water safety, water ecology, water environment, and water resources. For areas with significant water-related historical or social values, water culture is also considered in their sponge planning. Potential problem assessment approaches are listed in the ring next to sub-topics. The outermost ring includes objectives for tackling issues under each topic. Plans at the city and district levels all cover this content.

The framework in **Figure 4** describes three components of the planning process, i.e., planning, project, and responsible authorities. Three coloured frames represent different types of planning, i.e., master planning, detailed spatial planning, as well as Sponge City and other sectoral planning. The blue line and the green line represent the connection of different planning procedures concerning water and green systems, respectively. Coloured bullets in the Project component of **Figure 4** stand for different authorities, taking specific responsibilities in different project phases.

Analysis of this process framework is conducted from three perspectives:

1. The relationship between sponge city planning and other planning.

Sponge City planning is interwoven with other sector planning. Sponge City plans to integrate information, objectives, and implementation plans from other plans, such as urban spatial planning, water system planning, flood control planning, green system planning, ecological protection planning, etc., Vice-versa, Sponge City plans provide policy suggestions to these plans.

2. Downscaling Sponge City requirements.

Sponge City performance requirements are downscaled from larger administrative regions to smaller subzones. Nanjing's Sponge City plan has four subzone scales related to the normal spatial scales of city-district-neighbourhood, i.e., city, city divisions, drainage basins, and control units. Targets for Sponge City indicators are downscaled from city to district, and from there to drainage basins and control units. This ensures that objectives are achieved as the performance indicators of lower-level units are aggregated to upper-level units. Obligatory indicators such as VCRa and recommended indicators are assigned to each control unit and must be respected by land and project developers. Compensation of a deficit in one subzone by a surplus in another subzone is not allowed.

3. Involved authorities.

Many administrative authorities play an active role in guiding and assessing Nanjing's Sponge City planning. For example, Sponge Office (in pink), together with Natural Resource (in yellow) and Planning Bureau or Transport Bureau (in purple), is responsible for checking whether the (preliminary) design of a project fulfils Sponge City requirements before the construction permit is issued by Natural Resource and Planning Bureau (NPNRB, 2018b; 2018a). Intensive communication and information exchange is needed amongst different Bureaus, making the Sponge City planning process new and complex.

Comparative Analysis

Auckland's Water Sensitive Design (WSD)

To compare the Sponge City approach used in Nanjing to the WSD approach as applied in Auckland, several sources, especially guidelines, were studied (Healy et al., 2010; Lewis et al., 2015; Auckland Council, 2016; Cunningham et al., 2017; NPNRB, 2018b). Sponge City and WSD share many common elements

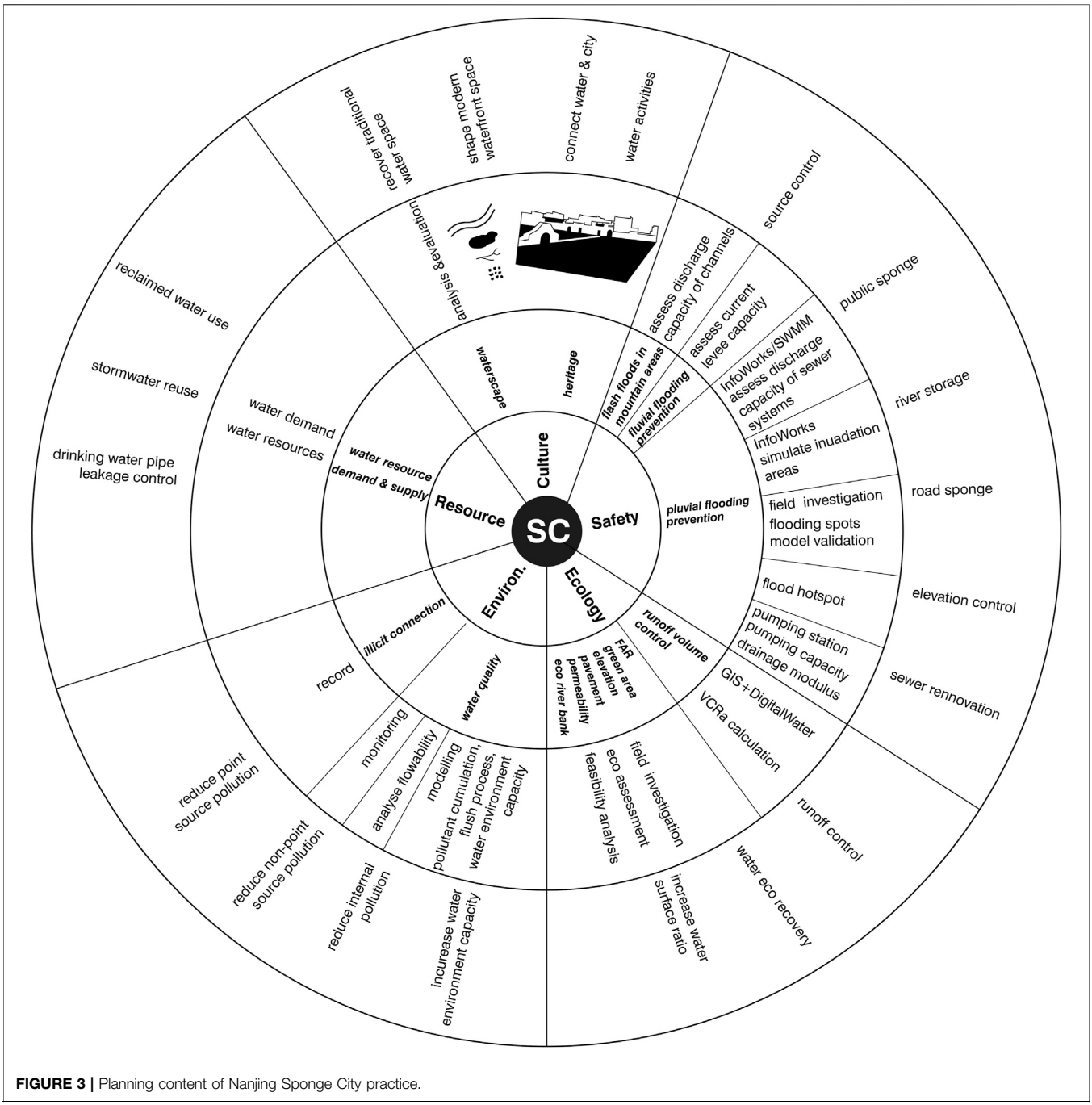

FIGURE 3 | Planning content of Nanjing Sponge City practice.

due to their similar philosophy. For example, both integrate the water and land development planning; However, the differences in guiding policies (demonstrated in **Supplementary Material SB**) lead to substantial differences in both contents and the structure of the planning process.

Content:

1. The objectives of Sponge City are indicator-oriented, setting standards or specific requirements. In contrast, WSD describes a clear vision, allows for flexibility, and leaves setting standards for indicators to the local stakeholders, depending on local conditions.
2. Unlike in Auckland's WSD, a comprehensive assessment of the local water system—as part of larger water and urban system—is missing in current Sponge City planning documents of Nanjing. For example, groundwater assessment and socio-cultural aspects are missing in both guidelines and plans of Nanjing Sponge City.
3. Principles outlined in WSD are explicit and clear, while vagueness in Sponge City guiding principles challenge its

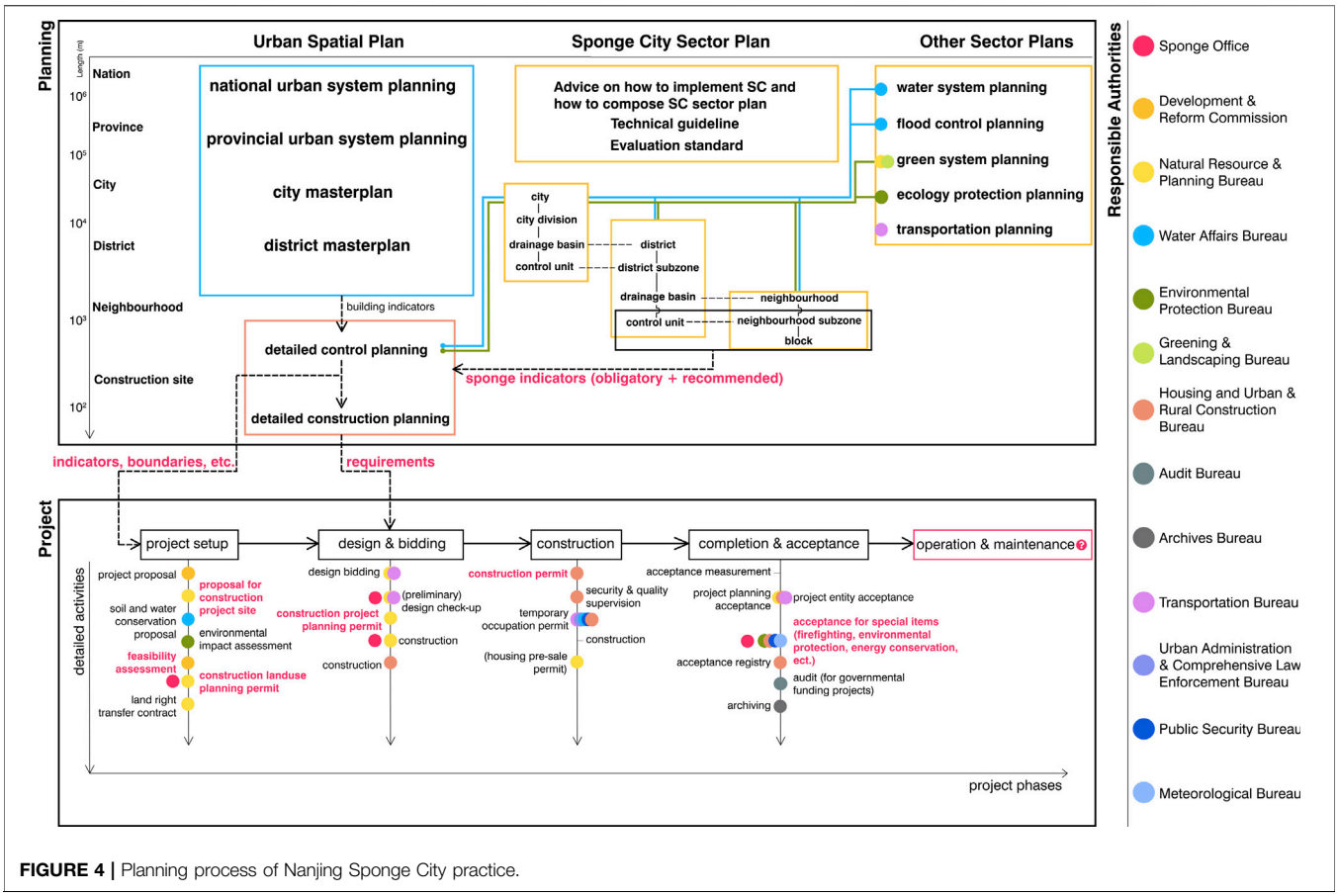

FIGURE 4 | Planning process of Nanjing Sponge City practice.

implementation; for example, the need to address stormwater close to its source is not mentioned.

4. WSD guidelines include an analysis of landscape and natural character values, as well as an analysis of past and expected future land development patterns. In contrast, spatial analysis in Sponge City planning mainly focuses on water and ecology.
5. In the Sponge City approach, the size of sponge measures is determined by the VCRa, an ecology-based indicator, similar to the Water Quality Volume in WSD. The VCRa, however, is *not* an indicator for designing sponge measures against pluvial flooding (Wang et al., 2015; Lin et al., 2019). No approach or calculation method is provided to design the sponge for pluvial flood protection. On the contrary, Auckland's WSD guidance documents distinguish measures for different spatial scales and different types of storms, which can be designed through standardized modelling and size calculation methods.

Process:

1. WSD is an inter-disciplinary design approach, whereas no specified inter-disciplinary collaboration mechanism is outlined in Sponge City approach.
2. WSD values the early engagement of local official actors and experts, which is not foreseen in the Sponge City approach.
3. WSD promotes the collaboration of stakeholders with regulators in the planning processes; while in the Sponge City approach, consultation of local inhabitants is not required, nor any co-creation/collaborative design of plans.
4. WSD and Sponge City both incorporate their requirements into the land development approval process; WSD illustrates the design procedure with regulatory checks, while Sponge City guidelines explicitly specify the roles of authorities in regulatory checks.
5. WSD provides rich information on the operation and maintenance of various commonly-used stormwater devices, including consideration of operating conditions, costs, and responsibilities. Operation and maintenance advice on sponge measures are given in Nanjing Sponge City guideline, but the responsibility of maintenance is not defined nor recommended to consider in planning.

Dutch Water Management Principles

Dutch water management experiences are insightful to other countries facing flooding, drought, and water quality issues. Dutch central government is embedding the following principles in its recent national water policy (Ministry of Infrastructure and Environment Affairs and Ministry of Economic, 2009):

- Comprehensive water management
  By considering the various tasks relating to water quantity (flood risk management and pluvial flooding), water quality,

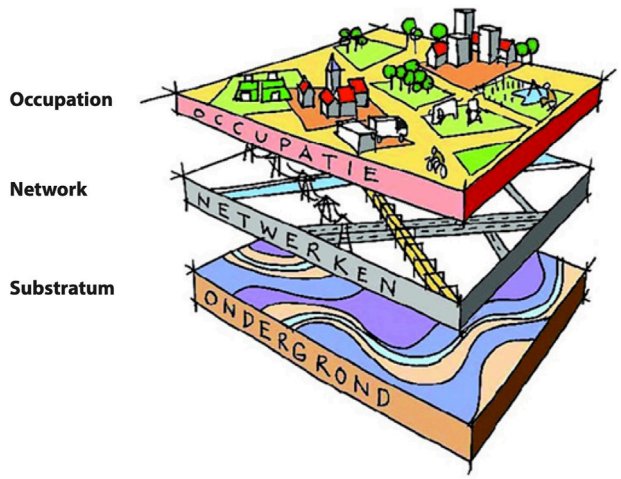

FIGURE 5 | *The illustration of the Dutch Layers Approach; the three layers from bottom to top are Substratum, Network, and Occupation* (De Hoog et al., 1998; Rijksplanologische Dienst, 2001).

and the use of fresh water under wet and dry circumstances in a coherent way, a comprehensive approach is achieved.

- Prevent shifting (or *Never Shift Problems* in Dutch)
  "Prevent shifting" is the centuries-old cornerstone of Dutch water management, which refers to preventing water quantity and quality problems being shifted in terms of space and time.
- Connecting space and water (including Layers Approach and Three Point Approach)
  By connecting water planning with spatial planning, it is often possible to improve water management while at the same time reinforcing the economy and the residents' living environment at lower costs. Before implementing measures, the activities are first coordinated with the other relevant spatial tasks and developments in an area; several approaches and guiding models are developed to support this integration, including the Layers Approach (see **Figure 5**) to spatial planning and the Three Points Approach (see **Figure 6**) to flood risk reduction.
  The Layers Approach (De Hoog et al., 1998; Rijksplanologische Dienst, 2001) distinguishes three layers of spatial planning tasks: substratum, networks, and occupation. Interventions in the occupation layer and the network layer are to be tuned to the properties of the subsurface and are to fit the water network, as well as other networks and objects in the occupation layer. The Three Points Approach is a method to help planning and designing flood risk reduction facilities (Fratini et al., 2012). Point 1 in **Figure 6** represents the design of facilities protecting up to the level of the design return period. Point 2 represents a situation where this level is exceeded, and the protection system fails. Spatial planning aims at minimizing the damage of that failing system by strengthening its coping and recovery capacity (de Graaf et al., 2007). Point 3 represents the everyday situation. Instead of being a hindrance, drainage and protection facilities ought to provide added value and services to society every day.
- Embed technical solutions in good governance
  The OECD published principles on water governance, covering 12 different aspects of governance (OECD, 2015). A more practical principle for evaluating the governance of interventions, however, is the PRIMO-chain approach (Adviesunit Resultaatgericht Beleid, Ministerie van Verkeer en Waterstaat, 1997): Policyi—Regulations and Legislation—Implementation capacity, execution capacity—Maintenance, monitoring and performance evaluation—Organisation and financing. If one of these elements is not in place, any intervention is doomed to fail.

These points allow for a comparison with the Sponge City approach (see **Supplementary Material SC**). Identified gaps in the current Sponge City planning approach are listed below.

Content:

1. Five water topics in Sponge City approach are treated separately, without addressing the synergies amongst them, which hinders the comprehensive management of the urban water system. Key water system components missing in the planning of sponge measures are groundwater management, pluvial flooding prevention, and drought mitigation.
2. There is a lack of sponge sizing method(s) to implement the principle *Never Shift Problems* in current Sponge City guidelines concerning pluvial flooding prevention.
3. The design method for additional resilience to future changes (Point 2 in **Figure 6**) is missing in Nanjing Sponge City planning. Moreover, everyday values (Point 3 in **Figure 6**), such as aesthetics, recreation values, etc., are not considered in current Sponge City planning.

Process:

1. Insufficient coordination between water and spatial planning experts while planning sponge measures.
2. Lack of involvement/engagement of various stakeholders to plan added values.

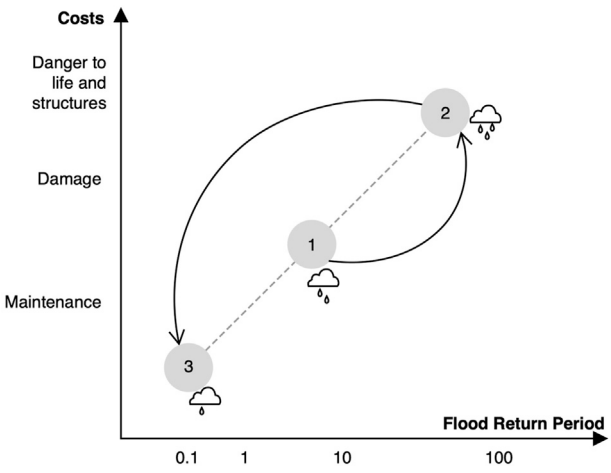

FIGURE 6 | The Three Points Approach scheme (adapted from Fratini et al., 2012).

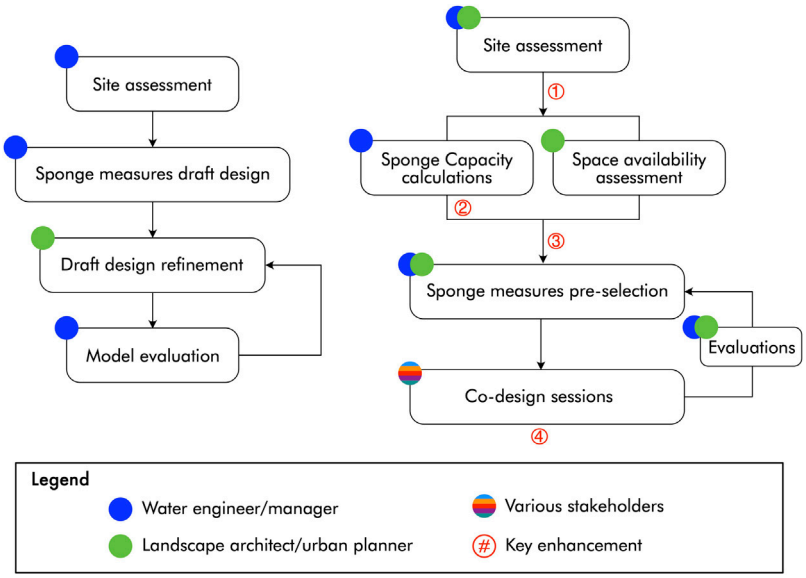

FIGURE 7 | Current (left, Chen, 2020) and proposed (right) sponge measures planning process.

3. Critical issues in perusing good governance include: 1). Performance evaluation: Whether proposed sponge interventions meet the regulations and standards is hardly evaluated; 2). Policy and regulations on groundwater management are not yet available; 3). Responsibility for maintenance remains unclear.

An Enhanced Version of Sponge City Planning Approach

Comparative analysis in the previous sections shed light on potential improvements of the current Sponge City planning approach. Many differences were found that can enhance the current approach. Key enhancements on both content and process are:

1. Elaborate the guiding principles based on local conditions.
2. Take a comprehensive water management approach; build on the local conditions; include pluvial flood prevention, drought mitigation, groundwater, and water quality management.
3. Create added values.
4. Co-design the plan, involving relevant experts and stakeholders.

Based on the ideas above, an enhanced approach for a new planning process was outlined, as represented in **Figure 7**.

As a first step, water engineers/managers and landscape architects/urban planners perform site assessments, based which they can jointly refine and customize guiding principles. Secondly, water engineers assess the flood and drought risks and calculate the required storage capacity; in parallel, landscape architects or urban planners analyse available urban space for potential interventions. Thirdly, a pre-selection stage is introduced to jointly shorten the long list of potential sponge measures considering local conditions. Fourthly, a participatory co-design workshop is organized for triggering discussion of sponge measure arrangement amongst relevant experts and stakeholders, e.g., urban designers, water engineers, civil engineers, local inhabitants, experts, governmental authorities, etc. During the workshop, participants are to be invited to share knowledge, expectations, preferences, etc., and make contributions to sponge measures selection and arrangement (van de Ven et al., 2016). Such co-design workshops are meant to produce one or more comprehensive conceptual intervention plans. This conceptual phase of planning is a timely opportunity for balancing interests and making choices (McEvoy et al., 2019). Finally, water engineers and urban designers collaborate in developing the conceptual Sponge City plan to a detailed design. Critical aspects such as environmental impact, cost-benefit analysis, etc., can thereby be evaluated, which might require involvement from other disciplines. Final decisions are based on this evaluation of expected impacts and effectiveness.

APPLICATION OF THE ENHANCED APPROACH

The enhanced approach was applied as far as possible in the Sponge City planning project for Qinhuai District. Limitations due to data availability, Covid-pandemic restrictions, and formal process requirements hindered a full use of the recommended approach. Nevertheless many new insights were gained.

Issues According to the Current Sponge City Approach

After spatial analysis, indicator assessment, and hydraulic modelling of the current situation, key issues regarding the

TABLE 2 | Key issues and relevant indicators in Qinhuai District regarding the five Sponge City topics NPNRB (2018b); Wei, personal communication, December 4, 2019).

Topic	Key issues	Standards in Sponge City planning of Qinhuai District (targets by 2030)
Water safety	• Flood events occur once every 8 years on average due to heavy rainfall in large areas of the district • Increasing imperviousness causes more runoff volume and higher runoff rate • Sewers were designed for return period of 0.5–1 year • Blue and green areas are shrinking due to urbanization, which weaken the storage capacity	• Design return period 50 years for pluvial flood prevention and control • Design return period 200 years for fluvial flood prevention and control • Design return period 3–5 years for sewer systems • Required storage capacity according to VCRa: 25.6 mm
Water ecology	• Average VCRa is 38% • 'Hard' banks account for 64% of total length	• VCRa: 75% for 80% of urban the built areas • Ecological embankment ratio: 80% for new built areas
Water environment	• Water quality was tested as Class V in six out of seven cross-sections of Qinhuai canals during 2015–2019. Class V is the poorest water quality category • Water quality of groundwater at two test wells both indicates Class V quality during 2015–2019 • Non-point source pollutants are estimated to be 1718 tons SS/year, generated from runoff over pavements • Point source pollution mainly happen along Yongfeng River, resulting from combined sewer overflow and illicit connections	• The ratio of water bodies achieving quality requirements: 85% • Non-point source pollution reduction ratio: 50% for 80% of built area • Water quality standard: Class IV or better
Water resource	• Pipe leakage ratio in Nanjing is above 16% • There is almost no stormwater reuse practice in Qinhuai District	• Stormwater reuse ratio: > 5% • Pipe leakage ratio: <10%
Water culture	Difficulties lie in water-related cultural heritage protection. Water culture has not been incorporated into the urban fabric and inhabitants' daily life	• Reshape historical spaces • Incorporate waterfronts into urban landscape

five water topics of the current Sponge City approach are identified, as summarized in **Table 2**.

Applying the Enhanced Version of Sponge City Planning Approach in Qinhuai District

A brief overview of results, based on the key enhancements mentioned above, is as follows:

1. Elaborate the guiding principles based on the local conditions.

Based on site analysis using the Layers Approach, guiding principles were used to connect water and space given the local conditions in the area. Three key principles for Qinhuai were:

1. Prevent shifting; retain and store, rather than quick drainage.

Retention and detention are essential in delaying peak flow and controlling runoff volumes. Storage can lead to other co-benefits such as mitigation of non-point source pollution, groundwater recharge, drought mitigation, stormwater reuse, etc.

The required storage capacity for pluvial flood prevention was assessed to be 86 mm on average, based on the required 50-years return period, the available pumping capacity in the (sub) districts, 10-years climate forcing (precipitation and evaporation), and catchment properties as inputs. More details on these storage capacity calculations and the underlying Storage-Discharge-Frequency (SDF) curves can be found in **Supplementary Material SF**. Storage requirements for each subzone are visualized in **Figure 8**. These storage depths are used as storage capacity targets in the planning of sponge measures.

2. Three Points Approach.

Introducing blue-green measures for creating storage capacity will deliver multi-functional land use and produce co-benefits concerning ecology, recreation, and urban heat island mitigation while providing storage, coping, and adaptive capacity as well as added value.

A long list of nature-based sponge measures is selected for four typical urban topologies (see **Figure 9** and **Supplementary Material SG**). **Figure 9** also includes the expected responsible authority in Nanjing for each of the adaptation measures and the bureaus that are possible (to be) involved in the planning, design, implementation, and maintenance of these facilities.

3. Logical priority of interventions.

As the long list of blue-green measures is large, a logical strategy is needed to prioritize different interventions. Given their potential sponge size and complexity of implementation, a logical hierarchy of spatial sponge interventions was made. Sponge retention was created in 1. Public green spaces; 2. Vacant lots and infrastructural spaces; 3. Residential green spaces; 4. Temporary sponges on small roads; 5. Green roofs (see **Figure 10**). Suggested interventions were prioritized accordingly.

2. Take a comprehensive water management approach.

It would have been preferable to first study the regional water system at the scale of the Qinhuai river basin before starting the Sponge City planning at the district scale. This could have answered the question on the acceptable capacity of the pumping stations that drain the subdistricts. However, limited data hinder such a basin-level water system analysis. This being unknown, it is assumed that the capacity of these stations should stay unchanged when assessing the required storage capacity in the sub-districts, as shown in **Figure 8**.

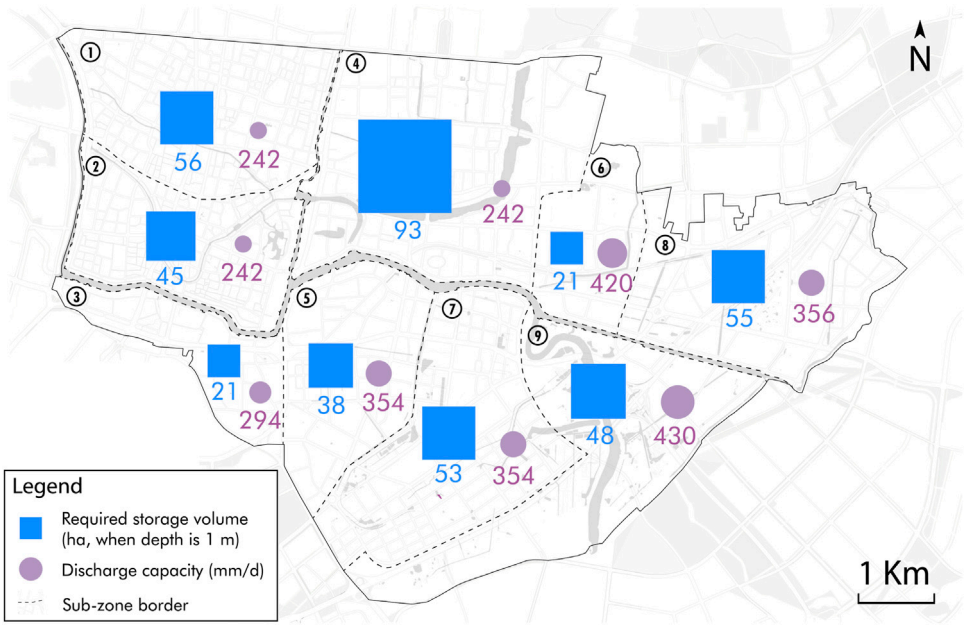

FIGURE 8 | The required storage capacities and discharge capacities for nine subzones of Qinhuai District.

The Urban Water Balance Model (Brolsma and Vergroesen, 2020) is employed to model the quantity of water components within Qinhuai subdistricts, including open water, unsaturated zone, groundwater (see **Supplementary Material SF**), etc. Modelling results are used to set the planning targets for pluvial flood prevention, drought mitigation, and groundwater management. The result shows that recharge of 0.72 mm/d or 68 mm in total can help mitigate the most severe drought event.

Although water quality data of some canal sections give indications to planning priority, the available data are insufficient to simulate the overall water quality of the district.

3. Plan for added value.

Mapping the structure of potential Sponge City intervention with added values follows two steps: 1. defining available spaces, including existing and planned green space, historical restrictions, existing small scale green space like roads/neighbourhoods; 2. defining preferred additional functions and services of interventions (either retention or detention). The resulting structure is shown in **Figure 11**, which consists of dotted, linear, patched, and nested sponges in public and private spaces aimed at strengthening the ecological, cultural, recreational, and social resilience of the district.

4. Co-design the plan, involving relevant experts and stakeholders.

The design of the final plan builds on established targets and requirements, the long list of potential interventions, the logical hierarchy of interventions, and the structure plan. Evidently, the planning of sponge solutions is not in the hands of a single bureau but requires coordination with experts from other bureaus as well as with representatives of the local population and businesses. Normally a collaborative design workshop with these representatives is to be held. The Covid-19 pandemic and lockdown, however, prevented such a meeting. Instead, local and international experts from the field of landscape architecture, urban water management, urban hydraulic engineering drafted a plan for pilot areas.

The Climate Resilient City Tool (van de Ven et al., 2016; McEvoy et al., 2018; McEvoy, 2019) was used to draft a plan for these pilot areas. One example area is shown in **Figure 12**. By adding a combination of bioswale (with drainage), infiltration boxes, water square, hollow roads, and rain gardens, this test area can reach 102 mm storage capacity (annual probability of exceedance less than 1/50) with co-benefits such as groundwater recharge (0.71 mm/d on average), runoff control and runoff pollution mitigation, etc. (see **Figure 13**). The measures in such an old city centre also improve biodiversity and, with aesthetic appeal, create opportunities for social interaction and recreational activities. Implementation enhances the attractiveness and liveability of the area every day, in addition to their hydrological functions.

DISCUSSION

Evaluation of the Case Study

The case study of Nanjing Qinhuai Sponge City planning demonstrates the feasibility and added value of applying the enhanced planning approach. Most of the proposed enhancements in aspects of planning content are successfully included in the analysis and results. From the perspective of the planning process, the case study demonstrates a comprehensive approach towards landscape design, water management, and spatial planning. Planning principles, site assessment, sponge measure selection, etc., were thoroughly discussed by the

FIGURE 9 | Sponge measure selections for four types of urban areas and responsible authorities for their design, implementation, and maintenance.

multi-disciplinary design team, during which local authorities were consulted to make adjustments.

The planning content also encountered obstacles. Calibration of the hydraulic models could not be performed due to the lack of data, which makes the assessment of flood-prone areas uncertain. On the other hand, the hydrologic water balance model could rely on data mainly available in the Qinhuai project; these include precipitation, land use and soil type. Hence, the results of this model are less uncertain. Moreover, the principle *Never Shift Problems*, resulting in a required storage capacity for pluvial flood protection, was not fully accepted by decision-makers; they considered the assessed capacity a recommended indicator rather than an obligatory one. As for the planning process, local inhabitants were not involved in the planning process. A co-design workshop could not be held due to Covid-19 restrictions. However, the final Qinhuai district Sponge City plan did highlight the importance of public involvement in future construction projects at smaller scales.

Reflections on the Sponge City Approach

The current Sponge City planning lacks fundamental building blocks to (re)design the water system in a comprehensive planning approach. (Li et al., 2017; Chan et al., 2018; Dai et al., 2018) which must be built on a hydrological analysis, consider land use and socio-economic situation, and contain a clear vision for the desired future situation. Without these essential frameworks, planners cannot deliver an integrative solution to complex issues of the local urban water management.

One crucial gap is that no quantified storage capacity is estimated for pluvial flood protection or drought mitigation. Sponge measure sizing is currently based on calculations of the VCRa, which is an ecological indicator that evoked debates

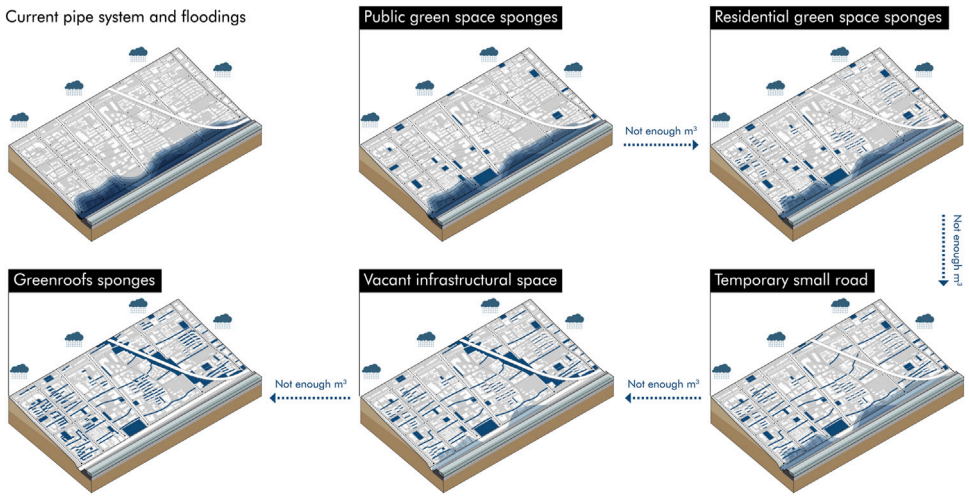

FIGURE 10 | Hierarchical sponge intervention priority.

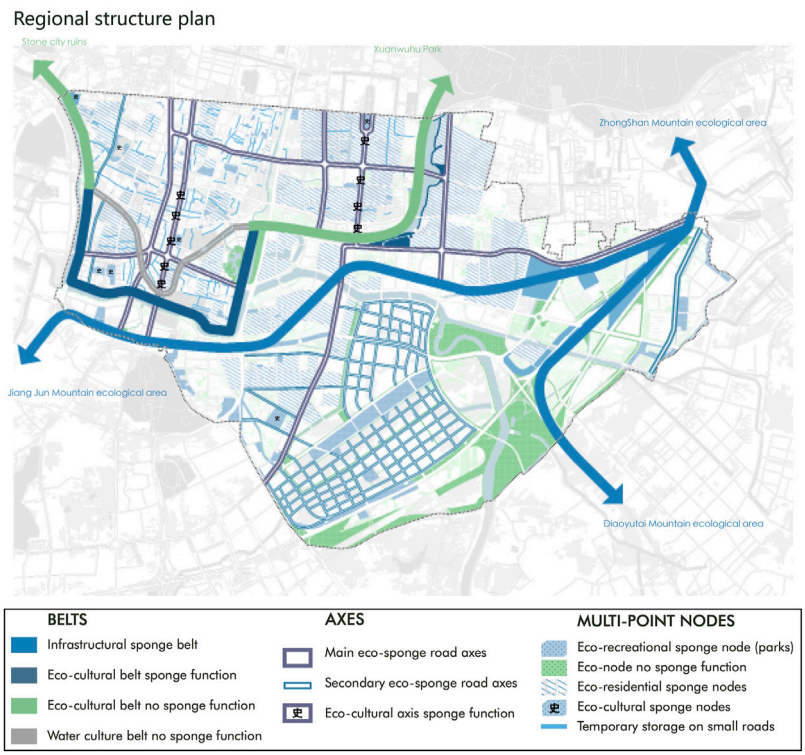

FIGURE 11 | The resulting sponge intervention structure plan.

in academia (Wang et al., 2015; Che et al., 2016) and caused confusion to practitioners. Pluvial flood protection, however, requires more retention (sponge) capacity, which can be determined by assessing SDF-curves for the local situation.

Space is often very limited in compact Chinese cities. Yet, for cities with similar climate and urban features as Nanjing's Qinhuai District, the case study sets an example of finding sufficient space for water storage by applying the enhanced planning approach. For cities with different climatic and urban conditions, the focus and strategy in planning may shift to other aspects such as drought mitigation or water ecology rehabilitation, based on local conditions. Tuning the approach to the local situation will be required. More research is needed to find out what would be the best way to do this.

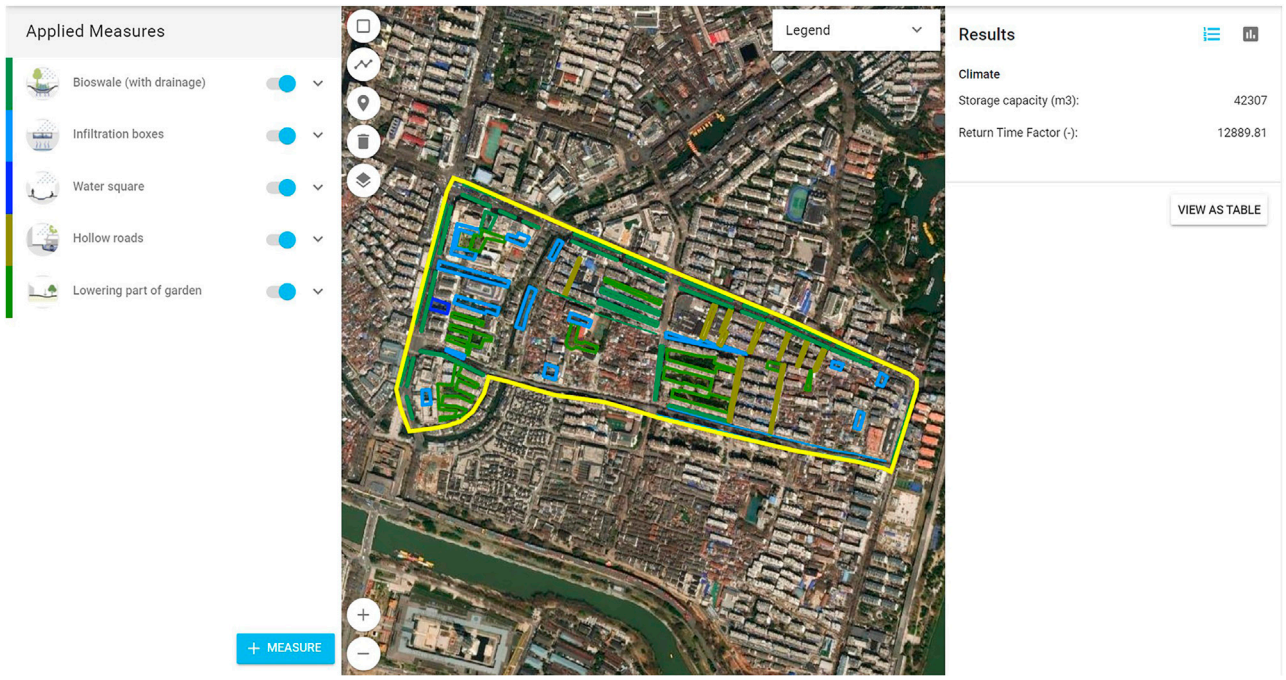

FIGURE 12 | Sponge interventions of a test area in topology 1.

Results

CLIMATE AND COSTS | CO BENEFITS

Measure	Surface	Storage capacity (m3)	Return Time Factor (-)	Groundwater recharge (mm/y)	Evapotranspira... (mm/y)	Heat reduction (°C)	Cool areas (-)	Construction	Maintenance
Bioswale (with drainage)	9537.51	3338	4.12	43	1	0.07	0	4291880	193135
Infiltration boxes	16657.13	15477	68.82	156	0	0	0	94945649	30192716
Water square	980.28	735	1.52	0	0	0.01	0	24262043	2620301
Hollow roads	5690.5	1707	1.01	0	1	0	0	1024290	138279
Lowering part of garden	23389.21	21050	25.16	61	3	0	0	3508382	210503

Results

CLIMATE AND COSTS | CO BENEFITS

Measure	Surface	Pathogen reduction (%)	Nutrient reduction (%)	Adsorbing pollutants (%)
Bioswale (with drainage)	9537.51	2	2	2
Infiltration boxes	16657.13	4	3	4
Water square	980.28	0	0	0
Hollow roads	5690.5	0	0	0
Lowering part of garden	23389.21	3	1	3

FIGURE 13 | Estimated performance and co-benefits of sponge interventions of a test area in topology 1.

As experienced during the implementation in the Qinhuai district, the enhanced approach encountered various challenges. Crucial ones include:

1. Data availability and accessibility.

Data plays an essential role in Sponge City planning. Data in this case study was not sufficient to support model calibration. The same problem appears in many other Chinese urban planning cases (Li et al., 2017). Therefore, including data collection in the enhanced approach requires Chinese cities to enhance monitoring of their water systems, including water quality and groundwater. Sponge City planning also requires renovating current data sharing mechanisms, e.g., by establishing a standardized, freely-accessible, public data platform (Cai, 2016).

2. Innovation and collaboration.

In parallel to similar experiences in environment management (Lo, 2020), local authorities are less motivated to make innovative local Sponge City plans given the strict governance, especially on performance indicators, from the central government. This results in local planning agencies rigidly pursuing the fulfilment of the required performance indicators at the expense of curtailing local innovations. For example, the local requirement of downscaling the VCRa to each small piece of land hinders planning larger scaled public sponge measures, e.g., at sub-district level. Moreover, the limited communication between decision-makers, policy developers, and experts is a well-known barrier to planning novel solutions (Davoudi, 2006). The co-design process proposed in the enhanced approach would be a stepping-stone for stimulating local innovations by simply bringing relevant experts and stakeholders around the table and enabling them to exchange knowledge and expectations (van de Ven et al., 2016). The successful application of a customized Climate Resilient City Tool in Xiangtan City (van de Ven et al., 2020) demonstrates the value of such a tools-supported planning approach, though the effectiveness of its application to other Chinese cities remains to see.

3. Local actors' willingness and awareness.

As Thomas et al. (2018) concluded on policy transferability, "softer" transferable lessons (e.g., good actor relationships, information sharing, etc.) are much more difficult to transfer than 'harder' technical tools. Sharing your thoughts and ideas with others requires the willingness to do this. Another challenge is the local decision makers' attitude towards *Never Shift Problems*. Policy makers should realize the importance of local retention/detention capacity to avoid flooding problems in areas downstream. Knowledge transfer and bridge-building between experts, policy developers, and decision-makers is essential for creating the awareness that this principle is at the heart of Sponge City planning.

Limitations of the Methodological Approach

Differences in local conditions result in other issues, other stakeholders, and, consequently, in slightly different planning processes. Auckland's WSD planning guidelines are not 100% representative of all WSD plans in New Zealand; and the Dutch also have other principles and use other tools in their water management planning. Likewise, Nanjing's Sponge City planning is not representative of all Sponge City planning in China. As a result, the enhanced approach as formulated and applied in this study for Qinhuai District is not the final solution. The approach needs customization to the local situation and can certainly be enriched and extended further by studying the success and failure of sustainable urban water planning in other cities in China and around the world. Moreover, insights in improving Sponge City planning, construction, and governance can be gained through collecting local stakeholders' experiences and feedback, in communities of practice, as well as by thoroughly monitoring and evaluating the effects of Sponge City interventions after implementation.

CONCLUSION

This paper presents the current Chinese Sponge City planning theory and local practice in Nanjing City. Through compare-and-contrast analysis between Nanjing's Sponge City planning approach and Auckland's Water Sensitive Design, as well as evaluation of Sponge City from the perspective of Dutch water management theories, gaps in the current policies were revealed, and potentials of enhancing planning approach were illuminated. An enhanced approach was proposed and applied in a case study of Nanjing's Qinhuai Sponge City planning project.

It can be concluded that the current performance-indicator-oriented Sponge City planning approach is insufficiently integrative and comprehensive: elements are missing, both in terms of content and process. Missing elements include assessing the required water storage capacity for both pluvial flood protection and drought mitigation, groundwater management, the search for added values from blue-green nature-based solutions and involvement of local actors and experts from related disciplines in the planning process, etc.

The enhanced approach, facilitated by hydrological, hydraulic, and planning support tools, contributes to comprehensive and integrative planning, with active engagement of local stakeholders and experts from many different disciplines and City Bureaus. Results from the case study demonstrate the successful application of the enhanced approach for Qinhuai District, including quantifying the required storage capacity, interdisciplinary cooperation in setting principles and selecting sponge measures, formulating a logical hierarchy of interventions, and drafting a conceptual sponge city plan. The new approach received positive results and reactions, which makes us conclude that the adapted approach we proposed is indeed an enhanced version. Barriers appeared mainly on data availability and the awareness of the *Never Shift Problems* principle.

To maximize the economic, ecological, and social co-benefits of Sponge City interventions, future research is needed to relate the local urban system and the local water system. Moreover, implementation can benefit from co-creative planning workshops with experts and local stakeholders to elaborate the plan in more detail. These workshops could not take place earlier due to the COVID pandemic restrictions. Such participatory planning activities facilitate the knowledge exchange amongst various stakeholders and ensure the soundness and justness of Sponge City planning. Lastly, the results of this study can be used by other cities to improve their Sponge City planning approach and by China's central government to inspire improvements of the national Sponge City guidelines. It is recommended that the central government provides more support to encourage bottom-up mechanisms of policy

implementation, including capacity building activities, financing, monitoring, data disclosure, and planning process evaluation studies.

DATA AVAILABILITY STATEMENT

The original contributions presented in the study are included in the article/**Supplementary Material**, further inquiries can be directed to the corresponding authors.

AUTHOR CONTRIBUTIONS

SC and FV contributed to conception and design of the study. LW collected and organised the data. SV contributed to the spatial analysis and the structural plan. SC wrote the first draft of the manuscript. All authors contributed to manuscript revision, read, and approved the submitted version.

ACKNOWLEDGMENTS

The research for this paper was supported by Delft University of Technology, Deltares, and China Europe Water Platform (CEWP). The Qinhuai case study could not be conducted without help from Nanjing Municipal Government, Qinhuai District Government, and Nanjing Hydraulic Research Institute (NHRI). Thanks to China Academy of Urban Planning and Design (CAUPD) for the collaboration in CEWP and for sharing their insights into Sponge City policy development, planning, and practice.

SUPPLEMENTARY MATERIAL

The Supplementary Material for this article can be found online at: https://www.frontiersin.org/articles/10.3389/fenvs.2021.748231/full#supplementary-material

REFERENCES

Adviesunit Resultaatgericht Beleid, Ministerie van Verkeer en Waterstaat (1997). Resultaatgericht beleid: advies bij beleidsontwikkeling, communicatie en samenwerking. Retrieved from https://puc.overheid.nl/PUC/Handlers/DownloadDocument.ashx?identifier=PUC_102580_31andversienummer=1.

Auckland Council (2016). The Auckland Code of Practice for Land Development and Subdivision. Retrieved from http://content.aucklanddesignmanual.co.nz/regulations/codes-of-practice/stormwatercodeofpractice/details/Documents/Auckland CoP Chapter 1 - Version 1 0_Final v8.pdf.

Brolsma, R., and Vergroesen, T. (2020). Urban Water Balance Model. Retrieved from https://publicwiki.deltares.nl/display/AST/Urban+Water+balance+model.

Brown, R. R., Keath, N., and Wong, T. H. F. (2009). Urban Water Management in Cities: Historical, Current and Future Regimes. *Water Sci. Tech.* 59 (5), 847–855. doi:10.2166/wst.2009.029

Cai, L. (2016). Shiyong yu "haimianchengshi" de shuiwen shuili moxing gaishu [Introduction of Hydrological and Hydraulic Models for "Sponge City"]. *Fengjing Yuanlin* 02, 33–43.

Chan, F. K. S., Griffiths, J. A., Higgitt, D., Xu, S., Zhu, F., Tang, Y.-T., et al. (2018). "Sponge City" in China-A Breakthrough of Planning and Flood Risk Management in the Urban Context. *Land Use Policy* 76 (March), 772–778. doi:10.1016/j.landusepol.2018.03.005

Che, W., Zhang, K., Zhang, W., and Zhao, Y. (2016). Chuqi yushui yu jingliu zongliang kongzhi de guanxi ji qi yingyong fenxi [Analysis of the relationship between initial rainwater and total runoff control and its application]. *Zhongguo jishui paishui* 32 (6), 9–14.

Che, W., and Zhang, W. (2019). "Urban Stormwater Management and Sponge City Concept in China," in *Urban Water Management for Future Cities: Technical and Institutional Aspects from Chinese and German Perspective*. Editors S. Köster, M. Reese, and J. Zuo (Springer International Publishing), 3–11. doi:10.1007/978-3-030-01488-9_1

Chen, S. (2020). *Sponge Design: A Study on Comprehensive Sponge City Design Approach*. Delft: Delft University of Technology. http://resolver.tudelft.nl/uuid:a758663f-fb34-49bd-8cb7-03726938bc72.

Costa, S., Peters, R., Martins, R., Postmes, L., Keizer, J. J., and Roebeling, P. (2021). Effectiveness of Nature-Based Solutions on Pluvial Flood hazard Mitigation: The Case Study of the City of Eindhoven (the netherlands). *Resources* 10 (3), 24. doi:10.3390/resources10030024

Cunningham, A., Colibaba, A., Hellberg, B., Silyn, G., Simcock, R., Speed, S., et al. (2017). *Stormwater Management Devices In the Auckland Region*.

Dai, Y., Jiao, S., Ding, G., and Shen, Y. (2018). Jin Shinian Haimianchengshi Jianshe Yanjiu Pingshu Yu Zhanwang [Review and prospect of Sponge City Construction in Recent Ten Years]. *Xiandai chengshi yanjiu* 8, 77–87. doi:10.3969/j.issn.1009-6000.2018.08.011

Davoudi, S. (2006). Evidence-Based Planning. *DisP - Plann. Rev.* 42 (165), 14–24. doi:10.1080/02513625.2006.10556951

de Graaf, R., van de Giesen, N., and van de Ven, F. (2007). Alternative Water Management Options to Reduce Vulnerability for Climate Change in the Netherlands. *Nat. Hazards* 51 (3), 407–422. doi:10.1007/s11069-007-9184-4

De Hoog, M., Sijmons, D., and Verschuuren, S. (1998). Herontwerp Van Het Laagland, in *Het Metropolitane Debat*. Editor D. H. Frieling (Bussum: Uitgeverij THOTH), 74–87.

European Commission (2019). The European Green Deal. *Eur. Comm.* 53 (9), 24. doi:10.1017/CBO9781107415324.004

Fratini, C. F., Geldof, G. D., Kluck, J., and Mikkelsen, P. S. (2012). Three Points Approach (3PA) for Urban Flood Risk Management: A Tool to Support Climate Change Adaptation through Transdisciplinarity and Multifunctionality. *Urban Water J.* 9 (5), 317–331. doi:10.1080/1573062x.2012.668913

He, Y., and Xing, H. (2006). Woguo Chengshi Shuiwuran Xianzhuang Ji Qi Duice [The Urban Water Pollution Status Quo and Countermeasures in China]. *Shuili Keji yu jingji* 01, 44–45.

Healy, K., Carmody, M., and Conaghan, A. (2010). *Operation and Maintenance of Stormwater Treatment Devices in the Auckland Region*. Auckland: Auckland Regional Council. Available at: https://knowledgeauckland.org.nz/publications/operation-and-maintenance-of-stormwater-treatment-devices-in-the-auckland-region/.

Hooimeijer, F. L. (2014). *The Making of Polder Cities: A fine Dutch Tradition*. Heijningen: Jap Sam Books.

Hurlimann, A., and Wilson, E. (2018). Sustainable Urban Water Management under a Changing Climate: The Role of Spatial Planning. *Water* 10 (5), 546. doi:10.3390/w10050546

Kumar, P., Debele, S. E., Sahani, J., Aragão, L., Barisani, F., Basu, B., et al. (2020). Towards an Operationalisation of Nature-Based Solutions for Natural Hazards. *Sci. Total Environ.* 731, 138855. doi:10.1016/j.scitotenv.2020.138855

Lewis, M., James, J., Shaver, E., Blackbourn, S., Leahy, A., Seyb, R., et al. (2015). *Water Sensitive Design For Stormwater (GD2015/004)*. Auckland: Auckland Council. Available at: http://content.aucklanddesignmanual.co.nz/project-type/infrastructure/technical-guidance/Documents/GD04 WSD Guide.pdf.

Li, H., Ding, L., Ren, M., Li, C., and Wang, H. (2017). Sponge City Construction in China: A Survey of the Challenges and Opportunities. *Water* 9 (9), 594. doi:10.3390/w9090594

Li, X., Li, J., Fang, X., Gong, Y., and Wang, W. (2016). Case Studies of the Sponge City Program in China. *World Environmental and Water Resources Congress*, 2016, 295–308. doi:10.1061/9780784479858.031

Lin, B., Liao, Y., and Ding, H. (2019). Differentiation of "Volume Capture Ratio of Annual Rainfall. *China Terminology* 21 (5), 4. doi:10.3969/j.issn.1673-8578.2019.05.01

Liu, H., and Han, D. (2014). Nanjing Laocheng Neihe Shuixi Xingtai Yanhua Jiedu [Interpretation of Inland River System Morphology Evolution in the Old City of Nanjing. *Jianzhu yu wenhua* 4, 12–19. doi:10.3969/j.issn.1672-4909.2014.04.002

Lo, K. (2020). Ecological Civilization, Authoritarian Environmentalism, and the Eco-Politics of Extractive Governance in China. *Extractive Industries Soc.* 7 (3), 1029–1035. doi:10.1016/j.exis.2020.06.017

Ma, Y., Jiang, Y., and Swallow, S. (2020). China's Sponge City Development for Urban Water Resilience and Sustainability: A Policy Discussion. *Sci. Total Environ.* 729, 139078. doi:10.1016/j.scitotenv.2020.139078

Mao, Y., Wu, H., Pei, H., He, P., and Liu, D. (2012). Jin 50a Nanjing xiaji jiangshui de qihou tezheng [Climate features of summer rainfall in Nanjing during recent 50a]. *Qixiang kexue* 32 (6), 646–652. doi:10.3969/2012jms.0047

McEvoy, S. (2019). *Planning Support Tools in Urban Adaptation Practice*. Delft: Delft University of Technology. doi:10.4233/uuid:48b7649c-5062-4c97-bba7-970fc92d7bbf

McEvoy, S., van de Ven, F. H. M., Blind, M. W., and Slinger, J. H. (2018). Planning Support Tools and Their Effects in Participatory Urban Adaptation Workshops. *J. Environ. Manage.* 207, 319–333. doi:10.1016/j.jenvman.2017.10.041

McEvoy, S., van de Ven, F. H. M., Brolsma, R., and Slinger, J. H. (2019). Evaluating a Planning Support System's Use and Effects in Urban Adaptation: An Exploratory Case Study from Berlin, Germany. *Sustainability* 12 (1), 173. doi:10.3390/su12010173

MHURD 住建部 (2018). *Haimian Chengshi Jianshe Pingjia Biaozhun [Evaluation Standards for Sponge City Construction*, GB/T51345. Beijing: China Architecture & Building Press. Retrieved from http://download.mohurd.gov.cn/bzgg/gjbz/GBT 51345-2018海绵城市建设评价标准.pdf.

MHURD 住建部 (2015). *Haimian Chengshi Jixiao Pingjia Yu Kaohe Zhibiao (Shixing)* [Sponge City Construction Performance Evaluation and Evaluation Index (Trial)]. Retrieved from http://www.mohurd.gov.cn/wjfb/201507/W020150715042911.doc.

MHURD 住建部 (2016). *Zhufang chengxiang jianshe bu guanyu yinfa haimian chengshi zhuanxiang guihua bianzhi zanxing guiding de tongzhi* [Notice of the Ministry of Housing and Urban-Rural Development on Printing and Distributing the Interim Provisions on the Preparation of the Special Planning for the Sponge City]. Retrieved from http://www.mohurd.gov.cn/wjfb/201603/t20160317_226932.html.

MHURD 住建部 (2014). *Zhufang chengxiang jianshe bu guanyu yinfa haimianchengshi jianshe jishu zhinan —— diyingxiang kaifa yushui xitong goujian (shixing) de tongzhi* [Notice of the Ministry of Housing and Urban-Rural Development on Issuing Technical Guidelines for Sponge City Construction-Low Impact Development Rainwater System Construction (Trial)]. Retrieved from http://www.mohurd.gov.cn/wjfb/201411/t20141102_219465.html.

Ministry of Infrastructure and Environment Affairs , & Ministry of Economic (2009). National Water Plan (2016-2021). Retrieved from https://www.government.nl/documents/policy-notes/2015/12/14/national-water-plan-2016-2021.

NPNRB 南京市规划局 (2018a). Guanyu Yinfa "Nanjing Shi Gongcheng Jianshe Xiangmu Lixiang Yongdi Guihua Xuke Jieduan Shenpi Shixiang Banli Guize" and "*Nanjing Shi Gongcheng Jianshe Xiangmu Gongcheng Jianshe Xuke Jieduan Shenpi Shixiang Banli Guize"* [Notice on Printing and Distributing the "Regulations for Approval in the Planning and Permit Phase of Land Use for Construction Projects in Nanjing" and "Rules for Approval in the Phase of Approval for Construction Permits for Engineering Construction Projects in Nanjing"] (NPNRB. Retrieved from http://ghj.nanjing.gov.cn/njsgtzyj/201811/P020181204726302150849.pdf.

NPNRB 南京市规划局 (2018b). *Nanjing Shi Haimian Chengshi Guihua Jianshe Zhinan* [Guidelines for Planning and Construction of Sponge City in Nanjing] (Office of the Leading Group for the Construction of Nanjing Sponge City 南京市海绵城市建设工作领导小组办公室. Retrieved from http://sjw.nanjing.gov.cn/tzgg/201807/P020181020788812936119.pdf.

OECD (2015). OECD Principles on Water Governance. Available at: https://www.oecd.org/cfe/regionaldevelopment/OECD-Principles-on-Water-Governance.pdf.

Qi, Y., Chan, F. K. S., Thorne, C., O'Donnell, E., Quagliolo, C., Comino, E., et al. (2020). Addressing Challenges of Urban Water Management in Chinese Sponge Cities via Nature-Based Solutions. *Water* 12 (10), 1–24. doi:10.3390/w12102788

Rijksplanologische Dienst (2001). Ruimtelijke Verkenningen 2000: Het Belang Van Een Goede Ondergrond. *Ministerie van Volkshuisvesting, Ruimtelijke Ordening en Milieu*. Netherlands: RPD The Hague.

State Council 国务院 (2015). Zhonggong zhongyang guowuyuan guanyu jiakuai tuijin shengtai wenming jianshe de yijian [Opinions of the Central Committee of the Communist Party of China and the State Council on Accelerating the Construction of Ecological Civilization. Retrieved from http://www.gov.cn/gongbao/content/2015/content_2864050.htm.

Stead, D. (2014). Urban Planning, Water Management and Climate Change Strategies: Adaptation, Mitigation and Resilience Narratives in the Netherlands. *Int. J. Sustain. Dev. World Ecol.* 21 (1), 15–27. doi:10.1080/13504509.2013.824928

Sun, Y., Chen, Z., Wu, G., Wu, Q., Zhang, F., Niu, Z., et al. (2016). Characteristics of Water Quality of Municipal Wastewater Treatment Plants in China: Implications for Resources Utilization and Management. *J. Clean. Prod.* 131, 1–9. doi:10.1016/j.jclepro.2016.05.068

Thomas, R., Pojani, D., Lenferink, S., Bertolini, L., Stead, D., and van der Krabben, E. (2018). Is Transit-Oriented Development (TOD) an Internationally Transferable Policy Concept. *Reg. Stud.* 52 (9), 1201–1213. doi:10.1080/00343404.2018.1428740

van de Ven, F. H. M., Brolsma, R., Hulsman, H., Chen, S., Zhang, W., Zhu, R., et al. (2020). Climate Risk and Vulnerability Assessment, and the Xiangtan Climate Resilient Toolbox. Available at: https://www.adb.org/sites/default/files/linked-documents/52230-001-sd-04.pdf.

van de Ven, F. H. M., Snep, R. P. H., Koole, S., Brolsma, R., van der Brugge, R., Spijker, J., et al. (2016). Adaptation Planning Support Toolbox: Measurable Performance Information Based Tools for Co-creation of Resilient, Ecosystem-Based Urban Plans with Urban Designers, Decision-Makers and Stakeholders. *Environ. Sci. Pol.* 66, 427–436. doi:10.1016/j.envsci.2016.06.010

Wang, F., Yan, Z., Huang, W., and Zhou, Q. (2012). Chengshi Yushui Neilao Chengyin Ji Duice [Causes and Countermeasures of Urban Water Logging]. *Zhongguo jishui paishui* 28 (12), 15–17. doi:10.3969/j.issn.1000-4602.2012.12.004

Wang, H., Ding, L., Cheng, X., and Li, N. (2015). Hydrologic Control Criteria Framework in the United States and its Referential Significance to China. 46, 1261–1271. doi:10.13243/j.cnki.slxb.20150670

Xia, J., Zhang, Y., Xiong, L., He, S., Wang, L., and Yu, Z. (2017). Opportunities and Challenges of the Sponge City Construction Related to Urban Water Issues in China. *Sci. China Earth Sci.* 60 (4), 652–658. doi:10.1007/s11430-016-0111-8

Yu, K., Li, D., Yuan, H., Fu, W., Qiao, Q., and Wang, S. (2015). Haimian Chengshi" Lilun Yu Shijian ["Sponge City": Theory and Practice]. *Chengshi guihua* 39 (06), 26–36.

Conflict of Interest: Author SV was employed by the company LOLA Landscape Architects. Author WZ was employed by the company Ewaters. Author LW was employed by the company Achterboschzantman International.

The remaining authors declare that the research was conducted in the absence of any commercial or financial relationships that could be construed as a potential conflict of interest.

Publisher's Note: All claims expressed in this article are solely those of the authors and do not necessarily represent those of their affiliated organizations, or those of the publisher, the editors and the reviewers. Any product that may be evaluated in this article, or claim that may be made by its manufacturer, is not guaranteed or endorsed by the publisher.

frontiers in Environmental Science

ORIGINAL RESEARCH
published: 15 October 2021
doi: 10.3389/fenvs.2021.762618

Optimization for Cost-Effectively Monitoring Ecological Effects of Water Diversion on the Urban Drinking Water Sources in a Large Eutrophic Lake

Jiangyu Dai[1], Zhonghua Feng[1], Xiufeng Wu[1], Shiqiang Wu[1], Yu Zhang[1], Fangfang Wang[1], Ang Gao[1], Xueyan Lv[2]* and Senlin Zhu[3]**

[1]State Key Laboratory of Hydrology-Water Resources and Hydraulic Engineering, Nanjing Hydraulic Research Institute, Nanjing, China, [2]Jiangsu Environment Monitoring Center, Nanjing, China, [3]College of Hydraulic Science and Engineering, Yangzhou University, Yangzhou, China

OPEN ACCESS

Edited by:
Michael Gormley,
Heriot-Watt University,
United Kingdom

Reviewed by:
Mohamed Hassaan,
National Institute of Oceanography and Fisheries (NIOF), Egypt
Baogang Zhang,
China University of Geosciences, China

***Correspondence:**
Xiufeng Wu
xfwu@nhri.cn
Xueyan Lv
ailvxy@126.com
Senlin Zhu
slzhu@yzu.edu.cn

Specialty section:
This article was submitted to Water and Wastewater Management, a section of the journal Frontiers in Environmental Science

Received: 22 August 2021
Accepted: 22 September 2021
Published: 15 October 2021

Citation:
Dai J, Feng Z, Wu X, Wu S, Zhang Y, Wang F, Gao A, Lv X and Zhu S (2021) Optimization for Cost-Effectively Monitoring Ecological Effects of Water Diversion on the Urban Drinking Water Sources in a Large Eutrophic Lake. Front. Environ. Sci. 9:762618. doi: 10.3389/fenvs.2021.762618

Due to the inputs of allochthonous pollutants and biological species from imported water, ecological effects of water diversion on urban drinking sources require long-term monitoring. Since spatial distributions of biological and environmental elements are always susceptible to water diversion, the monitoring specifications in water-receiving regions are always different from conventional ecological monitoring, especially in monitoring parameter selection and site distribution. To construct the method for selecting sensitive monitoring parameters and optimizing sites distribution in lakes, the large river-to-lake water diversion project, Water Diversion from Yangtze River to Lake Taihu in China, was taken as an example. The physicochemical properties and phytoplankton communities in the water-receiving Gonghu Bay and the referenced lake center were investigated and compared between the water diversion and non-diversion days in different seasons from 2013 to 2014. The comparative and collinearity analyses for selecting sensitive physicochemical parameters to water diversion, and the multidimensional scaling analysis based on the matrices of biological and sensitive physicochemical data, were integrated to optimize the monitoring in the water-receiving lake regions. Seven physicochemical parameters, including water temperature, pH, dissolved oxygen, total nitrogen, total phosphorus, chlorophyll a, and active silicate, were demonstrated to be sensitive to seasonal water diversion activities and selected for optimizing the site distribution and daily water quality monitoring. The nonmetric multidimensional scaling analysis results based on the data matrices of sensitive physicochemical parameters and phytoplankton communities were consistent for sites distribution optimization. For cost-effective monitoring, the sites distribution scheme could choose the optimizing results based on the Euclidean distance from 3.0 to 4.0 and the Bray-Curtis similarity from 40 to 60%. This scheme divided the Gonghu Bay into three water regions: the inflow river inlet, bay center, and bay mouth adjacent to the open water region. In each of the three regions, one representative site could be selected. If focusing on more details of each region, the standards with the Euclidean distance lower than 2.0 and the Bray-Curtis similarity higher than 60% should be considered. This

optimization method provided an available way to fulfill the cost-effective long-term monitoring of urban drinking water sources influenced by water diversion projects.

Keywords: water diversion, drinking water sources, physicochemical parameters, phytoplankton community, cost-effective monitoring

INTRODUCTION

Water diversion projects, as popular engineering projects for water supply and environmental improvement, have been implemented in many countries for over several decades (Hu et al., 2008). Originally, water diversion projects, such as the California Water Diversion Project, Mississippi River Diversion Project, and China South-to-North Water Diversion Project, were mainly used for agricultural irrigation, industrial production, residential water use, and ecological water supplement (Li et al., 2011, 2013). Since the global lake eutrophication problem became prominent in the 1960s, water diversion also has been taken as an efficient way to improve hydro-environments and to deal with cyanobacterial blooms in drinking water sources in many eutrophic lakes such as Lake Green in the USA (Oglesby, 1968), Lake Veluwe in the Netherlands (Jagtman et al., 1992), and others (Lake Taihu, Lake Chaohu, Lake Dianchi, Lake Baiyangdian, etc.) in China (Hu et al., 2008; Zhai et al., 2010; Li et al., 2011, 2013; Zhang et al., 2016; Chen et al., 2017; Cao et al., 2018; Dai et al., 2018, 2020; Qu et al., 2020; Zhang et al., 2021). As an emergent measure for protecting drinking water security, ecological effects induced by allochthonous inputs of nutrients and exotic species in water diversion projects have been receiving extensive attention.

To reveal the ecological effects of water diversion projects on drinking water sources in lakes, long-term ecological monitoring work is necessary. The ecological monitoring procedure for rivers and lakes always has standard specifications for sampling sites, sampling time, monitoring parameters, and other procedures (Wang et al., 2013). However, due to the dynamic inflow discharges of water diversion and their influences on water currents, the distributions of ecological elements are always influenced by the inflow discharges, allochthonous elements, and the lasting time of water diversion activities (Li et al., 2013). Therefore, the monitoring specifications, especially the site location, should be different from that of the normal monitoring methods. For example, due to the mixing effects of water diversion in the water-receiving regions, the original spatial differences in concentrations of some physicochemical parameters among the adjacent sites during the non-diversion period might be eliminated by the water diversion (Dai et al., 2020). Moreover, the normal specification of lake ecological monitoring always has many physicochemical parameters (Wang et al., 2013), some of which may not be sensitive to the water diversion. Thus, to save monitoring costs, sensitive physicochemical parameters should be selected for the long-term monitoring of the ecological effects induced by water diversion.

The site layout optimization research in lakes is mainly related to water quality monitoring (Behmel et al., 2016; Jiang et al., 2020; Liu et al., 2020). To optimize the water quality monitoring networks in drinking water sources of lakes, site layout optimization methods are usually based on water quality parameters correlation coefficients (Wang et al., 2014), the kriging variance (Beveridge et al., 2012), chlorophyll a remote sensing (Kiefer et al., 2015), and multivariate statistical analysis like cluster and discriminant analysis (Kovács et al., 2015; Tanos et al., 2015). These methods always use one or several representative water quality parameters to calculate differences among sites. But only a few studies provided a method for selecting the representative water quality parameters, mainly using the principal component analysis and collinearity analysis (Wang et al., 2014). Moreover, for optimizing ecological monitoring works in lakes, biological communities should also be considered. However, few studies provide a targeted methodology for optimizing the layout of ecological monitoring sites in drinking water sources of lakes, especially influenced by water diversion projects (Lepono et al., 2003; Zhang, 2009).

Lake Taihu is the third largest eutrophic shallow lake in the most developed middle and lower reaches of the Yangtze River, China. Due to anthropogenic and climatic disturbances, cyanobacterial blooms and pollution-induced water shortage have become the dominant ecological problems in the Taihu Basin (Qin et al., 2010). The Water Diversion from the Yangtze River to Lake Taihu (WDYT) project has been given the obligation to relieve these ecological problems in the Taihu Basin (Hu et al., 2008). Although the WDYT can quickly enhance the water exchange capacity and alleviate the cyanobacterial blooms in some drinking water sources of Lake Taihu (Li et al., 2013), the allochthonous input of nutrients and other pollutants have also sparked controversies (Hu et al., 2010; Dai et al., 2018; Yao et al., 2018; Qin et al., 2019). Therefore, long-term and cost-effective monitoring work should be carried out to objectively evaluate ecological effects of this project. In this study, we proposed a targeted methodology for selecting sensitive biotic and abiotic parameters and optimizing the location of monitoring sites in the water-receiving regions of Lake Taihu. As the numerous and active biota in lakes, phytoplankton are vitally sensitive to lake conditions such as the trophic level and hydrodynamic disturbance (Guo et al., 2019), and thus are taken as the representative biological index in ecological monitoring (Padisak et al., 2006). The physicochemical parameters and phytoplankton communities in the drinking water sources in Gonghu Bay were measured during the water diversion periods in different seasons. Based on these monitoring variables, an integrated method, combining comparative analysis, collinearity analysis, and multivariate statistical analysis, was constructed for optimizing the ecological monitoring sites distribution in lakes. This study intended to provide an available method which is cost-effective for long-term

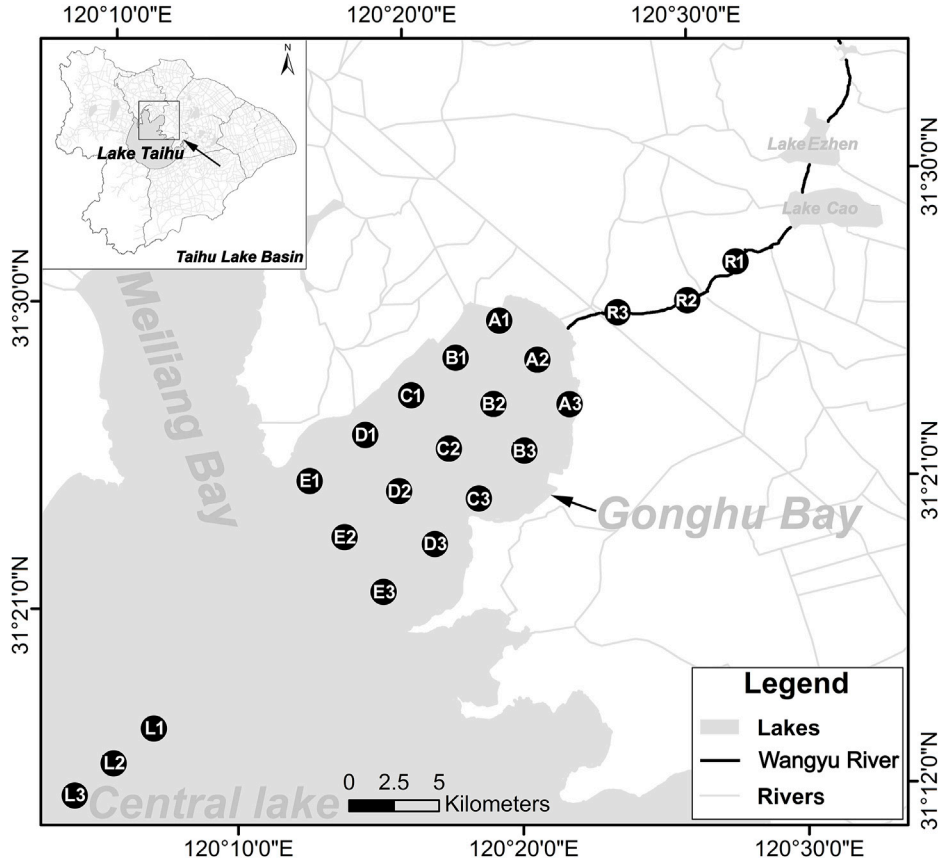

FIGURE 1 | The initial distribution of monitoring sites in Wangyu River, Gonghu Bay, and the lake center of Lake Taihu.

ecological monitoring, and thus could standardize the procedure of ecological monitoring for limnetic effects induced by water diversion projects.

MATERIALS AND METHODS

Study Area and Initial Monitoring Sites Distribution

Gonghu Bay, the northeastern part of Lake Taihu, is the main urban drinking water source for Wuxi city of the Taihu Basin and also the first water-receiving area connecting the main inflow channel of the Wangyu River and the central lake of Lake Taihu (**Figure 1**). It covers about 150 km^2 and has a multi-year average water depth of 1.8 m (Zhong et al., 2012). Due to the frequent serious cyanobacterial blooms in the north part of Lake Taihu from May to December in a year, Gonghu Bay is always threatened by *Microcystis* scums (Dai et al., 2018, 2020). According to the Technical Specifications Requirements for Environmental Monitoring of Surface Water and Waste Water (HJ/T 91-2002) issued by the Ministry of Ecology and Environment of P.R. China, we distributed the monitoring sites in a uniform grid with a 2.50 km distance among two sites in Gonghu Bay. We also laid three monitoring sites in Wangyu River and the central lake of Lake Taihu, respectively, (**Figure 1**). In Gonghu Bay, there were three site lines from the river mouth of Wangyu River to the central lake, of which two were along the west and east sides of Gonghu Bay, respectively. The other was of the central line of Gonghu Bay. Each line had five sites.

Water Sample Collection and Physicochemical Parameters Measurement

Since WDYT is always operated according to the water level of Lake Taihu (TBA, 2013). Once the water level of Lake Taihu is lower than the control water level for water supply which is ruled by the Taihu Basin Authority (TBA), the hydro-junctions in the Wangyu River will open to transfer Yangtze River water to Lake Taihu. Additionally, if Lake Taihu faces serious cyanobacterial blooms, the WDYT will also be urgently operated to relieve bloom disasters (Qin et al., 2010). Due to this reason, the WDYT has been regularly operated during the dry period in Taihu Basin from November to February year by year (TBA, 2013, 2014). In this study, we constantly monitored *in situ* on the middle days of July, August, November, and January from 2013 to 2014. Among these sampling days, the days of November and January in 2013 and July in 2014 were in the period without water

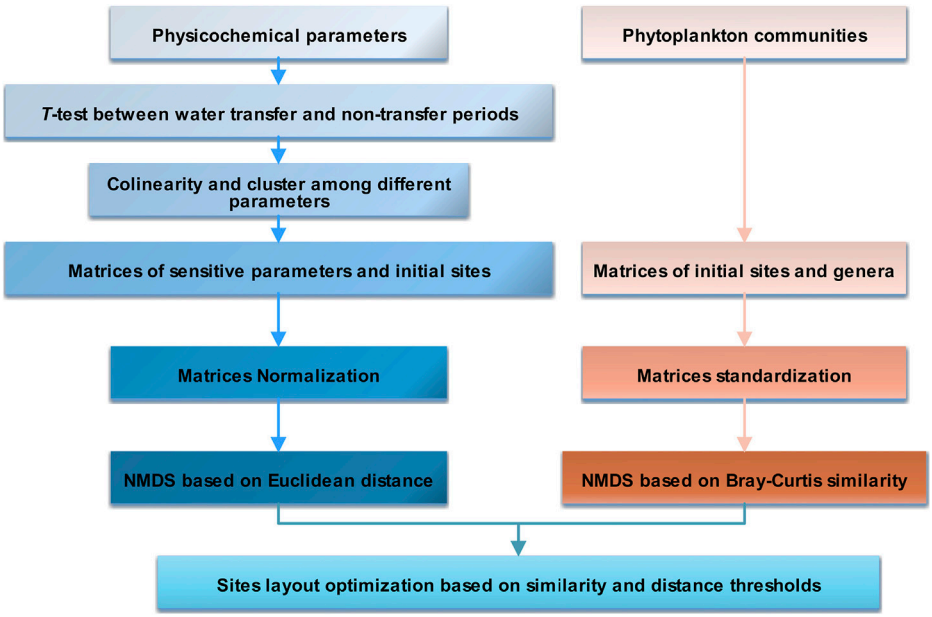

FIGURE 2 | The flow chart of sites optimization methodologies used in this study.

diversion, while the days in August of 2013 and November and January in 2014 were all in the water diversion period.

About a 2-L water sample (about 50 cm under the water surface) for each site was collected using the column water sampler. One liter was stored in a clean plastic bottle and used for measuring the physicochemical parameters in the laboratory in 24 h. Another 1-L water sample for each site was stored in a sterile plastic bottle and fixed with the 15 ml of 5% Lugol's iodine reagent (Jin and Tu, 1990), which was transported to the laboratory for phytoplankton community identification.

Physicochemical Parameters Measurement

Water temperature, pH, turbidity, and dissolved oxygen content were detected *in situ* using the Portable Multi-parameters Detection HQ30d (HACH, Shanghai, China) kit. The contents of total nitrogen (TN), total phosphorus (TP), ammonia (NH_3-N), nitrate (NO_3-N), soluble reactive phosphorus (SRP), permanganate index (COD_{Mn}), chlorophyll a (Chl a), and dissolved silicate (SiO_3-Si) were all measured in the laboratory according to the literature methods (Jin and Tu, 1990).

Phytoplankton Community Identification

After over 24 h of standing, the 1-L Lugol's fixed water sample for each site was concentrated to 50 ml in a sterile glass bottle using a separating funnel. Then, 0.1 ml of the concentrated sample was injected into the algae counting box and put in the Axiovert 200 (CARL ZEISS, Germany) optical microscope to uniformly capture 100 random views. This procedure was repeated three times for one sample. The cell abundances of phytoplankton species were identified according to the literature (Hu and Wei, 2006).

Optimization Methods

Sensitive Physicochemical Parameters Selection

The significance in physicochemical parameters between the periods of water diversion and non-diversion in the same month for different years was determined using the two-tailed *t*-test method (**Figure 2**) in the SPSS 16.0 statistic software (IBM, United States). The collinearities of the significant physicochemical parameters were tested by Pearson correlation analysis with the SPSS 16.0 software and were plotted using the R software. After this, the representative significant parameters without significant autocorrelation among them were selected to be the sensitive physicochemical parameters which would be further used for sites distribution optimization.

Sites Distribution Optimization

Nonmetric Multidimensional scaling analysis (NMDS) (Clarke and Gorley, 2006) was used to optimize the distribution and number of monitoring sites, based on the Euclidean distance of environmental data matrices and Bray-Curtis similarity of phytoplankton community matrices among initial monitoring sites, respectively, (**Figure 2**). The environmental data matrices were constructed by sensitive physicochemical parameters of the initial monitoring sites. The phytoplankton community matrices were constructed by the phytoplankton genera or species corresponding to the environmental data matrices. The threshold values, distinguishing sites revealing different ecological effects of water diversion, were selected as 1.0, 2.0, 3.0, 4.0, 5.0 of the Euclidean distance and 40, 50, 60, 70, 80% of the Bray-Curtis similarity, respectively. The NMDS biplots showing differences among sites on the water diversion days were plotted using the Primer-E software (Quest Research Limited, New Zealand) (Clarke and Gorley, 2006).

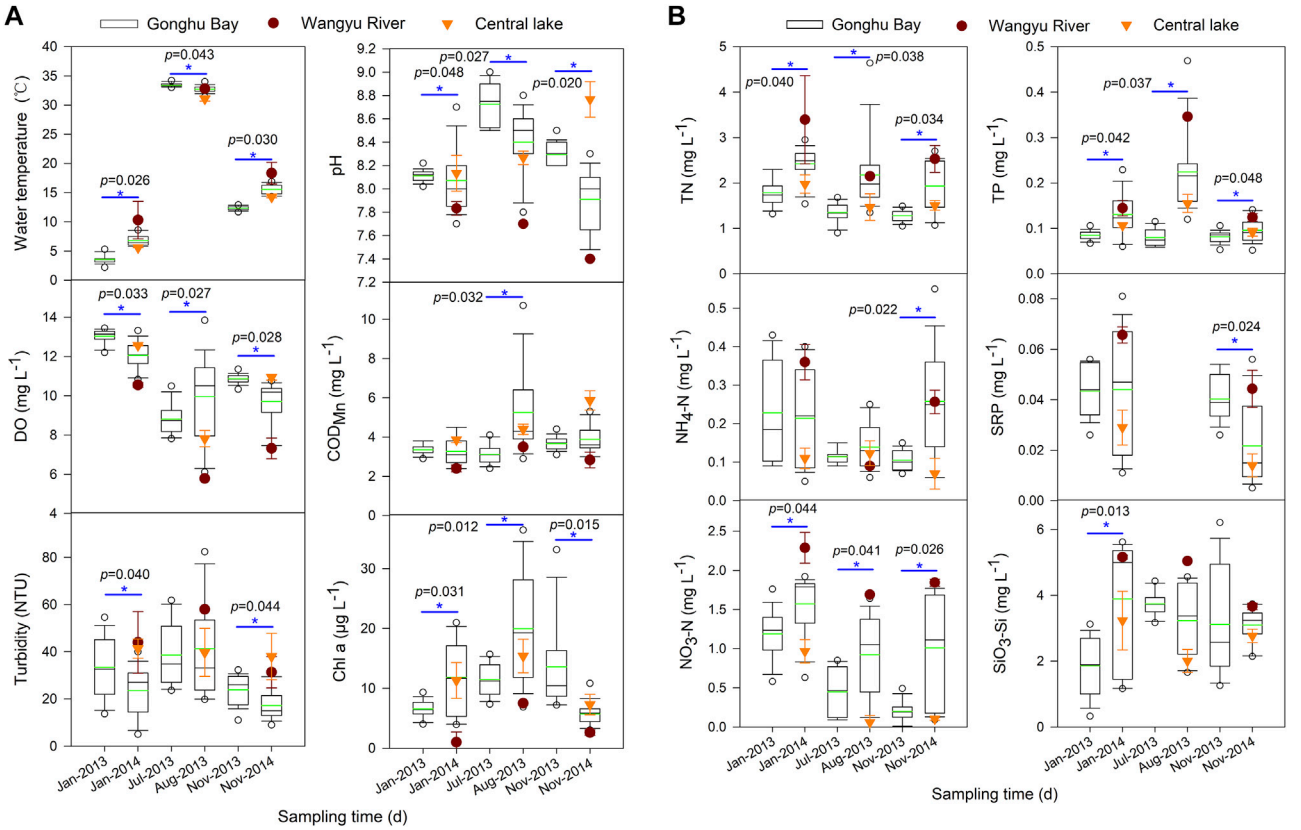

FIGURE 3 | The comparisons in mean values of the 12 physicochemical parameters between the same seasons during water diversion and non-diversion periods from 2013 to 2014 (DO, dissolved oxygen; SiO_3-Si, active silicate; NO_3-N, nitrate; NH_3-N, ammonia; TN, total nitrogen; TP, total phosphorus; Temp, water temperature; Chl a, chlorophyll a; COD_{Mn}, permanganate index; Jan, Aug, and Nov are the abbreviations of January, August, and November, respectively, the asterisk means significant difference in parameters between the water diversion and non-diversion periods in the same season; Significant *p* values between the water diversion and non-diversion periods in the same season are shown in the figure; the green line means the mean value in the physicochemical parameter from the 15 sites in the Gonghu Bay).

RESULTS AND DISCUSSION

Sensitive Physicochemical Parameters Determination

The investigated physicochemical parameters were differently sensitive to the water diversion in the three seasons (**Figure 3**). In the three seasons during 2013–2014, there were significant differences in the mean values of water temperature, DO, pH, Chl a, TN, NO_3-N, and TP in Gonghu Bay between the water diversion and non-diversion days. In some of the three seasons, significant differences were also found in the mean values of turbidity, COD_{Mn}, NH_3-N, SRP, and SiO_3-Si. Due to the lower contents of DO and pH (**Figure 3**) and the higher values of water temperature (**Figure 3**), TN, NH_3-N, NO_3-N, TP, and SiO_3-Si (**Figure 3**) in the Wangyu River on some of the water diversion days, the contents of water temperature, DO, pH, TN, NH_3-N, NO_3-N, TP, and SiO_3-Si were evidently different from those on the non-diversion days in the same season. Since the contents of turbidity in the Wangyu River and central lake were always higher than those in Gonghu Bay, this parameter was not sensitive to the water diversions in different seasons (**Figure 3**). The average contents of COD_{Mn} and Chl a in Gonghu Bay were more influenced by the growth of phytoplankton in Gonghu Bay, but the average content of Chl a was also lower on the water diversion days than that on the non-diversion days in autumn (**Figure 3**). The contents of SRP were also not sensitive to the water diversions in different seasons (**Figure 3**).

The collinearity analysis of the 12 monitored parameters on all six sampling days showed there were pronounced correlations among some of the physicochemical parameters (**Figure 4**). Based on the collinearities among the physicochemical parameters, seven physicochemical parameter groups were classified with the Pearson coefficient of 0.30: group A, COD_{Mn}, Chl a, and pH; group B, turbidity; group C: water temperature and TP; group D, DO; group E, TN and NO_3-N; group F, SiO_3-Si; group G, NH_3-N, and SRP (**Figure 5**). However, if selecting the higher Pearson coefficients, we could get more groups. Combining with the results of mean value comparisons and the convenience in data acquisition, seven physicochemical parameters, including water temperature, pH, DO, TN, TP, Chl a, and SiO_3-Si, were selected to be the sensitive physicochemical parameters used for sites distribution optimization and daily water quality monitoring.

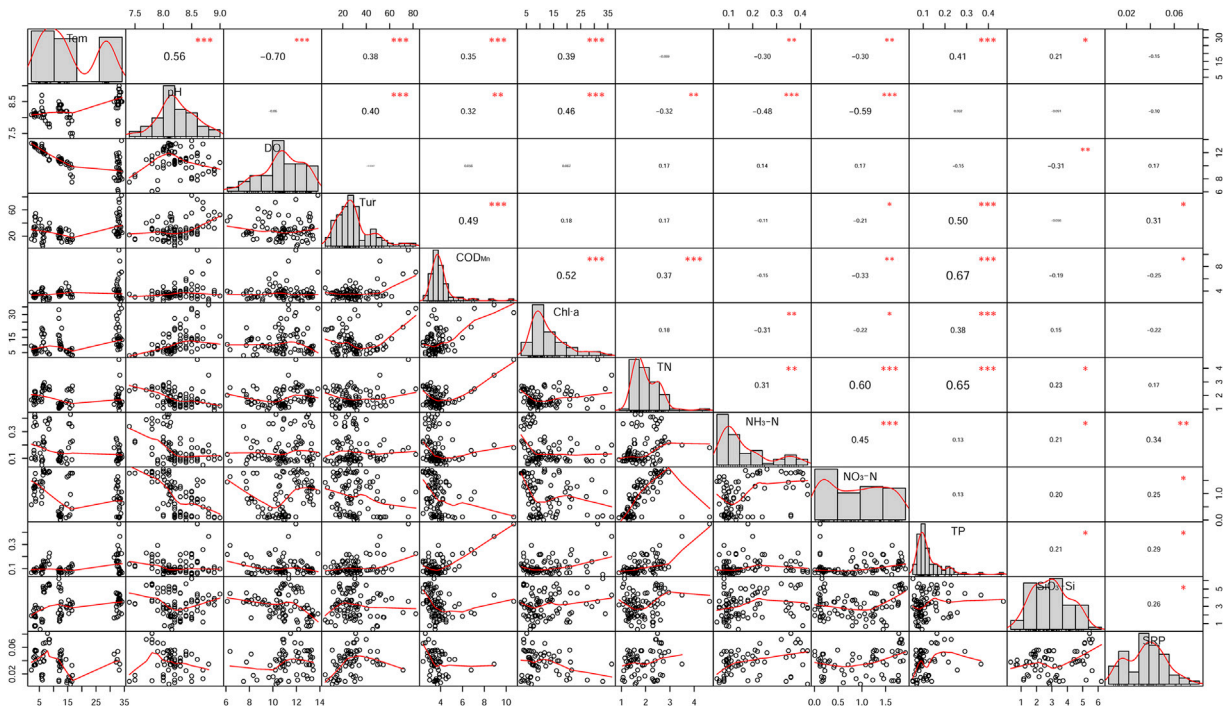

FIGURE 4 | The collinearity analysis of the 12 monitored physicochemical parameters on all six sampling days. [DO, dissolved oxygen; SiO_3-Si, active silicate; NO_3-N, nitrate; NH_3-N, ammonia; TN, total nitrogen; TP, total phosphorus; Temp, water temperature; Chl a, chlorophyll a; COD_{Mn}, permanganate index; the single asterisk represents significant correlations (Pearson correlation, $p \leq 0.05$); the double asterisk means highly significant correlations ($p \leq 0.01$); the triple asterisk means extremely significant correlations ($p \leq 0.001$)].

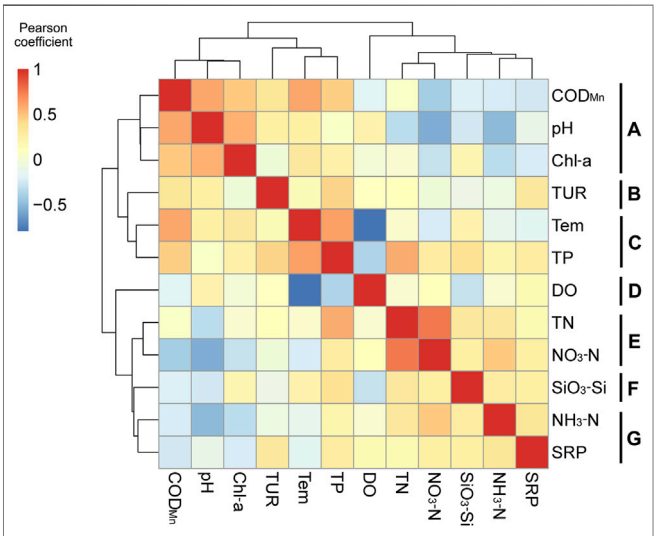

FIGURE 5 | The heatmap of Pearson correlations among the monitored physicochemical parameters in Gonghu Bay in the six sampling times. (The sample number of the Pearson correlation test is 90. DO, dissolved oxygen; SiO_3-Si, active silicate; NO_3-N, nitrate; NH_3-N, ammonia; TN, total nitrogen; TP, total phosphorus; Temp, water temperature; Chl a, chlorophyll a; COD_{Mn}, permanganate index).

The selected parameters represent different physicochemical features of the lake water.

Water temperature, reflecting seasonal and climate changes, is the basic physical parameter influencing characteristics of hydrodynamics, circulation of substance and energy, and life processes in lakes (O'Reilly et al., 2003; Elçi, 2008; Gudasz et al., 2010). The pH value is the comprehensive physicochemical index which reflects the dynamics of hydrogen ion determined by the contents of carbon dioxide, bicarbonate ion, and carbonate in water (Charlson and Rodhe, 1982). Due to the normally lower pH values in rivers than in lakes (Feng et al., 2017), the pH value which is always increased by the cyanobacterial blooms (Cao et al., 2016) in the water-receiving lake regions were decreased significantly. Dissolved oxygen is also a regular and critical environmental monitoring parameter which is easily obtained *in situ* using automatic monitoring equipment. The Chl a index represents not only the primary production but also the level of cyanobacterial blooms. Additionally, N, P, and Si are the basic elements of natural waters, and the nutrient parameters are also the normal monitoring indexes for drinking water sources (Wu et al., 2017). Finally, the selected physicochemical parameters not only reflected the sensitive characteristics of the physicochemical habitat in the water-receiving lake region, but also covered the most important monitoring water quality indexes for the drinking water sources.

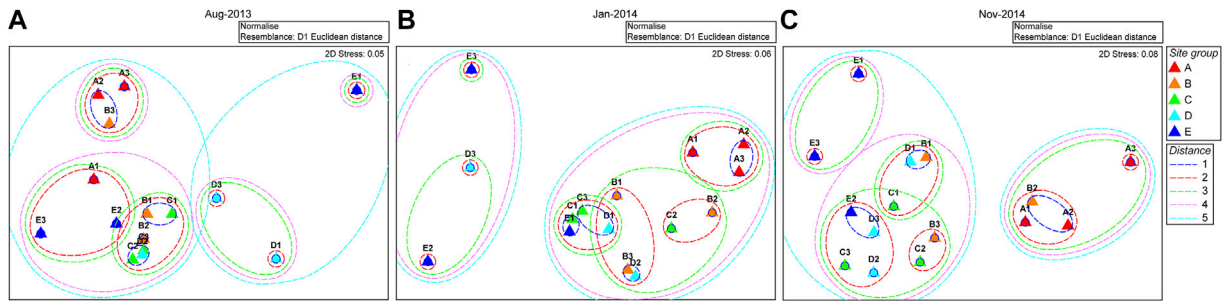

FIGURE 6 | The multi-scaling analysis biplots for monitoring sites in Gonghu Bay based on the Euclidean distance matrices of sensitive physicochemical parameters during the six sampling periods from 2013 to 2014. The classification of monitoring sites was based on three levels (1, 2, 3, 4, and 5).

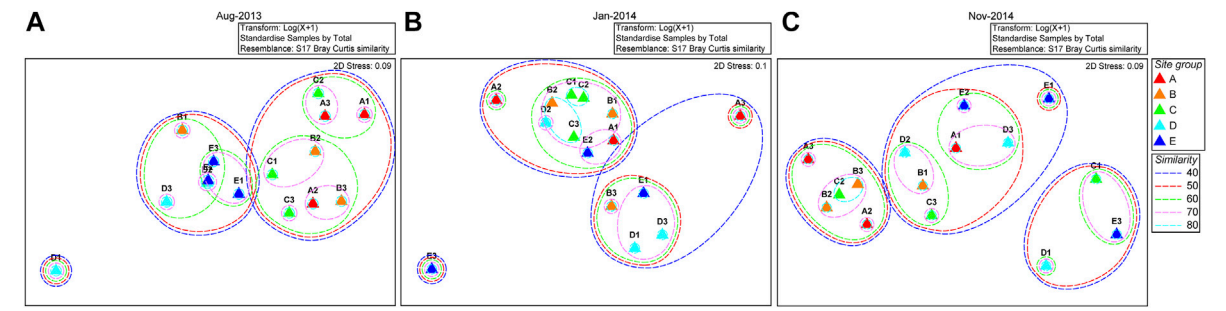

FIGURE 7 | The multi-scaling analysis biplots for monitoring sites in Gonghu Bay based on the Bray-Curtis similarity matrices of phytoplankton communities during the six sampling periods from 2013 to 2014. The classification of monitoring sites was based on three levels (40, 50, 60, 70, and 80%).

Sites Optimization Based on Matrices of Sensitive Physicochemical Parameters

The NMDS results based on the Euclidean distance matrices of the sensitive physicochemical parameters from 2013 to 2014 showed the pronounced differences among sites, with the gradient from the inflow river mouth of Gonghu Bay to the adjacent region between Gonghu Bay and the lake center on the water diversion days (**Figure 6**). The classification of sampling sites was different with different distance thresholds. Along with the increase of Euclidean distance, the number of site clusters decreased. At the 1.0 level of Euclidean distance, most of the sampling sites differed from each other on each water diversion day, while at the 5.0 level of Euclidean distance, only two site clusters were classified on the three water diversion days. Totally, at the Euclidean distance range from 3.0 to 4.0, three site groups were found in the inflow river mouth of Gonghu Bay, bay center, and the adjacent region between Gonghu Bay and the lake center during the water diversion periods, respectively (**Figure 6**). The Euclidean distance is the most popular dissimilarity index for measuring the distances among different environmental matrices (Hadjisolomou et al., 2018). In this current study, the classification result at the Euclidean distance range from 3.0 to 4.0 could reflect the heterogeneity in the spatial effect induced by water diversion. Therefore, based on the environmental matrices of sensitive physicochemical parameters, the sites distribution could be optimized which could also reflect the impacts of water diversion on the drinking water sources in lakes.

Sites Optimization Based on Phytoplankton Community Matrices

The NMDS on the Bray-Curtis similarity matrices of the phytoplankton communities showed obvious spatial heterogeneity in phytoplankton community structures on the three water diversion days of 2013–2014 (**Figure 7**). At the similarity level of 80%, the phytoplankton community in different sites was significantly different. The ecological structure of Gonghu Bay is complicate with the algae-dominated west region and the macrophyte-dominated east region (Gao et al., 2017). Moreover, the lake currents of some water regions in Gonghu Bay are sensitive to the disturbance induced by wind and water diversion activities (Lv, 2013). Therefore, the phytoplankton habitat in Gonghu Bay presented obvious spatial heterogeneity, which might be an important reason for the significant differences in phytoplankton communities among different sites at the similarity of 80%. However, from 60 to 40% of the similarity levels, most of the adjacent sites were grouped together and shaped several site groups in the inflow river mouth of Gonghu Bay, center, and the adjacent region between Gonghu Bay and the central lake during the water diversion periods,

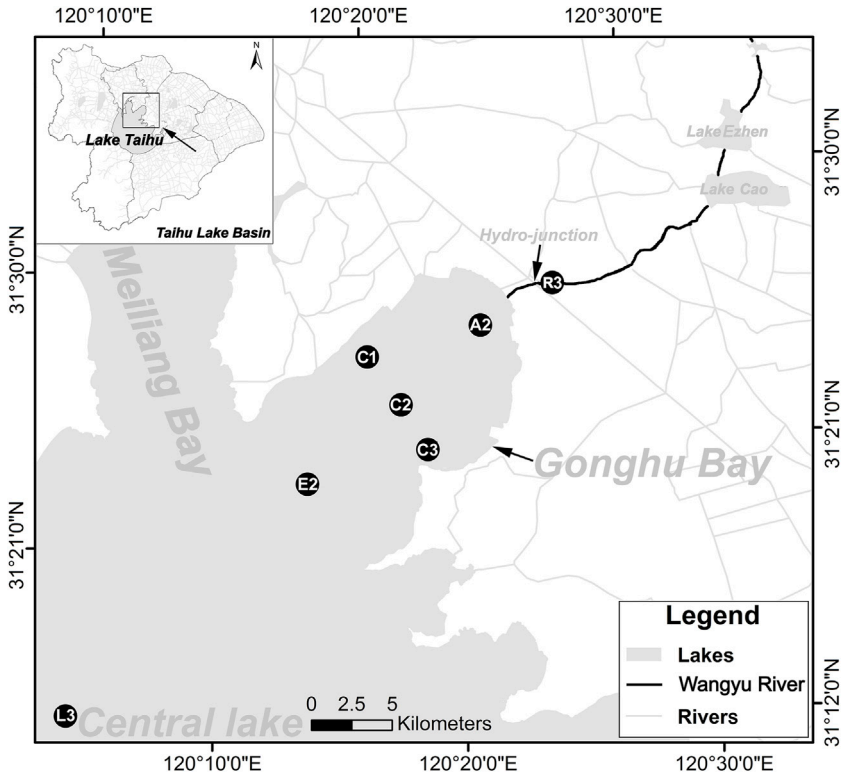

FIGURE 8 | The most cost-effective sites distribution in Wangyu River, Gonghu Bay, and the lake center of Lake Taihu.

respectively, (**Figure 7**). Consistent with the results of the NMDS analysis on sensitive physicochemical properties of water samples, the spatial distribution of the phytoplankton communities in Gonghu Bay during the water diversion days was similar. The similar distribution pattern for both the phytoplankton communities and their physicochemical habitats was demonstrated by some previous studies (Li et al., 2019; Kutlu et al., 2020). In this study, the thresholds for the cluster indices were determined to optimize the sampling sites distribution, which was alternative according to the monitoring requirements.

Determination of Sites Distribution Optimization and Methodology Application

In view of the above NMDS analysis results, taking into account the spatial distribution of monitoring sites and ecological functions of monitoring areas, the optimization of monitoring sites for the ecological effects of the water diversion project was optimized. The representative monitoring sites that can reflect the ecological effects of water diversion in Gonghu Bay were initially selected. Among them, the distance between every point in Gonghu Bay was optimized from the original 2.5–5 km.

As the only monitoring point of the Wangyu River, site R3 should be preserved to represent the characteristics of inflow water. As the most sensitive water area to water diversion activities, site A1 that linked the Wangyu River inlet and Gonghu Bay is also preserved. During the periods of water diversion, the physicochemical and biological elements of Gonghu Bay showed an evident spatial gradient along the Wangyu River inlet to the mouth of Gonghu Bay, so three monitoring sites (A2, C2, and E2) are preserved along the center line of Gonghu Bay. As a reference water area, lake center regions retained the original L3 monitoring site. The east and west regions of Gonghu Bay are two different types of ecosystems, and the southeast monsoon has a greater impact on Lake Taihu in the summer. Therefore, the monitoring sites (C1 and C3) were preserved for the east and west regions, respectively (**Figure 8**).

From the monitoring costs perspective, the sites layout scheme could choose the optimizing results based on the Euclidean distance of 3.0–4.0 or the Bray-Curtis similarity from 40 to 60%. This scheme divided Gonghu Bay into three water regions with the distance gradient far from the inflow river mouth. In each of the three regions, one representative site could be located. However, if focusing on more details of each region, the standards with the Euclidean distance lower than 2.0 and the Bray-Curtis similarity higher than 60% should be considered. At the same time, the marginal effect of the biological diversity of the shoreline ecosystem in lakes and the impact of wind directions in different seasons in Lake Taihu should be taken into consideration. The most representative

monitoring sites in the monitored area should be selected in different seasons.

CONCLUSION

Based on the two-tailed *t*-test and collinearity analysis, the six physicochemical parameters including pH, DO, turbidity, TP, NO_3-N, and SiO_3-Si were demonstrated to be sensitive physicochemical parameters that could be used for sites distribution optimization in Gonghu Bay. The sites distribution optimization method is available to the case study of Gonghu Bay influenced by the WDYT. The NMDS analysis results based on the Euclidean distance of physicochemical matrices and the Bray-Curtis similarity of phytoplankton communities were consistent. From the monitoring costs perspective, the sites distribution scheme could choose the optimizing results based on the Euclidean distance from 3.0 to 4.0 and the Bray-Curtis similarity from 40 to 60%. This scheme divided Gonghu Bay into three water regions of the Wangyu River inlet, center, and mouth of Gonghu Bay. In each of the three regions, one representative site could be located. However, if focusing on more details of each region, the standards with the Euclidean distance lower than 2.0 and the Bray-Curtis similarity higher than 60% should be considered. At the same time, the marginal effect of the biological diversity of the shoreline ecosystem in lakes and the impact of wind directions in different seasons in Lake Taihu should be taken into consideration. The most representative monitoring sites in the monitored area should be selected in different seasons.

DATA AVAILABILITY STATEMENT

The original contributions presented in the study are included in the article/Supplementary Material, further inquiries can be directed to the corresponding authors.

AUTHOR CONTRIBUTIONS

JD: Conceptualization, Investigation, Formal analysis, Writing—Original Draft ZF: Revision and Editing XW: Project administration, Funding acquisition SW: Supervision, Project administration, Funding acquisition YZ: Formal analysis FW: Investigation AG: Investigation XL: Investigation, Resources SZ: Writing—Review and Editing.

FUNDING

This work was jointly funded by the National Key R and D Program of China (2018YFE0206200), the Projects of National Natural Science Foundation of China (52179073), and the Special Research Fund of Nanjing Hydraulic Research Institute (Y120010).

ACKNOWLEDGMENTS

We are grateful to the Hydrology and Water Resources Investigation Bureau of Wuxi for their help in the field survey and sample collection.

REFERENCES

Behmel, S., Damour, M., Ludwig, R., and Rodriguez, M. J. (2016). Water Quality Monitoring Strategies - A Review and Future Perspectives. *Sci. Total Environ.* 571, 1312–1329. doi:10.1016/j.scitotenv.2016.06.235

Beveridge, D., St-Hilaire, A., Ouarda, T. B. M. J., Khalil, B., Conly, F. M., Wassenaar, L. I., et al. (2012). A Geostatistical Approach to Optimize Water Quality Monitoring Networks in Large Lakes: Application to Lake Winnipeg. *J. Great Lakes Res.* 38, 174–182. doi:10.1016/j.jglr.2012.01.004

Cao, X., Wang, Y., He, J., Luo, X., and Zheng, Z. (2016). Phosphorus Mobility Among Sediments, Water and Cyanobacteria Enhanced by Cyanobacteria Blooms in Eutrophic Lake Dianchi. *Environ. Pollut.* 219, 580–587. doi:10.1016/j.envpol.2016.06.017

Cao, Z.-G., Li, S., Zhao, Y.-E., Wang, T.-P., Bergquist, R., Huang, Y.-Y., et al. (2018). Spatio-Temporal Pattern of Schistosomiasis in Anhui Province, East China: Potential Effect of the Yangtze River - Huaihe River Water Transfer Project. *Parasitol. Int.* 67 (5), 538–546. doi:10.1016/j.parint.2018.05.007

Charlson, R. J., and Rodhe, H. (1982). Factors Controlling the Acidity of Natural Rainwater. *Nature* 295 (5851), 683–685. doi:10.1038/295683a0

Chen, X., Wang, F., Lu, J., Li, H., Zhu, J., and Lv, X. (2017). Simulation of the Effect of Artificial Water Transfer on Carbon Stock ofPhragmites Australisin the Baiyangdian Wetland, China. *Scientifica* 2017, 1–11. doi:10.1155/2017/7905710

Clarke, K., and Gorley, R. (2006). *PRIMER V6: User Manual/tutorial*. Plymouth: PRIMER-E Ltd.

Dai, J., Wu, S., Wu, X., Lv, X., Sivakumar, B., Wang, F., et al. (2020). Impacts of a Large River-To-Lake Water Diversion Project on Lacustrine Phytoplankton Communities. *J. Hydrol.* 587, 124938. doi:10.1016/j.jhydrol.2020.124938

Dai, J., Wu, S., Wu, X., Xue, W., Yang, Q., Zhu, S., et al. (2018). Effects of Water Diversion from Yangtze River to Lake Taihu on the Phytoplankton Habitat of the Wangyu River Channel. *Water* 10 (6), 759. doi:10.3390/w10060759

Elçi, Ş. (2008). Effects of thermal Stratification and Mixing on Reservoir Water Quality. *Limnology* 9 (2), 135–142. doi:10.1007/s10201-008-0240-x

Feng, Z., Su, B., Xiao, D.-D., and Ye, L.-Y. (2017). Study on pH Value and its Variation Characteristics of the Main Rivers into Dianchi Lake under the Anthropogenic and Natural Processes, Yunnan, China. *J. Inf. Optimization Sci.* 38 (7), 1197–1210. doi:10.1080/02522667.2017.1367501

Gao, H., Shi, Q., and Qian, X. (2017). A Multi-Species Modelling Approach to Select Appropriate Submerged Macrophyte Species for Ecological Restoration in Gonghu Bay, Lake Taihu, China. *Ecol. Model.* 360, 179–188. doi:10.1016/j.ecolmodel.2017.07.003

Gudasz, C., Bastviken, D., Steger, K., Premke, K., Sobek, S., and Tranvik, L. J. (2010). Temperature-Controlled Organic Carbon Mineralization in lake Sediments. *Nature* 466 (7305), 478–481. doi:10.1038/nature09186

Guo, K., Wu, N., Wang, C., Yang, D., He, Y., Luo, J., et al. (2019). Trait Dependent Roles of Environmental Factors, Spatial Processes and Grazing Pressure on lake Phytoplankton Metacommunity. *Ecol. Indicators* 103, 312–320. doi:10.1016/j.ecolind.2019.04.028

Hadjisolomou, E., Stefanidis, K., Papatheodorou, G., and Papastergiadou, E. (2018). Assessment of the Eutrophication-Related Environmental Parameters in Two Mediterranean Lakes by Integrating Statistical Techniques and Self-Organizing Maps. *Int. J. Environ. Res. Public Health* 15 (3), 547. doi:10.3390/ijerph15030547

Hu, H., and Wei, Y. (2006). *Chinese Freshwater Algae–System, Classification and Ecology*. 1st edition. Beijing: Science Press. (In Chinese).

Hu, L., Hu, W., Zhai, S., and Wu, H. (2010). Effects on Water Quality Following Water Transfer in Lake Taihu, China. *Ecol. Eng.* 36 (4), 471–481. doi:10.1016/j.ecoleng.2009.11.016

Hu, W., Zhai, S., Zhu, Z., and Han, H. (2008). Impacts of the Yangtze River Water Transfer on the Restoration of Lake Taihu. *Ecol. Eng.* 34 (1), 30–49. doi:10.1016/j.ecoleng.2008.05.018

Jagtman, E., Van der Molen, D. T., and Vermij, S. (1992). The Influence of flushing on Nutrient Dynamics, Composition and Densities of Algae and Transparency in Veluwemeer, The Netherlands. *Hydrobiologia* 233 (1-3), 187–196. doi:10.1007/978-94-011-2432-4_17

Jiang, J., Tang, S., Han, D., Fu, G., Solomatine, D., and Zheng, Y. (2020). A Comprehensive Review on the Design and Optimization of Surface Water Quality Monitoring Networks. *Environ. Model. Softw.* 132, 104792. doi:10.1016/j.envsoft.2020.104792

Jin, X., and Tu, Q. (1990). *The Standard Methods for Observation and Analysis of lake Eutrophication*. 2nd edition. Beijing: China Environmental Science Press. (In Chinese).

Kiefer, I., Odermatt, D., Anneville, O., Wüest, A., and Bouffard, D. (2015). Application of Remote Sensing for the Optimization of *In-Situ* Sampling for Monitoring of Phytoplankton Abundance in a Large Lake. *Sci. Total Environ.* 527-528, 493–506. doi:10.1016/j.scitotenv.2015.05.011

Kovács, J., Kovács, S., Hatvani, I. G., Magyar, N., Tanos, P., Korponai, J., et al. (2015). Spatial Optimization of Monitoring Networkson the Examples of a River, a Lake-Wetland System and a Sub-Surface Water System. *Water Resour. Manage.* 29 (14), 5275–5294. doi:10.1007/s11269-015-1117-5

Kutlu, B., Aydın, R., Danabas, D., and Serdar, O. (2020). Temporal and Seasonal Variations in Phytoplankton Community Structure in Uzuncayir Dam Lake (Tunceli, Turkey). *Environ. Monit. Assess.* 192 (2), 105–112. doi:10.1007/s10661-019-8046-3

Lepono, T., Du Preez, H. H., and Thokoa, M. (2003). Monitoring of Water Transfer from Katse Dam into the Upper Vaal River System: Water Utility's Perspective. *Water Sci. Technol.* 48 (10), 97–102. doi:10.2166/wst.2003.0548

Li, C., Feng, W., Chen, H., Li, X., Song, F., Guo, W., et al. (2019). Temporal Variation in Zooplankton and Phytoplankton Community Species Composition and the Affecting Factors in Lake Taihu-A Large Freshwater lake in China. *Environ. Pollut.* 245, 1050–1057. doi:10.1016/j.envpol.2018.11.007

Li, Y., Acharya, K., and Yu, Z. (2011). Modeling Impacts of Yangtze River Water Transfer on Water Ages in Lake Taihu, China. *Ecol. Eng.* 37 (2), 325–334. doi:10.1016/j.ecoleng.2010.11.024

Li, Y., Tang, C., Wang, C., Tian, W., Pan, B., Hua, L., et al. (2013). Assessing and Modeling Impacts of Different Inter-basin Water Transfer Routes on Lake Taihu and the Yangtze River, China. *Ecol. Eng.* 60 (11), 399–413. doi:10.1016/j.ecoleng.2013.09.067

Liu, G., Ai, J., Xu, J., Zheng, J., and Yao, D. (2020). Monitoring point Optimization in lake Waters. *Water Sup* 20 (6), 2348–2358. doi:10.2166/ws.2020.147

Lv, X. Y. (2013). *Impact of Water Diversion on the Growth of Dominant Eutrophic Algae in Lake Taihu*. Nanjing: Nanjing Hydraulic Research Institute. (In Chinese).

O'Reilly, C. M., Alin, S. R., Plisnier, P.-D., Cohen, A. S., and McKee, B. A. (2003). Climate Change Decreases Aquatic Ecosystem Productivity of Lake Tanganyika, Africa. *Nature* 424 (6950), 766–768. doi:10.1038/nature01833

Oglesby, R. T. (1968). Effects of Controlled Nutrient Dilution on a Eutrophic lake. *Adv. Water Pollut. Res.* 2, 747–757. doi:10.1016/0043-1354(68)90182-6

Padisák, J., Borics, G., Grigorszky, I., and Soróczki-Pintér, É. (2006). Use of Phytoplankton Assemblages for Monitoring Ecological Status of Lakes within the Water Framework Directive: The Assemblage Index. *Hydrobiologia* 553 (1), 1–14. doi:10.1007/s10750-005-1393-9

Qin, B., Paerl, H. W., Brookes, J. D., Liu, J., Jeppesen, E., Zhu, G., et al. (2019). Why Lake Taihu Continues to Be Plagued with Cyanobacterial Blooms through 10 Years (2007-2017) Efforts. *Sci. Bull.* 64 (6), 354–356. doi:10.1016/j.scib.2019.02.008

Qin, B., Zhu, G., Gao, G., Zhang, Y., Li, W., Paerl, H. W., et al. (2010). A Drinking Water Crisis in Lake Taihu, China: Linkage to Climatic Variability and lake Management. *Environ. Manage.* 45 (1), 105–112. doi:10.1007/s00267-009-9393-6

Qu, X., Chen, Y., Liu, H., Xia, W., Lu, Y., Gang, D.-D., et al. (2020). A Holistic Assessment of Water Quality Condition and Spatiotemporal Patterns in Impounded Lakes along the Eastern Route of China's South-To-North Water Diversion Project. *Water Res.* 185, 116275. doi:10.1016/j.watres.2020.116275

Tanos, P., Kovács, J., Kovács, S., Anda, A., and Hatvani, I. G. (2015). Optimization of the Monitoring Network on the River Tisza (Central Europe, Hungary) Using Combined Cluster and Discriminant Analysis, Taking Seasonality into Account. *Environ. Monit. Assess.* 187 (9), 575. doi:10.1007/s10661-015-4777-y

TBA (2013). *Annual Report of the Water Diversion Project from Yangtze River to Lake Taihu*. Shanghai: The Taihu Basin Authority. (In Chinese).

TBA (2014). *Annual Report of the Water Diversion Project from Yangtze River to Lake Taihu*. Shanghai: The Taihu Basin Authority. (In Chinese).

Wang, C., Wang, Z., and Zhang, H. (2013). Introduce of Sampling Design about Federal EPA Surface Water Quality Monitoring and Assessment. *Environ. Monit. China* 29 (5), 124–128. doi:10.3969/j.issn.1002-6002.2013.05.025

Wang, H., Wu, M., Deng, Y., Tang, C., and Yang, R. (2014). Surface Water Quality Monitoring Site Optimization for Poyang Lake, The Largest Freshwater lake in China. *Int. J. Environ. Res. Pub. He.* 11 (11), 11833–11845. doi:10.3390/ijerph111111833

Wu, Z., Zhang, D., Cai, Y., Wang, X., Zhang, L., and Chen, Y. (2017). Water Quality Assessment Based on the Water Quality index Method in Lake Poyang: The Largest Freshwater lake in China. *Sci. Rep.* 7 (1), 17999–18008. doi:10.1038/s41598-017-18285-y

Yao, X., Zhang, L., Zhang, Y., Du, Y., Jiang, X., and Li, M. (2018). Water Diversion Projects Negatively Impact lake Metabolism: A Case Study in Lake Dazong, China. *Sci. Total Environ.* 613-614, 1460–1468. doi:10.1016/j.scitotenv.2017.06.130

Zhai, S., Hu, W., and Zhu, Z. (2010). Ecological Impacts of Water Transfers on Lake Taihu from the Yangtze River, China. *Ecol. Eng.* 36 (4), 406–420. doi:10.1016/j.ecoleng.2009.11.007

Zhang, Q. (2009). The South-To-North Water Transfer Project of China: Environmental Implications and Monitoring Strategy. *J. Am. Water Resour. As.* 45 (5), 1238–1247. doi:10.1111/j.1752-1688.2009.00357.x

Zhang, X., Wang, G., Tan, Z., Wang, Y., and Li, Q. (2021). Effects of Ecological Protection and Restoration on Phytoplankton Diversity in Impounded Lakes along the Eastern Route of China's South-To-North Water Diversion Project. *Sci. Total Environ.* 795, 148870. doi:10.1016/j.scitotenv.2021.148870

Zhang, X., Zou, R., Wang, Y., Liu, Y., Zhao, L., Zhu, X., et al. (2016). Is Water Age a Reliable Indicator for Evaluating Water Quality Effectiveness of Water Diversion Projects in Eutrophic Lakes. *J. Hydrol.* 542, 281–291. doi:10.1016/j.jhydrol.2016.09.002

Zhong, C., Yang, G., Gao, Y., and Wang, L. (2012). Seasonal Variations of Macrozooplankton Community in Gonghu Bay of Lake Taihu. *J. Hydroecol.* 33 (1), 47–52. (In Chinese). doi:10.3969/j.issn.1003-1278.2012.01.010

Conflict of Interest: The authors declare that the research was conducted in the absence of any commercial or financial relationships that could be construed as a potential conflict of interest.

Publisher's Note: All claims expressed in this article are solely those of the authors and do not necessarily represent those of their affiliated organizations, or those of the publisher, the editors and the reviewers. Any product that may be evaluated in this article, or claim that may be made by its manufacturer, is not guaranteed or endorsed by the publisher.

frontiers in Environmental Science

ORIGINAL RESEARCH
published: 29 October 2021
doi: 10.3389/fenvs.2021.765227

A Framework for Methodological Options to Assess Climatic and Anthropogenic Influences on Streamflow

Yu Zhang[1], Xiufeng Wu[1], Shiqiang Wu[1]*, Jiangyu Dai[1]*, Lei Yu[1]*, Wanyun Xue[1], Fangfang Wang[1], Ang Gao[1] and Chen Xue[2]*

[1]State Key Laboratory of Hydrology-Water Resources and Hydraulic Engineering, Nanjing Hydraulic Research Institute, Nanjing, China, [2]China Energy Investment Corporation Science and Technology Research Institute Co.,Ltd., Nanjing, China

Climate change and human activities are having increasing impacts on the global water cycle, particularly on streamflow. Current methods for quantifying these impacts are numerous and have their merits and limitations. There is a lack of a guide to help researchers select one or more appropriate methods for attribution analysis. In this study, hydrological modeling, statistical analysis, and conceptual approaches were used jointly to develop a methodological options framework consisting of three modules, to guide researchers in selecting appropriate methods and assessing climatic and anthropogenic contributions to streamflow changes. To evaluate its effectiveness, a case study in the Upper Yangtze River Basin (UYRB) of China was conducted. The results suggest that the SWAT-based method is the best approach to quantify the influences of climate change and human activities on streamflow in the UYRB. The comprehensive assessment indicates that climate change is the dominant cause of streamflow changes in the UYRB, and the contribution of climate change, indirect human activities, and direct human activities to streamflow changes is about 7:1:2. The proposed framework is efficient and valuable in assisting researchers to find appropriate methods for attribution analysis of streamflow changes, which can help to understand the water cycle in changing environments.

Keywords: attribution analysis, climate change, human activities, streamflow changes, Upper Yangtze River Basin

OPEN ACCESS

Edited by:
Huiyu Dong,
Research Center for Eco-environmental Sciences (CAS), China

Reviewed by:
Chengji Shen,
Hohai University, China
Zhenduo Zhu,
University at Buffalo, United States

****Correspondence:***
Xiufeng Wu
xfwu@nhri.cn
Shiqiang Wu
sqwu@nhri.cn
Jiangyu Dai
jydai@nhri.cn
Lei Yu
yulei0405@foxmail.com

Specialty section:
This article was submitted to Water and Wastewater Management, a section of the journal Frontiers in Environmental Science

Received: *26 August 2021*
Accepted: *15 September 2021*
Published: *29 October 2021*

Citation:
Zhang Y, Wu X, Wu S, Dai J, Yu L, Xue W, Wang F, Gao A and Xue C (2021) A Framework for Methodological Options to Assess Climatic and Anthropogenic Influences on Streamflow. Front. Environ. Sci. 9:765227. doi: 10.3389/fenvs.2021.765227

INTRODUCTION

Streamflow is one of the most important elements of the hydrological cycle and is key to understanding hydrological processes at various spatial and temporal scales under changing environments (Penny et al., 2020; Jiang et al., 2021; Porter et al., 2021; Wright et al., 2021). However, streamflow has been significantly altered by the combined effects of climate change and human activities (Liu et al., 2019; Yasarer et al., 2020; Zeng et al., 2021). Changes in two important climatic variables, precipitation, and potential evapotranspiration, jointly influence the spatial and temporal distribution patterns of water resources (Borgwardt et al., 2020). The sixth assessment report of the IPCC (Intergovernmental Panel on Climate Change) notes that global mean precipitation and evaporation increase with global warming (high confidence). This will undoubtedly accelerate the change in streamflow. Human activities, including land use/land

cover changes, water consumption, urbanization, and dam construction, have also altered hydrological processes in many areas (Zhao et al., 2012; Jardim et al., 2020). It is worth noting that streamflow changes may have a significant impact on water use patterns in different sectors such as agriculture, domestic, industry, environment, and hydropower generation (Zhang et al., 2021b). Therefore, it is important to clarify streamflow changes and their drivers for water resources management under the changing environment.

The existing common methods used to quantitatively estimate the impacts of climate change and human activities on streamflow can be grouped into three categories: hydrological modeling, statistical analysis, and conceptual approaches (Wang, 2014; Dey and Mishra, 2017). The hydrological modeling method is based on various hydrological models, such as SWAT (Soil and Water Assessment Tool) model, GBHM (Geomorphology-Based Hydrological Model), and VIC (Variable Infiltration Capacity) model, to simulate the runoff process in a watershed and then analyze the influences of climate change and human activities on streamflow (Dey and Mishra, 2017; Hajihosseini et al., 2020). For instance, Zhang et al. (2021a) employed SWAT to evaluate the impacts of climate change and human activities on streamflow changes in the Upstream Yangtze River. The results showed that the main contributions to runoff change are 70% from climate change and 30% from human influence. However, the uncertainty introduced by the parameter estimations, structure, and input data of the model may lead to inaccurate results.

Statistical analysis methods are based on the observed streamflow and meteorological factors, and the contributions of meteorological factors to streamflow changes are calculated by statistical analysis, which requires a certain length of the observations series, and usually the longer the series, the better the results are obtained (Wang, 2014; Dey and Mishra, 2017). The common methods include multiple regression models and climate elasticity models, which have been widely applied in many case studies (Miao et al., 2011; Li et al., 2014). For instance, Zhang et al. (2020) used the simple linear regression method and sensitivity indicator method to separate impacts of climate variabilities and human activities on streamflow changes in a typical semi-arid basin (Guanting River Basin in China). Nevertheless, these methods have certain limitations. For example, multiple regression models cannot capture the nonlinear characteristics of streamflow changes, and climate elasticity models cannot quantify the effects of extreme hydroclimatic variability and human activities on streamflow changes.

The conceptual approaches mainly include those based on the Budyko framework and those based on the Tomer Schilling framework. The former uses estimated precipitation and potential evapotranspiration elasticity to assess the impact of climate change on streamflow changes, which has certain physical mechanisms, while the calculation is relatively simple and convenient, and is widely used (Li et al., 2020; Todhunter et al., 2020; Wang et al., 2020). For example, Liu et al. (2021) used the Budyko framework for attribution analysis of global runoff changes and found that other factors than precipitation and potential evaporation are the most significant drivers to global streamflow changes based on observed data. Tomer and Schilling (2009) proposed a conceptual approach that can distinguish the relative contributions of climate change and human activities to the streamflow changes based on a 25-years experiment in a small watershed, namely the Tomer Schilling framework. This method can only distinguish the relative contribution of climate change and human activities, and requires more data on precipitation and actual evapotranspiration (Wang, 2014). Also, Renner et al. (2012) noted that the method does not adhere to the water and energy limits. Thus, this method is not as widely used as the former.

As mentioned above, each method has its merits and limitations. Therefore, it is more valuable to combine and compare the results of multiple methods than a single method. At present, few studies have sorted out and integrated these methods and analyzed and identified the attribution of streamflow changes in the form of a framework. For instance, Wang (2014) compared currently-used methods to analyze the attribution of streamflow changes, assess assumptions and issues of the methods and provided a framework for gauged watersheds. However, the framework is limited to watersheds with negligible groundwater loss, and there is no application case. Also, Zhang et al. (2020) proposed a comprehensive assessment framework, including six Budyko-framework-based methods, hydrological simulation, sensitivity indicator method, and empirical statistics, to separate impacts of climate variability and human activity on streamflow. The difference between the ten attribution methods varied between 5 and 12% in their study, which showed that the multi-method framework can effectively avoid overestimation/underestimation and quantitative uncertainty. However, some of the methods involved in the framework may be inappropriate for some basins, which may easily lead to inaccurate evaluation. Moreover, the methods for attribution analysis of streamflow changes have some criteria and assumptions, which undoubtedly limit their generality (Dey and Mishra, 2017). Therefore, it is crucial to choose a suitable method for attribution analysis of streamflow changes.

Therefore, the main aim of this study is to propose a methodological options framework based on hydrological modeling, statistical analysis, and conceptual approach, which is to guide researchers in selecting appropriate methods and comprehensively assessing the impacts of climate change and human activities on streamflow. Specifically, the framework includes three modules: data preparation (Module Ⅰ), streamflow changes analysis and key driver identification (Module Ⅱ), and attribution analysis method selection and comprehensive assessment (Module Ⅲ). Also, the Upper Yangtze River Basin (UYRB) of China was taken as a case study to confirm the effectiveness of the proposed framework. The rest of this paper is organized as follows. ***Methodology*** clarifies the details of methods, including the proposed framework, fundamental techniques, and critical criteria and assumptions. ***Case Study*** provides the details of the case study. ***Results*** shows the results of the streamflow changes and their attribution analysis. ***Discussion*** discusses the results of the three

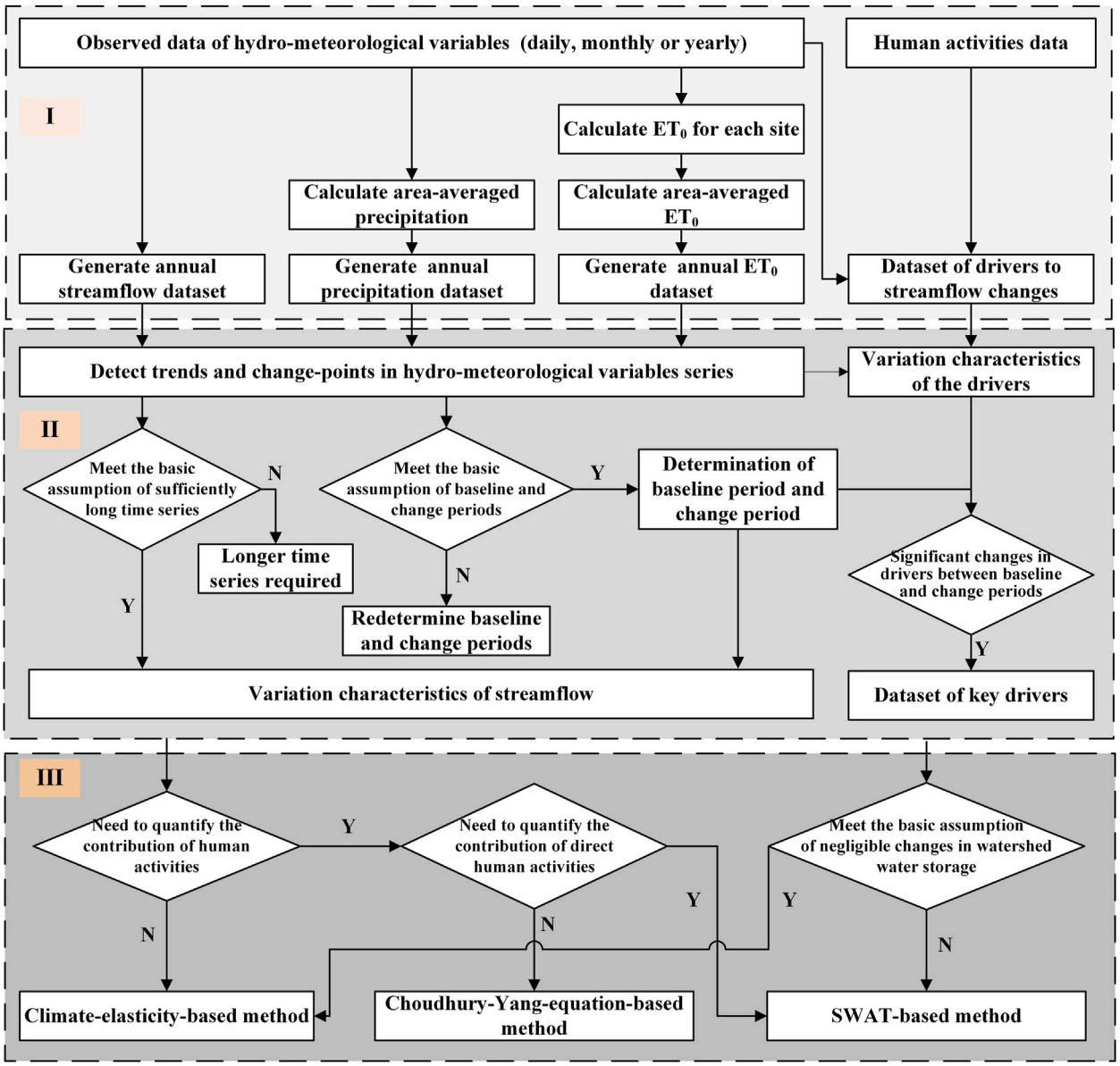

FIGURE 1 | Flowchart of the framework for methodological options to assess climatic and anthropogenic influences on streamflow.

methods and the implications of the proposed framework. Finally, ***Conclusion*** presents the conclusions of this study, summarizing the results of the comprehensive analysis and significance of the framework.

METHODOLOGY

Overview of the Framework

In this study, we proposed a framework for methodological options to assess climatic and anthropogenic influences on streamflow (**Figure 1**), which is mainly composed of three modules: (I) data preparation, (II) streamflow change analysis and key driver identification, and (III) attribution analysis method selection and comprehensive assessment.

Data Preparation

First, hydro-meteorological data of the study area were collected. Reference evapotranspiration (ET_0) is calculated for each meteorological station by the Penman-Monteith equation recommended by FAO (Food and Agriculture Organization), and the area-averaged precipitation and ET_0 are calculated. The streamflow dataset, precipitation dataset, and ET_0 dataset of the study area are constructed. At the same time, data on human activities were also collected and combined with data on meteorological elements to form a dataset regarding the drivers of streamflow changes.

Streamflow Change Analysis and Key Driver Identification

First, based on the dataset of streamflow, precipitation and ET_0 generated in Module I, time series analysis methods were used to clarify the trends in streamflow and other water cycle elements in the study area, and check whether the streamflow changes have a major abrupt change point, and whether the critical assumption of "time series is long enough" is satisfied, if not, it is considered that a longer time series is needed to assess climatic and anthropogenic influences on streamflow, but if it is satisfied, the steps continue. Second, the study period is divided into base period and change period according to the main abrupt change point of streamflow. Trends in streamflow, precipitation, ET_0 before the abrupt change point are tested to check whether the critical assumption of "base period and change period" is met, if not, the abrupt change point is considered to be lagging behind and needs to be re-divided into base and change periods, if it is met, two sub-periods are determined and the basin streamflow changes in the two sub-periods are calculated. Third, the drivers are analyzed for significant changes between the base and change periods, and the drivers with significant changes are selected to form the key driver set.

Attribution Analysis Method Selection and Comprehensive Assessment

In this study, the SWAT-based method, climate-elasticity-based method and Choudhury-Yang-equation-based method were selected as representatives of the hydrological modeling methods, conceptual methods and statistical methods, respectively. First, based on the research needs and identified key drivers, it is determined whether quantitative assessment of anthropogenic contributions is required; if not, then the climate-elasticity-based method is sufficient, and if so, then the Choudhury-Yang-equation-based or SWAT-based method is selected. Second, to determine whether the quantitative assessment for contributions of direct human activities is needed, if not, the Choudhury-Yang equation-based method is satisfied, if needed, the SWAT-based method is selected. Third, to determine whether the study basin satisfies the assumption of "negligible change in water storage", if not, the SWAT-based method is selected, and if so, the climate-elasticity-based method and Choudhury-Yang-equation based can be used.

Basic Methods

Time Series Analysis Methods

In this framework, time series analysis was used to detect the temporal trends and abrupt changes in hydro-meteorological series. Since different statistical methods may produce different results, four time series analysis methods were selected in this study, *i.e.*, the Mann-Kendall test (Mann, 1945; Kendall, 1975), the Spearman's Rho test (Lehmann, 1975), the Pettitt's test (Pettitt, 1979), the sequential clustering method (Dubes and Jain, 1980). The non-parametric Mann-Kendall test is highly recommended by the WMO (World Meteorological Organization) and widely used to detect monotonic trends in long-term hydro-meteorological variations. The Spearman's Rho test is a quick and simple test to determine whether correlation exists between two sub-series in the same series of observations. Both the Mann-Kendall test and the Spearman's Rho test are used to identify trends in hydro-meteorological series and evaluate the significance of the trends. The non-parametric Pettitt's test, same as the Mann-Kendall test, is a rank-based and distribution-free test. It is used to identify the occurrence of an abrupt change point in hydro-meteorological series. The sequential clustering method is used to detect the abrupt change point as a reconfirmation for Pettitt's test in this study.

Attribution Analysis Methods

Generally, the study period is divided into two sub-periods based on historical streamflow changes, i.e., baseline period and change period. The baseline period is affected by the changing environment to a negligible extent, and streamflow is in a natural or quasi-natural state. The streamflow during the change period, on the other hand, is affected by climate change and human activities, and undergoes significant changes under the influence. Based on this, the principles of the currently used attribution analysis methods can be summarized as follows:

$$\Delta R = \overline{R}_{ap} - \overline{R}_{bp} = \Delta R^C + \Delta R^H \tag{1}$$

$$\Delta R^C = \overline{R}^C_{ap} - \overline{R}_{bp} \tag{2}$$

$$\Delta R^H = \overline{R}^H_{ap} - \overline{R}_{bp} \tag{3}$$

where ΔR is the streamflow change; $\overline{R}_{ap}$ is the average annual streamflow during change period; $\overline{R}_{bp}$ is the average annual streamflow during baseline period. The streamflow change is considered to be caused by the combined effects of climate change and human activities, and their contributions are denoted as ΔR^C and ΔR^H. $\overline{R}^C_{ap}$ and $\overline{R}^H_{ap}$ are the average annual streamflow during change period influenced by climate change only and by human activities only. The contributions of climate change and human activities to streamflow change are estimated by $\overline{R}^C_{ap}$ and $\overline{R}^H_{ap}$ minus the average annual streamflow during baseline period $\overline{R}_{bp}$.

Equations 1–3 are the general ideas of attribution analysis methods, which are realized in different ways in different methods. The climate-elasticity-based method, Choudhury-Yang-equation-based method and SWAT-based method are used in this study to further clarify the implementation of the basic ideas of attribution analysis.

1) Climate-elasticity-based method

The climate elasticity model (Schaake, 1990) is a classical approach that was originally proposed to estimate the effect of only one driver (*i.e.*, precipitation) on streamflow, and the model can be expressed as:

$$\frac{\Delta R_i}{\overline{R}} = \varepsilon^p_R \frac{\Delta P_i}{\overline{P}} \tag{4}$$

where ΔR_i and ΔP_i are the deviations of streamflow and precipitation in the i^{th} year from the average annual value $\overline{R}$

and $\overline{P}$. ε_R^P is the elasticity coefficient of streamflow with respect to precipitation.

After this, a two-parameter model incorporating precipitation and temperature (Fu et al., 2007) was proposed and can be expressed as:

$$\frac{\Delta R_i}{\overline{R}} = \varepsilon_R^P \frac{\Delta P_i}{\overline{P}} + \varepsilon_R^T \frac{\Delta T_i}{\overline{T}} \tag{5}$$

where ΔT is deviations of temperature in the i^{th} year from the average annual value $\overline{T}$. ε_R^T is the elasticity coefficient of streamflow with respect to temperature.

Later, more meteorological factors were introduced and climate elasticity models with more parameters were established (Yang and Yang, 2011). After fitting the elasticity coefficients based on long series of observations, the contribution of each meteorological factor can be estimated. It can be seen that the more complete and longer the long series of observations of streamflow and each meteorological factor, the better the fitting effect and the more accurate the attribution analysis results.

2) Choudhury-Yang-equation-based method

The Budyko hypothesis (Budyko, 1974) can be expressed as the following equation:

$$\frac{E}{P} = F(E_0/P) \tag{6}$$

where E is the average annual actual evapotranspiration for a basin; P is the average annual precipitation; E_0 is the average annual potential evapotranspiration.

The function $F(\cdot)$ in **Eq. 6** is considered to have a general expression, and many scholars have proposed formulas without parameters, with one parameter or with two parameters. Among them, the Choudhury-Yang equation (Yang et al., 2008) is able to describe the interactions between climate, hydrology and watershed with the following expression:

$$E = \frac{PE_0}{\left(P^n + E_0^n\right)^{1/n}} \tag{7}$$

where n is a parameter related to the land surface. Using $E = P - R$ to estimate the E, n can be calculated from E, P and E_0.

For a closed watershed, the change in the multi-year average water storage can be neglected, and the long-term water balance can be expressed as:

$$R = P - E \tag{8}$$

The streamflow can be written as a function of precipitation (P), potential evapotranspiration (E_0) and land surface parameter (n):

$$R = f(P, E_0, n) \tag{9}$$

Further the streamflow change can be written in the following differential form:

$$dR = \frac{\partial f}{\partial P} dP + \frac{\partial f}{\partial E_0} dE_0 + \frac{\partial f}{\partial n} dn \tag{10}$$

$$\frac{dR}{R} = \left(\frac{\partial f}{\partial P}\frac{P}{R}\right)\frac{dP}{P} + \left(\frac{\partial f}{\partial E_0}\frac{E_0}{R}\right)\frac{dE_0}{E_0} + \left(\frac{\partial f}{\partial n}\frac{n}{R}\right)\frac{dn}{n} \tag{11}$$

$$\frac{dR}{R} = \varepsilon_P \frac{dP}{P} + \varepsilon_{E_0}\frac{dE_0}{E_0} + \varepsilon_n \frac{dn}{n} \tag{12}$$

where $\varepsilon_P = \frac{\partial f}{\partial P}\frac{P}{R}$, $\varepsilon_{E_0} = \frac{\partial f}{\partial E_0}\frac{E_0}{R}$, $\varepsilon_n = \frac{\partial f}{\partial n}\frac{n}{R}$ are elasticity coefficients of precipitation, potential evapotranspiration and land surface parameter.

Finally, the contributions of drivers to streamflow change are estimated as follows:

$$\Delta R_p = \varepsilon_P \frac{R}{P}\Delta P \tag{13}$$

$$\Delta R_{E_0} = \varepsilon_{E_0}\frac{R}{E_0}\Delta E_0 \tag{14}$$

$$\Delta R_n = \varepsilon_n \frac{R}{n}\Delta n \tag{15}$$

where ΔR_p, ΔR_{E_0}, ΔR_n are the contributions of precipitation P, potential evapotranspiration E_0 and land surface parameter n; ΔP, ΔE_0, Δn are the differences between the three drivers in the baseline period and the change period.

3) SWAT-based method

SWAT (Arnold et al., 1998) is a widely used, physically based distributed hydrological model for simulating surface streamflow, groundwater discharge, evapotranspiration, soil water content (Zhang et al., 2021a). It and has been certified as an effective tool for evaluating water resources at a wide range of scales. A two-driver example is given to clarify the implementation of the basic ideas of attribution analysis in the SWAT-based method.

The driving factors are first identified as climate change and human activities, which are expressed as C and H respectively, while the model inputs are abbreviated as C and H. The streamflow output of the model is written as a function of C and H. Then the streamflow change can be expressed in the form of **Eq. 1** as:

$$\Delta W = \overline{W_{(C_{ap},H_{ap})}} - \overline{W_{(C_{bp},H_{bp})}} = \Delta W^C + \Delta W^H \tag{16}$$

where ΔW is the streamflow change; $\overline{W_{(C_{ap},H_{ap})}}$ and $\overline{W_{(C_{bp},H_{bp})}}$ are the average annual streamflow simulated by SWAT during the change period and baseline period; ap and bp represent the change period and baseline period; C_{ap} and H_{ap} are the model inputs of climate and human activities during the change period; C_{bp} and H_{bp} are the model inputs of climate and human activities during the baseline period.

Contributions of climate change and human activities to streamflow change can be expressed in the form of **Eqs 2**, **3** as

$$\Delta W^C = \overline{W_{(C_{ap},H_{ap})}} - \overline{W_{(C_{bp},H_{bp})}} \tag{17}$$

$$\Delta W^H = W\left(\bar{C_{ap}}, H_{ap}\right) - W\left(\bar{C_{ap}}, H_{bp}\right) \tag{18}$$

where $W_{(\bar{C_{ap}},H_{bp})}$ is the average annual streamflow simulated with model inputs of climate during the baseline period and human activities during the change period.

Critical Criteria and Assumptions

Baseline Period and Change Period

The assumption that "the study period can be divided into a baseline period and a change period" is used in all the above three methods. It assumes streamflow is in a natural or quasi-natural state during the baseline period and undergoes significant changes during the change period because of the influence of climate change and human activities. Determining the baseline period and change period is the first step in attribution analysis. The time series analysis was used to detect the abrupt change point of the streamflow series, and the sub-period before the abrupt change point is recognized as the baseline period, and the sub-period after the abrupt change point is recognized as the change period. Commonly used methods include double cumulative curve, Pettitt test, Mann-Kendall test, sliding *t*-test, ordered clustering, *etc*. Two problems may arise when using the abrupt change point in streamflow to divide the base period and the change:

1) The abrupt change point in streamflow is later than the cut-off point between the baseline period and the change period. This occurs because human activities and climate change have opposite effects on the increase or decrease in streamflow between the cut-off point and the abrupt change, which cancel each other out at a certain statistical confidence level. From the general knowledge of water cycle, there should be no obvious trend of streamflow, precipitation and potential evapotranspiration in the natural period of a basin. Therefore, the accuracy of the baseline period determination is verified by detecting the trend of streamflow, precipitation and potential evapotranspiration in the baseline period.
2) For sufficiently long streamflow series, the time series analysis sometimes detects multiple abrupt change points, which are then divided into two cases: (a) Several abrupt change points with relatively low confidence level are detected after a major one. In this case, only the main abrupt change point is selected. (b) Multiple abrupt change points are scattered over the study period and it is difficult to determine which is the major one. In this case, the abrupt change points near the beginning and end of the study period are not included in the reliable points because the uncertainty is too large. The remaining points are filtered out one by one according to the streamflow changes or precipitation and potential evapotranspiration changes during sub-periods to find the major abrupt change point.

Impacts of Human Activities

At the watershed scale, human activities can be grouped into two categories: 1) human activities that directly affect streamflow (direct human activities), such as off-channel water use, damming, reservoir storage and discharge, and other activities that act directly on streamflow and have an immediate impact on streamflow once they are implemented. Direct human activities can increase or decrease streamflow, and for a single activity, the effect on streamflow is obvious and can be measured directly. However, as watersheds become larger and river systems increase, direct human activities will become more complex and difficult to observe comprehensively. 2) Human activities that indirectly affect streamflow (indirect human activities), such as land use change, soil and water conservation, urbanization, etc. The impact of an individual indirect human activity on the increase or decrease of streamflow is not obvious for a short duration, and usually needs to be accumulated for a certain period to produce a measurable impact. As the watershed grows larger, the impact of indirect human activities is instead more easily estimated with the help of remote sensing and other technical means.

The climate-elasticity-based method is only able to calculate the contribution of climate change to streamflow change. If the streamflow change minus climatic contribution is attributed to anthropogenic contribution, then the anthropogenic contribution contains an error term, and it is not able to distinguish between contributions of direct and indirect human activities. The Choudhury-Yang-equation-based method attributes streamflow changes exclusively to precipitation, potential evapotranspiration and land surface coefficient, i.e., to climate change and indirect human activities. The SWAT model allows for reservoirs and water extraction points in addition to inputs such as climate, soil, and land use. Therefore, the SWAT-based method is able to assess the effects of climate change, indirect human activities and direct human activities on streamflow. When the method is applied to a large watershed, the direct human activities are always too complex, so streamflow change minus contributions of climate change and indirect human activities is attributed to the effects of direct human activities, but an error term is included.

Length of Time Series

All three methods implicitly assume the length of the time series. That is, it is assumed that "the time series of streamflow is long enough". 1) The time series is long enough to include natural or quasi-natural period and periods of change, and to include natural and changing characteristics of streamflow. 2) It is long enough to distinguish between gradual and abrupt changes in streamflow, to detect the points of abrupt change, and to identify changes in climatic elements. 3) It is sufficient to reflect the impact of indirect human activities on streamflow. In practice, for a watershed where streamflow is influenced by changing environment, a streamflow series is considered long enough for attribution analysis if it can be detected with significant trend changes and abrupt change points. Therefore, analyzing the characteristics of streamflow changes, detecting the abrupt change points, and analyzing the characteristics of driver changes are also tests of the assumption that the time series length is sufficiently long. In addition, as far as the attribution analysis method is concerned, the time series length is long enough to facilitate the establishment of a mapping relationship between driving factors and streamflow, thus making the attribution analysis more accurate.

Changes in Watershed Water Storage

The Choudhury-Yang-equation-based method uses a simplified water balance equation for a watershed (**Eq (8)**. The simplified

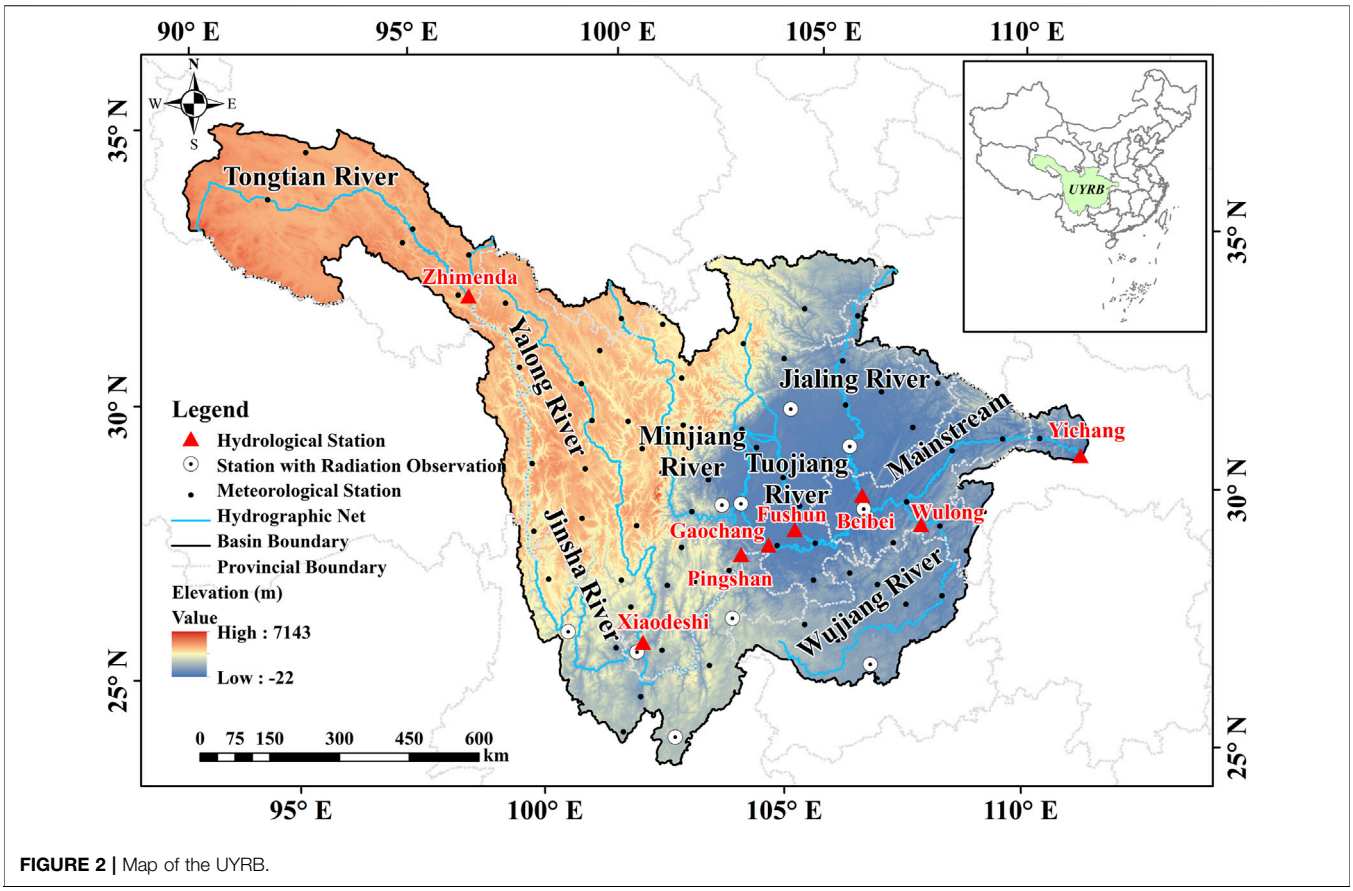

FIGURE 2 | Map of the UYRB.

water balance equation is based on the assumption that "the change in the multi-year average water storage in a closed watershed is negligible". However, if there is a significant decrease in streamflow and an increase in water storage in a study basin, attribution analysis under this assumption tends to exaggerate the contribution of climate change and underestimate the impact of human activities, while other cases may also produce biased attribution results. The climate-elasticity-based method aims to establish statistical relationships between streamflow and drivers. The watershed water storage is difficult to measure directly, so the climate-elasticity-based method is not able to take into account changes in water storage. As the SWAT model takes into account the watershed water storage and deep groundwater loss, the SWAT-based method can estimate the influence of changes in watershed water storage.

CASE STUDY

Study Area

The Upper Yangtze River Basin (UYRB) was selected as a case study area to quantify the contributions of climate change and human activities to its streamflow changes and confirm the effectiveness of the proposed framework. The Yangtze River is the longest river in Asia and the third-longest river in the world. The average annual streamflow of the Yangtze River is 996 km^3, making up 36% of the total streamflow in China, and the hydropower generation accounts for about 40% of the national total. The UYRB is located in the region between 90 and 112°E and 23 and 35°N, with a total area of 1 million km^2 (**Figure 2**). The UYRB is the streamflow formation area and hydropower storage area of the Yangtze River, accounting for 45% of basin water resources and 90% of basin hydropower resources (with a developable installed capacity of about 20×10^8 kW). It has a mean annual temperature of 16.8°C, mean annual precipitation of 1,130 mm. However, measured streamflow in most regions of the UYRB has been decreasing heavily in recent years, which greatly impacts economic development, social stability, and ecological security (Zhang et al., 2018). Therefore, it is necessary to conduct an attribution analysis of the streamflow changes in the basin.

Data Processing (Module I)

Daily streamflow series (1951–2013) from hydrological stations located at the mainstream and important tributaries (**Figure 2**) were collected from the China Annual Hydrological Reports. Meteorological data were collected from the National Meteorological Information Centre of China (NMIC), including daily observations of precipitation, air temperatures, relative humidity, wind speed, and sunshine duration for the period from 1951 to 2013. The topography is represented using the digital elevation model (DEM) with a spatial resolution of

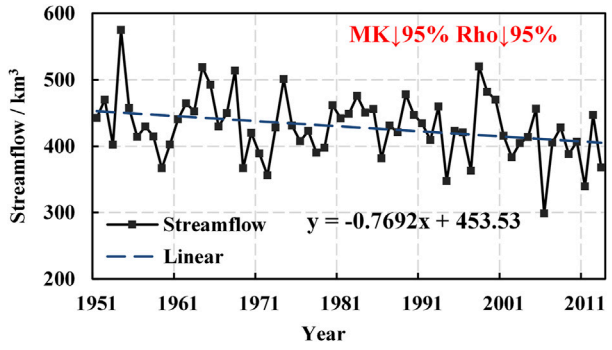

FIGURE 3 | Annual streamflow series observed in Yichang station (Note: ↓ represents decreasing trend; 95% represents a confidence level of 95%).

90 m, which was obtained from the Consultative Group on International Agricultural Research (CGIAR) Consortium for Spatial Information (CGIAR-CSI) (http://srtm.csi.cgiar.org). Geological characteristics data includes land use/cover data and soil type data. Land use/cover maps with a scale of 1: 100000 for 1980, 1990, 1995, 2000, 2005, 2010, and 2013 were collected from the Data Center for Resources and Environmental Sciences, Chinese Academy of Sciences (RESDC) (http://www.resdc.cn). ET_0 was calculated for each meteorological station by the FAO Penman-Monteith equation. The solar radiation was calculated using the Angstrom formula (Wang et al., 2021), in which the Angstrom coefficients were estimated by the measured radiation within the UYRB (**Figure 2**). The area-averaged precipitation and ET_0 were further calculated. The streamflow dataset, precipitation dataset, and ET_0 dataset of the UYRB were constructed and combined with data on human activities to form a dataset on the drivers of streamflow changes. At this point the data preparation in Module I is complete.

RESULTS

Long-Term Trend and Change in Streamflow (Module II)

Yichang station is the control station for the entire UYRB. Streamflow series observed in the Yichang station reflects the general characteristics of streamflow changes in the UYRB. The observed annual streamflow series of Yichang station is shown in **Figure 3**. It is clear that streamflow in the UYRB decreased by a rate of $-0.77\ km^3$ per year during 1951–2013. The long-term trend in streamflow and its significance were identified by the Mann-Kendall test and the Spearman's Rho test. Results obtained from the two methods are consistent, revealing a significant downward trend (at the 95% confidence level) in streamflow in the UYRB during the study period. A more detailed description and analysis of the spatio-temporal variability of streamflow can be found in our previous study (Zhang et al., 2021a).

The change point in streamflow series was identified by the Pettitt's test and the sequential clustering method. Both methods show that the abrupt change point of observed annual streamflow series at Yichang station occurred in 1993at 95% confidence level. More detailed results and analysis of the abrupt change can also be found in our previous study (Zhang et al., 2021a). According to the change point in streamflow series, the study period can be divided into two sub-periods (i.e., 1951–1993 and 1994–2013).

For baseline period determination, the changes of streamflow, precipitation and ET_0 during 1951–1993 were detected by Mann-Kendall test. The results indicate that there are no obvious changes in streamflow, precipitation or ET_0 series during the first sub-period (**Table 1**). Therefore, the basic assumption of "baseline period and change period" is valid. The sub-period 1951–1993 is confirmed as the baseline period and the sub-period 1994–2013 is determined as the change period.

Meanwhile, the mean value, standard deviation (SD) and coefficient of variation (CV) of the hydro-meteorology series in the baseline and change periods were separately calculated and listed in **Table 1**. Compared with the baseline period, the average annual streamflow in the change period decreased by 8.4%. A statistically significant difference can be found between the mean values of the annual streamflow for the two periods at the 95% confidence level, while the difference between the SD or CV is not statistically significant. Differences at the 95% confidence level are also found between the means of the precipitation and ET_0 series for the two periods. No statistically significant differences are found between the SD and CV of the precipitation and ET_0 series for the two periods. At this point in the analysis, it can be concluded that the hydro-meteorology series of the UYRB from 1951 to 2013 meets the two basic assumptions of "baseline period and change period" and "sufficient length of time series". In this case study, the SWAT-based method, climate-elasticity-based method and Choudhury-Yang-equation-based method are all applicable.

Driving Factors Identification (Module II)

Precipitation, evapotranspiration and streamflow are the basic elements of the water cycle. Precipitation is the water income item and evapotranspiration is the output item. Actual evapotranspiration is influenced by available water (i.e., precipitation, land surface conditions) on the one hand, and available energy (i.e., potential evapotranspiration) on the other. The potential evapotranspiration is mainly influenced by meteorological factors such as maximum temperature (Tmax), minimum temperature (Tmin), wind speed (WS), relative humidity (RH), sunshine hour (SH). In addition, streamflow is also influenced by indirect human activities such as land use/cover change (LUCC) and direct human activities. Therefore, P, Tmax, Tmin, RH, SH, WS, and LUCC data were initially selected to form the drivers of streamflow changes in Module I. It is noted that the direct human activities in the UYRB are too complex to collect detailed information. In this case study, the contribution of direct human activities was estimated by subtracting the contribution of other drivers from the total streamflow change.

In order to identify the key driving factors of streamflow change in the drivers dataset in Module I. The mean value of each meteorological factor in baseline period and change period were calculated and listed in **Table 2**. The *t*-test was used to detect differences of meteorological factors for the two periods.

TABLE 1 | Characteristics of the streamflow, precipitation and ET_0 series in the UYRB before and after change point (Note: – represents a confidence level lower than 80%).

Hydro-meteorology series	Sub-period 1951–1993				Sub-period 1994–2013			Change of mean
	Trend	Mean	SD	CV	Mean	SD	CV	
Streamflow/km^3	–	438.2	42.7	0.10	401.2	44.7	0.11	–37.0
Precipitation/mm	–	999.9	72.1	0.07	954.8	63.1	0.07	–45.1
ET_0/mm	–	1436.9	41.5	0.03	1479.0	50.8	0.03	42.1

TABLE 2 | Mean values of the meteorological factors in the UYRB for baseline period and change period.

Driving factors	Baseline period (1951–1993)	Change period (1994–2013)	Change of mean
P/mm	999.9	954.8	–45.1
Tmax/°C	17.9	18.6	0.7
Tmin/°C	7.5	8.1	0.6
RH/%	70.3	68.4	–1.9
SH/h	1754.1	1718.1	–36.0
WS/m·s–^{1}	1.8	1.6	–0.2

Differences at 99% confidence level are found between the mean values of P, Tmax, Tmin, WS, and RH for the two periods. Difference is not obvious in SH. Therefore, P, Tmax, Tmin, WS, and RH were selected as the meteorological driving factors. During the study period, land use/cover in the UYRB underwent obvious changes. As an indirect human activity, LUCC was also selected as a driver. Detailed description of LUCC can be found in our previous study (Zhang et al., 2021a).

Climatic and Anthropogenic Contributions to Streamflow Change (Module III)

Based on the judgments in Module III, it is clear that the SWAT-based method is the best method for assessing climatic and anthropogenic influences on streamflow in the UYRB, because it is capable of assessing the effects of climate change, indirect human activities and direct human activities on streamflow. The climate-elasticity-based method is the second-best choice, which does not distinguish between direct and indirect human activities. In this case study, the parameter n was not collected and needed to be estimated, so the Choudhury-Yang-equation-based method is the worst option. In this section, the SWAT-based method was selected, supplemented by the other two methods, to conduct a comprehensive attribution analysis. For the purpose of comparison between the three methods, streamflow changes were attributed to climate change, direct human activities, and indirect human activities.

1) SWAT-based method

According to the general steps of the method, the contributions of climate change (ΔW^C), LUCC (ΔW^L) and direct human activities (ΔW^D) can be calculated by the following equations:

$$\Delta W^C = \overline{W_{(C_{ap},L_{bp})}} - \overline{W_{(C_{bp},L_{bp})}} \quad (19)$$

$$\Delta W^C = \overline{W_{(C_{ap},L_{bp})}} - \overline{W_{(C_{bp},L_{bp})}} \quad (20)$$

$$\Delta W^T = \overline{W_{observed,ap}} - \overline{W_{(C_{bp},L_{bp})}} \quad (21)$$

$$\Delta W^D = \Delta W^T - \Delta W^C - \Delta W^L = \overline{W_{observed,ap}} - \overline{W_{(C_{ap},L_{ap})}} \quad (22)$$

where L_{ap} and L_{bp} are the land use inputs during change period and baseline period; ΔW^T is the total streamflow change; $\overline{W_{observed,ap}}$ is the average observed streamflow during change period.

The contributions of climate change, LUCC and direct human activities are listed in **Table 3**. The results suggest that the main contributions to streamflow change are from climatic variabilities (69%), LUCC (10%) and direct human activities (21%). Climate change appears to be the main cause of streamflow change with a contribution of -25.5 km^3.

2) Climate-elasticity-based method

A multi-parameter climate elasticity model was developed with the key driving factors as follows:

$$\frac{dR}{R} = \varepsilon_P \frac{dP}{P} + \varepsilon_{T_{max}} \frac{dT_{max}}{T_{max}} + \varepsilon_{T_{min}} \frac{dT_{min}}{T_{min}} + \varepsilon_{RH} \frac{dRH}{RH} + \varepsilon_{WS} \frac{dWS}{WS} \quad (23)$$

where ε_P, $\varepsilon_{T_{max}}$, $\varepsilon_{T_{min}}$, ε_{RH}, ε_{WS} are elasticity coefficients of the meteorological factors.

The contributions of climate change and human activities to streamflow were listed in **Table 3**. The climatic contribution is –22.6 km^3. The contribution of climate change and human activities to streamflow change is about 7:3.

3) Choudhury-Yang-equation-based method

The elasticity coefficients of precipitation, potential evapotranspiration and land surface parameter were first calculated according to the steps: $\varepsilon_P = 1.68$, $\varepsilon_{E_0} = -0.68$, $\varepsilon_n = -0.69$. The larger the absolute value of the elasticity

TABLE 3 | Climatic and anthropogenic contributions to streamflow changes.

Methods	Climatic contributions		Anthropogenic contributions		Total contributions
SWAT-based	$\triangle W^C$		$\triangle W^L$	$\triangle W^D$	$\triangle W^T$
	−25.5		−3.7	−7.8	−37.0
	(69%)		(10%)	(21%)	(100%)
Climate-elasticity-based	$\triangle W^C$		$\triangle W^H$		$\triangle W^T$
	−22.6		−14.4		−37.0
	(61%)		(39%)		(100%)
Choudhury-Yang-equation-based	$\triangle W^P$	$\triangle W^{E0}$	$\triangle W^n$		$\triangle W^T$
	−32.9	−12.7	7.0		−38.6
	(85%)	(33%)	(−18%)		(100%)
Multiple regression model	$\triangle W^C$		$\triangle W^H$		$\triangle W^T$
	−24.4		−12.6		−37.0
	(66%)		(34%)		(100%)

coefficient of the factor, the more sensitive the streamflow is to it. Thus, precipitation is the dominant factor of streamflow change. The contributions of precipitation, potential evapotranspiration and land surface parameter to streamflow were calculated and listed in **Table 3**.

DISCUSSION

Through the analysis in ***Climatic and Anthropogenic Contributions to Streamflow Change (Module III)***, the results based on the SWAT-based method and climate-elasticity-based method are relatively close, and the contribution of climate change and human activities to the streamflow changes are 7 : 3 and 6 : 4, respectively; where the contribution of climate change is −25.5 and −22.6 km^3, respectively. However, the contribution of climate change based on the Choudhury-Yang-equation-based method is -45.6 km^3, which is significantly larger than the above two methods. The possible reason for this is that n is calculated from precipitation and evapotranspiration.

Here, we used a multiple regression model, the most direct method for attribution analysis of streamflow changes under changing environment, to further verify the contribution of P and E_0 (climate factors) to streamflow changes. The specific expressions are as follows:

$$R = aP + bE_0 + c \tag{24}$$

where R, P and E_0 are streamflow, precipitation, and potential evapotranspiration; a, b and c are regression coefficients.

Based on the precipitation, potential evapotranspiration and streamflow data for the baseline period (1951–1993), the values of a, b and c are 0.426, 0.128, and 128.961 (at the 95% confidence level), respectively, with a correlation coefficient of 0.803. The results of calculating the attribution analysis in the UYRB are shown in **Table 3**. It can be seen that: the contribution of climate change is −24.4 km^3, and the contribution ratio of climate change and human activities to streamflow changes is 6.6 : 3.4, which is close to the results of the SWAT-based method and climate-elasticity-based method. Therefore, comprehensive analysis shows that climate change is the dominant driver of streamflow changes in the UYRB, and the contribution ratio of climate change, indirect human activities, and direct human activities to streamflow changes is about 7 : 1 : 2.

In general, the proposed framework was applied to assess climatic and anthropogenic influences on streamflow changes in the UYRB in this study, indicating that the dominant factor of streamflow changes in the basin from 1951 to 2013 was climate change, which is consistent with previous studies (Lu et al., 2019; Ye et al., 2020; Shao et al., 2021). For example, Wang and Xia (2015) employed water balance model to assess the impacts of climate change and human activities on streamflow changes in the UYRB, finding that 71.43% of streamflow decrease was due to climate change in the basin since 1993. Similarly, Ahmed et al. (2020) noted that climate change played a controlling role in streamflow changes in the UYRB. Recently, Shao et al. (2021) used the water balance equation, double mass curve, and linear regression analysis to quantify the contributions of climate change and anthropogenic activities to streamflow changes in the Jialing River (a main tributary of the upper Yangtze River) during 1960–2017. The results show that climate change had led to a significant reduction in annual streamflow (82.2%).

Different methods of attribution analysis have their own characteristics, limitations, critical criteria and assumptions, which in turn cause large variability and uncertainty in calculation results (Zhang et al., 2020). This is consistent with the findings of this study that the attribution results based on the Choudhury-Yang-equation-based method are significantly different from both the SWAT-based method and climate-elasticity-based method. This further emphasizes the importance of selecting an appropriate methodology to help properly assess the contribution of climate change and human activities to streamflow changes. Therefore, the proposed framework is valuable and effective in helping researchers to select the appropriate method, reduce the uncertainty introduced by the method, and avoid the misperceptions that may result from inappropriate methods. Indeed, the framework has some limitations, which need further research. We chose only one commonly used method as the most representative for the three categories of methods (i.e., hydrological modeling, statistical analysis, and conceptual approaches). However, the calculation

results of different methods in the same category may not be consistent. For instance, Zhang et al. (2020) used six Budyko framework-based methods to estimate the contributions of climate change and human activities to streamflow changes. The results showed that the uncertainty between these methods is about 5–7%.

CONCLUSION

This study aims to provide guidance for the selection of appropriate methods to quantify the climatic and anthropogenic influences on streamflow. Therefore, a method selection framework for attribution analysis was developed using the SWAT-based method, climate-elasticity-based method, and Choudhury-Yang-equation-based method jointly. The proposed framework consists of three modules, namely data preparation (Module Ⅰ), streamflow changes analysis and key driver identification (Module Ⅱ), and attribution analysis method selection and comprehensive assessment (Module Ⅲ). To evaluate its effectiveness, a case study in the UYRB was conducted. Under the framework, a significantly decreasing trend and changes were detected in observed annual streamflow in the UYRB. The study period was divided into a baseline period (1951–1993) and a change period (1994–2013) based on proposed criteria and assumptions. Subsequently, statistical indicators indicated that precipitation, maximum temperature, minimum temperature, wind speed, relative humidity, and LUCC are key drivers of streamflow changes in the UYRB. The analysis in Module Ⅲ indicates that the SWAT-based method is the best approach to assess climatic and anthropogenic influences on streamflow in the UYRB, and the climate-elasticity-based method and Choudhury-Yang-equation-based method are also applicable. The comprehensive attribution analysis suggests that climate change is the dominant cause of streamflow changes in the UYRB, and the contribution of climate change, indirect human activities, and direct human activities to streamflow changes is about 7:1:2. Overall, the proposed framework is efficient and valuable in assisting researchers to find appropriate methods for attribution analysis of streamflow changes under changing environments.

DATA AVAILABILITY STATEMENT

The original contributions presented in the study are included in the article/supplementary material, further inquiries can be directed to the corresponding authors.

AUTHOR CONTRIBUTIONS

All authors listed have made a substantial, direct, and intellectual contribution to the work and approved it for publication.

FUNDING

This work was supported by the National Key R&D Program of China (Grant No. 2018YFE0206200); the Project funded by China Postdoctoral Science Foundation (Grant No. 2019M661884); the Natural Science Foundation of Jiangsu Province, China (Grant No. BK20200160); the Special Research Fund of Nanjing Hydraulic Research Institute (Grant No. Y120006).

REFERENCES

Arnold, J. G., Srinivasan, R., Muttiah, R. S., and Williams, J. R. (1998). Large Area Hydrologic Modeling and Assessment Part I: Model Development. *J. Am. Water Resour. Assoc* 34, 73–89. doi:10.1111/j.1752-1688.1998.tb05961.x

Borgwardt, F., Unfer, G., Auer, S., Waldner, K., El-Matbouli, M., and Bechter, T. (2020). Direct and Indirect Climate Change Impacts on Brown Trout in Central Europe: How Thermal Regimes Reinforce Physiological Stress and Support the Emergence of Diseases. *Front. Environ. Sci.* 8. doi:10.3389/fenvs.2020.00059

Budyko, M. I. (1974). *Climate and Life*. New York: Academic Press, 508.

Dey, P., and Mishra, A. (2017). Separating the Impacts of Climate Change and Human Activities on Streamflow: A Review of Methodologies and Critical Assumptions. *J. Hydrol.* 548, 278–290. doi:10.1016/j.jhydrol.2017.03.014

Dubes, R., and Jain, A. K. (1980). Clustering Methodologies in Exploratory Data Analysis. *Adv. Comput.* 19, 113–228. doi:10.1016/S0065-2458(08)60034-0

Fu, G., Charles, S. P., and Chiew, F. H. S. (2007). A Two-Parameter Climate Elasticity of Streamflow index to Assess Climate Change Effects on Annual Streamflow. *Water Resour. Res.* 43 (11), W11419. doi:10.1029/2007WR005890

Hajihosseini, M., Hajihosseini, H., Morid, S., Delavar, M., and Booij, M. J. (2020). Impacts of Land Use Changes and Climate Variability on Transboundary Hirmand River Using SWAT. *J. Water Clim. Change* 11 (4), 1695–1711. doi:10.2166/wcc.2019.100

Jardim, P. F., Melo, M. M. M., Ribeiro, L. d. C., Collischonn, W., and Paz, A. R. d. (2020). A Modeling Assessment of Large-Scale Hydrologic Alteration in South American Pantanal Due to Upstream Dam Operation. *Front. Environ. Sci.* 8, 567450. doi:10.3389/fenvs.2020.567450

Jiang, S., Zhou, L., Ren, L., Wang, M., Xu, C.-Y., Yuan, F., et al. (2021). Development of a Comprehensive Framework for Quantifying the Impacts of Climate Change and Human Activities on River Hydrological Health Variation. *J. Hydrol.* 600, 126566. doi:10.1016/j.jhydrol.2021.126566

Kendall, M. G. (1975). *Rank Correlation Methods*. London: Griffin.

Lehmann, E. L. (1975). *Nonparametrics, Statistical Methods Based on Ranks*. California: Holden Day.

Li, B., Su, H., Chen, F., Li, H., Zhang, R., Tian, J., et al. (2014). Separation of the Impact of Climate Change and Human Activity on Streamflow in the Upper and Middle Reaches of the Taoer River, Northeastern China. *Theor. Appl. Climatol* 118 (1-2), 271–283. doi:10.1007/s00704-013-1032-8

Li, H., Shi, C., Zhang, Y., Ning, T., Sun, P., Liu, X., et al. (2020). Using the Budyko Hypothesis for Detecting and Attributing Changes in Runoff to Climate and Vegetation Change in the Soft sandstone Area of the Middle Yellow River basin, China. *Sci. Total Environ.* 703, 135588. doi:10.1016/j.scitotenv.2019.135588

Liu, J., You, Y., Zhang, Q., and Gu, X. (2021). Attribution of Streamflow Changes across the globe Based on the Budyko Framework. *Sci. Total Environ.* 794, 148662. doi:10.1016/j.scitotenv.2021.148662

Liu, X., Liu, W., Yang, H., Tang, Q., Flörke, M., Masaki, Y., et al. (2019). Multimodel Assessments of Human and Climate Impacts on Mean Annual Streamflow in China. *Hydrol. Earth Syst. Sci.* 23 (3), 1245–1261. doi:10.5194/hess-23-1245-2019

Lu, C.-h., Dong, X.-y., Tang, J.-l., and Liu, G.-c. (2019). Spatio-temporal Trends and Causes of Variations in Runoff and Sediment Load of the Jinsha River in China. *J. Mt. Sci.* 16 (10), 2361–2378. doi:10.1007/s11629-018-5330-6

Mann, H. B. (1945). Nonparametric Tests against Trend. *Econometrica* 13, 245–259. doi:10.2307/1907187

Miao, C., Yang, L., Liu, B., Gao, Y., and Li, S. (2011). Streamflow Changes and its Influencing Factors in the Mainstream of the Songhua River basin, Northeast China over the Past 50 Years. *Environ. Earth Sci.* 63 (3), 489–499. doi:10.1007/s12665-010-0717-x

Penny, G., Srinivasan, V., Apoorva, R., Jeremiah, K., Peschel, J., Young, S., et al. (2020). A Process-based Approach to Attribution of Historical Streamflow Decline in a Data-scarce and Human-dominated Watershed. *Hydrological Process.* 34 (8), 1981–1995. doi:10.1002/hyp.13707

Pettitt, A. N. (1979). A Non-parametric Approach to the Change-point Problem. *Appl. Stat.* 28 (2), 126–135. doi:10.2307/2346729

Porter, M. E., Hill, M. C., Harris, T., Brookfield, A., and Li, X. (2021). The DiscoverFramework Freeware Toolkit for Multivariate Spatio-Temporal Environmental Data Visualization and Evaluation. *Environ. Model. Softw.* 143, 105104. doi:10.1016/j.envsoft.2021.105104

Renner, M., Seppelt, R., and Bernhofer, C. (2012). Evaluation of Water-Energy Balance Frameworks to Predict the Sensitivity of Streamflow to Climate Change. *Hydrol. Earth Syst. Sci.* 16 (5), 1419–1433. doi:10.5194/hess-16-1419-2012

Schaake, J. C. (1990). "From Climate to Flow," in *Climate Change and U.S.Water Resources*. Editor P. E. Waggoner (New York: JohnWiley), 177–206.

Shao, Y., He, Y., Mu, X., Zhao, G., Gao, P., and Sun, W. (2021). Contributions of Climate Change and Human Activities to Runoff and Sediment Discharge Reductions in the Jialing River, a Main Tributary of the Upper Yangtze River, China. *Theor. Appl. Climatol* 145 (3-4), 1437–1450. doi:10.1007/s00704-021-03682-1

Todhunter, P. E., Jackson, C. C., and Mahmood, T. H. (2020). Streamflow Partitioning Using the Budyko Framework in a Northern Glaciated Watershed under Drought to Deluge Conditions. *J. Hydrol.* 591, 125569. doi:10.1016/j.jhydrol.2020.125569

Tomer, M. D., and Schilling, K. E. (2009). A Simple Approach to Distinguish Land-Use and Climate-Change Effects on Watershed Hydrology. *J. Hydrol.* 376 (1-2), 24–33. doi:10.1016/j.jhydrol.2009.07.029

Wang, M., Zhang, Y., Lu, Y., Gong, X., and Gao, L. (2021). Detection and Attribution of Reference Evapotranspiration Change (1951-2020) in the Upper Yangtze River Basin of China. *J. Water Clim. Change*, jwc2021011. doi:10.2166/wcc.2021.011

Wang, W., Zhang, Y., and Tang, Q. (2020). Impact Assessment of Climate Change and Human Activities on Streamflow Signatures in the Yellow River Basin Using the Budyko Hypothesis and Derived Differential Equation. *J. Hydrol.* 591, 125460. doi:10.1016/j.jhydrol.2020.125460

Wang, X. (2014). Advances in Separating Effects of Climate Variability and Human Activity on Stream Discharge: An Overview. *Adv. Water Resour.* 71, 209–218. doi:10.1016/j.advwatres.2014.06.007

Wright, M. S. P., Santelmann, M. V., Vaché, K. B., and Hulse, D. W. (2021). Modeling the Impact of Development Policies and Climate on Suburban Watershed Hydrology Near Portland, Oregon. *Landscape Urban Plann.* 214, 104133. doi:10.1016/j.lurbplan.2021.104133

Yang, H., and Yang, D. (2011). Derivation of Climate Elasticity of Runoff to Assess the Effects of Climate Change on Annual Runoff. *Water Resour. Res.* 47, W07526. doi:10.1029/2010WR009287

Yang, H., Yang, D., Lei, Z., and Sun, F. (2008). New Analytical Derivation of the Mean Annual Water-Energy Balance Equation. *Water Resour. Res.* 44, W034103. doi:10.1029/2007WR006135

Yasarer, L. M. W., Taylor, J. M., Rigby, J. R., and Locke, M. A. (2020). Trends in Land Use, Irrigation, and Streamflow Alteration in the Mississippi River Alluvial Plain. *Front. Environ. Sci.* 8, 66. doi:10.3389/fenvs.2020.00066

Ye, X., Zhang, Z., Xu, C.-Y., and Liu, J. (2020). Attribution Analysis on Regional Differentiation of Water Resources Variation in the Yangtze River Basin under the Context of Global Warming. *Water* 12 (6), 1809. doi:10.3390/w12061809

Zeng, X., Schnier, S., and Cai, X. (2021). A Data-Driven Analysis of Frequent Patterns and Variable Importance for Streamflow Trend Attribution. *Adv. Water Resour.* 147, 103799. doi:10.1016/j.advwatres.2020.103799

Zhang, K., Ruben, G. B., Li, X., Li, Z., Yu, Z., Xia, J., et al. (2020). A Comprehensive Assessment Framework for Quantifying Climatic and Anthropogenic Contributions to Streamflow Changes: A Case Study in a Typical Semi-arid North China basin. *Environ. Model. Softw.* 128, 104704. doi:10.1016/j.envsoft.2020.104704

Zhang, Y., Wang, M., Chen, J., Zhong, P.-a., Wu, X., and Wu, S. (2021a). Multiscale Attribution Analysis for Assessing Effects of Changing Environment on Runoff: Case Study of the Upstream Yangtze River in China. *J. Water Clim. Change* 12 (2), 627–646. doi:10.2166/wcc.2020.155

Zhang, Y., Yu, L., Wu, S., Wu, X., Dai, J., Xue, W., et al. (2021b). A Framework for Adaptive Control of Multi-Reservoir Systems under Changing Environment. *J. Clean. Prod.* 316, 128304. doi:10.1016/j.jclepro.2021.128304

Zhang, Y., Zhong, P.-a., Wang, M., Xu, B., and Chen, J. (2018). Changes Identification of the Three Gorges Reservoir Inflow and the Driving Factors Quantification. *Quat. Int.* 475, 28–41. doi:10.1016/j.quaint.2016.02.064

Zhao, Q., Liu, S., Deng, L., Dong, S., Yang, J., and Wang, C. (2012). The Effects of Dam Construction and Precipitation Variability on Hydrologic Alteration in the Lancang River Basin of Southwest China. *Stoch Environ. Res. Risk Assess.* 26, 993–1011. doi:10.1007/s00477-012-0583-z

Conflict of Interest: CX was employed by the China Energy Investment Corporation Science and Technology Research Institute Co., Ltd

The remaining authors declare that the research was conducted in the absence of any commercial or financial relationships that could be construed as a potential conflict of interest.

The reviewer CS declared a shared affiliation, with no collaboration, with one of the authors, LY, to the handling editor at the time of the review.

Publisher's Note: All claims expressed in this article are solely those of the authors and do not necessarily represent those of their affiliated organizations, or those of the publisher, the editors and the reviewers. Any product that may be evaluated in this article, or claim that may be made by its manufacturer, is not guaranteed or endorsed by the publisher.

frontiers in Earth Science

ORIGINAL RESEARCH
published: 16 November 2021
doi: 10.3389/feart.2021.739804

Mass Exchange of Water and Soil on the Soil Surface in the Rainfall Splash Erosion

Sun Sanxiang[1,2]*, *Zhang Yunxia*[1] and *Lei Pengshui*[1,2]

[1]School of Environmental and Municipal Engineering, Lanzhou Jiaotong University, Lanzhou, China, [2]Engineering Research Center for Cold and Arid Regions Water Resource Comprehensive Utilization, Ministry of Education, Lanzhou, China

This research aims to unfold the mass exchange mechanism of water and soil on the soil surface in the rainfall splash erosion process. We regard the rainfall splash erosion process as a collision process between the raindrop and the soil particle on the soil interface. This recognition allows us to incorporate research approaches from the spring vibrator model, which has been developed for simulating the impact of liquid drops on solid surface. We further argue that because a same set of factors determine the splash amount and infiltration amount and it is relatively simpler to observe the infiltration amount, an investigation into the relationship between the splash amount and infiltration amount would be able to provide a new channel for quantifying the splash erosion. This recognition leads us to examining the relationship between single raindrop, rainfall kinetic energy and splash erosion from both theoretical and empirical angles, with an emphasis on the relationship between the infiltration amount and the splash erosion. Such an investigation would add value to the collective effort to establish mass exchange law in water-soil interface during rainfall splash erosion. It is found that during the rainfall splash process, the splash erosion is proportional to the rainfall kinetic energy; and has a linear relation to the infiltration amount, with the rainfall intensity as one of important parameters and the slope depending on the unit conversation of the infiltration amount and the splash erosion. If the units of two items are same, the slope is the ratio of the soil and water density, and the splash erosion velocity of the rainfall is half of the rainfall terminal velocity. The single raindrop kinetic energy and the splash erosion have a quadratic parabola relation, and the splash velocity is about 1/3 of single raindrop terminal velocity.

Keywords: rainfall, splash erosion amount, infiltration amount, mass exchange, equivalent spring damping model

OPEN ACCESS

Edited by:
Zhan Tian,
Southern University of Science and Technology, China

Reviewed by:
Kuishuang Feng,
University of Maryland, United States
Jiangyu Dai,
Nanjing Hydraulic Research Institute, China

***Correspondence:**
Sun Sanxiang
sunsanxiang@mail.lzjtu.cn

Specialty section:
This article was submitted to Environmental Informatics and Remote Sensing, a section of the journal Frontiers in Earth Science

Received: *12 July 2021*
Accepted: *13 October 2021*
Published: *16 November 2021*

Citation:
Sanxiang S, Yunxia Z and Pengshui L (2021) Mass Exchange of Water and Soil on the Soil Surface in the Rainfall Splash Erosion. Front. Earth Sci. 9:739804. doi: 10.3389/feart.2021.739804

INTRODUCTION

Rainfall splash is mainly composed of rainfall, infiltration and splash factors. There has been a better understanding of the relationship between rainfall and infiltration than that between rainfall and splash in the literature (Li et al., 2011; Wang et al., 2015). One of the current research trends on the latter relationship is to establish the statistical relationship between splash erosion rate or amount and the characteristics of rainfall and earth surface. Publications in this stream of research use statistical regression and dimension analysis to deal with the experiment data, and some of them apply the force analysis and the momentum theorem without considering the momentum loss (Li et al., 2011). The studies on the relationship between the infiltration amount and the splash erosion are confined into experimental analysis. However, the regression results of such experimental analysis vary with experiment conditions. In addition, the theoretical analysis model of the relation has not yet been

established (Sun, 1997; Wang et al., 2015). There is an urgent need to advance both theoretical and empirical researches about the relationship across the splash erosion, rainfall and infiltration amount, as well as the mechanism of splash erosion mechanics.

It is widely recognized that the splash erosion mainly depends on the characteristics of earth surface and rainfall. The former includes slope, canopy vegetation and soil layer formation, and the latter includes rainfall, rain intensity, rainfall energy, raindrop's diameter, raindrop's velocity and rainfall duration, etc., (Sun, 1997; Wang et al., 2015).

A large number of experimental tests have been done to quantify the relationship between characteristics of earth surface and splash erosion, including studies on the effect of different diameter of aggregate on the loessal soil splash erosion velocity (Hu, 2015); the relationship among the soil initial moisture content, the red earth splash erosion and the moisture content of early stage corresponding to the raindrop splash amount with constant soil bulk density 1.2g/cm3 (Zhao et al., 2003; Ma et al., 2014); the influence of the changing grain size of red earth aggregate on the splash (Ma et al., 2013); the influence of purple soil, loess and chernozen soil crust on the splash, and the time history of the splash erosion (Bu et al., 2014); and the influence of bulk density, porosity, angle of internal friction, cohesion, and the soil particle size distribution on splash erosion rate after mixing different quality of silty clay, sand clay and sand (Wei et al., 2015). In the case of calcareous soil surface, compared with the influences caused by shear strength (SS), mean weight diameter (MWD), organic matter (OM), calcium carbonate, clay content, silt and sand fraction estimation, Saedi et al. (2016)argue that SS, MWD are the key indicators of the splash erosion. Based on the monitoring data of natural rainfall splash erosion across different soil types in NE Spain, Angulo et al. (2012)find that the splash erosion has little difference across different soil types.

Similarly, there also a large body of empirical researches to assess the influence of rainfall characteristics on the splash erosion. For example, based on indoor artificial rainfall experiments, Yin et al. (2011) regress the raindrop splash erosion on distance, the surface layer thickness, and raindrop kinetic energy and find that the kinetic energy increases with the splash erosion amount; Zheng et al. (2016) established statistical relationships between disturbance water-course thickness and sediment splash erosion under the condition of single and multiple raindrop splash with different soil types such as soil, loess and chernozen soil. Based on outdoor artificial rainfall experiments, Cheng et al. (2015) showed that the fine sand with the grain diameter 0.05–0.2 mm was most vulnerable to splash erosion, while the small size with the grain diameter less than 0.002 mm and the large size with the grain diameter larger than 0.2 mm were not easy to be splashed. They drawed conclusion that the splash erosion amount had an exponential relationship with the rainfall intensity and a linear relationship with the rainfall kinetic energy; and the splash rate had an exponential relationship with the duration of rainfall and a negative exponential relationship with the distance of the splash erosion. Qin et al. (2014) carried out splash tests with the raindrops generator and their experiment results show that, if the raindrop kinetic energy is less than 0.0674×10^{-3} J, there is no splash erosion being produced, and that the splash erosion grows linearly with the raindrop kinetic energy within a certain range of raindrop diameter. The results of the indoor artificial rainfall experiments reported in Hu et al. (2016) indicate that the critical energy of the splash erosion is 3~ 6$Jm^{-2}mm^{-1}$;each of the uphill, downhill, net, total splash erosion amounts has a power function relation with the rainfall energy, respectively, whereas the side-slope splash erosion has a quadratic polynomial relation with the rainfall energy. Majid et al. (2016) conducted outdoor runoff plot experiment to investigate the plausible relationship between the splash erosion and the runoff erosion under different rainfall intensities and slopes.

In this paper, we will analyze the mass exchange mechanism on the soil surface based on the concept of energy balance and with the assistance of the spring damping model (Zhou et al., 2012). We regard the rainfall splash erosion process as a collision process between the raindrop and the soil particle on the soil interface. This recognition allows us to incorporate research approaches from the spring model, which has been developed for analyzing collision process between solid and solid objects, and between liquid and solid objects; from the spring vibrator model, which has been developed for explaining the process of the droplets impacting the super-hydrophobic surface (Miao et al., 2012; Yang et al., 2010); and the mass-spring model, which has been developed for simulating the impact of liquid drops on solid surface (Zang et al., 2015). In addition, because a same set of factors determine the splash amount and infiltration amount, and it is relatively simpler to observe the infiltration amount, an investigation into the relationship between the splash amount and infiltration amount would be able to provide a new channel for quantifying the splash erosion. This recognition leads us to examining the relationship between single raindrop, rainfall kinetic energy and splash erosion from both theoretical and empirical angles, with an emphasis on the relationship between the infiltration amount and the splash erosion. Such an investigation would add value to the collective effort to establish mass exchange law in water-soil interface during rainfall splash erosion.

RAINDROP KINETIC ENERGY MODEL

Equivalent Spring Damping Model Based on Energy Balance

Spring damping method treats the collision process as a continuous dynamics problem, and thus regarding the contact force being equivalent to a spring damping model. Based on the Hunt's assumption, energy is dissipated during the collision. The hysteretic damping coefficient and the relationship between the two speeds before and after the collision are determined by the energy balance relationship. With the assistance of Newton recovery coefficient e, the kinetic energy loss is calculated according to **Eq. 1** (Zhang et al., 2013; Lin et al., 2016):

$$\Delta E = \frac{1}{2}\frac{m_1 m_2}{m_1 + m_2}(v_1 - v_{20})^2\left(1 - e^2\right) \tag{1}$$

Where ΔE is kinetic energy loss(J), m_1,v_1 are the mass (kg) and the terminal velocity (m/s) of the raindrops, respectively, m_2, v_{20} are the mass (kg) and the splash speed (m/s)of the soil particles, respectively; e is newton's coefficient of restitution(unitless).

The Relationship Between Single Raindrop Kinetic Energy and Splash Erosion Amount

In general, the collision process is composed of compaction and recover phases. In the compaction phase, raindrops generate deformation along the normal line of the contact surface, until the relative speed decreases to zero, when the relative deformation reaches maximum. Subsequently parts of raindrops adhere to the soil particle, other raindrops separate from the soil particle, and at this moment, the collision process finishes. The following section will analyze the scenario under which the soil surface slope is zero.

Since the soil particle is hydrophilic, the Newton recovery coefficient equals to zero, therefore the kinetic energy loss of the rainfall splash erosion system is shown during the collision process as follow:

$$\Delta E = \frac{1}{2}\frac{m_1 m_2}{m_1 + m_2}(v_1 - v_{20})^2 \tag{2}$$

Assuming that there is no rebounding after the raindrops collide with the soil particle, meaning that v_{20} (m/s) equals to 0. For convenience of analysis, the kinetic energy of the raindrops is taken as E(J), the mass of the soil particle after splash erosion is M_2 (kg), which includes the mass of the attached water, and the splash speed is v2 (m/s). Combining kinetic energy theorem with **Eq. 1**, we have

$$\frac{1}{2}\frac{m_1 M_2}{m_1 + M_2}v_1^2 = \frac{1}{2}m_1 v_1^2 - \frac{1}{2}M_2 v_2^2 \tag{3}$$

$$M_2 E = \left(E - \frac{1}{2}M_2 v_2^2\right)(m_1 + M_2)$$

$$E = \frac{1}{2}M_2 v_2^2 + \frac{1}{2}\frac{M_2^2}{m_1}v_2^2 \tag{4}$$

Eq. 4 demonstrates that the relationship between the kinetic energy of single raindrop and splash erosion is quadratic parabola, the coefficient depends on the splash speed and the rainfall capacity.

RESULTS AND DISCUSSION

The Relationship Between the Single Raindrops Terminal Velocity and the Soil Particle Splash Speed

There is little literature on the relationship between the raindrops speed and the soil particle splash speed during the collision process. When the single raindrop collides with the liquid wall surface with certain depth, the speeds of single raindrop before and after the collision present a linear relation according to (Song et al., 2013). Thus the quantitative relation between the speeds of a raindrop and the soil particle is $v_1 = kv_2$.

Table 1 demonstrates that the raindrops terminal speed and the coefficient with different diameter, if $v_1 = 3v_2$, the coefficient of $M_2{}^2$ in **Eq. 4** is about 120.0 ~ 240.0, which coincide with the value 146.4–250.8 (Angulo et al., 2012).

TABLE 1 | Comparison of the single raindrops terminal velocity and the coefficient with different raindrops diameter.

Raindrops diameter (mm)	Raindrops terminal velocity (m/s)	$\frac{1}{2}\frac{v_2^2}{m_1}$
3.07	8.09	240.0
3.28	8.26	205.2
3.38	8.34	191.1
3.65	8.53	158.8
3.86	8.66	138.4
4.09	8.79	120.0

Collision Model of Rainfall Flow on Slope

Because of the diversity of the size distribution of the raindrops and of the landing speed of the raindrops group, it is highly necessary to analyze the relationship between the splash erosion, the kinetic energy of the raindrops and the infiltration. In addition, it is of great importance to understand the splash erosion generated by the rainfall. Now, take the rainfall raindrops as a whole, the kinetic physical model of the rainfall can be constructed based on the concept of the rainfall flow proposed by Wang (Wang et al., 2005), to verify the feasibility of **Eq. 3**.

The Relationship Between the Rainfall Flow Mean Kinetic Energy and the Splash Erosion

According to the physical model presented by Wang (Wang et al., 2005), the average terminal velocity of the rainfall flow is expressed by

$$v_d = \frac{I}{k_1(C_1 + C_2 I)} \tag{5}$$

Where k_1 is the unit conversion factor, k_1 = 60,000; I represents the rainfall intensity(mm/min).

The mass of the rainfall flow (m_1, with the unit kg/m^3) is

$$m_1 = \frac{\rho_w}{C_1 + C_2 I} \tag{6}$$

Where ρ_w is the density of water (kg/m^3); C_1 represents the volume ratio of the rainfall critical raindrops group (mm^3/mm^3); C_2 is the coefficient of rainfall intensity effect, which stands for the volume ratio increment of the rainfall raindrops group caused by adding one unit rainfall intensity (min/mm). If 15 times test rainfall intensity is 0.492–3.694 mm/min, the average terminal velocity of the rainfall is 5.276–5.766 m/s, C_1 and C_2 are determined as 1.52519×10^{-7}, 2.84913×10^{-6} by experiment, respectively.

Combined with the rainfall intensity presented by Cheng (Cheng et al., 2015), the second item $1/m_1$ in the right of equation is 10^{-3}—10^{-4}kg^{-1}, which is 10^{-3}–10^{-4} times of the first item, therefore, the second item can be ignored, simplify **Eq. 4**:

$$E = \frac{1}{2}M_2 v_2^2 \tag{7}$$

TABLE 2 | Comparison of calculation and test results.

Rain intensity (mm/h)	Mean terminal velocity of rainfall flow (m/s)	$\frac{2}{v_2^2}$
26.4	5.057	312.8
31.4	5.307	302.4
43.7	5.274	287.6
51.2	5.326	282.0
67.2	5.402	274.1
77.0	5.431	271.2
95.3	5.473	267.1
117.0	5.505	264.0
136.0	5.526	262.0

M_2*with the unit kg, E with the unit Jin* ***Eq. 7*** *and* ***Eq. 8****.*

We can deem that it is linear proportional between the splash erosion and the kinetic energy of the rainfall, which tally with the literatures (Liu et al., 2011; Cheng et al., 2015; Zheng et al., 2016; Kinnell, 2019; Nives et al., 2021).

The Relationship Between Mean Terminal Velocity of Rainfall Flow and the Soil Particles Splash Speed

The terminal velocity of single raindrops with the diameter 1.8 mm is 6.09 m/s, which is larger than the average terminal velocity of the rainfall flow, 5.276–5.766 m/s. Therefore, it is necessary to verify the relationship between the average terminal velocity of rainfall flow and the soil particles splash speed. In order to compare with test data, convert **Eq. 7** into:

$$M_2 = \frac{2}{v_2^2}E \tag{8}$$

Table 2 shows the comparison of the coefficient of **Eq. 8** by calculating the average terminal velocity with the test rain intensity presented by Cheng (Cheng et al., 2015). Take the interplay between raindrops into consideration, there is $v_d = 2v_2$.

The rain splash erosion experiment selected 31.4, 67.2, 95.3 mm/h rainfall intensity, nine duration rainfalls (3, 6, 10, 15, 20, 25, 30, 40, 50 min), and the test slope was determined as 5. The splash erosion plate is made of steel plate, with the inner diameter 100 cm, outer diameter 220 cm, which is applied to measure the splash erosion quantity. The datum of the up, down, left, right slope four azimuths splash erosion quantity and the rainfall kinetic energy was analyzed with regression analysis. As a result, the linear fitting results are best shown in **Table 3**.

Compare the coefficient term of E in **Table 3** with that of **Table 2**, it can be seen that the average terminal velocity of the rainfall is approximately twice of the speed of the splash particle. Although there regresses different slopes, the coefficient of the three rainfall intensities 31.4, 67.2 and 95.3 mm/h are 302.4, 274.1and 267.2, respectively, which is near to the coefficient of the E item in **Table 3**, while there exists some difference with the situation of the up and down slope, this may cause by the influence of the position potential energy.

Relational Model of the Splash Erosion and Infiltration Amount

Theoretical Relation Model

Because the relationship, which is of the splash erosion and the average kinetic energy of single raindrop and of rainfall, accords with the experiment, it is of rational to describe the splash erosion process with the equivalent spring damping model based on the energy balance. Now it would be right time to apply the proposed model to analyze the relationship between the splash erosion and the infiltration amount.

Assumed that the rainfall was deducted the infiltration, the rest raindrops and the soil particle were splashed together. Suppose the mass of the splashed water is $m_1 f$, according to the energy conservation, the kinetic energy loss is the difference of the kinetic energy of splash erosion born before and after the splash.

$$\frac{1}{2}\frac{m_1(m_2+m_1-f)}{2m_1+m_2-f}v_1^2 = \frac{1}{2}m_1v_1^2 - \frac{1}{2}(m_2+m_1-f)v_2^2 \tag{9}$$

Simply **Eq. 9**, there is

$$v_2^2f^2 - (3m_1v_2^2 + 2m_2v_2^2)f = -m_2^2v_2^2 - 3m_1m_2v_2^2 + m_1^2v_1^2 - 2m_1^2$$

Further finishing:

$$v_2^2(f-m_2)^2 - 3m_1v_2^2(f-m_2) + m_1^2(v_1^2-2) = 0$$

$$f - m_2 = \frac{3}{2}m_1 + \frac{1}{2v_2}m_1\sqrt{9v_2^2 - 4v_1^2 + 8} \tag{10}$$

Eq. 10 demonstrates that the relationship between the splash erosion m_2 and the infiltration amount f is linearly proportional.

There are several important points by analyzing **Eq. 10**:

1) The slope of the linear ration of the former two items is determined by the unit conversion relation. Additionally, **Eq. 10** provides a new method for identifying the splash erosion amount.
2) The line intercept depends on the rainfall, raindrop terminal velocity and the soil splash erosion velocity. While the intercept is ultimately determined by the rainfall intensity according to **Eq. 5** and **Eq. 6**.
3) If $\frac{3}{2}m_1 > \frac{1}{2v_2}m_1\sqrt{9v_2^2 - 4v_1^2 + 8}$ there is $f > m_2$ and the average terminal velocity of the rainfall $v_2 > \sqrt{2}$, which shows that the infiltration amount is larger than the splash erosion. Based on **Eq. 5** and **Eq. 6**, the corresponding rainfall intensity is 0.017 mm/min. However, when the rainfall intensity is greater than 0.017 mm/min, the infiltration amount is larger than the splash erosion.
4) In the process of the individual rainfall splash, it can increase the difference of the infiltration amount and the splash erosion by decreasing the value v_2, which is one of the major measures to increase the surface roughness in practical.
5) In the rainfall process, there exists the mass exchange between the infiltration and the splash erosion on the soil surface.
6) If the practical energy of the raindrop splash erosion is less than the critical energy (Qin et al., 2014; Hu et al., 2016), there will not generate the splash erosion, that is $v_2 = 0$, **Eq. 10** and the above conclusions can be false.

Model Validation

The experiment soil is the loess soil collected from the Loess Hilly and gully region, the northwest water Ansaichafang Experiment

TABLE 3 | The fitting function between the splash erosion and the rainfall kinetic energy of four azimuths.

Different azimuth	Formula between splash erosion and rainfall kinetic energy	The correlation coefficients
Left slope	M_2 = 272.62E +1.0140	0.9711
Right slope	M_2 = 272.91E + 1.0254	0.968 5
Up slope	M_2 = 212.87E + 1.046 2	0.938 5
Downhill	M_2 = 349.49E + 1.106 0	0.958 3

M_2*with the unit g,* E *with the unit J in samples13.*

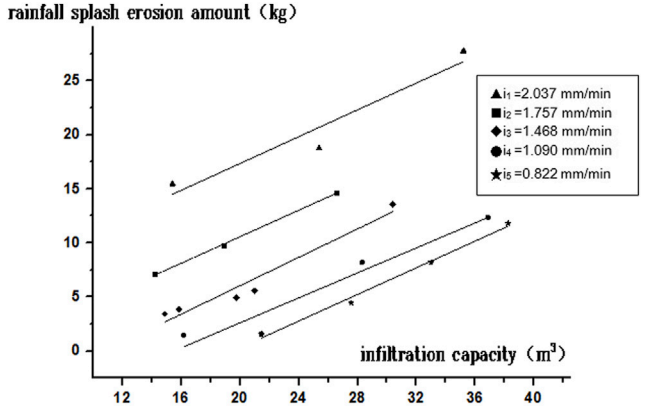

FIGURE 1 | Experimental results of the relationship between rainfall splash erosion amount and infiltration volume.

Station mountain range. The rainfall area is 2 m × 3 m, the rainfall intensity is 0.822, 1.090,1.468,1.757, 2.037 mm/min, the slope is 10°, 15°, 20°, 25°, 30°. The soil equipment is a wooden box with 40 cm width, 35 cm height and 100 cm projected length. The wall tops of the box are made into wedge-shaped, the bottom of the box is drilled with many micropores with the diameter 2.5mm, these micropores are designed in quincunx-shape in order to simulate the natural channel. The other side of the box are installed to observe the splash erosion (Wu et al., 1992).

Figure 1 shows the relationship between the infiltration amount and the rainfall splash erosion.

The results manifest that the relationship presents a cluster of li nes, different rainfall intensities correspond to different intercepts, and the relationship mainly depends on the rainfall intensity, which tally with **Eq. 10**, further verify that the rest raindrops and the soil particles adhere each other and are splashed together.

The slopes of the five lines are 0.577–0.657, which can be approximately as the reciprocal of the loessal soil density 1,500–1700 kg/m^3. If convert the ordinate and abscissa, i.e. the infiltration amount is the ordinate, the line slope just is the soil density, which manifest that the slope is determined by the unit conversion relationship. This conclusion also agrees with **Eq. 10**.

CONCLUSION

In summary, this paper clearly verified the relationships of single raindrop, the average kinetic energy of the rainfall and the splash erosion with the equivalent spring damper model based on some relevant experiments datum, it comes out several major conclusions as follow:

Basically reasonable the rainfall kinetic energy and the splash erosion by the equivalent spring damping model in the process of rainfall splash erosion, there exist the mass exchange of infiltration and splash erosion on the soil surface, which provides a new approach to identify the splash erosion. The equivalent spring damping model is usefull to describe the relationship between spatter amount and infiltration amount, rainfall (flow) kinetic energy and spatter amount.

Under the condition of the rainfall splash erosion, it is a linear relation between the splash erosion amount and the infiltration amount, which slope is determined by the unit conversion of two former items. If select the same units, the slope is the ratio of the soil density and the water density. The ratio is identified by rainfall mass, terminal velocity and the splash erosion of soil particle, while these three parameters are determined by the rain intensity in the end, and there have different intercepts corresponding with different rain intensities.

In the case of rainfall splash erosion, the kinetic energy of rainfall is linearly proportional to the amount of splash erosion, the rainfall terminal velocity is two times of the soil erosionrate. If consider the single raindrop, the kinetic energy and the splash erosion amount are quadric parabolic relation, and the raindrop terminal velocity is three times of the soil erosion rate.

These proposed results are summarized without considering the influence of the position potential energy, however which has little effect on the results, when dealing with the practical problems, it can be considered specially.

DATA AVAILABILITY STATEMENT

The original contributions presented in the study are included in the article/Supplementary Materials, further inquiries can be directed to the corresponding author/s.

AUTHOR CONTRIBUTIONS

ZY and LP Mainly engaged in testing and analysis work.

FUNDING

This work was supported by the National Key R& D Program of China (2018YFE0206200) and the National Natural Science Foundation of China (51869009).

ACKNOWLEDGMENTS

We also appreciate the helpful data from authors of paper and suggestions from the reviewers.

REFERENCES

Angulo-Martínez, M., Beguería, S., Navas, A., and Machín, J. (2012). Splash Erosion under Natural Rainfall on Three Soil Types in NE Spain. *Geomorphology* 175-176, 38–44. doi:10.1016/j.geomorph.2012.06.016

Bu, C.-f., Wu, S.-f., and Yang, K.-b. (2014). Effects of Physical Soil Crusts on Infiltration and Splash Erosion in Three Typical Chinese Soils. *Int. J. Sediment Res.* 29, 491–501. doi:10.1016/s1001-6279(14)60062-7

Cheng, J. H., Qin, Y., Zhang, H. J., Cong, Y., Yang, F., and Yan, Y. Q. (2015). Splash Erosion under Artificial Rainfall in Rocky Mountain Area of Northern China. *Trans. Chin. Soc. Agric. Machinery* 46, 153–161. doi:10.6041/j.issn.1000-1298.2015.02

Hu, W., Zheng, F. L., and Bian, F. (2016). Effects of Raindrop Kinetic Energy on Splash Erosion in Typical Black Soil Region of Northeast China. *Acta Ecol. Sinica* 36, 4708–4717 10. doi:10.5846/stxb201412312613

Hu, X. (2015). Effect of Granular Structure on Soil Splash Erosion Rate and Soil Crust Development of Loessial Soil. *Chin. Agric. Sci. Bull.* 31, 229–235.

Kinnell, P. I. A. (2019). Comment on "Evaluating and modelling splash detachment capacity based on laboratory experiments" by Wu et al. (2019). Catena 176, 189–196. *Catena* 183, 104189. doi:10.1016/j.catena.2019.104189

Li, W. J., Li, D. X., and Wang, X. K. (2011). Study on Raindrop Splash Detachment Model. *J. Basic Sci. Eng.* 19, 689–699.

Lin, J., Lin, Y., and Qian, J. (2016). Adhesive Contact Mechanics: from Deterministic to Stochastic Description. *Chin. Sci. Bull.* 61, 701–706. doi:10.1360/n972015-00736

Liu, H. P., Fu, S. H., Wang, X. Y., Xu, L., Fang, N., Liu, B. Y., et al. (2011). Effects of Slope Gradient on Raindrop Splash Erosion. *Acta Pedologica Sinica* 48, 479–486.

Ma, R. M., Cai, C. F., Li, Z. X., Wang, J. G., Feng, J. Y., Wu, X. G., et al. (2014). Effect of Antecedent Soil Moisture on Aggregate Stability and Splash Erosion of Krasnozem. *Trans. Chin. Soc. Agric. Eng.* 30, 95–103.10.3969/j.issn.1002-6819.2014.03.013.

Ma, R. M., Wang, J. G., Li, Z. X., Cai, C. F., and Wang, S. (2013). Effects of Dynamic Distribution of Aggregate Size on Splash Erosion under Rainfall in Red Soils. *Resour. Environ. Yangtze Basin* 22, 779–784.

Mahmoodabadi, M., and Sajjadi, S. A. (2016). Effects of Rain Intensity, Slope Gradient and Particle Size Distribution on the Relative Contributions of Splash and Wash Loads to Rain-Induced Erosion. *Geomorphology* 253, 159–167. doi:10.1016/j.geomorph.2015.10.010

Miao, S. G., Dou, J. X., Chen, F., Li, J., and Li, A. G. (2012). Analysis of Observations on the Urban Surface Energy Balance in Beijing. *Sci. China:earth Sci.* 42, 1394–1402. doi:10.1007/s11430-012-4411-6

Qin, Y., Cheng, J. H., Zhang, H. J., and Li, Z. (2014). A Study of the Raindrop Impact to Splash Erosion. *J. Soil Water Conservation* 28, 74–78. doi:10.13870/j.cnki.stbcxb.2014.02.014

Saedi, T., Shorafa, M., Gorji, M., and Khalili Moghadam, B. (2016). Indirect and Direct Effects of Soil Properties on Soil Splash Erosion Rate in Calcareous Soils of the central Zagross, Iran: A Laboratory Study. *Geoderma* 271, 1–9. doi:10.1016/j.geoderma.2016.02.008

Song, Y. C., Ning, Z., Sun, C. H., Lv, M., Yan, K., and Fu, J. (2013). Movement and Splashing of a Droplet Impacting on a Wet Wall. *Chin. J. Theor. Appl. Mech.* 45, 833–842. doi:10.6052/0459-1879-13-053

Sun, S. X. (1997). Study on Relationship between Rainfall Splash Erosion and Infiltration on Loess Slopeland. *J. Soil Water Conservation* 3, 92–94.

Wang, B., Ma, J. M., Cheng, J. H., Yu, X. Y., Dai, Q. J., Lv, P. Y., et al. (2015). Effects of Gravel Coverage on Splash Erosion in the Mountainous Region of Northern China. *Sci. Soil Water Conservation* 13, 93–98. doi:10.16843/j.sswc.2015.05.016

Wang, Z. L., Sun, Q. M., Zheng, F. L., and Niu, Z. H. (2005). Physically-Based Model of Rain Fall Flow Kinetic Energy. *J. Hydraulic Eng.* 36, 1280–1285.

Wei, Y. J., Wu, X. L., and Cai, C. F. (2015). Splash Erosion of Clay-Sand Mixtures and its Relationship with Soil Physical Properties: The Effects of Particle Size Distribution on Soil Structure. *CATENA* 135, 254–262. doi:10.1016/j.catena.2015.08.003

Wu, P. T., and Zhou, P. H. (1992). The Action of Rain Drop Splash on Sheet Flow Erosion. *Bull. Soil Water Concervation* 12, 19–47. doi:10.13961/j.cnki.stbctb.1992.04.003

Yang, J., Zhang, Y., Liu, D., and Wei, X. (2010). CFD-DEM Simulation of Three-Dimensional Aeolian Sand Movement. *Sci. China Phys. Mech. Astron.* 53, 1306–1318. doi:10.1007/s11433-010-4038-6

Yin, W. J., Wang, J., and Liu, D. D. (2011). Effect of Surface Water Thickness on the Amount of Splash Erosion. *J. Irrigation Drainage* 30, 115–117. doi:10.13522/j.cnki.ggps.2011.04.011

Zambon, N., Johannsen, L. L., Strauss, P., Dostal, T., Zumr, D., Cochrane, T. A., et al. (2021). Splash Erosion Affected by Initial Soil Moisture and Surface Conditions under Simulated Rainfall. *Catena* 196, 104827. doi:10.1016/j.catena.2020.104827

Zang, D., Li, Y., Chen, Z., Li, J., Geng, X. G., and Cheng, X. P. (2015). Shape Evolution of Free Falling Deformed Droplets. *Chin. Sci. Bull.* 60, 917–921.

Zhang, R., Zhu, W., and Zheng, X. J. (2013). Investigation into the Three-Dimensional Sand Particle-Bed Collision Process. *J. Lanzhou Univ. Nat. Sci.* 49, 861–869. doi:10.13885/j.issn.0455-2059.2013.06.013

Zhao, X. G., and Shi, H. (2003). Prescription of Soil Anti-erosion Capability under Water Erosion. *Arid Land Geogr.* 26, 12–16. doi:10.13826/j.cnki.cn65-1103/x.2003.01.003

Zheng, T. H., Xing, Y. Y., He, K. X., Teng, F., and Li, G. L. (2016). Rain Splash and Sheet Flow Mixed Sediment Transport Mechanism. *J. Northwest A F Univ. Nat. Sci. Edition* 44, 211–218. doi:10.13207/j.cnki.jnwafu.2016.03.029

Zhou, Z. C., Wu, X. Y., Zhang, W. Q., and Xie, Z. W. (2012). Study on Contact Dynamics Based Springy Damper Model. *J. Hubei Univ. Technology* 27, 125–128.

Conflict of Interest: The authors declare that the research was conducted in the absence of any commercial or financial relationships that could be construed as a potential conflict of interest.

frontiers in Environmental Science

ORIGINAL RESEARCH
published: 17 January 2022
doi: 10.3389/fenvs.2021.778598

Urban Catchment-Scale Blue-Green-Gray Infrastructure Classification with Unmanned Aerial Vehicle Images and Machine Learning Algorithms

Jinlin Jia[†], *Wenhui Cui*[†] *and Junguo Liu* *

School of Environmental Science and Engineering, Southern University of Science and Technology, Shenzhen, China

OPEN ACCESS

Edited by:
Laixiang Sun,
University of Maryland, United States

Reviewed by:
Kun Zhang,
Marquette University, United States
Jonathan Nuttall,
Deltares, Netherlands

***Correspondence:**
Junguo Liu
junguo.liu@gmail.com
liujg@sustech.edu.cn

[†]*These authors have contributed equally to this work and share first authorship*

Specialty section:
This article was submitted to Environmental Informatics and Remote Sensing, a section of the journal Frontiers in Environmental Science

Received: *17 September 2021*
Accepted: *22 December 2021*
Published: *17 January 2022*

Citation:
Jia J, Cui W and Liu J (2022) Urban Catchment-Scale Blue-Green-Gray Infrastructure Classification with Unmanned Aerial Vehicle Images and Machine Learning Algorithms. Front. Environ. Sci. 9:778598. doi: 10.3389/fenvs.2021.778598

Green infrastructure (GI), such as green roofs, is now widely used in sustainable urban development. An accurate mapping of GI is important to provide surface parameterization for model development. However, the accuracy and precision of mapping GI is still a challenge in identifying GI at the small catchment scale. We proposed a framework for blue-green-gray infrastructure classification using machine learning algorithms and unmanned aerial vehicle (UAV) images that contained digital surface model (DSM) information. We used the campus of the Southern University of Science and Technology in Shenzhen, China, as a study case for our classification method. The UAV was a DJI Phantom 4 Multispectral, which measures the blue, green, red, red-edge, and near-infrared bands and DSM information. Six machine learning algorithms, i.e., fuzzy classifier, *k*-nearest neighbor classifier, Bayes classifier, classification and regression tree, support vector machine (SVM), and random forest (RF), were used to classify blue (including water), green (including green roofs, grass, trees (shrubs), bare land), and gray (including buildings, roads) infrastructure. The highest kappa coefficient was observed for RF and the lowest was observed for SVM, with coefficients of 0.807 and 0.381, respectively. We optimized the sampling method based on a chessboard grid and got the optimal sampling interval of 11.6 m to increase the classification efficiency. We also analyzed the effects of weather conditions, seasons, and different image layers, and found that images in overcast days or winter days could improve the classification accuracy. In particular, the DSM layer was crucial for distinguishing green roofs and grass, and buildings and roads. Our study demonstrates the feasibility of using UAV images in urban blue-green-gray infrastructure classification, and our infrastructure classification framework based on machine learning algorithms is effective. Our results could provide the basis for the future urban stormwater management model development and aid sustainable urban planning.

Keywords: green infrastructure, blue infrastructure, classification, unmanned aerial vehicle images, machine learning

1 INTRODUCTION

Green infrastructure (GI) is a collection of areas that function as natural ecosystems and open spaces (Benedict and McMahon, 2006; Palmer et al., 2015), and it can maintain and improve the quality of air and water and provide multiple benefits for people and wildlife (Palmer et al., 2015; Benedict and McMahon, 2006; Environmental Protection Agency, 2015; Hashad et al., 2021). As an important part of urban ecosystems (Hu et al., 2021), GI provides green spaces for cities, and benefit people's physical and mental health (Venkataramanan et al., 2019; Zhang et al., 2021). In addition, GI can alleviate urban flooding and urban heat island effect (Venkataramanan et al., 2019; Dai et al., 2021; Ouyang et al., 2021; Bartesaghi-Koc et al., 2020), and accelerate sustainable development (Hu et al., 2021).

GI and other infrastructures are important land types that have different runoff coefficients, which are essential for stormwater management models and urban energy balance models (Cui and Chui, 2021; Yang et al., 2021). Nitoslawski et al. (2021) pointed out that it is valuable to use emerging technologies to study urban green infrastructure mapping. However, the current related studies only carry out classification and mapping for part of infrastructure. For example, Narziev et al. (2021) mapped irrigation system, while Man et al. (2020) and Furberg et al. (2020) mapped urban grass and trees. There is a need to perform a more comprehensive classification and mapping of infrastructures.

Generally, infrastructures are the facilities needed by the society, while the land covers are divided based on their natural and physical characteristics (Environmental Protection Agency, 2019; Gregorio and Jansen, 2000). For example, green roofs can be used to reduce the runoff and increase the aesthetic of buildings, which is one kind of GI. But it cannot be regarded as the land cover. To our best knowledge, there are no specific methods for the classification of GI. Boonpook et al. (2021) pointed out that the distinction between green roofs and ground grass is difficult because their spectral information is similar. Moreover, GI is usually scattered over urban areas and has different forms with a fine spatial scale. The mapping of GI based on remote sensing images with insufficient spatial resolution or fewer data features has a large uncertainty (Bartesaghi-Koc et al., 2020).

In recent decades, using remote sensing for automatic classification and mapping of infrastructure is valuable for avoiding manual identification, which is time-consuming and laborious (Shao et al., 2021). Satellites, airborne vehicles, and unmanned aerial vehicles (UAVs) have usually been used to obtain images as inputs for automatic classification and mapping. Satellites can collect data and make repeated observations at regular intervals, even in difficult-to-reach locations (Gašparović and Dobrinić, 2021). Satellite images have been widely used for GI identification. For example, Gašparović and Dobrinić (2021) used satellite synthetic aperture radar images to identify water, bare soil, forest, and low vegetation, and Furberg et al. (2020) used satellite images to analyze the changes in urban grassland and forest. However, the acquisition of satellite images is strongly affected by the atmospheric cloud conditions (Gašparović and Dobrinić, 2021; Wang et al., 2019), and the accuracy and precision are limited by the spatial resolution (Bartesaghi-Koc et al., 2020; Wang et al., 2019), especially in urban areas with complex features (Furberg et al., 2020).

Airborne vehicles provide high-resolution images and can adjust the angles, positions, and instruments as required (Alakian and Achard, 2020). For example, Man et al. (2020) extracted grass and trees in urban areas based on airborne hyperspectral and LiDAR data. However, the costs of airborne vehicles are prohibitive and they require logistics management (Bartesaghi-Koc et al., 2020). Nowadays, the cost of UAVs is decreasing (Wang et al., 2019) and UAVs can carry a variety of sensors (e.g., multispectral cameras, LiDAR, and thermal infrared cameras) that can obtain targeted high-resolution data on a centimeter scale (Jiang et al., 2021). The amount of research on GI using UAV data has been increasing; for example, urban GI thermal effects (Khalaim et al., 2021), GI vegetation health (Dimitrov et al., 2018), and the classification of plant species (Fan and Lu, 2021; Jiang et al., 2021; Miura et al., 2021) have been investigated. Therefore, UAV data is more suitable for small catchment studies.

Machine learning algorithms, such as fuzzy classifier (FC) (Trimble Germany GmbH, 2014a; Cai and Kwan, 1998), *k*-nearest neighbor classifier (KNN) (Bai et al., 2021; Li et al., 2016), Bayes classifier (Bayes) (Han et al., 2012; Brunner et al., 2021), classification and regression tree (CART) (Li et al., 2016; Zhang and Yang, 2020), support vector machine (SVM) (He et al., 2007; Ismail et al., 2021), and random forest (RF) (Li et al., 2016; Dobrinić et al., 2021) algorithms, have been widely used in land surface automatic classification, especially in land use/cover classification. For example, Zhang and Yang (2020) improved land cover classification based on the CART method; Dobrinić et al. (2021) built an accurate vegetation map using a RF algorithm. However, these algorithms have still not been effectively applied in the infrastructure classification in small urban catchments, and the optimal algorithm is still not clear.

At present, although UAVs have advantages in vegetation identification, such as the classification of crops, trees, and grass species (Garzon-Lopez and Lasso, 2020; Fan and Lu, 2021; Jiang et al., 2021; Miura et al., 2021; Sudarshan Rao et al., 2021; Wicaksono and Hernina, 2021), the application of UAVs for infrastructure classification is still rare. Machine learning algorithms have not been widely used for infrastructure classification. In the present study, we take green infrastructure (all different green open spaces), blue infrastructure (surface water bodies), and gray infrastructure (artificial structures without vegetation) as the study objects, and classify the blue-green-gray infrastructure using an UAV at a small catchment scale (i.e., 0.1–10 km^2), and develop a high-resolution object-based method using machine learning algorithms. In addition, we optimize the sampling method and discuss the effects of weather conditions, seasons, and different image layers on classification.

2 MATERIALS AND METHODS

2.1 Study Area and Data Acquisition

The Southern University of Science and Technology (SUSTech) is located in Shenzhen, China (**Figure 1**), which has a subtropical

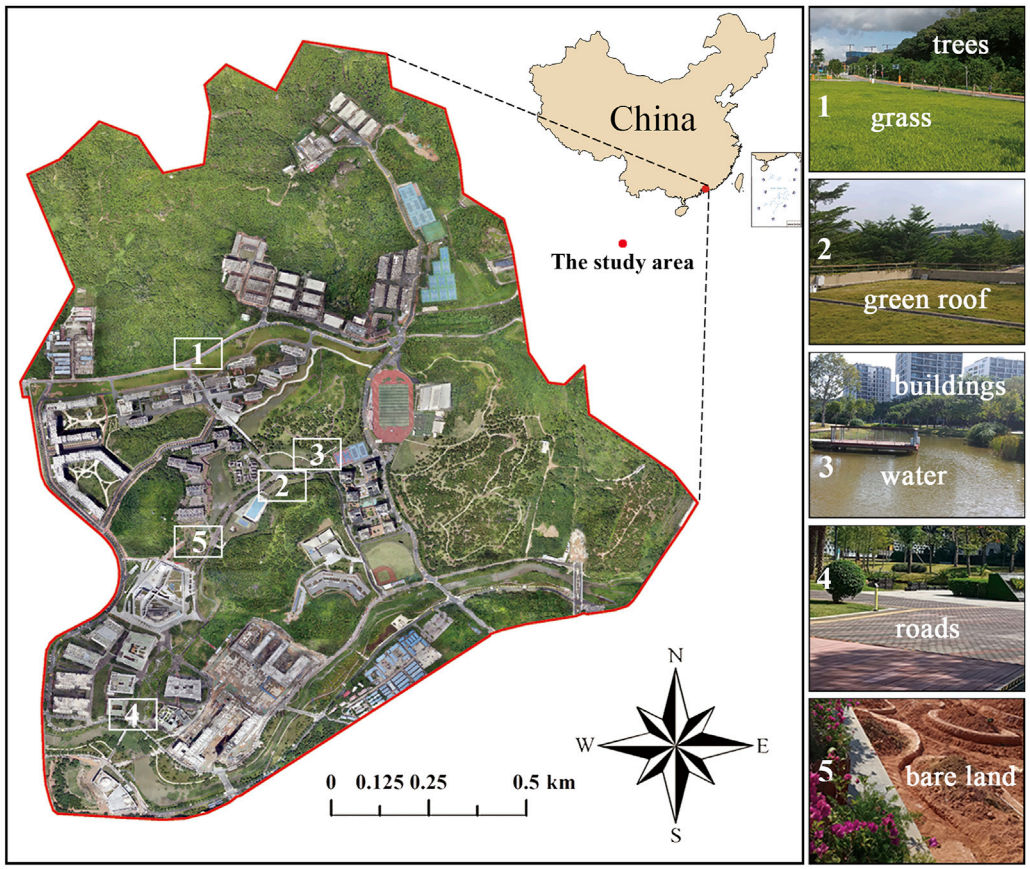

FIGURE 1 | The orthophoto map of study area. The numbers 1–5 show the locations of typical infrastructure in the campus, which corresponding pictures are displayed on the right.

monsoon climate with annual mean precipitation of 1935.8 mm (Meteorological Bureau of Shenzhen Municipality, 2021; Hu et al., 2008). The whole area of the campus is about 2 km^2. There are hills in the northern and central parts of the campus, and a river runs through the southern part (**Figure 1**). The combination of terrain and campus walls creates a small catchment. The vegetation is mainly plantation community, including lemon eucalyptus (*Eucalyptus citriodora Hook. f.*) community, acacia mangium (*Acacia mangium Willd.*) community, and lychee (*Litchi chinensis Sonn.*) forest (Hu et al., 2008). The buildings with various forms of roofs, asphalt roads and permeable pavements are mosaic in the campus. There are also lakes, streams and a river, and so on. Although they were built in different periods but all of them were constructed within 10 years. Their pictures could be found in **Supplementary Figure S1**.

There are several types of GI (e.g., green roofs, trees, grass, and bare land), blue infrastructure (e.g., water), and gray infrastructure (e.g., buildings and roads) distributed across the campus (**Figure 1**). To test the application of UAV images and the method of classifying different types of infrastructure, the SUSTech campus was chosen as the study area.

A DJI Phantom 4 Multispectral (DJI P4M) (DJI, https://www.drdrone.ca/pages/p4-multispectral) UAV was used in this study to obtain the images. The UAV has a built-in stabilizing imaging system, integrating one RGB camera and five multispectral cameras, covering blue (B; 450 ± 16 nm), green (G; 560 ± 16 nm), red (R; 650 ± 16 nm), red-edge (RE; 730 ± 16 nm), and near-infrared (NIR; 840 ± 26 nm), all at two megapixels with a global shutter and on a three-axis gimbal.

Flying missions were performed when the weather conditions were feasible (generally sunny) and the wind was below force 4 (wind speed <6 m/s), at regular intervals of 2–4 weeks. Due to the battery capacity of the UAV, we divided the study area into nine subareas to perform the flying missions. Each mission was carried out between 11:00 and 13:30 in adjacent 2 days and we acquired a total of about 24,600 images from 4,100 photo locations. The UAV can record the precision position information, which could be used for post processed kinematics (PPK) to synthesize the images (https://www.drdrone.ca/pages/p4-multispectral). We used DJI Terra (version 3.0) with orthophoto image correction algorithm to synthesize the images and generate the RGB orthophoto image, the spectral images for the five bands, the digital

TABLE 1 | Six machine learning algorithms adopted in this study.

Algorithm and abbreviation	Algorithm theory	Advantages	Disadvantages	References
Fuzzy classifier (FC)	Establishes the membership function of a class based on a variety of features and predicts an object's class by its membership value	General and accurate; Stable accuracy	Difficult to interpret Heavy calculation burden	Trimble Germany GmbH, (2014a); Trimble Germany GmbH, (2014b); Cai and Kwan, (1998)
k-Nearest neighbor (KNN)	Classifies an object based on the majority of its *k*-nearest training examples in the feature space	Fast training speed; Generalizes better with a large training set Not sensitive to outliers	High computer memory requirements Slow prediction stage	Trimble Germany GmbH, (2014b); Bai et al. (2021); Mohammadpoor and Eshghizadeh, (2021); Li et al. (2016)
Bayes (Bayes)	Applies Bayes' theorem with strong independence assumptions to predict an object's class	Stable classification efficiency; Needs a small amount of training data	Assumes distribution independence Need to calculate the prior probability	Trimble Germany GmbH, (2014b); Han et al. (2012); Brunner et al. (2021); Li et al. (2016)
Classification and regression tree (CART)	Segments data into homogeneous subgroups by a series of decisions	White box: is easy to interpret; More features can be processed	Easy to overfit Unstable	Trimble Germany GmbH, (2014b); Li et al. (2016); Zhang and Yang, (2020)
Support vector machine (SVM)	Maps samples to points in feature space, uses decision planes to segment the space, and then classifies new objects according to the same spatial attributes	Can solve small sample problems; Can solve high-dimensional and complex problems	Difficult to train large samples Difficult to solve multi-class problems	Trimble Germany GmbH, (2014b); Bai et al. (2021); Mohammadpoor and Eshghizadeh, (2021); Ismail et al. (2021); He et al. (2007)
Random forest (RF)	Builds decision trees with each tree generated by randomly selecting subsets of training samples or feature spaces	Can deal with noise and high-dimensional and unbalanced datasets High parallel processing capability	Not suitable for small amounts of data or low-dimensional data Easy to overfit	Trimble Germany GmbH, (2014b); Bai et al. (2021); Li et al. (2016); Dobrinić et al. (2021)

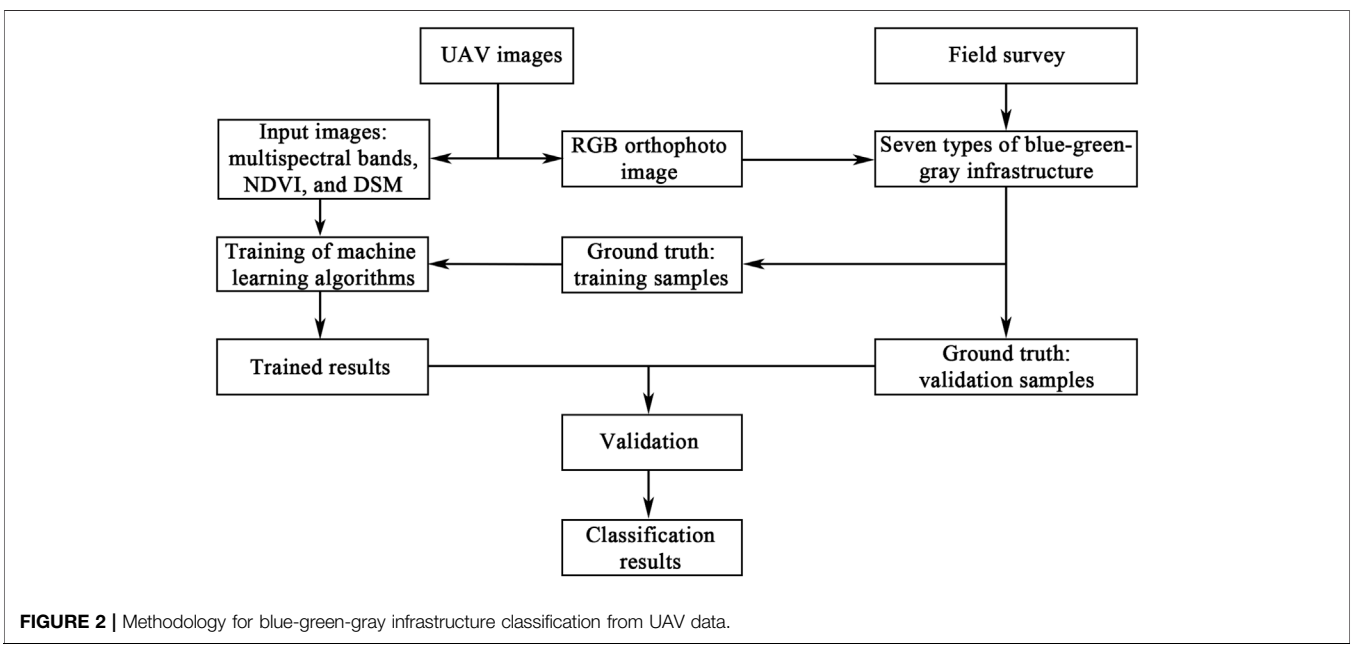

FIGURE 2 | Methodology for blue-green-gray infrastructure classification from UAV data.

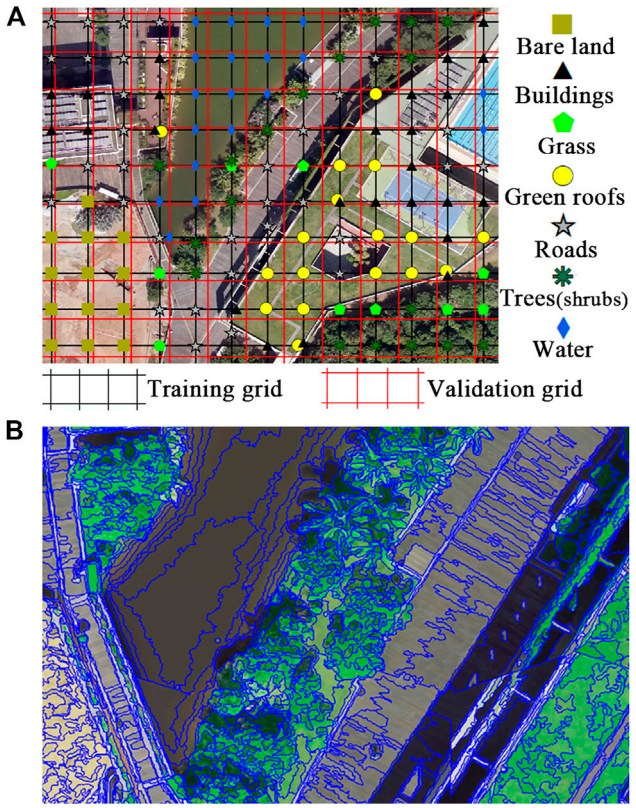

FIGURE 3 | (A) Chessboard grid sampling method for making samples. The dots are sample points at the grid intersections. **(B)** Objects created by multiresolution segmentation, shown as blue polygons.

surface model (DSM), and the normalized difference vegetation index (NDVI) maps (**Supplementary Figure S2**). The DSM had a resolution of 0.114 m and the other images had a resolution of 0.057 m.

2.2 Classification Algorithms

In this study, six widely used machine learning algorithms were compared. Descriptions, advantages, and disadvantages of the algorithms are shown in **Table 1**. Detailed explanations and the hyperparameter settings associated with the algorithms are given in **Supplementary material S1**.

2.3 Methodology

Figure 2 shows the steps for extracting and classifying the blue-green-gray infrastructure based on the UAV images. Firstly, the input images and RGB orthophoto image were retrieved from the UAV images. Secondly, with the RGB orthophoto image and field survey, we created the training and validation samples for different kinds of infrastructure. Thirdly, based on input images and training samples, we trained the algorithms and got the trained results. Finally, the validation accuracy and classification results were made based on the validation samples and trained results.

2.3.1 Sample Creation

Based on the classification categories of the European Commission (Maes et al., 2016), we classified blue-green-gray infrastructure in the SUSTech campus as water, trees (shrubs), grass, green roofs, bare land, buildings (no vegetation), and roads.

The seven types of samples were made for model training and validation of the machine learning algorithms. ArcMap (version 10.6, included in ArcGIS for Desktop, Esri) was used to pre-process input images (**Supplementary Figure S2**) and make the sample shapefiles for training and validation (**Figure 3A**). To ensure that the samples were random and the process could be repeated, we applied an equidistant sampling method (chessboard grid sampling method, **Figure 3A**), which made the samples uniformly distributed (Zhao et al., 2017). To avoid the overlap of samplings, the grids for the validation was obtained by shifting the grids for training, as shown in **Figure 3A**.

To achieve a better trade-off between classification accuracy and efficiency, we compared the results derived from samples with different sampling intervals (i.e., 2.9, 5.8, 8.7, 11.6, 14.5, and 17.4 m) in the central part of the campus (referred to as the core area, which is subarea No. 10 in **Supplementary Figure S3**). The classification accuracies were evaluated at different sampling intervals, and the optimal sampling interval was determined.

2.3.2 Algorithm Training and Validation

Different machine learning algorithms were assessed with Trimble eCognition Developer (eCognition) (version 9.0.2) based on the object-based image analysis method (Trimble Germany GmbH, 2014a). Multiresolution segmentation was used to divide the UAV images into small objects (**Figure 3B**). The classes were assigned to the objects corresponding to the training samples, and the features of the image layers were extracted to the objects. Each machine learning algorithm was used for training and classification (**Figure 4**). The accuracy was assessed by the error matrix based on the validation samples and trained results.

We used five widely used indices, producer's accuracy, user's accuracy, mean accuracy of different classes, kappa coefficient, and overall accuracy (OA), to evaluate the classification accuracy (Talebi et al., 2014; Dobrinić et al., 2021; Wang et al., 2019; Man et al., 2020). The producer's accuracy is the ratio of the number of correctly classified objects to validation objects for a class, and the user's accuracy is the ratio of the number of correctly classified objects to classified objects for a class (Talebi et al., 2014; Dobrinić et al., 2021). The mean accuracy is the average of the producer's accuracy and user's accuracy. The kappa coefficient uses information about the entire error matrix to evaluate the classification accuracy and is calculated as (Wang et al., 2019; Man et al., 2020)

$$\kappa = \frac{N \times \Sigma_{i=1}^{k} n_{ii} - \Sigma_{i=1}^{k} (n_{i+} \times n_{+i})}{N^2 - \Sigma_{i=1}^{k} (n_{i+} \times n_{+i})} \quad (1)$$

where N is the total number of objects, k is the number of classes of the classification, n_{ii} is the number of correctly classified objects in class i, n_{i+} is the objects number classified as class i, and n_{+i} is the number of validation objects of class i.

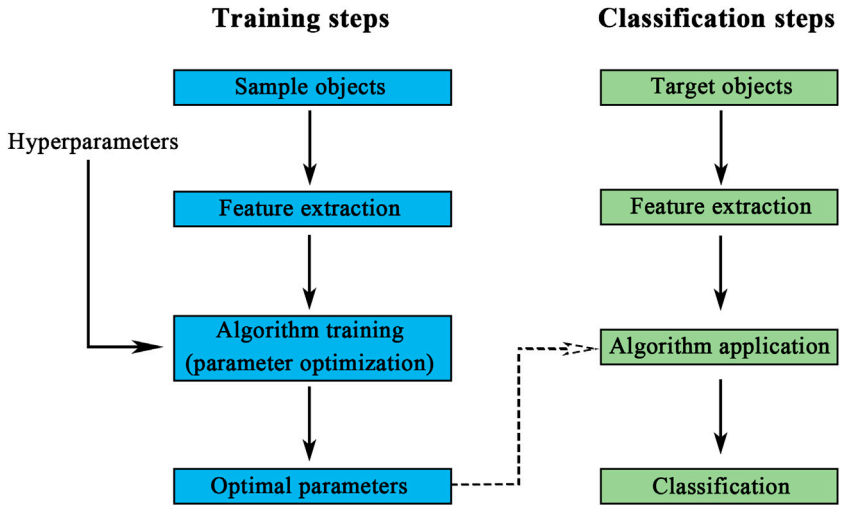

FIGURE 4 | Training and classification steps for machine learning algorithms.

TABLE 2 | Accuracy assessment of classification at different sampling intervals.

Sampling interval (m)	Number of samples	Mean accuracy							Kappa	OA
		Roads	Buildings	Grass	Trees (shrubs)	Bare land	Water	Green roofs		
2.9	16,162	0.952	0.953	0.843	0.932	0.967	0.992	0.842	0.897	0.922
5.8	4,088	0.923	0.931	0.787	0.909	0.939	0.980	0.753	0.855	0.890
8.7	1,812	0.877	0.901	0.788	0.911	0.898	0.956	0.697	0.836	0.875
11.6	1,061	0.857	0.883	0.749	0.891	0.875	0.954	0.667	0.804	0.851
14.5	702	0.861	0.900	0.717	0.886	0.886	0.909	0.646	0.793	0.843
17.4	477	0.820	0.856	0.720	0.890	0.846	0.960	0.669	0.783	0.836

The OA is the proportion of all sample objects that are correctly classified (Man et al., 2020) and a larger OA value means a better classification result. OA is calculated as (Wang et al., 2019)

$$OA = \frac{\Sigma_{i=1}^{k} n_{ii}}{N} \quad (2)$$

The optimal algorithm was obtained by comparing the kappa coefficients and OAs. To test the stability of the best algorithm, we selected the core area and five subareas for accuracy comparison from the total 17 subareas of the study area using a random number generator (**Supplementary Figure S3**). According to the trial-and-error accuracy assessment, we optimized the selected image layers further by increasing or decreasing the number of layers (see **Section 3.6** for details).

3 RESULTS AND DISCUSSION

3.1 Optimization of Sampling Method

Our sampling method was first implemented with RF algorithm in the core area, which covered an area of 126,857 m^2 and contained seven types of infrastructure. The accuracies of different sampling interval scenarios for various infrastructure types are shown in **Table 2**. For all infrastructure types, a finer sampling interval corresponded to a higher classification accuracy. A kappa coefficient between 0.80 and 1.00 indicates almost perfect classification, whereas a coefficient between 0.60 and 0.80 indicates substantial classification (Landis and Koch, 1977). The number of samples represents the manual sampling load, and a smaller number indicates higher efficiency. Considering the trade-off between accuracy and sampling efficiency, an optimal sampling interval of 11.6 m was used in this study.

Common methods for creating sample data include manual selection of the region of interest (Wang et al., 2019), simple random sampling, and equidistant sampling (Zhao et al., 2017). Manual selection is subjective and arbitrary, and thus the results depend on the operator. Simple random sampling is easy to perform, but it may cause polarization and give poor training results (Zhao et al., 2017). The equidistant sampling method, chessboard grid sampling, is objectively random and repeatable. The method produces uniformly distributed samples and mitigates polarization (Zhao et al., 2017), so it can be widely used in other areas. The optimal sampling interval may vary due to the differences in infrastructure type in the target area (e.g.,

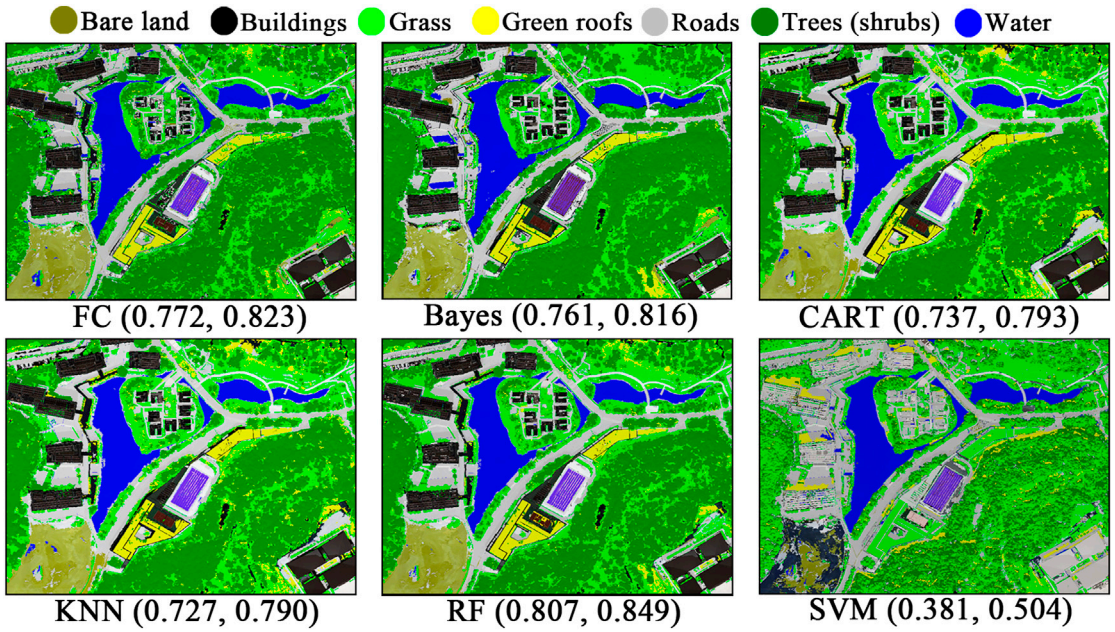

FIGURE 5 | Results for the classification algorithms and their kappa coefficients and OAs.

college communities and typical urban areas) and the scale of the infrastructure. Similarly, prioritizing efficiency or accuracy requires different optimal sampling intervals. However, in the areas of the same type (e.g., different college communities), the optimal sampling interval is representative.

3.2 Comparison of Classification Algorithms

Figure 5 shows the classification results of six algorithms in the core area, with a sampling interval of 11.6 m for both training samples and validation samples. The kappa coefficient and OA had the same ranking result, so we took kappa as a representative index for our analysis.

The RF algorithm exhibited the best performance in the core area, with a kappa coefficient of 0.807, demonstrating the advantages of this algorithm in processing high-dimensional data. The following two best classification methods were FC and Bayes, which had similar kappa coefficients of 0.772 and 0.761, respectively. The results calculated with the CART and KNN algorithms showed slightly worse performance. However, the classification results for the SVM algorithm were the worst, with a low kappa coefficient of 0.381. The main reason for this poor performance may be that the SVM algorithm has difficulty in handling large samples and multi-class problems (Bai et al., 2021; He et al., 2007).

3.3 Validation in Other Subareas

The subareas selected for the stability test with RF algorithm were Nos. 3, 5, 13, 14, 17, and 10 (the core area) (**Supplementary Figure S3**). The classification results, kappa coefficients, and OAs are shown in **Figure 6** and **Table 3**. The kappa coefficients of the five subareas and OAs of the six subareas were greater than 0.8, which reflected an almost perfect performance (Landis and Koch, 1977). The kappa coefficient of subarea No. 3 was 0.592, which was moderate (0.4–0.6) (Landis and Koch, 1977), but the OA was as high as 0.867. This was because the proportion of trees in the training sample set reached about 75% (692/930), which reduced the relative consistency in the calculation (**Eq. 1**). The mean accuracies of bare land and roads in subarea No. 3 and bare land in subarea No. 13 were below 0.6 (**Table 3**), which could be associated with the insufficient number of training samples for the related infrastructures. The training samples of them are less than 20. Meanwhile, the classification results were better based on training samples more than 30. From this perspective, to achieve a good result of mapping infrastructure, the training samples should be more than 30.

3.4 Effect of Weather Conditions on Classification

In the images taken between August 24, 2020 and December 26, 2020, there were eleven sunny days, three partly cloudy days, and one overcast day. The classification results with RF algorithm were better for the images taken on the overcast day than those taken on the sunny days. We discuss the results from the images taken on December 17, 2020 (overcast) and December 21, 2020 (sunny) as an example. The kappa coefficient and OA for the images taken on the overcast day were greater than those for the sunny day (**Table 4**). For each type of infrastructure, the mean accuracies of the results derived from the overcast day were higher than those from the sunny day for grass, buildings, and roads. However, for green roofs, better results were obtained from the sunny day.

The spectral similarity of grass, trees and green roofs is high (Boonpook et al., 2021). Therefore, we used DSM elevation to

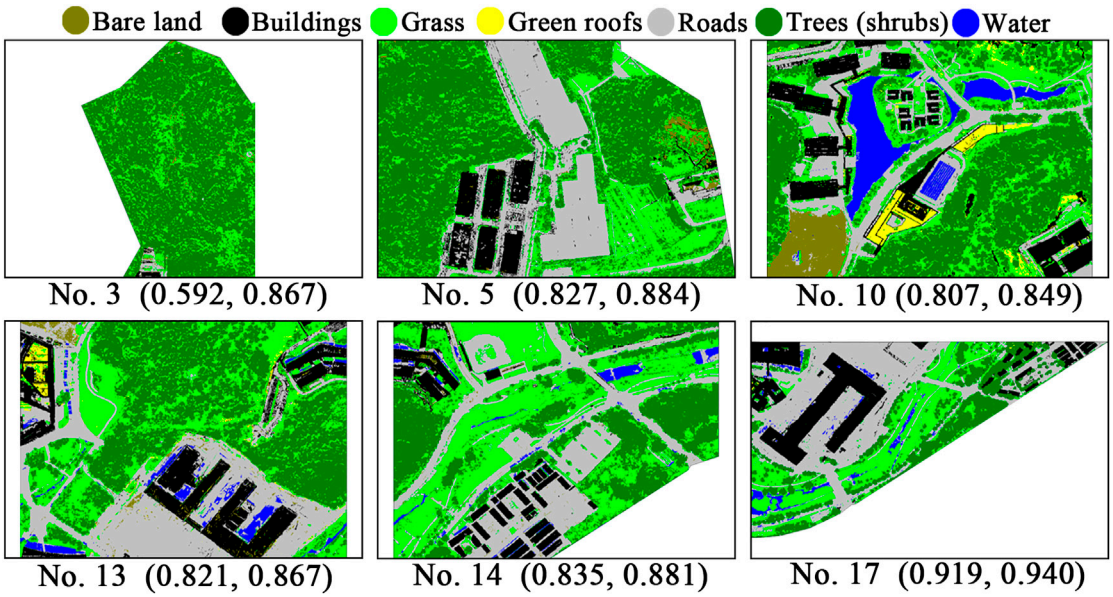

FIGURE 6 | Classification results in subareas of the study area, and the kappa coefficients and OAs.

TABLE 3 | Classification accuracy assessment in different subareas.

Subarea	Area (m^2)	Mean accuracy							Kappa	OA
		Green roofs	Grass	Trees (shrubs)	Bare land	Buildings	Roads	Water		
No. 3	117,258	—	0.633	0.928	0.487	0.875	0.458	—	0.592	0.867
No. 5	127,549	—	0.770	0.919	0.680	0.862	0.935	—	0.827	0.884
No. 10	126,857	0.617	0.714	0.883	0.897	0.921	0.894	0.974	0.807	0.849
No. 13	126,330	0.690	0.811	0.897	0.438	0.895	0.911	0.742	0.821	0.867
No. 14	111,530	—	0.871	0.886	0.000	0.891	0.914	0.668	0.835	0.881
No. 17	118,552	0.833	0.924	0.944	0.000	0.964	0.954	0.732	0.919	0.940

TABLE 4 | Comparison of classification accuracy under different weather conditions.

Weather	Mean accuracy							Kappa	OA
	Green roofs	Grass	Trees (shrubs)	Bare land	Buildings	Roads	Water		
Sunny	0.775	0.734	0.874	0.762	0.936	0.940	0.986	0.852	0.879
Overcast	0.720	0.784	0.871	0.762	0.986	0.961	0.993	0.868	0.892

increase the difference between green roofs on buildings and vegetation on the ground. Analysis of the locations and image features of the error points (red circles in **Figure 7**) showed that on a sunny day, the distinction between grass in the shadow of trees and green roofs at the same elevation increased (red circles 6 and 7). In addition, stronger sunlight increased the reflection intensity of leaves on the sunny side of trees (red circles 5 and 6), so the distinction between trees and green roofs also increased. Therefore, accuracy for green roofs was better on the sunny day than on the overcast day. On the sunny day, trees shadows had a strong shading effect on grass (red circle 8), which made it easy to confuse grass with the shaded side of trees. Similarly, shadows of tall buildings blocked out trees and grass (red circles 2 and 3); thus, vegetation in shaded areas could also be misclassified. Therefore, the accuracy of grass was better on the overcast day than on the sunny day. Shadows of tall buildings on the roads were easy to misclassify as water on the sunny day, but not on the overcast day (red circle 1). Under strong Sun on the sunny day, some special coatings on the buildings, such as solar panels, reflected sunlight, which could easily lead to misclassification (red circle 4). On balance, these effects meant that the overcast day image data resulted in better classification results. If the purpose of the flying mission is to obtain spectral data for classification, we recommend doing it on an overcast day with plenty of light.

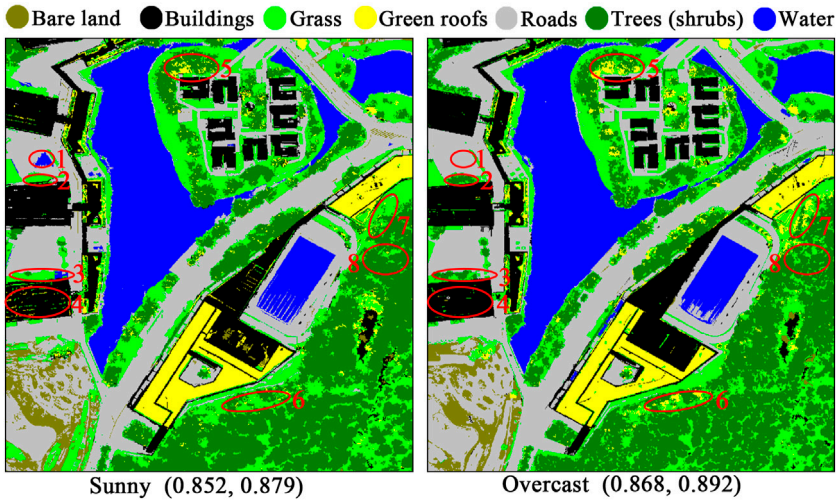

FIGURE 7 | Results on a sunny day (left) and an overcast day (right), and the kappa coefficients and OAs. The red circles indicate the main differences between the two subfigures.

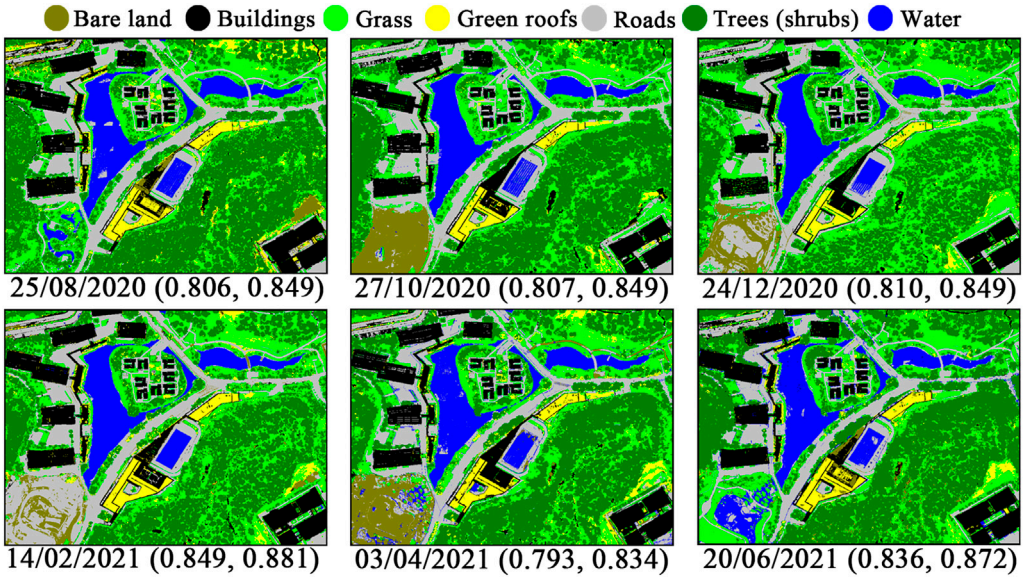

FIGURE 8 | Results for different seasons, and the kappa coefficients and OAs.

3.5 Effect of Seasons on Classification

The kappa coefficients and OAs with RF algorithm in different months of the year (**Figure 8**) showed that the best classification results were in February (winter) and June (summer), and the kappa coefficient and OA for February were better than those for June.

Table 5 shows that accuracies for grass, roads, and water for February were better than those for June. This may be because the grass was withered or dead in winter, and thus was more easily distinguished from trees on the spectrum. In addition, the tree canopies shrank, so that the increased quantity of light made it easier to identify grass in gaps. As discussed in **Section 3.4**, shadows made the classification results worse. The area of shadows increases in winter, which could decrease the accuracy. However, grass and trees accounted for a large proportion of the total area, whereas the area of shadows was small, leading to a better classification result in winter. Because the sunlight was weaker in winter, there was a smaller difference between the roads in shadow and the roads in sunlight. Therefore, the mean accuracy of roads was better in winter than in summer. In addition, when the sunlight was close to direct in summer, water surfaces tended to generate mirror reflections, which produced noisy points in the UAV images. Therefore, misclassification of water occurred easily,

TABLE 5 | Comparison of classification accuracy for February and June.

Month	Mean accuracy							Kappa	OA
	Green roofs	Grass	Trees (shrubs)	Bare land	Buildings	Roads	Water		
February	0.646	0.812	0.903	0.701	0.913	0.944	1.000	0.849	0.881
June	0.699	0.802	0.912	0.748	0.920	0.910	0.914	0.836	0.872

as shown in the center of the subfigures in **Figure 8** (April, June, and August).

Comparing the February and June classification results in **Figure 8** and **Table 5**, the mean accuracy for green roofs in June (i.e., 0.699) was better than that in February (i.e., 0.646). This may be because strong summer sunlight made other vegetation more distinct from the green roofs, which is consistent with the discussion in **Section 3.4**. Campus construction work caused the change in bare land area that resulted in the difference between the 2 months.

3.6 Effect of Different Image Layers on Classification

The combination of seven image layers (B, G, R, RE, NIR, NDVI, DSM) were used as the benchmark for comparing the results with RF algorithm. By comparing the classification accuracies after reducing the number of image layers, the effects of different layers on the results were analyzed. For convenience, we refer to the results from different layer combinations as cases I–VIII (**Figure 9**).

Case I was the benchmark that included all seven layers. Except for green roofs, the mean accuracies in case I were the best. However, the classification result for water was not significantly affected by the different layers, with the accuracies in all the cases larger than 0.94. In most cases, the average accuracies of green roofs and grass were less than 0.8, which indicated that they were easily confused classes.

Case II (B, G, R, RE, NIR, NDVI) did not include the DSM layer. Because green roofs and grass, as well as roads and buildings, have similar features (Boonpook et al., 2021), when the DSM layer was not included, the accuracies of green roofs, grass, buildings, and roads were considerably lower. Therefore, the DSM layer was key information that distinguished green roofs and grass, as well as buildings and roads. To improve the classification accuracy further, the method identifying the four types of infrastructure should be developed in future research. Because green roofs are located on buildings, it may be effective to first extract the buildings, and then identify vegetation on buildings as green roofs. For building recognition, some researchers have used manual extraction (Shao et al., 2021), which is time-consuming and laborious. Due to the different colors and types of building roofs, it is difficult to identify them effectively with only spectral images (Kim et al., 2011). Demir and Baltsavias (2012) and Wang et al. (2018) combined the slope from DSM, spectral images, and other information to identify buildings, and the accuracy was above 0.9. Kim et al. (2011) analyzed LiDAR data to obtain normalized digital surface model (nDSM), and then combined it with airborne images to identify buildings. The nDSM, which is the difference between DSM and digital elevation model, is created from a point cloud (Talebi et al., 2014; Sun and Lin, 2017; Kodors, 2019). Talebi et al. (2014) also used nDSM to distinguish roads, building roofs, and pervious surfaces, and the mean accuracy of building recognition was above 0.8. In summary, using the slope from DSM or nDSM combined with spectral images is effective for identifying buildings, and green roofs, grass, and roads can be accurately classified further.

Case III (B, G, R, RE, NIR, DSM) did not include the NDVI layer. Comparing the results of cases I and III, the accuracies of most classes in case I were higher than those in case III, except for green roofs. The classification subfigures (**Supplementary Figure S4**) showed that green roofs were overclassified in case I, decreasing the accuracy for green roofs. In case IV (B, G, R, RE, NDVI, DSM), which did not include the NIR layer, the accuracy for green roofs was greatly improved, whereas the OA was still as good as that in case I. The results for case V (B, G, R, NIR, NDVI, DSM), which did not include the RE layer, were similar to those for case IV, but the accuracies for bare land and buildings were lower.

Case VI (B, G, R, NDVI, DSM) did not include the RE and NIR layers, and the accuracy for green roofs was increased substantially by 0.2. The accuracies for grass and roads were decreased, but the other changes were small. The decrease in OA was small, and the classification results were good in general. Case VII (NIR, RE, NDVI, DSM) did not include the B, G, and R bands, and the accuracy for green roofs increased by 0.13. Cases VI and VII showed that appropriate redundancy removal of spectral image layers helped to identify green roofs accurately.

In case VIII (B, G, R, DSM), which did not include the NIR, RE, and NDVI layers, in addition to green roofs and bare land, the accuracies of the other classes were decreased considerably. For overall evaluation, the OA was below 0.8. In particular, the accuracy of grass dropped below 0.6. Case VIII demonstrates the problem of insufficient data layers.

This analysis demonstrated that the DSM layer is crucial for distinguishing green roofs and grass, as well as buildings and roads. Furthermore, appropriate removal of redundant spectral image layers increased the accuracy for green roofs. Case VI (B, G, R, NDVI, DSM) used five image layers, and the green roof accuracy was increased by 0.2 at the cost of decreasing the accuracy for grass by 0.034. The accuracies for the other classes were maintained, which indicated that case VI was the most appropriate combination.

3.7 Limitations

Firstly, although there have been several represented types of infrastructure considered in this study, some other types of green

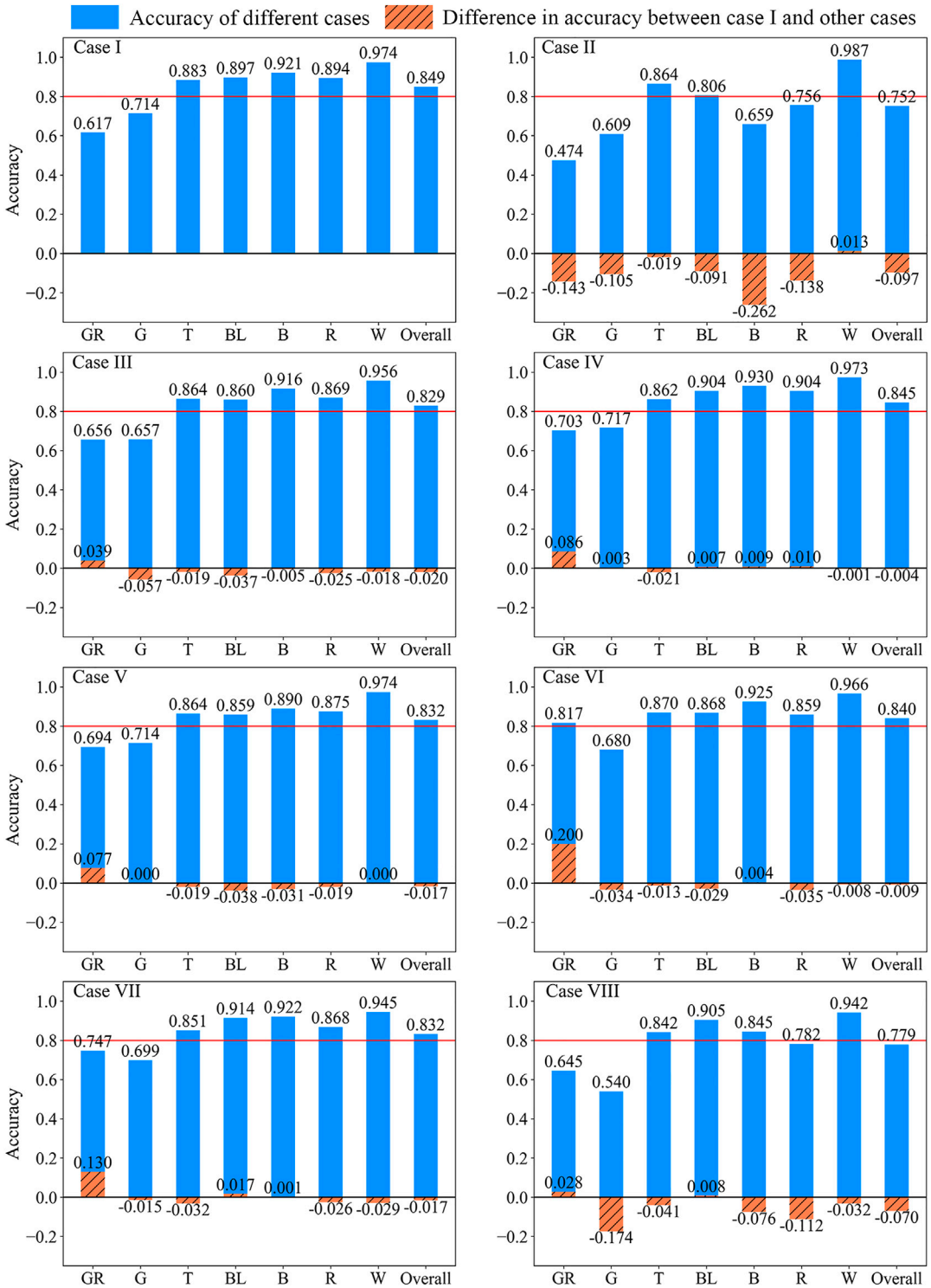

FIGURE 9 | Accuracies of classification results with different image layers. The abbreviations for the classes on the abscissa are as follows: GR. green roofs, G. grass, T. trees (shrubs), BL. bare land, B. buildings, R. roads, W. water.

infrastructure (e.g., rain garden) are still missed. Besides, in gray infrastructure, roads can be further subdivided into asphalt roads and porous brick pavements. The porous pavement cannot be recognized in this study. The algorithms and multispectral data used in this paper are capable to recognize the green roofs but not able to distinguish the above finer types effectively.

Secondly, in terms of the sampling method, we only get the optimal sampling interval for college communities. For different types of study areas, we need to conduct trial and error tests to get the optimal sampling interval. This step will still require further improvement.

Thirdly, the remote sensing data we used is limited. If LiDAR point cloud data or DEM data are available, in conjunction with DSM and spectral data, the classification accuracy of green roofs, grass, trees, buildings and roads will be greatly improved.

4 CONCLUSION

We developed a method to classify blue-green-gray infrastructure accurately using machine learning algorithms and UAV image data. Because the resolution of UAV images is on the centimeter scale, this method could identify all types of infrastructure on a sub-meter scale.

The chessboard grid sampling method was used to ensure the randomness and objectivity of samples. Evaluating the accuracies with different sampling intervals showed that a sampling interval of 11.6 m ensured that the kappa coefficient and OA were in the almost perfect range (>0.8) and that the number of samples was reduced, which increased working efficiency.

There are many machine learning algorithms that can be used for infrastructure classification. The different principles of the algorithms cause differences in their applicability. Evaluating the accuracies of the classification results from six widely used algorithms showed that the RF, FC, and Bayes algorithms were suitable for recognizing different infrastructure. RF was the best algorithm because of its ability to process high-dimensional data well. In addition, the results in other subareas, in which the kappa coefficient and OA were generally greater than 0.8, showed that this method had universal applicability. For any type of infrastructure, more than 30 training samples were needed to ensure the reliability of classification.

Comparing the classification results on a sunny day and an overcast day showed that overcast day data increased the recognition of grass, trees, and roads in shadow. The misclassification of roads in shadow as water was also reduced. The angle of sunlight changes with seasons, which in turn alters the shadow area. In winter, the shadow area is larger, which may reduce the classification accuracy. However, because trees and grass were the main infrastructure types in the study area, shriveled grass in winter increased the spectral difference and classification accuracy. The combination of the two effects resulted in more accurate classification in winter.

To obtain better classification results, we used seven image layers. Through trial and error, we showed that appropriate removal of redundant spectral image layers, such as RE and NIR, increased the recognition accuracy of green roofs. The DSM layer was crucial for improving the distinction considerably between green roofs and grass, and buildings and roads. Using only five image layers (B, G, R, NDVI, and DSM) increased the accuracy for green roofs greatly at the cost of a small decrease in the accuracy for grass.

Our method can identify small facilities on a sub-meter scale, and can obtain a distribution map of blue-green-gray infrastructure in urban small catchments ($0.1–10\ km^2$) accurately and quickly. The classification of GI is fundamental for rational management and planning of GI, and contributes to sustainable development of urban areas. Combined with the rainwater use characteristics of various infrastructure, an accurate GI distribution map can help to simulate stormwater management and use effectiveness accurately in small urban catchments.

DATA AVAILABILITY STATEMENT

The raw data supporting the conclusion of this article will be made available by the authors, without undue reservation.

AUTHOR CONTRIBUTIONS

JJ wrote the manuscript, built the method, acquired data, and conducted data processing and analysis. WC conceived the study, built the method, together wrote this manuscript, and supervised this study. JL conceived the study, acquired funding, supervised the study, and contributed to the manuscript writing.

FUNDING

This work was supported by the National Key R&D Program of China (2018YFE0206200) and Strategic Priority Research Program of Chinese Academy of Sciences (XDA20060402). It was also supported by the National Natural Science Foundation of China (NSFC) (grant No. 41625001) and the High-level Special Funding of the Southern University of Science and Technology (grant Nos. G02296302 and G02296402).

ACKNOWLEDGMENTS

We acknowledge Dr. Wenfang Cao and Pengfei Wang of the iTOWER group for their help with software.

SUPPLEMENTARY MATERIAL

The Supplementary Material for this article can be found online at: https://www.frontiersin.org/articles/10.3389/fenvs.2021.778598/full#supplementary-material

REFERENCES

Alakian, A., and Achard, V. (2020). Classification of Hyperspectral Reflectance Images with Physical and Statistical Criteria. *Remote Sensing* 12, 2335. doi:10.3390/rs12142335

Bai, Y., Zhang, S., Bhattarai, N., Mallick, K., Liu, Q., Tang, L., et al. (2021). On the Use of Machine Learning Based Ensemble Approaches to Improve Evapotranspiration Estimates from Croplands across a Wide Environmental Gradient. *Agric. For. Meteorology* 298-299, 108308. doi:10.1016/j.agrformet.2020.108308

Bartesaghi-Koc, C., Osmond, P., and Peters, A. (2020). Quantifying the Seasonal Cooling Capacity of 'green Infrastructure Types' (GITs): An Approach to Assess and Mitigate Surface Urban Heat Island in Sydney, Australia. *Landscape Urban Plann.* 203, 103893. doi:10.1016/j.landurbplan.2020.103893

Benedict, M. E., and McMahon, E. T. (2006). *Green Infrastructure*. Washington, DC: Island Press.

Boonpook, W., Tan, Y., and Xu, B. (2021). Deep Learning-Based Multi-Feature Semantic Segmentation in Building Extraction from Images of UAV Photogrammetry. *Int. J. Remote Sensing* 42, 1–19. doi:10.1080/01431161.2020.1788742

Brunner, M., Von Felten, J., Hinz, M., and Hafner, A. (2021). Central European Early Bronze Age Chronology Revisited: A Bayesian Examination of Large-Scale Radiocarbon Dating. *PLOS ONE* 15, e0243719. doi:10.1371/journal.pone.0243719

Cui, W., and Chui, T. F. M. (2021). Measurements and Simulations of Energy Fluxes over a High-Rise and Compact Urban Area in Hong Kong. *Sci. Total Environ.* 765, 142718. doi:10.1016/j.scitotenv.2020.142718

Dai, X., Wang, L., Tao, M., Huang, C., Sun, J., and Wang, S. (2021). Assessing the Ecological Balance between Supply and Demand of Blue-green Infrastructure. *J. Environ. Manage.* 288, 112454. doi:10.1016/j.jenvman.2021.112454

Demir, N., and Baltsavias, E. (2012). Automated Modeling of 3D Building Roofs Using Image and LiDAR Data. *ISPRS Ann. Photogramm. Remote Sens. Spat. Inf. Sci.* I-4, 35–40. doi:10.5194/isprsannals-I-4-35-2012

Dimitrov, S., Georgiev, G., Georgieva, M., Gluschkova, M., Chepisheva, V., Mirchev, P., et al. (2018). Integrated Assessment of Urban green Infrastructure Condition in Karlovo Urban Area by *In-Situ* Observations and Remote Sensing. *One Ecosystem* 3, e21610. doi:10.3897/oneeco.3.e21610

Dobrinić, D., Gašparović, M., and Medak, D. (2021). Sentinel-1 and 2 Time-Series for Vegetation Mapping Using Random forest Classification: A Case Study of Northern Croatia. *Remote Sensing* 13 (12), 2321. doi:10.3390/rs13122321

Environmental Protection Agency (2019). Land Cover. United States Environmental Protection Agency. Available at: https://cfpub.epa.gov/roe/indicator.cfm?i=49 (Accessed on November 1, 2021).

Environmental Protection Agency (2015). What Is Green Infrastructure? United States Environmental Protection Agency. Available at: https://www.epa.gov/green-infrastructure/what-green-infrastructure (Accessed on July 12, 2021).

Fan, C., and Lu, R. (2021). UAV Image Crop Classification Based on Deep Learning with Spatial and Spectral Features. *IOP Conf. Ser. Earth Environ. Sci.* 783, 012080. doi:10.1088/1755-1315/783/1/012080

Furberg, D., Ban, Y., and Mörtberg, U. (2020). Monitoring Urban green Infrastructure Changes and Impact on Habitat Connectivity Using High-Resolution Satellite Data. *Remote Sensing* 12, 3072. doi:10.3390/RS12183072

Garzon-Lopez, C. X., and Lasso, E. (2020). Species Classification in a Tropical alpine Ecosystem Using UAV-Borne RGB and Hyperspectral Imagery. *Drones* 4, 69. doi:10.3390/drones4040069

Gašparović, M., and Dobrinić, D. (2021). Green Infrastructure Mapping in Urban Areas Using sentinel-1 Imagery. *Croat. J. For. Eng. (Online)* 42, 337–356. doi:10.5552/crojfe.2021.859

Gregorio, A. D., and Jansen, L. J. M. (2000). Land Cover Classification System (LCCS): Classification Concepts and User Manual. Food and Agriculture Organization. Available at: https://www.fao.org/3/x0596e/X0596e00.htm (Accessed on November 1, 2021).

Han, J. W., Kamber, M., and Pei, J. (2012). *Data Mining: Concepts and Techniques*. Beijing: China Machine Press.

Hashad, K., Gu, J., Yang, B., Rong, M., Chen, E., Ma, X., et al. (2021). Designing Roadside green Infrastructure to Mitigate Traffic-Related Air Pollution Using Machine Learning. *Sci. Total Environ.* 773, 144760. doi:10.1016/j.scitotenv.2020.144760

He, L. M., Shen, Z. Q., Kong, F. S., and Liu, Z. K. (2007). Study on Multi-Source Remote Sensing Images Classification with SVM (In Chinese). *J. Image Graphics* 4, 648–654. doi:10.3969/j.issn.1006-8961.2007.04.015

Hu, J., Cai, A. Y., Xiao, X. C., Yang, Z. P., Zhou, C., Zhou, W. B., et al. (2008). *Feasibility Study Report of Campus Construction Project of South University of Science and Technology (In Chinese)*. Shenzhen: Shenzhen Quncui Real Estate Appraisal and Construction Consulting Co. Ltd.

Hu, T., Chang, J., and Syrbe, R. U. (2021). Green Infrastructure Planning in Germany and China: a Comparative Approach to green Space Policy and Planning Structure. *Res. Urbanism Ser.* 6, 99–126. doi:10.7480/rius.6.96

Ismail, A., Juahir, H., Mohamed, S. B., Toriman, M. E., Kassim, A. M., Zain, S. M., et al. (2021). Support Vector Machines for Oil Classification Link with Polyaromatic Hydrocarbon Contamination in the Environment. *Water Sci. Techn.* 83, 1039–1054. doi:10.2166/wst.2021.038

Jiang, Y., Zhang, L., Yan, M., Qi, J., Fu, T., Fan, S., et al. (2021). High-resolution Mangrove Forests Classification with Machine Learning Using Worldview and UAV Hyperspectral Data. *Remote Sensing* 13, 1529. doi:10.3390/rs13081529

Khalaim, O., Zabarna, O., Kazantsev, T., Panas, I., and Polishchuk, O. (2021). Urban green Infrastructure Inventory as a Key Prerequisite to Sustainable Cities in Ukraine under Extreme Heat Events. *Sustainability* 13, 2470. doi:10.3390/su13052470

Kim, Y., Han, Y., Byun, Y., Choi, J., Han, D., and Kim, Y. (2011). "Object-based Classification of an Urban Area through a Combination of Aerial Image and Airborne Lidar Data," in American Society for Photogrammetry and Remote Sensing Annual Conference 2011, 265–270. Available at: https://www.scopus.com/inward/record.uri?eid=2-s2.0-84868623294&partnerID=40&md5=67b8f95b588f1f61c8865bc09fd897b6.

Kodors, S. (2019). Comparison of Algorithms for Construction Detection Using Airborne Laser Scanning and nDSM Classification. *Environ. Techn. Resour. Proc. Int. Scientific Pract. Conf.* 2, 79–83. doi:10.17770/etr2019vol2.4032

Landis, J. R., and Koch, G. G. (1977). The Measurement of Observer Agreement for Categorical Data. *Biometrics* 33, 159–174. doi:10.2307/2529310

Li, M., Ma, L., Blaschke, T., Cheng, L., and Tiede, D. (2016). A Systematic Comparison of Different Object-Based Classification Techniques Using High Spatial Resolution Imagery in Agricultural Environments. *Int. J. Appl. Earth Observation Geoinformation* 49, 87–98. doi:10.1016/j.jag.2016.01.011

Lynn Yaling Cai, L. Y., and Hon Keung Kwan, H. K. (1998). Fuzzy Classifications Using Fuzzy Inference Networks. *IEEE Trans. Syst. Man. Cybern. B* 28, 334–347. doi:10.1109/3477.678627

Machine Learning (2018). A Step by Step CART Decision Tree Example. Sefik Ilkin Serengil. Available at: https://sefiks.com/2018/08/27/a-step-by-step-cart-decision-tree-example/(Accessed on July 12, 2021).

Maes, J., Zulian, G., Thijssen, M., Castell, C., Baro, F., Ferreira, A., et al. (2016). *Mapping and Assessment of Ecosystems and Their Services: Urban Ecosystems 4th Report*. Luxembourg: Publication Office of the European Union. JRC101639. doi:10.2779/625242

Man, Q., Dong, P., Yang, X., Wu, Q., and Han, R. (2020). Automatic Extraction of Grasses and Individual Trees in Urban Areas Based on Airborne Hyperspectral and LiDAR Data. *Remote Sensing* 12, 2725. doi:10.3390/RS12172725

Meteorological Bureau of Shenzhen Municipality (2021). Climate Situation and Characteristics of Seasons in Shenzhen. Meteorological Bureau of Shenzhen Municipality. Available at: http://weather.sz.gov.cn/qixiangfuwu/qihoufuwu/qihouguanceyupinggu/qihougaikuang/(accessed on July 12, 2021).

Miura, N., Koyanagi, T. F., Yamada, S., and Yokota, S. (2021). Classification of Grass and Forb Species on Riverdike Using UAV LiDAR-Based Structural Indices. *Int. J. Automation Technol.* 15, 268–273. doi:10.20965/ijat.2021.p0268

Mohammadpoor, M., and Eshghizadeh, M. (2021). Introducing an Intelligent Algorithm for Extraction of Sand Dunes from Landsat Satellite Imagery in Terrestrial and Coastal Environments. *J. Coast Conserv* 25, 3. doi:10.1007/s11852-020-00789-x

Narziev, J., Nikam, B., and Gapparov, F. (2021). Infrastructure Mapping and Performance Assessment of Irrigation System Using GIS and Remote Sensing. *E3s Web Conf.* 264, 03005. doi:10.1051/e3sconf/202126403005

Nitoslawski, S. A., Wong-Stevens, K., Steenberg, J. W. N., Witherspoon, K., Nesbitt, L., and Konijnendijk van den Bosch, C. C. (2021). The Digital Forest: Mapping a

Decade of Knowledge on Technological Applications for Forest Ecosystems. *Earth's Future* 9 (8), e2021EF002123. doi:10.1029/2021EF002123

Ouyang, W., Morakinyo, T. E., Ren, C., Liu, S., and Ng, E. (2021). Thermal-irradiant Performance of green Infrastructure Typologies: Field Measurement Study in a Subtropical Climate City. *Sci. Total Environ.* 764, 144635. doi:10.1016/j.scitotenv.2020.144635

Palmer, M. A., Liu, J., Matthews, J. H., Mumba, M., and D'Odorico, P. (2015). Manage Water in a green Way. *Science* 349 (6248), 584–585. doi:10.1126/science.aac7778

Shao, H., Song, P., Mu, B., Tian, G., Chen, Q., He, R., et al. (2021). Assessing City-Scale green Roof Development Potential Using Unmanned Aerial Vehicle (UAV) Imagery. *Urban For. Urban Green.* 57, 126954. doi:10.1016/j.ufug.2020.126954

Sudarshan Rao, B., Hota, M., and Kumar, U. (2021). Crop Classification from UAV-Based Multi-Spectral Images Using Deep Learning. *Comm. Com. Inf. Sc.* 1376, 475–486. doi:10.1007/978-981-16-1086-8_42

Sun, X. F., and Lin, X. G. (2017). Random-forest-ensemble-based Classification of High-Resolution Remote Sensing Images and nDSM over Urban Areas. *Int. Arch. Photogramm. Remote Sens. Spat. Inf. Sci.* XLII-2/W7, 887–892. doi:10.5194/isprs-archives-XLII-2-W7-887-2017

Talebi, L., Kuczynski, A., Graettinger, A. J., and Pitt, R. (2014). Automated Classification of Urban Areas for Storm Water Management Using Aerial Photography and LiDAR. *J. Hydrol. Eng.* 19, 887–895. doi:10.1061/(ASCE)HE.1943-5584.0000815

Trimble Germany GmbH (2014a). *eCognition Developer 9.0 Reference Book*. Munich: Trimble Germany GmbH.

Trimble Germany GmbH (2014b). *eCognition Developer 9.0 User Guide*. Munich: Trimble Germany GmbH.

Venkataramanan, V., Packman, A. I., Peters, D. R., Lopez, D., McCuskey, D. J., McDonald, R. I., et al. (2019). A Systematic Review of the Human Health and Social Well-Being Outcomes of green Infrastructure for Stormwater and Flood Management. *J. Environ. Manage.* 246, 868–880. doi:10.1016/j.jenvman.2019.05.028

Wang, H., Han, D., Mu, Y., Jiang, L., Yao, X., Bai, Y., et al. (2019). Landscape-level Vegetation Classification and Fractional Woody and Herbaceous Vegetation Cover Estimation over the Dryland Ecosystems by Unmanned Aerial Vehicle Platform. *Agric. For. Meteorology* 278, 107665. doi:10.1016/j.agrformet.2019.107665

Wang, J. B., Jin, Q., Yang, G. D., Zhang, X. Q., Zhan, G. Q., and Shao, P. (2018). A Building Extraction Method Based on Object-Oriented Technology and DSM Image (In Chinese). *Glob. Geology.* 37, 1258–1264. doi:10.3969/j.issn.1004-5589.2018.04.026

Wicaksono, A., and Hernina, R. (2021). Urban Tree Analysis Using Unmanned Aerial Vehicle (UAV) Images and Object-Based Classification (Case Study: University of Indonesia Campus). *IOP Conf. Ser. Earth Environ. Sci.* 683, 012105. doi:10.1088/1755-1315/683/1/012105

Yang, Y., Li, J., Huang, Q., Xia, J., Li, J., Liu, D., et al. (2021). Performance Assessment of Sponge City Infrastructure on Stormwater Outflows Using Isochrone and SWMM Models. *J. Hydrol.* 597, 126151. doi:10.1016/j.jhydrol.2021.126151

Zhang, F., and Yang, X. (2020). Improving Land Cover Classification in an Urbanized Coastal Area by Random Forests: The Role of Variable Selection. *Remote Sensing Environ.* 251, 112105. doi:10.1016/j.rse.2020.112105

Zhang, J., Feng, X., Shi, W., Cui, J., Peng, J., Lei, L., et al. (2021). Health Promoting green Infrastructure Associated with green Space Visitation. *Urban For. Urban Green.* 64, 127237. doi:10.1016/j.ufug.2021.127237

Zhao, H.-S., Zhu, X.-C., Li, C., Wei, Y., Zhao, G.-X., and Jiang, Y.-M. (2017). Improving the Accuracy of the Hyperspectral Model for Apple Canopy Water Content Prediction Using the Equidistant Sampling Method. *Sci. Rep.* 7, 11192. doi:10.1038/s41598-017-11545-x

Conflict of Interest: The authors declare that the research was conducted in the absence of any commercial or financial relationships that could be construed as a potential conflict of interest.

Publisher's Note: All claims expressed in this article are solely those of the authors and do not necessarily represent those of their affiliated organizations, or those of the publisher, the editors and the reviewers. Any product that may be evaluated in this article, or claim that may be made by its manufacturer, is not guaranteed or endorsed by the publisher.

frontiers in Environmental Science

REVIEW
published: 19 January 2022
doi: 10.3389/fenvs.2021.816093

Stormwater Management Modeling in "Sponge City" Construction: Current State and Future Directions

Qianhui Liu[1†], *Wenhui Cui*[1†], *Zhan Tian*[1], *Yingdong Tang*[2], *Martin Tillotson*[3] *and Junguo Liu*[1*]

[1]School of Environmental Science and Engineering, Southern University of Science and Technology, Shenzhen, China, [2]Power China Huadong Engineering Corporation Limited (HDEC), Hangzhou, China, [3]School of Civil Engineering, University of Leeds, Leeds, United Kingdom

In response to urban pluvial flooding and pollution, the Chinese government proposed a "sponge city" policy in 2013 that aims to improve urban stormwater management and promote sustainable urban development. However, at present, sponge city construction is still in its exploratory stage. It is still not clear which models are capable of simulating the six key processes (i.e., "retention," "infiltration," "storage," "purification," "discharge," and "utilization") of sponge city practices. Its various benefits (e.g., social, economic and environmental benefits) have not yet been systematically investigated in the context of the sponge city. In this study, we reviewed and compared 19 urban stormwater management models (including 13 hydrological models and 10 decision-support tools, as there are 4 overlap ones) and investigated their application in China. Firstly, we examined the mechanisms behind the hydrological models and compared the abilities of the models to simulate various processes. Secondly, we analyzed what kinds of benefits can be addressed by these decision support tools (DSTs). Finally, we discussed the applications and limitations of the models in various climate zones in China. The findings suggest that none of the models consider the impact of climate change on the sponge city practices (SCP) and none of DSTs can simulate the negative performance of SCP. Furthermore, the lack of sufficient databases in China limited the applications of many of the models. Additionally, we found that the hydrological processes corresponding to "storage" were given more attention in southern China, and "infiltration" of stormwater was of greater concern in northern China. In the context of sponge city construction, this paper provides suggestions for future model development of urban stormwater management in China, such as the development of a stormwater database and the incorporation of long-term climate change impacts into the model.

Keywords: stormwater management, sponge city, green stormwater infrastructure, model comparison, stormwater utilization

OPEN ACCESS

Edited by:
Pedro Neves Carvalho,
Aarhus University, Denmark

Reviewed by:
Jun Xia,
Wuhan University, China
An Liu,
Shenzhen University, China

****Correspondence:***
Junguo Liu
junguo.liu@gmail.com

[†]These authors have contributed equally to this work and share first authorship

Specialty section:
This article was submitted to Water and Wastewater Management, a section of the journal Frontiers in Environmental Science

Received: *16 November 2021*
Accepted: *20 December 2021*
Published: *19 January 2022*

Citation:
Liu Q, Cui W, Tian Z, Tang Y, Tillotson M and Liu J (2022) Stormwater Management Modeling in "Sponge City" Construction: Current State and Future Directions. Front. Environ. Sci. 9:816093. doi: 10.3389/fenvs.2021.816093

1 INTRODUCTION

Rapid urbanization increases impervious surface area and reduces opportunities for stormwater infiltration, altering the urban hydrological cycle (Oudin et al., 2018; Hou et al., 2019; Rosenberger et al., 2021; Wang and Palazzo et al., 2021). In the context of climate change, extreme rainfall events have increased in frequency, resulting in greater urban flooding potential, non-point source

pollution, and more frequent discharges from combined sewer overflows (Hou et al., 2020; Mishra et al., 2021, Yang et al., 2021). Due to the inadequacy of conventional stormwater management systems, countries have begun to explore novel and more sustainable stormwater management techniques such as low impact development (LID), best management practices (BMPs), and green infrastructure (GI) in the United States, water sensitive urban design (WSUD) in Australia, sustainable drainage systems (SUDs) in the United Kingdom, low impact city design and development (LIUDD) in New Zealand, as well as the active, beautiful, clean (ABC) water program in Singapore (Chang et al., 2018; Zhang et al., 2019; Kazantsev et al., 2020; Islam et al., 2021). In 2013, the Chinese government proposed its own urban water management programme, the national "sponge city" initiative, meaning that cities can promote infiltration, retain, store, and purify stormwater like a sponge to utilize stormwater resources and alleviate the problems of flooding, water shortages, and pollution (Li H et al., 2017; Wang et al., 2017). Such SCP have significantly impacted urban hydrological processes and stormwater-resource utilization in China (Suppakittpaisarn et al., 2017; Traver and Ebrahimian, 2017; Li C et al., 2019). They can increase the permeability of urban surfaces and infiltration, alleviate the negative impacts caused by stormwater runoff (e.g., flooding and non-point source pollution), and also replenish groundwater (Fanelli et al., 2017). Moreover, through SCP, stormwater resources are collected and treated in sustainable, cost-effective ways for urban public and residential applications such as firefighting, road cleaning, and toilet flushing (Sartor et al., 2018; Grytsenko et al., 2020). "Sponge city" has been mentioned in the sixth IPCC report as one of effective practices. Chinese government also strongly promotes it in the new urban planning and defined six words to mark the functions of sponge city (i.e., "retention," "infiltration," "storage," "utilization," "purification" and "discharge") (Xia et al., 2017). The six processes have the specific Chinese words for each of them, which are proposed in an official document issued by the Chinese State Council (i.e., *Zhi* for retention, *Shen* for infiltration, *Xu* for storage, *Yong* for utilization, *Jing* for purification, and *Pai* for discharge) (Liu H et al., 2017). They are used to describe the process from rainwater dropped from the sky to it is discharged through the surface or pipes. However, the practices lack the scientific instructions for the successful implementation.

Numerous studies have applied hydrological models to simulate processes and evaluate the cost effectiveness of various SCP configurations. For example, Li et al. (2018) used Hydrus-1D to investigate the operational effects of bioretention on tanks in Xi'an, Shanxi Province. Zhang et al. (2021) used SWMM and SUSTAIN to assess the cost effectiveness of SCP in Dali, Yunnan Province. Additionally, DSTs have supported policymakers or stakeholders in making better and more effective decisions. For example, the Spatial Suitability ANalysis TOol (SSANTO) was used in Melbourne, Australia to involve stakeholders in urban planning through integration of WSUD (Kuller et al., 2019), and STORMKIT was applied in the Australian state of Victoria to assist in the design of a stormwater system using minimum input requirements (Imteaz, 2015). A few studies have reviewed or compared model applications in multiple situations. For example, Jayasooriya and Ng (2014) selected 10 models and conducted a series of comparisons relating to data requirements, model accuracy, simulation approaches etc., and Elliott and Trowsdale (2007) compared 10 models in terms of application range, calculation methods, contaminant removal, SCP devices, and user interfaces. Haris et al. (2016) reviewed 12 models to explore their functionality, accessibility, characteristics, and components.

These studies have, however, not compared the application of stormwater models in the context of China's sponge city policy. For example, how do models or algorithms embedded in stormwater models correspond to the six mandated functions for sponge city construction? The variables and parameters used as inputs to the models are not yet summarized for sponge city policymakers and other related stakeholders. Moreover, are current DSTs capable of supporting a cost benefit analysis of sponge city construction? These questions require further elucidation, hence our study has investigated the performance of 19 urban stormwater management models in terms of hydrological simulations and decision support in the context of the sponge city. Given that the six hydrological processes (i.e., "retention," "infiltration," "storage," "utilization," "purification" and "discharge," **Figure 1**) are mandated in the construction of sponge cities (Jia et al., 2017), we have analyzed hydrological simulations based on these six processes. Additionally, sponge city practices provide environmental, economic and social benefits, an understanding of which can provide support to decision making. However, their relevant benefits in China have not been systematically summarized and evaluated (He et al., 2019; She et al., 2021). Therefore, our study also aims to evaluate DST from this perspective.

2 MATERIALS AND METHODS

In this paper, we firstly reviewed the stormwater modelling and tools, which are currently assessed worldwide. Then we found the assessed their applications in China based on the published articles.

Firstly, we identified 33 stormwater models from published articles, conference papers, project websites, government technical reports and modeling guidelines. Amongst these, we selected ones simulating different SCP processes which are currently available and widely used. After manually screening, we identified 19 models, which detail information and their advantages and shortcomings are included in the Supplementary Tables. Based on their main features, we divided the models into two types: hydrological models (13 no.) and DSTs (10 no.). Amongst the 19 models, LIDRA, L-THIA LID, MUSIC, and SUSTAIN were able to model both hydrological and DST functions, hence were included in both categories. Then we compared the mechanisms and the required input variables of the hydrological models with regard to retention, infiltration, storage, utilization, purification, and discharge. We also compared the DSTs in terms of their ability to model social, economic, and environmental benefits.

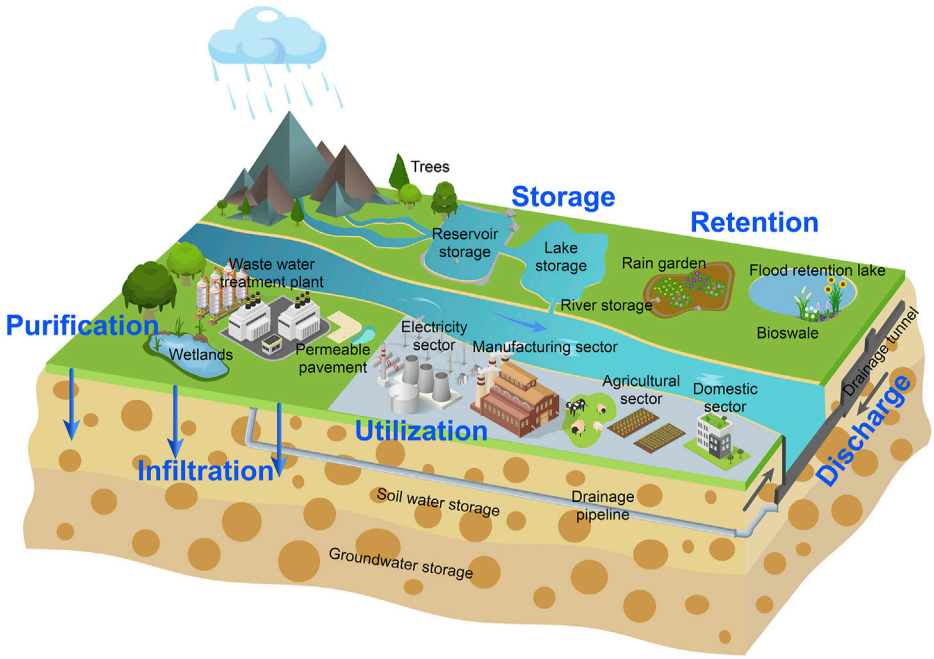

FIGURE 1 | The six hydrological processes in sponge city design.

Secondly, to assess the application of these 19 models in Chinese sponge city construction, we reviewed related articles in Web of Science and Scopus, excluded the review articles. Given that LID practices were firstly applied in Beijing since 2000, articles published from January 1, 2000 were investigated. The search terms in this study were "Model name + Stormwater or Rainwater". After the manual filtering, 199 case studies were retrieved.

3 RESULTS

3.1 Hydrological Performance of Models

The internal mechanisms and input variables for simulating the six main processes of each hydrological model are summarized in **Table 1**. The mathematical algorithms associated with different processes are displayed in the mechanism row. Some processes are not explicitly described in the user manual of several reviewed models, and these are shown as blanks. The comparison of the six main processes simulated by these models is described below.

3.1.1 Retention

Retention is an important component in calculating surface runoff, and it is usually embedded in the rainfall-runoff module (i.e., SWMM, SUSTAIN, MIKE-URBAN, L-THIA LID, and MUSIC) (Zhang D et al., 2018; Liu et al., 2019). Retention is regarded as a process related to ground conditions such as slope, surface storage and roughness (Sharior et al., 2019). The input parameters of the models are similar, including slope, surface manning coefficient, storage depth, vegetative cover and width. However, specific algorithms for retention are not separated from the runoff calculation.

The retention process in the RECARGE and HEC-HMS models include interception and surface depression. The former calculates surface depression as a function of zone thickness and storage layer thickness based on the water balance model (Tu A et al., 2020), while the latter uses an empirical equation to estimate the interception and surface depression as an empirical value may vary with different surface conditions (Roy et al., 2013; Gebre, 2015). The SWAT model can estimate retention based on soil profile water content or accumulated plant evapotranspiration (Elçi, 2017; Cheng et al., 2021). The LIDRA model considers retention as tree canopy interception, which is related to rainfall depth (Horton, 1919). Retention cannot be simulated in Hydrus-1D because the model only considers the longitudinal movement of stormwater in the soil layer and ignores its horizontal movement on the surface. GIF Mod and P8 lack specific algorithms to calculate the retention process.

3.1.2 Infiltration

With the exception of GIF Mod, all other models can simulate infiltration. LIDRA, MUSIC and Hydrus-1D use specific methods related to soil properties to calculate infiltration, whilst the others estimate infiltration based on algorithms embedded in the surface runoff modules. The most widely used methods are the Green-Ampt method and the Soil Conservation Service (SCS) curve method. SWMM, SUSTAIN, HEC-HMS and MIKE-URBAN have several methods to calculate infiltration (see below). StormTac calculates infiltration as a residual of the water

TABLE 1 | Comparison of the mechanisms and input variables of hydrological models in terms of the six mandated processes in sponge city design.

Model name	Types	Retention	Infiltration	Storage	Utilization	Purification	Discharge
SWMM	Mechanism	a process related to the ground conditions such as slope, surface storage, and roughness	Horton infiltration equation; Green-Ampt method; SCS curve method	1. Function Area = A × (Depth)B + C to describe how surface area varies with depth; 2. Tabulated area versus depth curve	LID facility storage layer	power function, exponential function, saturation function, exponential wash-off function and rating curve wash-off function	Manning equation
	Input variables	slope, manning coefficient, impervious rate, storage rate, width	Horton: max and min infiltration rate, decay constant, drying time, max infiltration volume; Green-Ampt: suction head, conductivity, initial deficit; SCS Curve: SCS number, conductivity, drying time	storage area; volume or depth	storage depth	pollutant initial buildup, street sweeping interval, street sweeping availability, last swept; buildup: pollutant, function, buildup rate constant, power/sat. constant, scaling factor, time series, normalizer; wash-off: pollutant, function, coefficient, exponent, cleaning efficiency, bmp efficiency	seepage rate value (in/hr or mm/hr)
SUSTAIN	Mechanism	a process related to the ground conditions such as slope, surface storage, and roughness	Horton infiltration equation; Green-Ampt method; SCS curve method	1. Function Area = A × (Depth) B + C to describe how surface area varies with depth; 2. Tabulated area versus depth curve	LID facility storage layer	VFSMOD algorithms for sediment interception	Manning equation
	Input variables	slope, manning coefficient, impervious rate, storage rate, width	Horton: max and min infiltration rate, decay constant, drying time, max infiltration volume; Green-Ampt: suction head, conductivity, initial deficit; SCS Curve: SCS number, conductivity, drying time	storage area; volume or depth	storage depth	pollutant initial buildup, street sweeping interval, street sweeping availability, last swept; buildup: pollutant, function, buildup rate constant, power/sat. constant, scaling factor, time series, normalizer; wash-off: pollutant, function, coefficient, exponent, cleaning efficiency, bmp efficiency	seepage rate value (in/hr or mm/hr)
MIKE-URBAN	Mechanism	the catchment editor can perform the retention related to surface conditions	Kinematic Wave and Linear Reservoir: Horton infiltration equation UHM: SCS curve method RDI	Kinematic Wave: surface storage RDI: snow storage, surface storage, unsaturated zone (root zone) storage, and groundwater storage	LID facility storage layer	—	—
	Input variables	storage depth, vegetative cover, surface roughness, surface slope, swale side slope	Horton: minimum and maximum infiltration capacity, infiltration time constant for wet and dry conditions SCS: curve number, initial abstraction depth, initial antecedent moisture condition	height, porosity, conductivity, clogging factor	storage volume parameters	—	—

(Continued on following page)

TABLE 1 | (*Continued*) Comparison of the mechanisms and input variables of hydrological models in terms of the six mandated processes in sponge city design.

Model name	Types	Retention	Infiltration	Storage	Utilization	Purification	Discharge
RECARGA	Mechanism	surface depression water balance model	Green-Ampt method	—	—	—	van Genuchten equation
	Input variables	SCP to connected impervious area ratio, roof depression storage	saturated hydraulic conductivity, average capillary suction head, ponded depth, the initial soil water deficit	—	—	—	soil layer dimensionless water content, the limiting hydraulic conductivity
HEC-HMS	Mechanism	interception and surface depressions	The deficit and constant loss model; The exponential loss model; The Green and Ampt loss model; The initial and constant loss model; The SCS curve number loss model; The Smith Parlange loss model; The soil moisture accounting (SMA) loss model	The relationship between storage and other variables, i.e., Elevation-Storage-Discharge, Storage-Discharge, Elevation-Area, and Elevation-Storage (identified by routing method)	—	Transport potential functions	Outflow Curve, Specified release, and Outflow Structures
	Input variables	empirical value	The deficit and constant loss model: maximum deficit, percolation rate, and initial deficit; Green and Ampt Loss Model: initial loss, hydraulic conductivity, wetting front suction, volume moisture deficit; Initial and Constant Loss Model: loss rates; SCS Curve Number: soil cover, land use, and antecedent moisture; SMA model: the maximum infiltration rate, evapotranspiration (ET), volume of soil storage	—	—	the specific gravity of the sediment grains, the density of dry clay sediment	—
GIF Mod	Mechanism	—	—	head-storage relationship: Van Genuchten-Mualem equation	—	transport of solid particles and dissolved and Solid-Associated water quality constituents governing equation	head-flow equations: Van Genuchten-Mualem equation, Manning equation, and Darcy equation
	Input variables	—	—	—	—	bottom area, initial water depth, depth, saturated moisture content, initial particle concentration	external flux, inflow time series
StormTac	Mechanism	An equation quantifying acceptable recipient loads considers retention; different SCP have different equations to calculate retention volume	Losses such as evaporation, ET and infiltration are considered in water balance calculations	—	—	The total pollutant concentration is calculated as a flow-weighted average of stormwater and baseflow concentrations	—
	Input variables	—	—	—	—	the catchment area	—

(Continued on following page)

TABLE 1 | (*Continued*) Comparison of the mechanisms and input variables of hydrological models in terms of the six mandated processes in sponge city design.

Model name	Types	Retention	Infiltration	Storage	Utilization	Purification	Discharge
SWAT	Mechanism	2 methods: vary with soil profile water content or accumulated plant ET	Green-Ampt method				Manning's equation
	Input variables	Water content, ET					
P8	Mechanism		SCS curve method			Particle concentrations in runoff are calculated using an empirical equation	Manning's equation
	Input variables						
L-THIA-LID	Mechanism	The initial abstraction, which describes all losses of precipitation (interception, infiltration, surface storage, and evaporation), is a function of the CN (SCS method)				NPS pollutant masses are computed by multiplying runoff depth for a land use by the area of that land use and the appropriate EMC value and converting units	
	Input variables	Soil properties				Land use properties	
Hydrus-1D	Mechanism	—	soil hydraulic function	—	—	—	deep drainage from the soil profile function
	Input variables	—	scaled unsaturated soil hydraulic conductivity, pressure head, scaling factor for the water content, scaling factor for the hydraulic conductivity, scaling factor for the pressure head, scaled volumetric water content, residual soil water content, scaled residual soil water content	—	—	—	empirical parameter in the deep drainage function, empirical parameter in the deep drainage function, the reference position of the groundwater level, pressure head
MUSIC	Mechanism	a process related to the ground conditions	the infiltration rate is defined as an exponential function of the soil moisture storage	impervious storage, pervious storage: soil moisture storage, and groundwater storage		Transfer functions; The graphical relationship between the inflow and outflow concentration	—
	Input variables	sub-catchment properties, impervious store capacity	soil moisture store capacity, maximum infiltration loss, infiltration loss exponent, soil moisture, field capacity, groundwater data	catchment properties		pollutant concentration information	rainfall and ET
LIDRA	Mechanism	the rainfall interception from tree canopy is related to rainfall	The soil infiltration rate is a function of soil type	—	—	—	—
	Input variables	Rainfall depth	Soil type, hydraulic conductivity	—	—	—	—

balance model. RECARGA, L-THIA LID and P8 use the SCS curve method and SWAT uses the Green-Ampt method.

In SWMM and SUSTAIN, infiltration can be calculated using the Horton infiltration equation, the Green-Ampt method or the SCS curve method. Users can choose a specific method according to their research needs and data availability. For example, the Horton infiltration equation is applicable when exploring a small watershed or when soil data is inadequate; however, a limitation is

that it does not consider the conditions of the saturated and unsaturated zones (Wang and Chu, 2020; Yang et al., 2020). The Green-Ampt method has strict data requirements i.e., requires comprehensive soil data (Huo et al., 2020; Salifu et al., 2021). The SCS curve method is applicable to large watersheds, but a limitation is that it does not reflect the influence of rainfall intensity and rainfall processes on runoff (Nile et al., 2018; Lian et al., 2020).

HEC-HMS calculates infiltration based on loss models, e.g., the exponential loss model, Green and Ampt loss model or the Smith Parlange loss model (Zema et al., 2017). Different models corresponded to various parameters, and users can choose the appropriate model according to research needs or data availability.

The algorithm to calculate infiltration in MIKE-URBAN is incorporated in the four surface runoff models, which are Time-Area Method, Kinematic Wave Method, Linear Reservoir Method, Unit Hydrograph Method (UHM), and one continuous hydrological model called MOUSE Rainfall Dependent Infiltration (RDI) (DHI, 2017). In the Time-Area method, infiltration is included as runoff loss, and it is not defined separately (Akram et al., 2014; Fariborzi et al., 2019). Both the Kinematic Wave and Linear Reservoir methods apply the Horton infiltration equation to calculate the infiltration (Yin et al., 2020). For UHM, the SCS Curve method is used to estimate the infiltration (Kocsis et al., 2020; Strapazan et al., 2021). In RDI, there are two methods for simulating the infiltration process: Fast Response Component (FRC) and Slow Response Component (SRC) (Zhang S et al., 2018). If the soils' previous hydrological conditions are considered, users can choose the SRC method (Ohlin Saletti, 2021).

L-THIA LID cannot calculate infiltration based on independent methods. The infiltration coefficient in StormTac can be estimated from its relationship with runoff. LIDRA estimates soil infiltration rate from the hydraulic conductivity of different soil types (Rawls et al., 1982). In MUSIC, the infiltration rate of the soil can be calculated from an exponential function of soil moisture storage (https://wiki.ewater.org.au/display/MD6). When the soil water reserve is empty, the infiltration rate reaches its maximum value, and when the soil water reserve is full the infiltration rate gradually decreases to its minimum value. Hydrus-1D uses a soil hydraulic function which can more precisely simulate infiltration compared with the above-mentioned models, however it requires more input variables than other models (Feitosa and Wilkinson, 2016; Hilten et al., 2008; Jiang et al., 2010; Tu et al., 2021).

3.1.3 Storage

The calculation of storage is mainly based on two methods. Some models (e.g., SWMM) directly calculate storage by detecting its relationship with other parameters (e.g., catchment area and depth) (Rossman et al., 2015). Some other models (e.g., MUSIC) divide storage into different parts and calculate each part based on various corresponding methods (https://wiki.ewater.org.au/display/MD6), as shown below.

The storage curve is used in SWMM and SUSTAIN to calculate storage based on the relationship between storage and water depth (Yazdi et al., 2019; Tu et al., 2020). The former uses a linear equation to calculate storage area, while the latter applies a tabulated method (Liu et al., 2018; Deitch and Feirer, 2019); both require water depth or volume as input variables.

GIF Mod applies the Van Genuchten-Mualem equation to estimate catchment wide storage, which identifies catchment storage based on the relationship between storage and water head (Onoja et al., 2019; Weber et al., 2020). In HEC-HMS storage is computed by various equations revealing the relationship between storage and other variables such as catchment area, elevation and discharge (https://www.hec.usace.army.mil/confluence/hmsdocs/hmstrm).

In MIKE-URBAN storage is calculated using the Kinematic Wave method, which considers the surface storage as three parts: snow surface, unsaturated zone ("root zone") and ground water in RDI (Hernes et al., 2020; Thrysøe et al., 2021). The input variables are height, porosity, conductivity and clogging factor.

In MUSIC, storage is divided into impervious storage and pervious storage. Impervious storage is a user defined constant, and pervious storage consists of soil moisture storage and groundwater storage. The specific equations are however not publicly available (https://wiki.ewater.org.au/display/MD6).

3.1.4 Purification

The number of pollutants that can be removed from stormwater by SCP is difficult to accurately simulate. Amongst the models we reviewed only MUSIC and L-THIA LID are able to simulate purification performance by different types of SCP. However, most models (such as SWMM, SUSTAIN, HEC-HMS, GIF Mod, L-THIA LID, StormTac, and P8) can calculate the concentration of sedimentation or pollutants.

For pollutant accumulation models such as SWMM and SUSTAIN, pollutant accumulation and wash-off are simulated based on the accumulation and wash-off functions (Johannessen et al., 2019). However, both functions only estimate the pollutant reduction within the runoff flow volume (Rossman et al., 2015). SUSTAIN uses the Vegetative Filter Strip Model algorithms for sediment interception, which is more accurate than SWMM (Shoemaker et al., 2009). The input variables in each process are pollutant initial buildup, street sweeping interval, street sweeping availability, and last swept. In StormTac, the total pollutant concentration is calculated as a flow-weighted average of stormwater and baseflow concentrations (Lindgren, 2019; Wu J et al., 2021). In P8, particle concentrations in runoff are calculated using an empirical equation (Walker, 1990). For pollutant transporting models, GIF Mod uses a governing equation to calculate the transport of solid particles and other water quality constituents (Massoudieh et al., 2017). HEC-HMS calculates pollutant transport with potential functions (MacAsieb et al., 2021).

In L-THIA LID, NPS pollutant concentration masses can be calculated by the runoff depth, multiplying the area and the appropriate Event Mean Concentration (EMC) value (Engel and Harbor, 2017). The treated pollutants by SCP was estimated by

the treatment node in MUSIC, using the transfer functions (Gavrić et al., 2019). These transfer functions calculate the effluent concentration of stormwater based on the simple graphical relationship between inflow and outflow concentrations. Therefore, compared with other models, MUSIC can simulate stormwater quality more accurately.

Hydrus-1D and LIDRA do not include algorithms to simulate water quality.

3.1.5 Utilization

Here, it should be noted that the collection function of SCP, such as rainwater collected by rainwater harvesting tanks or cisterns, is regarded as a function of "utilization" in the context of China's sponge cities. Therefore, only models with rainwater harvesting simulation capability (e.g., SWMM, SUSTAIN and MIKE-URBAN) were investigated in this category. These models have specific SCP modules, and users can define the collecting capacity by relevant input variables such as storage layer parameters. For example, Campisano et al. (2017) estimated rainwater harvesting and evaluated the performance of rain tanks based on SWMM. They found that SWMM overestimated this value, especially for rain tanks smaller than 2 m^3. Li et al. (2021) simulated rainwater harvesting and reuse of rain barrels in Brentwood watershed (Texas, United States) and designed the optimizing parameters of rain barrels for efficient stormwater management, based on SWAT.

However, utilization functionality is still in development and there are different interpretations of it. Some researchers found stormwater utilization is associated with stormwater storage capacity, domestic water demand and current technologies (Hamdan, 2009; Nnadi et al., 2015). For example, the capability of stormwater storage is related to the size of rain tank or reservoir (Vargas et al., 2019; Kim et al., 2021). Domestic water demand can be affected the public policies and local population and industries (Takagi et al., 2018; Fernandes et al., 2020). Sustainable stormwater management can alleviate the water scarcity with some degree (Morales-Torres et al., 2016). Additionally, the development of advanced purification technologies and the new materials can also influence the stormwater utilization (Kolavani and Kolavani, 2020; Awang Ali et al., 2021).

3.1.6 Discharge

Discharge describes the movement of stormwater through drainage pipes, and models calculate this using various hydraulic equations (Chang et al., 2015; Cao et al., 2021). SWMM and SUSTAIN calculate the runoff routing in the pipeline based on the St. Venant flow equations for the dynamic wave and kinematic wave. Regarding the steady flow, the joint solution of Manning and continuous equation is used to calculate the flow rate (Rossman, 2015). SWAT uses the Manning equation to model stormwater movement in drainage systems, while P8 applies the curve number method to simulate runoff from pervious and indirectly connected with imperious surface (Minnesota Stormwater Manual). RECARGA and GIF Mod use the van Genuchten equation. The MIKE-URBAN module features an advanced Real-Time Control (RTC) simulation capability for urban drainage and sewer systems in the form of overflow pipes, weirs, orifices, etc. The stormwater between two nodes can be calculated with Muskingum Cunge method in MUSIC. The outflow hydrograph and pollutograph can be estimated by the continuity of mass equation (Peters, 2012). Hydrus-1D and LIDRA do not consider stormwater discharge in the urban drainage system. The processes of retention, infiltration, storage, and discharge are well simulated in SWMM, SUSTAIN, MIKE-URBAN, and MUSIC. The algorithms adopted in SWMM and SUSTAIN to simulate the above processes are similar, such that the required input parameters are the same. MIKE-URBAN can more accurately simulate the movement of stormwater in the drainage system given that it adapts five hydraulic methods depending on the process in question. The purification process, which corresponds to the improvement of water quality and the removal of pollutants, was fully simulated by MUSIC, i.e., it simulates the entire removal of various pollutants. SWMM and SUSTAIN only model the reduction in runoff mass load caused by the reduced runoff flow volume (Rossman et al., 2015; Shoemaker et al., 2009). None of these models can simulate the process of stormwater utilization and this is an area requiring further research.

3.2 The Performance of Stormwater Management Models in Decision Support and Policy Making

Amongst the 10 selected DSTs there were two free online tools, one free GIS-based tool, two commercially available software programs, two free software programs, and three free MS Excel-based tools. Specially MUSIC, WinSLAMM, UrbanBEATS and E^2 STORMED DST, as stand-alone software, have more complex operating processes than the online and spreadsheet tools. The environmental, economic and social benefits evaluated by the 10 DSTs are summarized in **Table 2**.

3.2.1 Environmental Benefits

The environmental benefits of SCP include improved hydrological performance (Dagenais et al., 2017; Spahr et al., 2020) such as stormwater quality improvement, flood mitigation, runoff reduction and groundwater recharge, as well as indirect benefits related to ecosystem services (Andersson et al., 2015; Dietrich and Rahul Yarlagadda, 2016; Gallo et al., 2020). Improved ecosystem services include adjustment to the local microclimate, carbon sequestration and storage, biodiversity conservation and restoration, and air pollution (Gómez-Baggethun and Barton, 2013; Ando and Netusil, 2018; Kazak et al., 2018).

Most models containing DST capability only address the hydrological aspects of environmental benefits, for example the reduction of water quantity and the improvement of water quality. LIDRA, for example, evaluates the benefits related to runoff reduction in various SCP scenarios. SWMM, SUSTAIN, MUSIC, winSLAMM, WMOST, and UrbanBEATS can evaluate

TABLE 2 | Comparison of DSTs.

Model name	Free or not	User interface	Simulated benefit		
			Economic	Social	Environmental
E^2 STORMED DST	√	Software	√		√
GI Valuation toolkit	√	Excel-internal tool	√	√	√
GVC	√	Online tool	√		
LIDRA	√	Online tool	√		√
L-THIA LID	√	Online tool	√		
MUSIC	×	Software	√		√
SUSTAIN	√	GIS-based tool	√		√
UrbanBEATS	√	Software		√	√
winSLAMM	×	Software	√		√
WMOST	√	Excel-internal tool	√		√

the benefits associated with runoff reduction and water-pollutant removal by various SCP.

The benefits associated with ecosystem services may also be assessed. For example, the E^2 STORMED DST can evaluate CO_2 reduction and energy benefits resulting from SCP. Additionally, the GI valuation toolkit can incorporate climate change adaptation and mitigation, as well as the biodiversity conservation related to SCP.

3.2.2 Economic Benefits

There are three main methods for evaluating the economic benefits of SCP. The first method calculates the life cycle cost of various SCP configurations. E^2 STORMED DST, GI Valuation Toolkit, LIDRA and MUSIC utilize this method. The second method generates a cost-benefit curve or report to help with decision making, and is used by SUSTAIN, WinSLAMM and WMOST. SUSTAIN has an optimization module to generate the most cost-effective scenarios based on the scatter search method and the non-dominated sorting genetic algorithm II method. Regardless of the cost related to improving water quantity, WinSLAMM provides the most cost-effective solutions for urban stormwater quality requirements (Pitt et al., 2002). In WMOST, a Pareto Frontier or trade-off curve can be generated by setting control experiments. The third method is associated with net present value (NPV), which is a widely used method to assess financial viability. This method incorporates the time value of money into decision making based on discounted cash flow techniques (Ye and Tiong, 2000). In the GVC this method is adopted to evaluate economic benefits.

In terms of life cycle costs MUSIC can calculate more types of cost compared with E^2 STORMED, LIDRA and L-THIA LID. More specifically, the life cycle cost of MUSIC includes the total acquisition cost, annual establishment cost, typical annual maintenance cost, renewal/adaptation cost, decommissioning cost and nominal cost. The types of cost in other models are mainly limited to construction costs and maintenance costs, for example LIDRA and L-THIA LID.

3.2.3 Social benefits

The social benefits related to SCP involve the improvement of aesthetics, public health, human welfare, public acceptability and city sustainability, noise reduction and entertainment (Keeley et al., 2013; Chini et al., 2017; BenDor et al., 2018; Bell et al., 2019). Only two tools amongst the reviewed models were found to be able to evaluate social benefits: UrbanBEATS and GI Valuation Toolkit. UrbanBEATS is a spatial planning tool with advanced visual outputs; it considers the influence of urban population density and the urban drainage system to help stakeholders make better decisions. The GI Valuation Toolkit can evaluate the improvements in community performance, health and wellbeing, tourism and recreation, and leisure related to SCP.

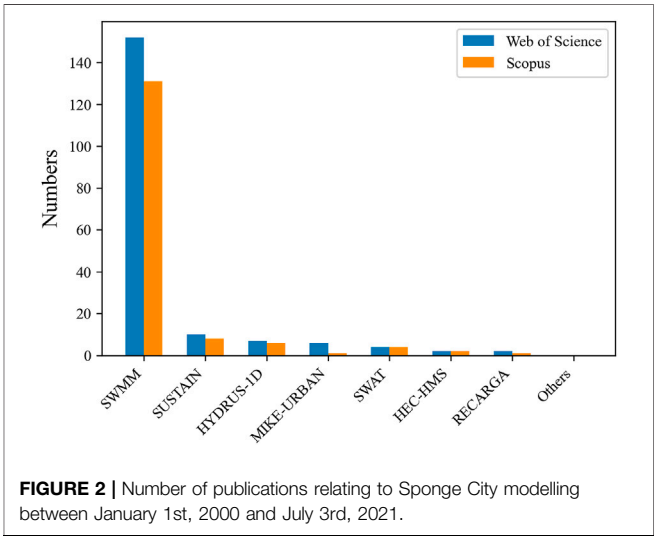

FIGURE 2 | Number of publications relating to Sponge City modelling between January 1st, 2000 and July 3rd, 2021.

In conclusion, with the exception of UrbanBEATS, all other tools were found to be able to evaluate the economic benefits of SCP by calculating the NPV of the sponge system or by identifying the cost of SCP under various scenarios. Amongst the reviewed models only the GI Valuation Toolkit and UrbanBEATS can evaluate social benefits. At present, the methods used to evaluate the social benefits of SCP are mainly indicator based screening and quantification (Dagenais et al., 2017; He et al., 2019; Li H et al., 2019). Because the original purpose of SCP is to reduce urban runoff and remove pollutants, all models except GVC can evaluate environmental benefits (Steffen et al., 2013; Berland et al., 2017).

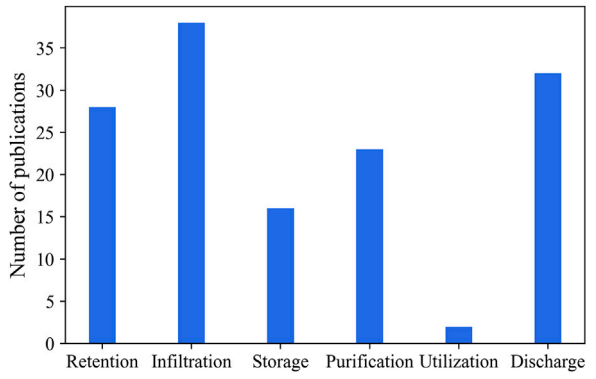

FIGURE 3 | Breakdown of the six hydrological processes included in Sponge City case studies in China.

4 CASE STUDIES IN CHINA

Among the filtered 199 studies, 146 cases with a defined municipal study area were selected. Specially, 66 of the 146 cases are in northern China, while the remainder are in southern China. Only 5 studies were published before 2010, which reflects the increased application of stormwater modeling over the last decade. Moreover, we found that most of studies were based on experiments at community or neighborhood scales. The results were mainly based on monitoring and simulations for single or multiple rainfall events, rather than long-term monitoring or simulations.

Amongst the articles we reviewed there were only seven models applied in China (**Figure 2**), of which SWMM was the most widely used. SWMM was capable of not only addressing the hydrological performance of SCP but, when coupled with other land use planning software, achieving real-time stormwater management and comprehensive performance evaluation (Li C et al., 2019; Zeng et al., 2021). Hydrus-1D was used to simulate infiltration-based SCP such as green roofs, permeable pavements, and bioretention (Qin et al., 2016; Fu et al., 2020; Li et al., 2020). MIKE-URBAN was useful for simulating urban stormwater drainage system performance, such as urban waterlogging (Luan et al., 2018). SUSTAIN was applied in both SCP hydrological performance assessment and assisting in the planning of SCP (Gao et al., 2015; Zhang et al., 2021). RECARGA was used to simulate the influence of bioretention on the water balance in an expressway service area in China and the appropriate parameters for bioretention was identified (Gao et al., 2018). HEC-HMS was applied to compare and analyze comprehensive regulation effects of three different storm water management scenarios (Liu et al., 2020). SWAT performed the cost-benefit analysis of SCP in Xiangxi River, China (Liu et al., 2014).

Early studies focused on the simulation of water quality and water quantity, as well as evaluation of the environmental benefits of SCP in terms of runoff and pollution control (Meng et al., 2014; Li et al., 2016). Outcomes identified optimal scheme choice and spatial layout amongst different configurations of SCP (Liao et al., 2015; Xu et al., 2017). Amongst the literature investigated, Guo et al. (2008) conducted the first stormwater modeling application study in Beijing with SWMM, and analyzed the different rainfall-runoff characteristics of various rainfall densities. Recently, studies related to improving the accuracy, efficiency, and robustness of hydrological models have been highlighted (Pang et al., 2020; Yin et al., 2020; Tang et al., 2021). Moreover, these stormwater management models are increasingly coupled with other platforms or models to achieve more comprehensive functions or to run simulations at larger spatial scales (Duan and Gao, 2019; Liang et al., 2020; Xu et al., 2021). Hydrological models were also integrated with remote sensing techniques, and neural networks have become more popular (Wang et al., 2021; Wu Z et al., 2021).

We further summarized the simulations of the six physical processes involved in the 199 case studies (**Figure 3**). Only 2 cases refer to utilization, and both of these used the SWAT model. Most studies focused on infiltration (38 no.) and discharge (32 no.). Thus, these two physical processes are well simulated in current models, whereas other processes such as storage and utilization were relatively uncommon.

Amongst the 199 case studies, 146 cases focused on specific study areas. We extracted these and further summarized model applications to climatic zones in China. The climate classification map is based on data retrieved from the Resource and Environment Science and Data Center (**Figure 4**, https://www.resdc.cn/data.aspx?DATAID=243). It may be seen that these cases are mainly distributed in eastern China where precipitation is higher and sponge city pilot projects are mostly located. The cases were spread amongst 57 cities, in which Beijing has the largest portion, corresponding to stormwater-resource management demands (Zhang D et al., 2018).

We further analyzed these cases and found that in northern China hydrological model use tends to focus on simulation of infiltration processes of SCP (Luan et al., 2017; Li et al., 2018). Precipitation in northern China is low, and unsaturated zones can reach hundreds of meters. As a result, rainfall exhibits low

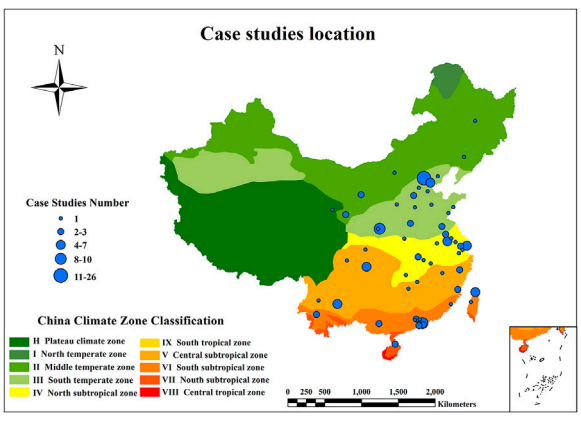

FIGURE 4 | Spatial distribution of case studies, retrieved from Web of Science and Scopus between January 1st, 2000 and July 3rd, 2021.

infiltration and field capacity is rarely reached (Han and Banin, 1999; Li H et al., 2019). Improving soil infiltration capacity is an effective way of reducing runoff, recharging groundwater and reducing surface water flooding (Li Z et al., 2017). In the southeast coastal area, application of hydrological models focused on simulating the storage of SCP (Qin et al., 2016; Mao et al., 2017). Because rainfall is more abundant and groundwater levels are high, soil moisture content is also high in the early stages. It is vital therefore to increase stormwater storage capacity through SCP in order to reduce flood risk.

DST functionality has not yet been widely applied in China. At present, sponge city planning mainly relies on a combination of hydrological models and other decision-support methods, such as multi-objective decision making (MODM), analytic hierarchy process (AHP), and a multi-objective evolutionary algorithm (MOEA) (Jia et al., 2015; Xu et al., 2017; Zhu et al., 2021). There are no systematic social and environmental evaluation criteria for sustainable stormwater management in China.

5 DISCUSSION AND CONCLUSION

This research reviewed 19 stormwater models, of which 13 models can perform hydrological simulations and 10 can function as decision support tools. We primarily analyzed the hydrological models for six key processes, as mandated by the Chinese government for sponge city construction. We also compared various DSTs in evaluating the economic, social, and environmental benefits of SCP. Finally, we collected case studies of model applications in China and analyzed the spatial variability and simulation advantages in various climatic zones.

This study reveals some deficiencies in the current simulation for SCP. First, the changes in the nature of SCP over time, such as change in plant coverage and/or the volume of water storage facilities, were not longitudinally studied. In the context of climate change and more intense and frequent rainfall, greater pressure is being placed on the urban ecosystem. Hence, the related hydrological impacts have not been validated by stormwater management models. Observations for vegetation and hydrologic changes need to be recorded to enable improved performance of stormwater management models.

Second, models are known to perform well in different regions of the world, but need further refinement for more meaningful application in sponge city construction in China. For example, the construction standards of rain gardens in China are different to those in other countries, so the parameters related to the capacity of stormwater treatment are also different (Wang et al., 2009). Moreover, these hydrological models cannot fully simulate the entire circulation of stormwater in the context of a sponge city. Case studies in China have mainly focused on reducing stormwater runoff and mitigating stormwater pollution; there is no coherent analysis of how stormwater replenishes groundwater, thus requires further research. Additionally, how stormwater is utilized, such as toilet flushing and irrigation of public green spaces, is still unknown. The model algorithms for understanding how SCP affect the six processes also need to be further optimized.

Third, it should be noted that rainwater harvesting by rainwater tanks or cisterns is classified as "utilization" in the context of China's sponge cities (Peng J et al., 2018; Peng S et al., 2018; Wei et al., 2019). How the collected water is then used (e.g., toilet flushing and urban irrigation) cannot be simulated by current stormwater management models, to our best knowledge. In the "utilization" category, we've clarified how to assign collected rainwater or treated stormwater (Takagi et al., 2018; Fernandes et al., 2020; Hajani and Rahman, 2014).

Finally, current DSTs only focus on evaluating the positive benefits of SCP and ignore the negative effects of SCP. Many studies have shown that SCP can also have negative effects. For example, rain gardens may accidentally increase the phosphorus content in stormwater (Hatt et al., 2009), and wetlands may cause eutrophication of water bodies (Heal et al., 2006). Reservoirs may act as a sink for pollution, endangering health in wildlife and humans (Paus et al., 2014). Data on economic costs in DSTs are lacking in China and require further study. Another limitation of DSTs is the lack of social-benefit assessment modules. Modules that evaluate the social benefits of SCP would assist in the long-term implementation of more SCP in communities. In addition, combining increased stakeholder participation with DSTs is becoming a crucial aspect of sponge city construction (Cousins, 2017; Qiao et al., 2018); DSTs are still not fully used in policy and decision-making.

Overall, for Chinese sponge cities, most models are capable of simulating the hydrological performance of SCP, however the application of DSTs is relatively poor and ineffective in China. Decision-making involves many social, economic, and political factors which may be different from the countries in which the DSTs were developed. Therefore, developing models that can adapt to China's sponge city conditions is crucial. Our review of case studies application in China show that stormwater models use is mainly distributed to central and eastern China. In northern China, studies tend to focus on simulating infiltration, whilst in southern China studies focus on the storage functions of SCP. This finding is significant in terms of selecting an appropriate model according to climatic zone and simulation functions. In summary, in this study, we have evaluated and compared the physical mechanisms embedded in stormwater models based on water retention, infiltration, storage, utilization, purification, and discharge; these factors are important in sponge city construction in China. Additionally, our study explored the social, environmental, and economic benefits of sponge city practices, which can be simulated by current decision-support tools. Furthermore, the application of these tools was also investigated in various climatic zones in China. The study not only improves the understanding of processes involved in the construction of a sponge city, but also provides insight into the development of future stormwater models.

AUTHOR CONTRIBUTIONS

QL wrote the manuscript, built the method, acquired data, and conducted data processing and analysis. WC conceived the study,

built the method, and wrote the manuscript together. JL conceived the study, acquired the funding, and contributed to the manuscript writing. MT, YT and ZT contributed to the manuscript editing.

FUNDING

This work was supported by the National Key R&D Program of China (No. 2018YFE0206200). It was also supported by the High-level Special Funding of the Southern University of Science and Technology (Grant Nos. G02296302 and G02296402).

ACKNOWLEDGMENTS

We acknowledge Dr. Wenfang Cao of the School of Environmental Science and Engineering, Southern University of Science and Technology (SUSTech) for helping edit the figures.

SUPPLEMENTARY MATERIAL

The Supplementary Material for this article can be found online at: https://www.frontiersin.org/articles/10.3389/fenvs.2021.816093/full#supplementary-material

REFERENCES

Akram, F., Rasul, M. G., Masud, M., Khan, K., Imam, S., and Amir, I. (2014). Comparison of Different Hydrograph Routing Techniques in XPSTORM Modelling Software : A Case Study. *Int. J. Environ. Ecol. Geol. Mining Eng.* 8 (3), 213–223. doi:10.5281/zenodo.1093034

Andersson, E., McPhearson, T., Kremer, P., Gomez-Baggethun, E., Haase, D., Tuvendal, M., et al. (2014). Scale and Context Dependence of Ecosystem Service Providing Units. *Ecosystem Services* 12, 157–164. doi:10.1016/j.ecoser.2014.08.001

Ando, A., and Netusil, N. (2018). *Valuing the Benefits of Green Stormwater Infrastructure*. Oxford: Oxford Research Encyclopedia of Environmental Science. Available at: https://oxfordre.com/environmentalscience/view/10.1093/acrefore/9780199389414.001.0001/acrefore-9780199389414-e-605 (Accessed June 27, 2021).

Awang Ali, A. N., Bolong, N., and Abdul Taha, N. (2021). A Review on the Application of Granular Filter Media and the Utilization of Agro-Industrial Wastes for Stormwater Quality Improvement. *Jurnal Teknologi.* 83 (4), 75–90. doi:10.11113/jurnalteknologi.v83.15159

Bach, P. M., Kuller, M., McCarthy, D. T., and Deletic, A. (2020). A Spatial Planning-Support System for Generating Decentralised Urban Stormwater Management Schemes. *Sci. Total Environ.* 726, 138282. doi:10.1016/j.scitotenv.2020.138282

Bean, R., Pitt, R. E., Pitt, R. E., Voorhees, J., and Elliott, M. (2021). Urban Tree Rainfall Interception Measurement and Modeling in WinSLAMM, the Source Loading and Management Model. *Jwmm.* 2021, 29. doi:10.14796/jwmm.c475

Bell, C. D., Spahr, K., Grubert, E., Stokes-Draut, J., Gallo, E., McCray, J. E., et al. (2019). Decision Making on the Gray-Green Stormwater Infrastructure Continuum. *J. Sustainable Water Built Environ.* 5 (1), 04018016. doi:10.1061/jswbay.0000871

BenDor, T. K., Shandas, V., Miles, B., Belt, K., and Olander, L. (2018). Ecosystem Services and U.S. Stormwater Planning: An Approach for Improving Urban Stormwater Decisions. *Environ. Sci. Pol.* 88 (July), 92–103. doi:10.1016/j.envsci.2018.06.006

Berland, A., Shiflett, S. A., Shuster, W. D., Garmestani, A. S., Goddard, H. C., Herrmann, D. L., et al. (2017). The Role of Trees in Urban Stormwater Management. *Landscape Urban Plann.* 162, 167–177. doi:10.1016/j.landurbplan.2017.02.017

Campisano, A., Catania, F. V., and Modica, C. (2017). Evaluating the SWMM LID Editor Rain Barrel Option for the Estimation of Retention Potential of Rainwater Harvesting Systems. *Urban Water J.* 14 (8), 876–881. doi:10.1080/1573062X.2016.1254259

Cao, Y., Xu, M., Ni, P., and Mei, G. (2021). Physical and Numerical Modelling of Infiltration from Drainage Holes for Perforated Storm Sewer. *Acta Geotech.* 2021, 1–17. doi:10.1007/s11440-021-01247-0

Castiglia Feitosa, R., and Wilkinson, S. (2016). Modelling green Roof Stormwater Response for Different Soil Depths. *Landscape Urban Plann.* 153, 170–179. doi:10.1016/j.landurbplan.2016.05.007

Chang, N.-B., Lu, J.-W., Chui, T. F. M., and Hartshorn, N. (2018). Global Policy Analysis of Low Impact Development for Stormwater Management in Urban Regions. *Land Use Policy.* 70 (January), 368–383. doi:10.1016/j.landusepol.2017.11.024

Chang, T.-J., Wang, C.-H., and Chen, A. S. (2015). A Novel Approach to Model Dynamic Flow Interactions between Storm Sewer System and Overland Surface for Different Land Covers in Urban Areas. *J. Hydrol.* 524, 662–679. doi:10.1016/j.jhydrol.2015.03.014

Cheng, J., Gong, Y., Zhu, D. Z., Xiao, M., Zhang, Z., Bi, J., et al. (2021). Modeling the Sources and Retention of Phosphorus Nutrient in a Coastal River System in China Using SWAT. *J. Environ. Manage.* 278 (P2), 111556. doi:10.1016/j.jenvman.2020.111556

Chini, C., Canning, J., Schreiber, K., Peschel, J., and Stillwell, A. (2017). The green experiment: Cities, green Stormwater Infrastructure, and Sustainability. *Sustainability.* 9 (1), 105–121. doi:10.3390/su9010105

Cousins, J. J. (2017). Infrastructure and Institutions: Stakeholder Perspectives of Stormwater Governance in Chicago. *Cities.* 66, 44–52. doi:10.1016/j.cities.2017.03.005

Dagenais, D., Thomas, I., and Paquette, S. (2017). Siting green Stormwater Infrastructure in a Neighbourhood to Maximise Secondary Benefits: Lessons Learned from a Pilot Project. *Landscape Res.* 42 (2), 195–210. doi:10.1080/01426397.2016.1228861

Deitch, M. J., and Feirer, S. T. (2019). Cumulative Impacts of Residential Rainwater Harvesting on Stormwater Discharge through a Peri-Urban Drainage Network. *J. Environ. Manage.* 243 (May), 127–136. doi:10.1016/j.jenvman.2019.05.018

DHI (2017). *MIKE Urban Collection System - Modelling of Storm Water Drainage Networks and Sewer Collection Systems (User Guide)*, 423. Horsholm: MIKE Powered by DHI. Available at: http://d.g.wanfangdata.com.cn/Periodical_mkhjbh201605010.aspx.

Dietrich, A., and Rahul Yarlagadda, C. G. (2016). Estimating the Potential Benefits of Green Stormwater Infrastructure on Developed Sites Using Hydrologic Model Simulation. *Sustainable Energ.* 33 (3), 676–680. doi:10.1002/ep.12428

Duan, H.-F., and Gao, X. (2019). Flooding Control and Hydro-Energy Assessment for Urban Stormwater Drainage Systems under Climate Change: Framework Development and Case Study. *Water Resour. Manage.* 33 (10), 3523–3545. doi:10.1007/s11269-019-02314-8

Elliott, A., and Trowsdale, S. (2007). A Review of Models for Low Impact Urban Stormwater Drainage. *Environ. Model. Softw.* 22 (3), 394–405. doi:10.1016/j.envsoft.2005.12.005

Elçi, A. (2017). Evaluation of Nutrient Retention in Vegetated Filter Strips Using the SWAT Model. *Water Sci. Technology* 76 (10), 2742–2752. doi:10.2166/wst.2017.448

Engel, B., and Harbor, J. (2017). *The L-THIA LID Model Description*. West Lafayette: Purdue University. Lid. Available at: https://engineering.purdue.edu/mapserve/LTHIA7/lthianew/lidIntro.php.

Fanelli, R., Prestegaard, K., and Palmer, M. (2017). Evaluation of Infiltration-based Stormwater Management to Restore Hydrological Processes in Urban Headwater Streams. *Hydrol. Process.* 31 (19), 3306–3319. doi:10.1002/hyp.11266

Fariborzi, H., Sabzevari, T., Noroozpour, S., and Mohammadpour, R. (2019). Prediction of the Subsurface Flow of Hillslopes Using a Subsurface Time-Area Model. *Hydrogeol J.* 27 (4), 1401–1417. doi:10.1007/s10040-018-1909-9

Feitosa, R. C., and Wilkinson, S. (2016). Modelling Green Roof Stormwater Response for Different Soil Depths. *Landscape Urban Plann* 153, 170–179. doi:10.1016/j.landurbplan.2016.05.007

Fernandes, S., Bonfante, M. C., de Oliveira, C. T., Maldonado, M. U., and Campos, L. M. S. (2020). Decentralized Water Supply Management Model: a Case Study of Public Policies for the Utilization of Rainwater. *Water Resour. Manage.* 34 (9), 2771–2785. doi:10.1007/s11269-020-02575-8

Fu, X., Liu, J., Shao, W., Mei, C., Wang, D., and Yan, W. (2020). Evaluation of Permeable brick Pavement on the Reduction of Stormwater Runoff Using a Coupled Hydrological Model. *Water* 12 (10), 2821. doi:10.3390/w12102821

Gallo, E. M., Bell, C. D., Panos, C. L., Smith, S. M., and Hogue, T. S. (2020). Investigating Tradeoffs of green to Grey Stormwater Infrastructure Using a Planning-Level Decision Support Tool. *Water.* 12 (7), 2005. doi:10.3390/w12072005

Gao, J., Pan, J., Hu, N., and Xie, C. (2018). Hydrologic Performance of Bioretention in an Expressway Service Area. *Water Sci. Technology* 77 (7), 1829–1837. doi:10.2166/wst.2018.048

Gao, J., Wang, R., Huang, J., and Liu, M. (2015). Application of BMP to Urban Runoff Control Using SUSTAIN Model: Case Study in an Industrial Area. *Ecol. Model.* 318, 177–183. doi:10.1016/j.ecolmodel.2015.06.018

Gavrić, S., Leonhardt, G., Marsalek, J., and Viklander, M. (2019). Processes Improving Urban Stormwater Quality in Grass Swales and Filter Strips: A Review of Research Findings. *Sci. Total Environ.* 669, 431–447. doi:10.1016/j.scitotenv.2019.03.072

Gebre, S. L. (2015). Application of the HEC-HMS Model for Runoff Simulation of Upper Blue Nile River Basin. *Hydrol. Curr. Res* 06 (02), 1. doi:10.4172/2157-7587.1000199

Gómez-Baggethun, E., and Barton, D. N. (2013). Classifying and Valuing Ecosystem Services for Urban Planning. *Ecol. Econ.* 86, 235–245. doi:10.1016/j.ecolecon.2012.08.019

Grytsenko, A., Rybalova, O., Matsak, A., and Artemiev, S. (2020). Using of Production Wastes in Stormwater Drainage Purification. *Msf.* 1006, 194–201. doi:10.4028/www.scientific.net/MSF.1006.194

Guo, L., and Jing, S. (2008). Analysis of Rainfall in Beijing Rivers Based on SWMM. *Computer Simulation* 2008 (04), 282–285+329. doi:10.3969/j.issn.1006-9348.2008.04.072

Hajani, E., and Rahman, A. (2014). Rainwater Utilization From Roof Catchments in Arid Regions: A Case Study for Australia. *J. Arid Environ.* 111, 35–41. doi:10.1016/j.jaridenv.2014.07.007

Hamdan, S. M. (2009). A Literature Based Study of Stormwater Harvesting as a New Water Resource. *Water Sci. Technology* 60 (5), 1327–1339. doi:10.2166/wst.2009.396

Han, F. X., and Banin, A. (1999). Long-term Transformation and Redistribution of Potentially Toxic Heavy Metals in Arid-Zone Soils: II. Incubation at the Field Capacity Moisture Content. *Water Air Soil Pollut.* 114 (3–4), 221–250. doi:10.1023/A:1005006801650

Haris, H., Chow, M. F., Usman, F., Sidek, L. M., Roseli, Z. A., and Norlida, M. D. (2016). Urban Stormwater Management Model and Tools for Designing Stormwater Management of Green Infrastructure Practices. *IOP Conf. Ser. Earth Environ. Sci.* 32 (1), 012022. doi:10.1088/1755-1315/32/1/012022

Hatt, B. E., Fletcher, T. D., and Deletic, A. (2009). Hydrologic and Pollutant Removal Performance of Stormwater Biofiltration Systems at the Field Scale. *J. Hydrol.* 365 (3–4), 310–321. doi:10.1016/j.jhydrol.2008.12.001

He, B.-J., Zhu, J., Zhao, D.-X., Gou, Z.-H., Qi, J.-D., and Wang, J. (2019). Co-benefits Approach: Opportunities for Implementing Sponge City and Urban Heat Island Mitigation. *Land Use Policy.* 86, 147–157. doi:10.1016/j.landusepol.2019.05.003

Heal, K. V., Hepburn, D. A., and Lunn, R. J. (2006). Sediment Management in Sustainable Urban Drainage System Ponds. *Water Sci. Technology.* 53 (10), 219–227. doi:10.2166/wst.2006.315

Hernes, R. R., Gragne, A. S., Abdalla, E. M. H., Braskerud, B. C., Alfredsen, K., and Muthanna, T. M. (2020). Assessing the Effects of Four SUDS Scenarios on Combined Sewer Overflows in Oslo, Norway: Evaluating the Low-Impact Development Module of the Mike Urban Model. *Hydrol. Res.* 51 (6), 1437–1454. doi:10.2166/nh.2020.070

Hilten, R. N., Lawrence, T. M., and Tollner, E. W. (2008). Modeling Stormwater Runoff from green Roofs with HYDRUS-1D. *J. Hydrol.* 358 (3–4), 288–293. doi:10.1016/j.jhydrol.2008.06.010

Horton, R. E. (1919). Rainfall Interception. *Mothly Waeather Rev.* 12 (306), 731–732. doi:10.1126/science.12.306.731-a

Hou, J., Mao, H., Li, J., and Sun, S. (2019). Spatial Simulation of the Ecological Processes of Stormwater for Sponge Cities. *J. Environ. Manage.* 232 (539), 574–583. doi:10.1016/j.jenvman.2018.11.111

Hou, X., Guo, H., Wang, F., Li, M., Xue, X., Liu, X., et al. (2020). Is the Sponge City Construction Sufficiently Adaptable for the Future Stormwater Management under Climate Change? *J. Hydrol.* 588 (May), 125055. doi:10.1016/j.jhydrol.2020.125055

Huo, W., Li, Z., Zhang, K., Wang, J., and Yao, C. (2020). GA-PIC: An Improved Green-Ampt Rainfall-Runoff Model with a Physically Based Infiltration Distribution Curve for Semi-arid Basins. *J. Hydrol.* 586 (March), 124900. doi:10.1016/j.jhydrol.2020.124900

Imteaz, M. A. (2015). STORMKIT: A Decision Support Tool for Stormwater System Analysis and Design. *Int. J. Computer Aided Eng. Technology.* 7 (3), 305–320. doi:10.1504/IJCAET.2015.071294

Islam, A., Hassini, S., and El-Dakhakhni, W. (2021). A Systematic Bibliometric Review of Optimization and Resilience within Low Impact Development Stormwater Management Practices. *J. Hydrol.* 599 (November 2020), 126457. doi:10.1016/j.jhydrol.2021.126457

Jayasooriya, V. M., and Ng, A. W. M. (2014). Tools for Modeling of Stormwater Management and Economics of green Infrastructure Practices: A Review. *Water Air Soil Pollut.* 225 (8), 1–20. doi:10.1007/s11270-014-2055-1

Jia, H., Wang, Z., Zhen, X., Clar, M., and Yu, S. L. (2017). China's Sponge City Construction: A Discussion on Technical Approaches. *Front. Environ. Sci. Eng.* 11 (4), 1–11. doi:10.1007/s11783-017-0984-9

Jia, H., Yao, H., Tang, Y., Yu, S. L., Field, R., and Tafuri, A. N. (2015). LID-BMPs Planning for Urban Runoff Control and the Case Study in China. *J. Environ. Manage.* 149, 65–76. doi:10.1016/j.jenvman.2014.10.003

Jiang, S., Pang, L., Buchan, G. D., Šimůnek, J., Noonan, M. J., and Close, M. E. (2010). Modeling Water Flow and Bacterial Transport in Undisturbed Lysimeters under Irrigations of Dairy Shed Effluent and Water Using HYDRUS-1D. *Water Res.* 44 (4), 1050–1061. doi:10.1016/j.watres.2009.08.039

Johannessen, B. G., Hamouz, V., Gragne, A. S., and Muthanna, T. M. (2019). The Transferability of SWMM Model Parameters between green Roofs with Similar Build-Up. *J. Hydrol.* 569 (January), 816–828. doi:10.1016/j.jhydrol.2019.01.004

Kazak, J., Chruściński, J., and Szewrański, S. (2018). The Development of a Novel Decision Support System for the Location of green Infrastructure for Stormwater Management. *Sustainability.* 10 (12), 4388. doi:10.3390/su10124388

Kazantsev, P., Marus, Y., and Smelovskaya, A. (2020). Landscape and Climate Specifics for Water Sensitive Urban Design in Vladivostok. *IOP Conf. Ser. Mater. Sci. Eng.* 753 (4), 042057. doi:10.1088/1757-899X/753/4/042057

Keeley, M., Koburger, A., Dolowitz, D. P., Medearis, D., Nickel, D., and Shuster, W. (2013). Perspectives on the Use of green Infrastructure for Stormwater Management in cleveland and milwaukee. *Environ. Manage.* 51 (6), 1093–1108. doi:10.1007/s00267-013-0032-x

Kim, J. E., Teh, E. X., Humphrey, D., and Hofman, J. (2021). Optimal Storage Sizing for Indoor arena Rainwater Harvesting: Hydraulic Simulation and Economic Assessment. *J. Environ. Manage.* 280, 111847. doi:10.1016/j.jenvman.2020.111847

Kocsis, I., Haidu, I., Haidu, I., and Maier, N. (2020). "Application of a Hydrological MIKE HYDRO River - UHM Model for Valea Rea River (Romania). Case Study, Flash Flood Event Occurred on August 1st, 2019," in Air and Water – Components of f the Environment Conference Proceedings, 257–272. doi:10.24193/awc2020_24

Kolavani, N. J., and Kolavani, N. J. (2020). Technical Feasibility Analysis of Rainwater Harvesting System Implementation for Domestic Use. *Sustainable Cities Soc.* 62 (June), 102340. doi:10.1016/j.scs.2020.102340

Kristvik, E., Kleiven, G. H., Lohne, J., and Muthanna, T. M. (2018). Assessing the Robustness of Raingardens under Climate Change Using SDSM and Temporal Downscaling. *Water Sci. Technology.* 77 (6), 1640–1650. doi:10.2166/wst.2018.043

Kuller, M., Bach, P. M., Roberts, S., Browne, D., and Deletic, A. (2019). A Planning-Support Tool for Spatial Suitability Assessment of green Urban Stormwater Infrastructure. *Sci. Total Environ.* 686, 856–868. doi:10.1016/j.scitotenv.2019.06.051

Lee, J. G., Selvakumar, A., Alvi, K., Riverson, J., Zhen, J. X., Shoemaker, L., et al. (2012). A Watershed-Scale Design Optimization Model for Stormwater Best Management Practices. *Environ. Model. Softw.* 37, 6–18. doi:10.1016/j.envsoft.2012.04.011

Li, C., Peng, C., Chiang, P.-C., Cai, Y., Wang, X., and Yang, Z. (2019). Mechanisms and Applications of green Infrastructure Practices for Stormwater Control: A Review. *J. Hydrol.* 568 (September 2018), 626–637. doi:10.1016/j.jhydrol.2018.10.074

Li, H., Qi, Z., Qi, Z., Gui, D., and Zeng, F. (2019). Water Use Efficiency and Yield Responses of Cotton to Field Capacity-Based Deficit Irrigation in an Extremely Arid Area of China. *Int. J. Agric. Biol. Eng.* 12 (6), 91–101. doi:10.25165/j.ijabe.20191206.4571

Li, J., Li, Y., and Li, Y. (2016). SWMM-based Evaluation of the Effect of Rain Gardens on Urbanized Areas. *Environ. Earth Sci.* 75 (1), 1–14. doi:10.1007/s12665-015-4807-7

Li, J., Zhao, R., Li, Y., and Chen, L. (2018). Modeling the Effects of Parameter Optimization on Three Bioretention Tanks Using the HYDRUS-1D Model. *J. Environ. Manage.* 217, 38–46. doi:10.1016/j.jenvman.2018.03.078

Li, J., Zhao, R., Li, Y., and Li, H. (2020). Simulation and Optimization of Layered Bioretention Facilities by HYDRUS-1D Model and Response Surface Methodology. *J. Hydrol.* 586 (March), 124813. doi:10.1016/j.jhydrol.2020.124813

Li, Q., Wang, F., Yu, Y., Huang, Z., Li, M., and Guan, Y. (2019). Comprehensive Performance Evaluation of LID Practices for the Sponge City Construction: A Case Study in Guangxi, China. *J. Environ. Manage.* 231 (May 2018), 10–20. doi:10.1016/j.jenvman.2018.10.024

Li, S., Liu, Y., Her, Y., Chen, J., Guo, T., and Shao, G. (2021). Improvement of Simulating Sub-daily Hydrological Impacts of Rainwater Harvesting for Landscape Irrigation with Rain Barrels/cisterns in the SWAT Model. *Sci. Total Environ.* 798, 149336. doi:10.1016/j.scitotenv.2021.149336

Li, H., Ding, L., Ren, M., Li, C., and Wang, H. (2017). Sponge City Construction in China: A Survey of the Challenges and Opportunities. *Water* 9 (9), 594–617. doi:10.3390/w9090594

Li, Z., Chen, X., Liu, W., and Si, B. (2017). Determination of Groundwater Recharge Mechanism in the Deep Loessial Unsaturated Zone by Environmental Tracers. *Sci. Total Environ.* 586, 827–835. doi:10.1016/j.scitotenv.2017.02.061

Lian, H., Yen, H., Huang, J.-C., Feng, Q., Qin, L., Bashir, M. A., et al. (2020). CN-China: Revised Runoff Curve Number by Using Rainfall-Runoff Events Data in China. *Water Res.* 177, 115767. doi:10.1016/j.watres.2020.115767

Liang, C., Zhang, X., Xia, J., Xu, J., and She, D. (2020). The Effect of Sponge City Construction for Reducing Directly Connected Impervious Areas on Hydrological Responses at the Urban Catchment Scale. *Water.* 12 (4), 1163. doi:10.3390/W12041163

Liao, Z. L., Zhang, G. Q., Wu, Z. H., He, Y., and Chen, H. (2015). Combined Sewer Overflow Control with LID Based on SWMM: An Example in Shanghai, China. *Water Sci. Technology.* 71 (8), 1136–1142. doi:10.2166/wst.2015.076

Lindgren, J. (2019). *Evaluation of Different Methods for Modelling Stormwater Quality*. Gothenburg: Chalmers tekniska högskola/Institutionen för arkitektur och samhällsbyggnadsteknik ACE.

Liu, H., Jia, Y., and Niu, C. (2017). "Sponge City" Concept Helps Solve China's Urban Water Problems. *Environ. Earth Sci.* 76 (14), 1–5. doi:10.1007/s12665-017-6652-3

Liu, R., Zhang, P., Wang, X., Wang, J., Yu, W., and Shen, Z. (2014). Cost-effectiveness and Cost-Benefit Analysis of BMPs in Controlling Agricultural Nonpoint Source Pollution in China Based on the SWAT Model. *Environ. Monit. Assess.* 186 (12), 9011–9022. doi:10.1007/s10661-014-4061-6

Liu, W., Feng, Q., Chen, W., Wei, W., and Deo, R. C. (2019). The Influence of Structural Factors on Stormwater Runoff Retention of Extensive green Roofs: New Evidence from Scale-Based Models and Real Experiments. *J. Hydrol.* 569 (October), 230–238. doi:10.1016/j.jhydrol.2018.11.066

Liu, Y., Cibin, R., Bralts, V. F., Chaubey, I., Bowling, L. C., and Engel, B. A. (2016). Optimal Selection and Placement of BMPs and LID Practices with a Rainfall-Runoff Model. *Environ. Model. Softw.* 80, 281–296. doi:10.1016/j.envsoft.2016.03.005

Liu, Z., Lu, T., Ye, J., Wang, G., Dong, X., Withers, R., et al. (2018). Antiferroelectrics for Energy Storage Applications: a Review. *Adv. Mater. Technol.* 3 (9), 1800111–1800121. doi:10.1002/admt.201800111

Luan, Q., Fu, X., Song, C., Wang, H., Liu, J., and Wang, Y. (2017). Runoff Effect Evaluation of LID through SWMM in Typical Mountainous, Low-Lying Urban Areas: A Case Study in China. *Water.* 9 (6), 439. doi:10.3390/w9060439

Luan, Q., Zhang, K., Liu, J., Wang, D., and Ma, J. (2018). The Application of Mike Urban Model in Drainage and Waterlogging in Lincheng County, China. *Proc. IAHS.* 379, 381–386. doi:10.5194/piahs-379-381-2018

MacAsieb, R. Q., Orozco, C. R., and Resurreccion, A. C. (2021). Application of Coupled Hec-Hms and Us Epa Wasp for Transport Modelling of Mercury in the Mining-Impacted Ambalanga River. *ASEAN Eng. J.* 11 (3), 158–176. doi:10.11113/AEJ.V11.17052

Mao, X., Jia, H., and Yu, S. L. (2017). Assessing the Ecological Benefits of Aggregate LID-BMPs through Modelling. *Ecol. Model.* 353, 139–149. doi:10.1016/j.ecolmodel.2016.10.018

Massoudieh, A., Maghrebi, M., Kamrani, B., Nietch, C., Tryby, M., Aflaki, S., et al. (2017). A Flexible Modeling Framework for Hydraulic and Water Quality Performance Assessment of Stormwater green Infrastructure. *Environ. Model. Softw.* 92, 57–73. doi:10.1016/j.envsoft.2017.02.013

Meng, Y., Wang, H., Chen, J., and Zhang, S. (2014). Modelling Hydrology of a Single Bioretention System with HYDRUS-1D. *Scientific World J.* 2014, 1–10. doi:10.1155/2014/521047

Mishra, A., Alnahit, A., and Campbell, B. (2021). Impact of Land Uses, Drought, Flood, Wildfire, and Cascading Events on Water Quality and Microbial Communities: A Review and Analysis. *J. Hydrol.* 596, 125707. doi:10.1016/j.jhydrol.2020.125707

Morales-Torres, A., Escuder-Bueno, I., Andrés-Doménech, I., and Perales-Momparler, S. (2016). Decision Support Tool for Energy-Efficient, Sustainable and Integrated Urban Stormwater Management. *Environ. Model. Softw.* 84, 518–528. doi:10.1016/j.envsoft.2016.07.019

Yazdi, M. N., Ketabchy, M., Sample, D. J., Scott, D., and Liao, H. (2019). An Evaluation of HSPF and SWMM for Simulating Streamflow Regimes in an Urban Watershed. *Environ. Model. Softw.* 118 (March), 211–225. doi:10.1016/j.envsoft.2019.05.008

Nile, B. K., Hassan, W. H., and Esmaeel, B. A. (2018). An Evaluation of Flood Mitigation Using a Storm Water Management Model [SWMM] in a Residential Area in Kerbala, Iraq. *IOP Conf. Ser. Mater. Sci. Eng.* 433 (1), 012001. doi:10.1088/1757-899X/433/1/012001

Nnadi, E. O., Newman, A. P., Coupe, S. J., and Mbanaso, F. U. (2015). Stormwater Harvesting for Irrigation Purposes: An Investigation of Chemical Quality of Water Recycled in Pervious Pavement System. *J. Environ. Manage.* 147, 246–256. doi:10.1016/j.jenvman.2014.08.020

Nordman, E. E., Isely, E., Isely, P., and Denning, R. (2018). Benefit-cost Analysis of Stormwater green Infrastructure Practices for Grand Rapids, Michigan, USA. *J. Clean. Prod.* 200, 501–510. doi:10.1016/j.jclepro.2018.07.152

Ohlin Saletti, A. (2021). *Infiltration and Inflow to Wastewater Sewer Systems - A Literature Review on Risk Management*, 56. Gothenburg: Chalmers University of Technology.

Onoja, M. U., Ahmadinia, M., Shariatipour, S. M., and Wood, A. M. (2019). Characterising the Role of Parametric Functions in the Van Genuchten Empirical Model on CO2 Storage Performance. *Int. J. Greenhouse Gas Control.* 88 (January), 233–250. doi:10.1016/j.ijggc.2019.06.004

Oudin, L., Salavati, B., Furusho-Percot, C., Ribstein, P., and Saadi, M. (2018). Hydrological Impacts of Urbanization at the Catchment Scale. *J. Hydrol.* 559, 774–786. doi:10.1016/j.jhydrol.2018.02.064

Palmstrom, N., and Walker, W. W. (1990). The P8 Urban Catchment Model for Evaluating Nonpoint Source Controls at the Local Level. *Enhancing States' Lake Management Programs.*

Pang, B., Shi, S., Zhao, G., Shi, R., Peng, D., and Zhu, Z. (2020). Uncertainty Assessment of Urban Hydrological Modelling from a Multiple Objective Perspective. *Water.* 12 (5), 1393. doi:10.3390/W12051393

Paus, K. H., Morgan, J., Gulliver, J. S., and Hozalski, R. M. (2014). Effects of Bioretention Media Compost Volume Fraction on Toxic Metals Removal, Hydraulic Conductivity, and Phosphorous Release. *J. Environ. Eng.* 140 (10), 04014033. doi:10.1061/(asce)ee.1943-7870.0000846

Peng, J., Zhang, X. M., and Zhang, Y. H. (2018). Study on Combining Flood Control with Rainwater Utilization of Airports in China. *IOP Conf. Ser. Earth Environ. Sci.* 191 (1), 012133. doi:10.1088/1755-1315/191/1/012133

Peng, S., Cui, H., and Ji, M. (2018). Sustainable Rainwater Utilization and Water Circulation Model for Green Campus Design at Tianjin University.

J. Sustainable Water Built Environ. 4 (1), 04017015. doi:10.1061/jswbay.0000841

Peters, R. W. (2012). Hydrology and Floodplain Analysis, 5th Edition. *Environ. Prog. Sustainable Energ.* 31 (3), 332–334. doi:10.1002/ep.11677

Pitt, R., Voorhees, J., and Burger, C. (2002). " *Low Impact Development " Calculations Using the Source Loading and Management Model (WinSLAMM)*. Tuscaloosa, 1–22.

Qiao, X.-J., Kristoffersson, A., and Randrup, T. B. (2018). Challenges to Implementing Urban Sustainable Stormwater Management from a Governance Perspective: A Literature Review. *J. Clean. Prod.* 196, 943–952. doi:10.1016/j.jclepro.2018.06.049

Qin, H.-p., Peng, Y.-n., Tang, Q.-l., and Yu, S.-L. (2016). A HYDRUS Model for Irrigation Management of green Roofs with a Water Storage Layer. *Ecol. Eng.* 95, 399–408. doi:10.1016/j.ecoleng.2016.06.077

Rawls, W. J., Brakensiek, C. L., and Saxtonn, K. E. (1982). Estimation of Soil Water Properties. *Trans. - Am. Soc. Agric. Eng.* 25 (5), 1316–1320. doi:10.13031/2013.33720

Rosenberger, L., Leandro, J., Pauleit, S., and Erlwein, S. (2021). Sustainable Stormwater Management under the Impact of Climate Change and Urban Densification. *J. Hydrol.* 596 (March), 126137. doi:10.1016/j.jhydrol.2021.126137

Rossman, I. A. (2015). Storm Water Management Model User'S Manuel. Version Ii. *Environ. Prot. Technol. Ser. EPA.* 670, 2015, 2015 ./2-75–017.

Roy, D., Begam, S., Ghosh, S., and Jana, S. (2013). Calibration and Validation of HEC-HMS Model for a River basin in Eastern India. *ARPN J. Eng. Appl. Sci.* 8 (1), 40–56.

Salifu, A., Abagale, F. K., and Kranjac-Berisavljevic, G. (2021). Estimation of Infiltration Models' Parameters Using Regression Analysis in Irrigation Fields of Northern Ghana. *Ojss.* 11 (03), 164–176. doi:10.4236/ojss.2021.113009

Sapdhare, H., Myers, B., Beecham, S., Brien, C., Pezzaniti, D., and Johnson, T. (2019). A Field and Laboratory Investigation of Kerb Side Inlet Pits Using Four media Types. *J. Environ. Manage.* 247 (June), 281–290. doi:10.1016/j.jenvman.2019.06.021

Sartor, J., Mobilia, M., and Longobardi, A. (2018). Results and Findings from 15 Years of Sustainable Urban Storm Water Management. *Int. J. SAFE.* 8 (4), 505–514. doi:10.2495/SAFE-V8-N4-505-514

Seo, M., Jaber, F., Srinivasan, R., and Jeong, J. (2017). Evaluating the Impact of Low Impact Development (LID) Practices on Water Quantity and Quality under Different Development Designs Using SWAT. *Water.* 9 (3), 193. doi:10.3390/w9030193

Shahed Behrouz, M., Zhu, Z., Matott, L. S., and Rabideau, A. J. (2020). A New Tool for Automatic Calibration of the Storm Water Management Model (SWMM). *J. Hydrol.* 581 (December 2019), 124436. doi:10.1016/j.jhydrol.2019.124436

Sharior, S., McDonald, W., and Parolari, A. J. (2019). Improved Reliability of Stormwater Detention basin Performance through Water Quality Data-Informed Real-Time Control. *J. Hydrol.* 573 (March), 422–431. doi:10.1016/j.jhydrol.2019.03.012

She, L., Wei, M., and You, X.-y. (2021). Multi-objective Layout Optimization for Sponge City by Annealing Algorithm and its Environmental Benefits Analysis. *Sustainable Cities Soc.* 66 (January), 102706. doi:10.1016/j.scs.2021.102706

Shoemaker, L., Riverson, J. J., Alvi, K., Zhen, J. X., Paul, S., and Rafi, T. (2009). *SUSTAIN - A Framework for Placement of Best Management Practices in Urban Watersheds to Protect Water Quality*. Cincinnati: Environmental Protection, 1–8. Available at: http://www.epa.gov/nrmrl/wswrd/wq/models/sustain/.

Spahr, K. M., Bell, C. D., McCray, J. E., and Hogue, T. S. (2020). Greening up Stormwater Infrastructure: Measuring Vegetation to Establish Context and Promote Cobenefits in a Diverse Set of US Cities. *Urban For. Urban Green.* 48 (December 2019), 126548. doi:10.1016/j.ufug.2019.126548

Stagnitta, T., Detenbeck, N., Piscopo, A., and Epa, U. S. (2018). *An Overview of the U . S . EPA ' S Watershed Management Optimization Support Tool (WMOST): A Case Study in Taunton , Massachusetts an Overview of the U . S . EPA ' S Watershed Management Optimization Support Tool (WMOST)*. Singapore: A case study in Taunton.

Steffen, J., Jensen, M., Pomeroy, C. A., and Burian, S. J. (2013). Water Supply and Stormwater Management Benefits of Residential Rainwater Harvesting in U.S. Cities. *J. Am. Water Resour. Assoc.* 49 (4), 810–824. doi:10.1111/jawr.12038

Strapazan, C., Haidu, I., Haidu, I., and Irimus, I. A. (2021). A Comparative Assessment of Different Loss Methods Available in Mike Hydro River-Uhm. *Carpath. J. Earth Environ. Sci.* 16 (1), 261–273. doi:10.26471/cjees/2021/016/172

Suppakittpaisarn, P., Jiang, X., and Sullivan, W. C. (2017). Green Infrastructure, Green Stormwater Infrastructure, and Human Health: A Review. *Curr. Landscape Ecol. Rep.* 2 (4), 96–110. doi:10.1007/s40823-017-0028-y

Takagi, K., Otaki, M., and Otaki, Y. (2018). Potential of Rainwater Utilization in Households Based on the Distributions of Catchment Area and End-Use Water Demand. *Water* 10 (12), 1706. doi:10.3390/w10121706

Tang, S., Jiang, J., Zheng, Y., Hong, Y., Chung, E.-S., Shamseldin, A. Y., et al. (2021). Robustness Analysis of Storm Water Quality Modelling with LID Infrastructures from Natural Event-Based Field Monitoring. *Sci. Total Environ.* 753, 142007. doi:10.1016/j.scitotenv.2020.142007

Thrysøe, C., Balstrøm, T., Borup, M., Löwe, R., Jamali, B., and Arnbjerg-Nielsen, K. (2021). FloodStroem: A Fast Dynamic GIS-Based Urban Flood and Damage Model. *J. Hydrol.* 600 (May), 126521. doi:10.1016/j.jhydrol.2021.126521

Traver, R. G., and Ebrahimian, A. (2017). Dynamic Design of green Stormwater Infrastructure. *Front. Environ. Sci. Eng.* 11 (4), 1–6. doi:10.1007/s11783-017-0973-z

Tu A, A., Li, Y., Mo, M., and Nie, X. (2020). Hydrologial Efffects of Design Parameters Optimization of Bioretention Based on RECARGA Model. *J. Soil Water Conservation* 34(01), 149–153. doi:10.13870/j.cnki.stbcxb.2020.01.022

Tu, M., Wadzuk, B., and Traver, R. (2020). Methodology to Simulate Unsaturated Zone Hydrology in Storm Water Management Model (SWMM) for green Infrastructure Design and Evaluation. *PLoS ONE.* 15 (7), e0235528–19. doi:10.1371/journal.pone.0235528

Tu, A., Xie, S., Mo, M., Song, Y., and Li, Y. (2021). Water Budget Components Estimation for a Mature Citrus Orchard of Southern China Based on HYDRUS-1D Model. *Agric. Water Management.* 243 (April 2020), 106426. doi:10.1016/j.agwat.2020.106426

Vargas, D., Dominguez, I., Ward, S., and Oviedo-Ocaña, E. R. (2019). Assisting Global Rainwater Harvesting Practitioners: A Decision Support Tool for Tank Sizing Method Selection under Uncertainty. *Environ. Sci. Water Res. Technol.* 5 (3), 506–520. doi:10.1039/c8ew00707a

Walker, W. W. (1990). *P8 Urban Catchment Model - Program Documentation Version 1.1*. Prepared for IEP, Inc. and Narragansett Bay Project(October). Wisconsin.

Wang, N., and Chu, X. (2020). Revised Horton Model for Event and Continuous Simulations of Infiltration. *J. Hydrol.* 589 (June), 125215. doi:10.1016/j.jhydrol.2020.125215

Wang, S., and Palazzo, E. (2021). Sponge City and Social Equity: Impact Assessment of Urban Stormwater Management in Baicheng City, China. *Urban Clim.* 37 (February), 100829. doi:10.1016/j.uclim.2021.100829

Wang, S., Yang, L., and Bai, W. (2009). Perfect Combination of Art and Technology—Study on the Construction of Rain Garden. *Chinese Landscape Architecture* 25 (06), 54–57. doi:10.3969/j.issn.1000-6664.2009.06.013

Wang, X., Tian, W., and Liao, Z. (2021). Offline Optimization of Sluice Control Rules in the Urban Water System for Flooding Mitigation. *Water Resour. Manage.* 35 (3), 949–962. doi:10.1007/s11269-020-02760-9

Wang, Y., Sun, M., and Song, B. (2017). Public Perceptions of and Willingness to Pay for Sponge City Initiatives in China. *Resour. Conservation Recycling.* 122, 11–20. doi:10.1016/j.resconrec.2017.02.002

Weber, T. K. D., Finkel, M., Gonçalves, M., Vereecken, H., and Diamantopoulos, E. (2020). Pedotransfer Function for the Brunswick Soil Hydraulic Property Model and Comparison to the Van Genuchten-Mualem Model. *Water Resour. Res.* 56 (9), 1–22. doi:10.1029/2019WR026820

Wei, Z., Sun, S., and Ji, X. (2019). The Inspiration of Rainwater Utilization of Foreign Sponge Campus Landscape Planning for Beijing. *IOP Conf. Ser. Earth Environ. Sci.* 227 (5), 052019. doi:10.1088/1755-1315/227/5/052019

Whitehouse, A. (2017). Common Economic Oversights in Green Infrastructure Valuation. *Landscape Res.* 42 (2), 230–234. doi:10.1080/01426397.2016.1228860

Wu J, J., Larm, T., Wahlsten, A., Marsalek, J., and Viklander, M. (2021). Uncertainty Inherent to a Conceptual Model StormTac Web Simulating Urban Runoff Quantity, Quality and Control. *Urban Water J.* 18 (5), 300–309. doi:10.1080/1573062X.2021.1878240

Wu Z, Z., Ma, B., Wang, H., Hu, C., Lv, H., and Zhang, X. (2021). Identification of Sensitive Parameters of Urban Flood Model Based on Artificial Neural Network. *Water Resour. Manage.* 35 (7), 2115–2128. doi:10.1007/s11269-021-02825-3

Xia, J., Zhang, Y., Xiong, L., He, S., Wang, L., and Yu, Z. (2017). Opportunities and Challenges of the Sponge City Construction Related to Urban Water Issues in China. *Sci. China Earth Sci.* 60 (4), 652–658. doi:10.1007/s11430-016-0111-8

Xu, T., Jia, H., Wang, Z., Mao, X., and Xu, C. (2017). SWMM-based Methodology for Block-Scale LID-BMPs Planning Based on Site-Scale Multi-Objective Optimization: a Case Study in Tianjin. *Front. Environ. Sci. Eng.* 11 (4), 1–12. doi:10.1007/s11783-017-0934-6

Xu, Z., Qu, Y., Wang, S., and Chu, W. (2021). Diagnosis of Pipe Illicit Connections and Damaged Points in Urban Stormwater System Using an Inversed Optimization Model. *J. Clean. Prod.* 292, 126011. doi:10.1016/j.jclepro.2021.126011

Yang, M., Zhang, Y., and Pan, X. (2020). Improving the Horton Infiltration Equation by Considering Soil Moisture Variation. *J. Hydrol.* 586 (January), 124864. doi:10.1016/j.jhydrol.2020.124864

Yang, Y., Li, J., Huang, Q., Xia, J., Li, J., Liu, D., et al. (2021). Performance Assessment of Sponge City Infrastructure on Stormwater Outflows Using Isochrone and SWMM Models. *J. Hydrol.* 597 (February), 126151. doi:10.1016/j.jhydrol.2021.126151

Ye, S., and Tiong, P. (2000). NPV-AT-Risk Method in Infrastructure Project Investment Evaluation. *J. Construction Eng. Management* 126 (June), 227–233. doi:10.1061/(asce)0733-9364(2000)126:3(227)

Yin, D., Evans, B., Wang, Q., Chen, Z., Jia, H., Chen, A. S., et al. (2020). Integrated 1D and 2D Model for Better Assessing Runoff Quantity Control of Low Impact Development Facilities on Community Scale. *Sci. Total Environ.* 720, 137630. doi:10.1016/j.scitotenv.2020.137630

Yu, Z., Montalto, F., and Behr, C. (2018). Probabilistic green Infrastructure Cost Calculations Using a Phased Life Cycle Algorithm Integrated with Uncertainties. *J. Hydroinformatics.* 20 (5), 1201–1214. doi:10.2166/hydro.2018.107

Zema, D. A., Labate, A., Martino, D., and Zimbone, S. M. (2017). Comparing Different Infiltration Methods of the HEC-HMS Model: The Case Study of the Mésima Torrent (Southern Italy). *Land Degrad. Develop.* 28 (1), 294–308. doi:10.1002/ldr.2591

Zeng, Z., Yuan, X., Liang, J., and Li, Y. (2021). Designing and Implementing an SWMM-Based Web Service Framework to Provide Decision Support for Real-Time Urban Stormwater Management. *Environ. Model. Softw.* 135 (September 2020), 104887. doi:10.1016/j.envsoft.2020.104887

Zhang, C., He, M., and Zhang, Y. (2019). Urban Sustainable Development Based on the Framework of Sponge City: 71 Case Studies in China. *Sustainability.* 11 (6), 1544–1621. doi:10.3390/su11061544

Zhang, D., Hølland, E. S., Lindholm, G., and Ratnaweera, H. (2018). Hydraulic Modeling and Deep Learning Based Flow Forecasting for Optimizing Inter Catchment Wastewater Transfer. *J. Hydrol.* 567, 792–802. doi:10.1016/j.jhydrol.2017.11.029

Zhang, S., Li, Y., Ma, M., Song, T., and Song, R. (2018). Storm Water Management and Flood Control in Sponge City Construction of Beijing. *Water.* 10 (8), 1040–1111. doi:10.3390/w10081040

Zhang, Z., Szota, C., Fletcher, T. D., Williams, N. S. G., Werdin, J., and Farrell, C. (2018). Influence of Plant Composition and Water Use Strategies on green Roof Stormwater Retention. *Sci. Total Environ.* 625, 775–781. doi:10.1016/j.scitotenv.2017.12.231

Zhang, Z., Gu, J., Zhang, G., Ma, W., Zhao, L., Ning, P., et al. (2021). Design of Urban Runoff Pollution Control Based on the Sponge City Concept in a Large-Scale High-Plateau Mountainous Watershed: A Case Study in Yunnan, China. *J. Water Clim. Change.* 12 (1), 201–222. doi:10.2166/wcc.2019.120

Zhu, Y., Li, H., Yang, B., Zhang, X., Mahmud, S., Zhang, X., et al. (2021). Permeable Pavement Design Framework for Urban Stormwater Management Considering Multiple Criteria and Uncertainty. *J. Clean. Prod.* 293, 126114. doi:10.1016/j.jclepro.2021.126114

Conflict of Interest: Author Dr. YT is employed by Power China Huadong Engineering Corporation Limited.

The remaining authors declare that the research was conducted in the absence of any commercial or financial relationships that could be construed as a potential conflict of interest.

Publisher's Note: All claims expressed in this article are solely those of the authors and do not necessarily represent those of their affiliated organizations, or those of the publisher, the editors and the reviewers. Any product that may be evaluated in this article, or claim that may be made by its manufacturer, is not guaranteed or endorsed by the publisher.

frontiers | Frontiers in Environmental Science

ORIGINAL RESEARCH
published: 22 June 2022
doi: 10.3389/fenvs.2022.887446

Prediction of River Pollution Under the Rainfall-Runoff Impact by Artificial Neural Network: A Case Study of Shiyan River, Shenzhen, China

Zhan Tian [1,2], Ziwei Yu [1], Yifan Li [1], Qian Ke [3], Junguo Liu [1], Hongyan Luo [4] and Yingdong Tang [5]*

[1]School of Environmental Science and Engineering, Southern University of Science and Technology, Shenzhen, China, [2]Pengcheng Laboratory, Shenzhen, China, [3]Delft University of Technology, Delft, Netherlands, [4]Meteorological Bureau of Shenzhen Municipality, Shenzhen, China, [5]PowerChina Huadong Engineering Corporation Limited, Hangzhou, China

Climate change and rapid urbanization have made it difficult to predict the risk of pollution in cities under different types of rainfall. In this study, a data-driven approach to quantify the effects of rainfall characteristics on river pollution was proposed and applied in a case study of Shiyan River, Shenzhen, China. The results indicate that the most important factor affecting river pollution is the dry period followed by average rainfall intensity, maximum rainfall in 10 min, total amount of rainfall, and initial runoff intensity. In addition, an artificial neural network model was developed to predict the event mean concentration (EMC) of COD in the river based on the correlations between rainfall characteristics and EMC. Compared to under light rain (< 10 mm/day), the predicted EMC was five times lower under heavy rain (25–49.9 mm/day) and two times lower under moderate rain (10–24.9 mm/day). By converting the EMC to chemical oxygen demand in the river, the pollution load under non-point-source runoff was estimated to be 497.6 t/year (with an accuracy of 95.98%) in Shiyan River under typical rainfall characteristics. The results of this study can be used to guide urban rainwater utilization and engineering design in Shenzhen. The findings also provide insights for predicting the risk of rainfall-runoff pollution and developing related policies in other cities.

Keywords: rainfall-runoff pollution, rainfall characteristics, EMC, integrated learning methods, ANN

OPEN ACCESS

Edited by:
Mohamed Hasnain Isa, University of Technology Brunei, Brunei

Reviewed by:
An Liu, Shenzhen University, China
Chandra Ojha, Indian Institute of Technology Roorkee, India

****Correspondence:***
Junguo Liu
junguo.liu@gmail.com

Specialty section:
This article was submitted to Water and Wastewater Management, a section of the journal Frontiers in Environmental Science

Received: *01 March 2022*
Accepted: *20 May 2022*
Published: *22 June 2022*

Citation:
Tian Z, Yu Z, Li Y, Ke Q, Liu J, Luo H and Tang Y (2022) Prediction of River Pollution Under the Rainfall-Runoff Impact by Artificial Neural Network: A Case Study of Shiyan River, Shenzhen, China. Front. Environ. Sci. 10:887446. doi: 10.3389/fenvs.2022.887446

1 INTRODUCTION

Rapid urbanization has adverse effects on the natural environment, especially in aquatic environments. Due to changes in the hydrological cycle and the high diversity of pollutants, urban rainfall-runoff pollution has become a major problem (Kammen and Sunter, 2016). Especially in the initial stage of rainfall, the river pollutant content is the highest in the entire runoff process, which is referred to as the first flush effect (Gnecco et al., 2005; Feng et al., 2017). Common contaminants of river mainly include suspended solids, nutrients and heavy metals which have a major effects on the water quality of urban rivers (Perera et al., 2019; Yang et al., 2021).

Rapid urbanization has increased the impervious areas in cities, thereby reducing rainwater infiltration and increasing the total amount of runoff into urban rivers and the pollution load of urban surface runoff (Chen et al., 2017; He et al., 2018). Li et al. (2021) found that human activity has contributed to long-term reductions in the total amount and frequency of weak precipitation and the significant increases in the total amount and frequency of heavy precipitation in China. Human

activities such as land use and land cover change, the construction of dams and irrigation canals, and mining have altered urban river runoff (Adeyeri et al., 2020) and significantly affected the rainfall characteristics. Urban rainfall-runoff pollution has become the main cause of global urban water pollution (Wang et al., 2021). Thus, identifying the factors affecting this type of pollution is critically important for controlling urban river pollution.

To make timely predictions related to rainfall-runoff pollution with minimal data, researchers have begun to apply machine learning methods. These methods do not require a comprehensive understanding of the mechanism underlying the interactions between various parameters. These methods are also effective for simulating nonlinear and non-stationary hydrological environmental processes (Wang and Yao, 2013; Badrzadeh et al., 2015). Machine learning-based methods have shown advantages for the analysis of rainfall-runoff pollution, and with the development of data science, various machine learning methods have been explored and developed to predict rainfall-runoff pollution in urban rivers (Jeung et al., 2019). These methods including random forest (RF), gradient boosting decision tree (GBDT), and extreme gradient boosting (XGBoost) methods, which have been applied to analyze the relationships between rainfall characteristics and runoff pollution (Wu et al., 2014; Wang et al., 2015). RF algorithms have been used to rank the importance of multiple rainfall characteristics affecting the initial scouring effect of river runoff, revealing the following six most important characteristics: total rainfall amount; maximum rainfall intensity in 5 min; rainfall duration; total amount of runoff; peak runoff; and average rainfall intensity (Alias et al., 2014; Perera et al., 2019). By using the boosting method, GBDT will integrate multiple decision trees (DT) for analysis, which has shown a good prediction performances (Liang et al., 2020). Huan et al. (2020) applied a GBDT method to select characteristic factors with strong effects on dissolved oxygen and used these factors as input data to reduce the time needed for calculations. Joslyn (2018) evaluated the performance of XGBoost in predicting nine water quality factors (each factor was separately predicted using the other eight factors) and obtained success rates ranging from 80% to 90%.

Rainfall characteristics can also significantly affect the concentrations of river pollutants (Feng et al., 2015; Zhang et al., 2021), and rainfall duration and rainfall intensity are two of the most important factors affecting hydrological processes (Ran et al., 2012). Rainfall-runoff pollution is also affected by other rainfall characteristics such as the total amount of rainfall, which can affect the scouring effect of runoff (Liu et al., 2014), and the dry period (Zhang, 2011; Pang et al., 2012). Jeung et al. (2019) assessed the effects of rainfall characteristics on water quality parameters in urban rivers and found that different water quality parameters were affected by different rainfall characteristics; for example, biochemical oxygen demand and chemical oxygen demand (COD) were closely related to rainfall intensity, whereas total organic carbon and total phosphorus were strongly affected by the dry period. Gnecco et al. (2005) analyzed the event mean concentrations (EMCs) of various pollutants in urban rivers and found a strong correlation between maximum rainfall intensity and EMC.

Although several previous studies have analyzed rainfall characteristics and their qualitative effects on rainfall-runoff pollution, few studies have quantitatively analyzed the effects of rainfall characteristics on its pollution. Neural network models including artificial neural network (ANN), convolutional neural network, and back-propagation neural network models can consider multiple rainfall features together to predict rainfall-runoff pollution (Wu et al., 2014; Wang et al., 2015; Chau, 2017; Fotovatikhah et al., 2018). Some researchers have used neural network models to generalize the complex relationships between rainfall characteristics and water quality parameters to enhance the accuracy of rainfall-runoff simulation and prediction (Fernandes et al., 2020). For example, ANN models can be used to accurately determine whether the surface water quality meets the criteria set by national regulations or quantify the characteristics of water bodies (Palani et al., 2008; Shi et al., 2018). Using rainfall characteristics such as rainfall duration and confluence area as inputs and EMC as a training target, a back-propagation neural network model showed high accuracy for evaluating the total amount of pollutants in rainwater runoff (Tian, 2016). Ye et al. (2020) summarized the characteristics of neural network models used in environmental pollution research and found that ANN models can significantly improve the efficiency of pollutant prediction in rivers.

The objectives of this study were to analyze the CODs of Shiyan River and Shiyan Reservoir and explore the relationships between COD and rainfall characteristics. To achieve these objectives, we: 1) ranked the importance of different rainfall characteristics in terms of their effects on rainfall-runoff pollution using various integrated learning methods; 2) quantified the relationships between rainfall characteristics and runoff pollution in Shiyan River using an ANN model; and 3) estimated the non-point-source pollution load based on the typical EMC in the Shiyan River. As verified in this paper, the data-driven method presented herein can quickly predict the COD of the river. The findings provide a reference for water quality analysis in other fields.

2 DATA AND METHODS

2.1 Study Area

Over the past 40 years, precipitation and extreme precipitation in the western urban area of Shenzhen have increased. Changes in the underlying surface and rainfall characteristics have also affected the temporal and spatial distributions of non-point-source pollution. In this study, Shiyan River in Shenzhen, China is taken as a research case, as can be seen in **Figure 1**. Shiyan River is located in Shiyan Street, Bao'an District and is a first-level tributary in the Maozhou River Basin. The total length of Shiyan River is 10.44 km, and the catchment area of the basin is 27.05 km^2. The Shiyan River eventually merges into the Shiyan Reservoir, which is one of the four major reservoirs in Shenzhen and one of the largest sources of drinking water in Bao'an District. With the rapid economic development of Bao'an District, Shiyan

TABLE 1 | Typical rainfall characteristics under different rainfall types (2013–2018) (Li, 2020).

Rainfall characteristics	Light rain	Moderate rain	Heavy rain	Torrential rain	Rainstorm	Extraordinary rainstorm
Total amount of rainfall (mm)	4.03	6.28	17.11	34.20	96.34	165.04
Rainfall duration (min)	108.82	153.26	239.43	556.12	761.93	1698.12
Maximum rainfall per minute (mm)	0.32	0.49	1.06	1.58	1.63	1.75
Maximum rainfall in 10 min (mm)	0.92	1.83	6.38	7.74	9.33	13.76
Rainfall intensity (mm/h)	0.70	1.03	1.53	2.03	3.19	4.03
Dry period (h)	34.00	22.43	20.10	22.10	26.30	14.67

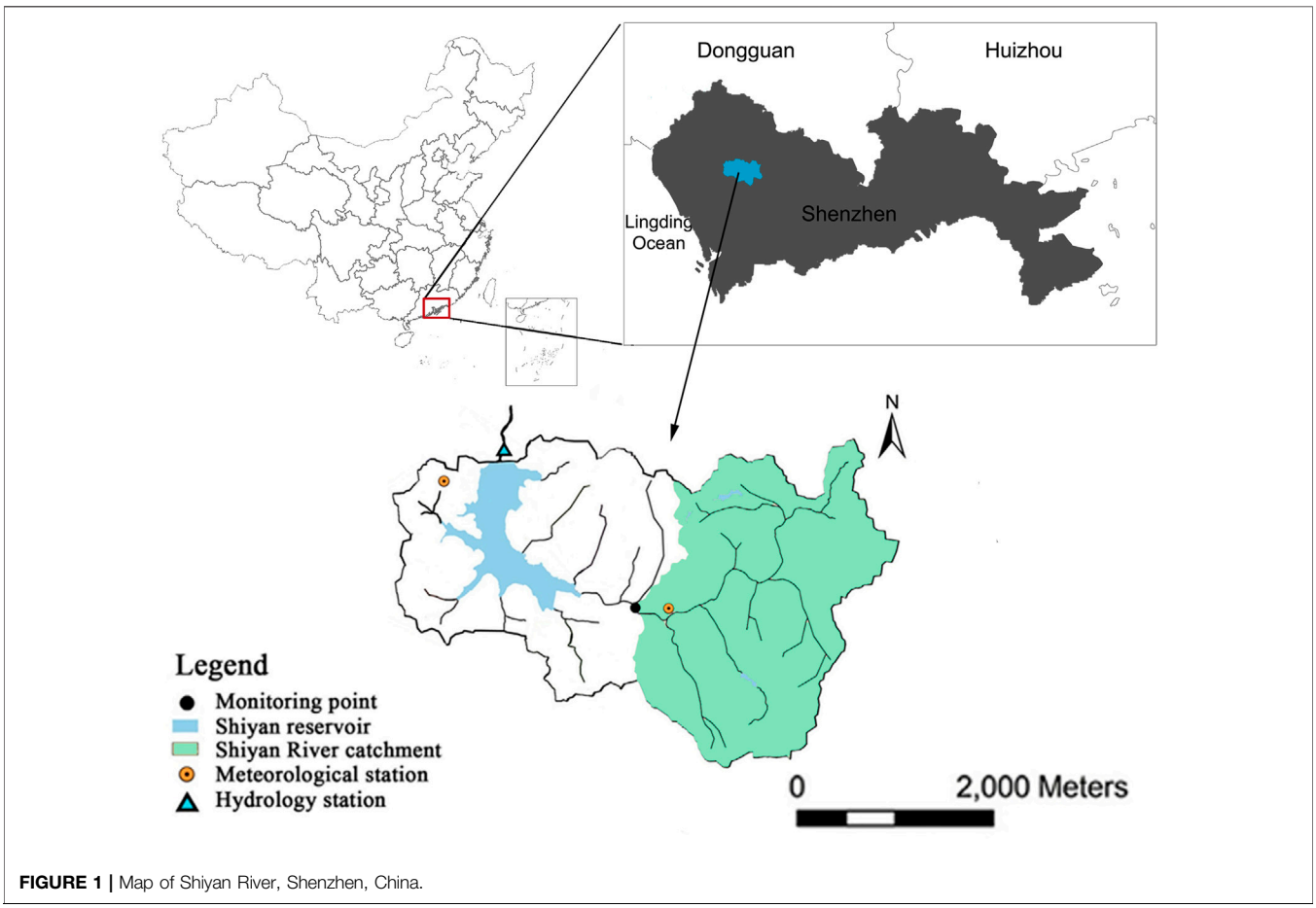

FIGURE 1 | Map of Shiyan River, Shenzhen, China.

River and Shiyan Reservoir will play increasingly important roles in water supply.

2.2 Data

The following data were used in this study. First, the hourly/daily/annual river discharge (m^3/s) and COD data (mg/L) for Shiyan River from 2009 to 2012 were obtained from Qin et al. (2013). We also used data from Qin et al. (2013) to select the most influential rainfall characteristics for EMC and build the ANN model based on rainfall characteristics to predict the EMC value. Rainfall-runoff data (mm/min) for 2013–2018 were obtained from Li (2020).

Due to the uncertainty of rainfall events, there is currently no uniform and clear criteria for classifying rainfall events. Based on recent research considering the effects of rainfall confluence time and rainfall duration, 180 min was used as the minimum time interval between two rainfall events, and the cumulative rainfall of each event had to be greater than 3 mm (Huang et al., 2021). According to the amount of rainfall in 24 h, all rainfall events were divided into six categories: light rain (< 10 mm); moderate rain (10–24.9 mm); heavy rain (25–49.9 mm); torrential rain (50–99.9 mm); rainstorm (100–249.9 mm); and extraordinary rainstorm (> 250 mm). Based on the above definitions of rainfall event and rainfall type, we obtained the typical rainfall characteristics (total amount of rainfall, rainfall duration, maximum rainfall per minute, maximum rainfall in 10 min, rainfall intensity, and dry period) for the study area and used

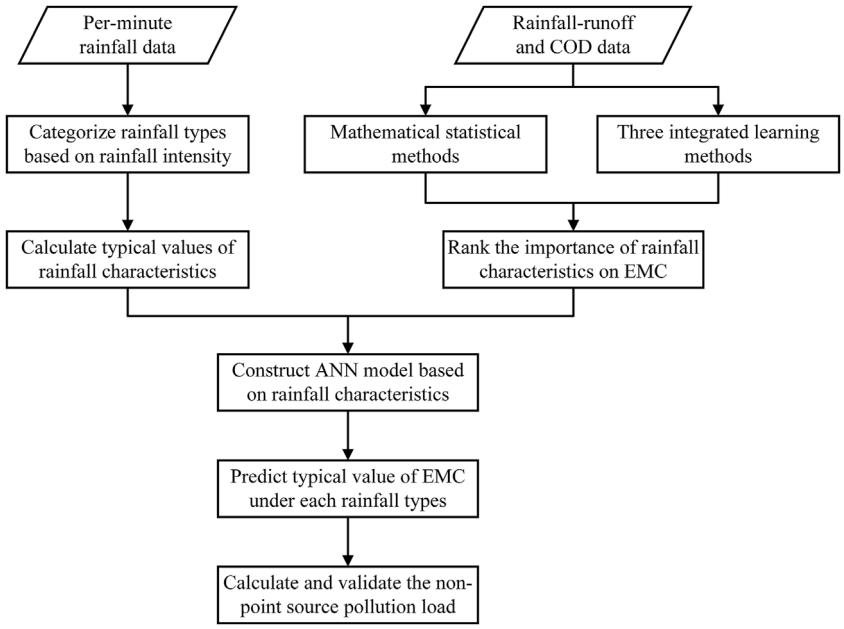

FIGURE 2 | Research framework for this study.

them in the subsequent verification of the pollution load of Shiyan River (**Table 1**).

2.3 Methods

As shown in **Figure 2**, we first processed the minute-level rainfall data (2013–2018) into different rainfall characteristics (total amount of rainfall, rainfall duration, maximum rainfall per minute, maximum rainfall in 10 min, rainfall intensity, and dry period). Subsequently, we identified the rainfall characteristics that most strongly affect EMC using mathematical statistical methods and three integrated learning methods (RF, GBDT, and XGBoost). Next, we developed an ANN model to predict the EMC values of Shiyan River by inputting typical rainfall characteristics under different rainfall types in terms of rainfall intensity per 24 h (namely, light rain, moderate rain, heavy rain, and torrential rain). Finally, we calculated and verified the runoff pollution load of the Shiyan Reservoir using the predicted EMC value.

2.3.1 Integrated Learning Methods

The integrated learning methods mainly completes research tasks by building and combining multiple different approaches, which can have a high accuracy rate. In this study, three widely used integrated learning algorithms (RF, GBDT, and XGBoost) were used to analyze the importance of various rainfall characteristics. RF is one of the most popular algorithms for solving classification and regression problems in recent years, with extremely high accuracy. GBDT can process a wide range of data types, and tuning parameter is relatively easy. XGBoost is efficient and flexible, which prevent overfitting and reduce model complexity.

2.3.1.1 Random Forest

RF is a method for accurately classifying large amounts of data by creating multiple decision trees. The RF algorithm consists of a combination of tree classifiers where each classifier is generated using a random vector sampled independently from the input vector, and each tree casts a unit vote for the most popular class to classify an input vector. The decision trees use the CART algorithm to select variables based on the splitting criteria of the root node and make judgments based on the characteristic evaluation standard; the root node recursively generates child nodes through the internal node. The internal nodes represent the judgments of the characteristics, and each child node represents a regression result. Random attributes are introduced into the training process of decision trees, and the results are determined by the predicted mean values of multiple decision trees. Averaging can alleviate the problem of high variance and high deviation by finding a natural balance between the two extremes. Because RFs are often used as black-box models, they can generate reasonable predictions for data without configuration.

2.3.1.2 Gradient Boosting Decision Tree

GBDT is a characteristics selection method with high interpretability. GBDT has high nonlinear processing ability when considering the interactions of multiple groups of characteristics (Huan et al., 2020). GBDT is a powerful machine learning tool consisting of three parts: regression decision tree, gradient boosting, and shrinkage. GBDT is based on the linear combination of basic functions; multiple rounds of iteration are performed, and each round of iteration produces a weak classifier (regression decision tree). Each classifier is trained based on the gradient of the previous classifiers, and the accuracy of the result is continuously improved by reducing the deviation. The algorithm aims to obtain a set of decision rules using the original characteristics as input to create a new decision tree (He et al., 2014).

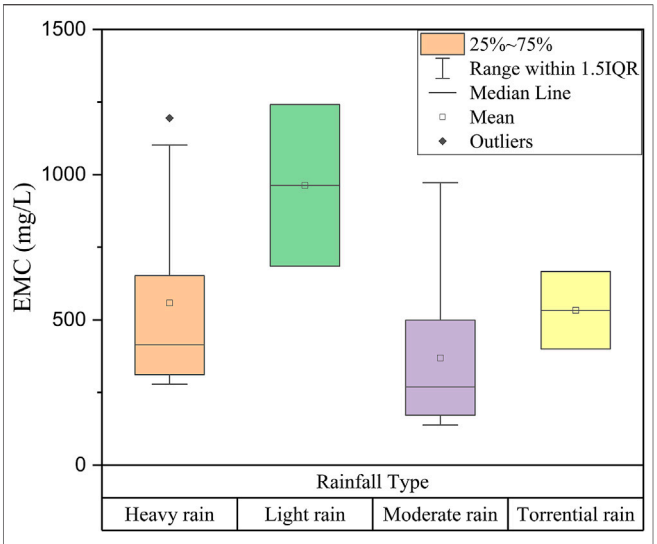

FIGURE 3 | EMC values under different rainfall types.

2.3.1.3 Extreme Gradient Boosting

XGBoost is an integrated machine learning algorithm based on decision trees that uses a gradient boosting framework. XGBoost has been widely used for regression, classification, and other applications. The core idea of XGBoost is to increase the number of decision trees by continuously splitting characteristics. Every time a tree is added, a new function $f(x)$ is learned to fit the residual of the last prediction. When the training is completed, resulting in k trees, the score of a sample is predicted based on the characteristics of this sample, and the score corresponding to each tree is added to the predicted value of the sample. This method uses normalization in the objective function to prevent overfitting and reduce the complexity of the model.

2.3.2 Artificial Neural Network Models

ANN models are networks of parallel distributed information processing systems that link input vectors to output vectors. They are composed of many information processing elements called neurons or nodes (Bisht et al., 2013). ANNs are mainly composed of three parts: the input layer, hidden layer, and output layer. The input layer primarily provides input data for the ANN model, and the hidden layer performs various transformations of the data (fitting the data by adjusting the function type and the number of neurons in the hidden layer), thus enhancing the network's ability to simulate complex functions. The output layer is considered to be a summary of the parallel calculation results performed by the hidden layer. The result of each neuron is the input of neurons existing in the next layer of the network, and the result of the output layer can be compared with the observed result (Haghiabi et al., 2018). Because the model is relatively simple and convenient for practical applications and prediction, it is a powerful tool for modeling many nonlinear hydrological processes; for example, ANN models have proven effective for use in the fields of water quality analysis and prediction.

2.3.3 Definition of Event Mean Concentration

Rainfall-runoff pollution events are characterized by uncertainty, and river runoff pollution is affected by factors such as the rainfall characteristics and underlying surface types. Instantaneous

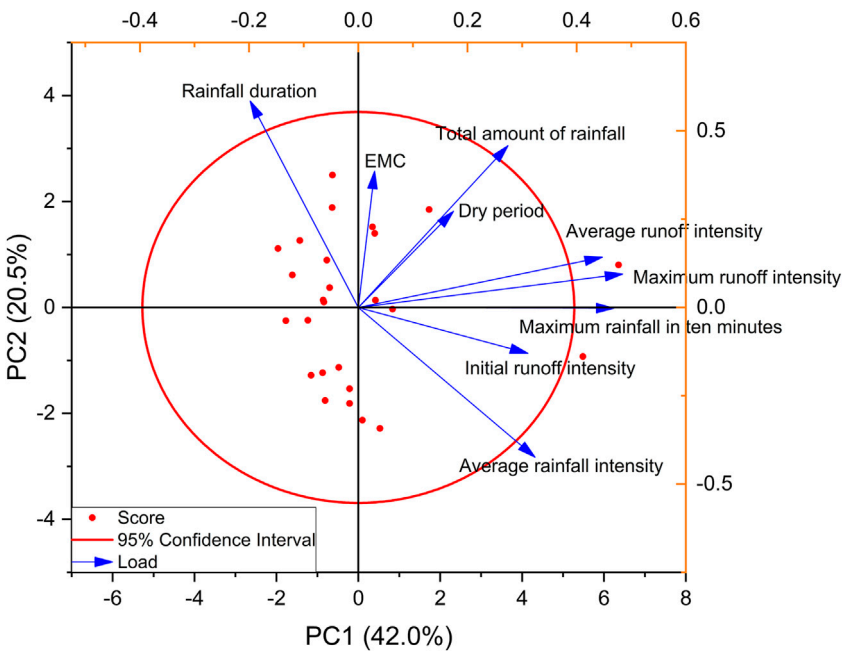

FIGURE 4 | PCA results between rainfall characteristics and EMC. PC1 and PC2 represent 42% and 20.5% of the total variance of the data, respectively. Red dots represent the scores of rainfall events. The red circle represents the 95% confidence interval. The blue arrows represent the proportions contributed by rainfall characteristics to PC1 and PC2.

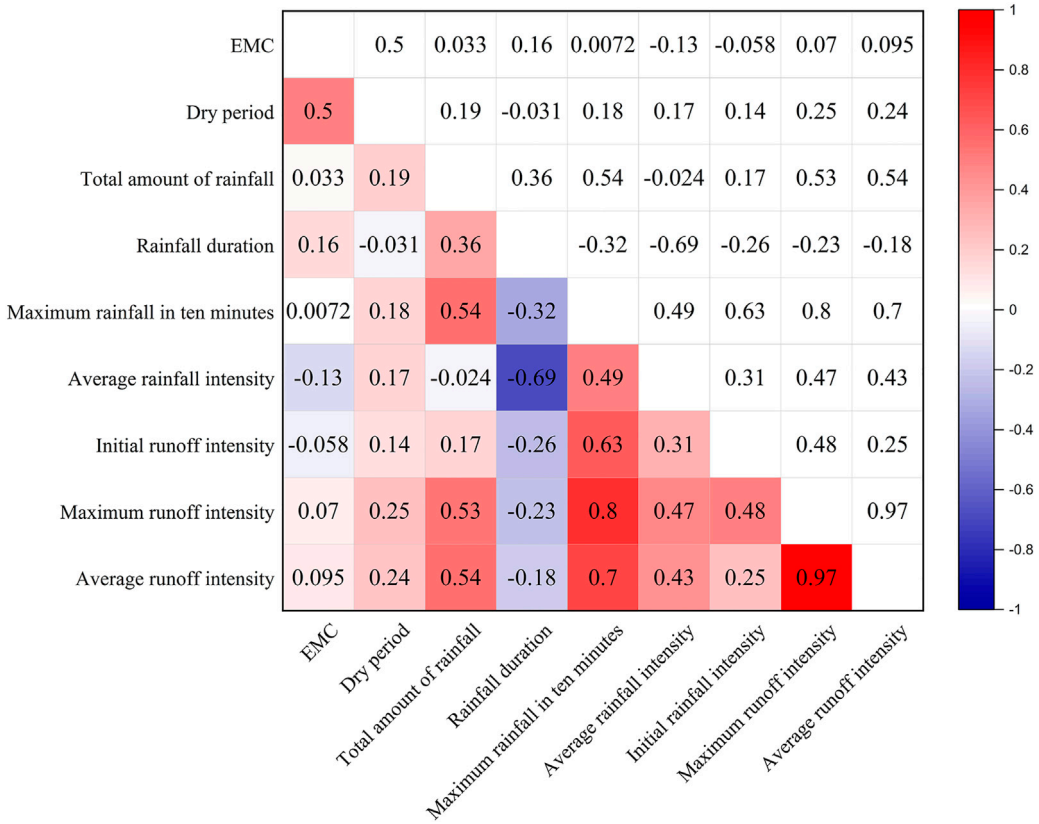

FIGURE 5 | Correlations between rainfall characteristics and EMC. Red and blue squares represent positive and negative correlations between two characteristics, respectively. Deeper color indicates a stronger correlation.

pollution concentrations do not accurately capture the characteristics of runoff pollution (Lee et al., 2011), it is necessary to find a variable to describe the pollution concentration in each rainfall-runoff pollution event. Therefore, in each event, COD was used to characterize water quality, and the degree of rainfall-runoff pollution was analyzed based on the event mean concentration (EMC) (Kim et al., 2007), which was calculated as the following equation (EMC formula):

$$\mathrm{EMC} = \frac{M}{V} = \frac{\int_0^T C_t Q_t dt}{\int_0^T Q_t dt} \tag{1}$$

Where: EMC = event mean concentration, mg/L; M = amount of pollutant, mg/L; V = runoff volume, m^3; T = rainfall duration, s; C_t = concentration of pollutant over time, mg/L; and Q_t = flow rate over time, m^3/s.

2.3.4 Model for Estimating Rainfall-Runoff Pollution

Due to the randomness of surface runoff discharge, the annual pollution load is usually to estimate the pollution load concentration of urban surface runoff, that is, the total amount of pollutants discharged from surface runoff caused by multiple rainfall events in a year (Li et al., 2010). The annual non-point-source runoff pollution load of Shiyan River was estimated based on the EMC values under typical rainfall characteristics. This estimation method has been widely used both within and outside of China (Wang, 2015). The annual runoff pollution load based on the EMC of the site was calculated using the following formula:

$$L_y = C_F \times \psi \times A \times P \times C \tag{2}$$

where: L_y = annual pollution load, t; C_F = proportion of rainfall events that produce runoff, usually taken when data are lacking, 0.9 was the empirical coefficient (Wang, 2015); Ψ = runoff coefficient; A = catchment area, km_2; P = average annual rainfall, mm; and C = EMC, mg/L.

3 RESULTS

3.1 Effects of Rainfall Characteristics on Event Mean Concentration

In this study, Shiyan River and Shiyan Reservoir were taken as typical research areas to explore the correlation between rainfall characteristics and runoff pollution. COD was used as a typical metric for pollution analysis. For convenience, the EMC formula was used to convert COD to EMC. Due to the low frequency of rainstorms and extraordinary rainstorms (0.03 and 0.01,

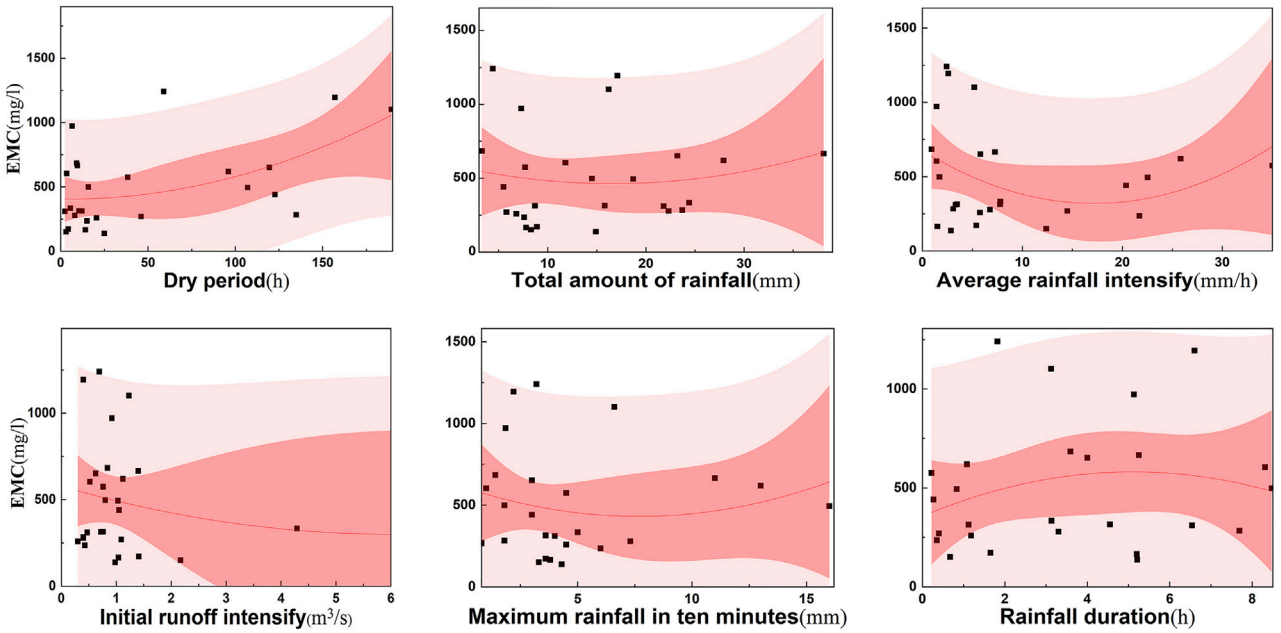

FIGURE 6 | Relationship between EMC and rainfall characteristics. Each black dot represents the EMC value of a rainfall event. The dark orange range represents the 95% confidence interval, while the light orange range represents the 95% prediction interval.

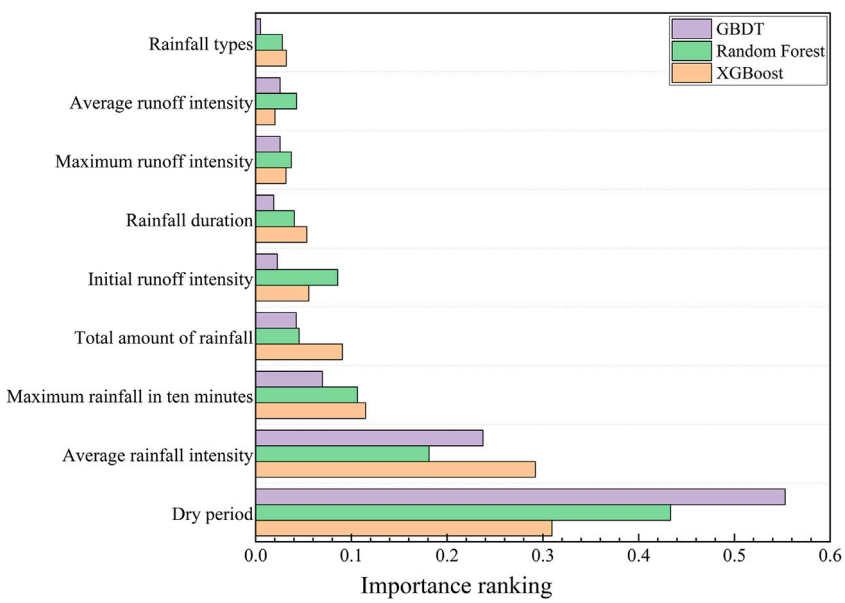

FIGURE 7 | Importance rankings of different rainfall characteristics in terms of their effect on EMC based on GBDT, RF, and XGBoost algorithms.

respectively), these rainfall types were combined with torrential rainfall events in this analysis.

Figure 3 shows the relationships between rainfall type and EMC based on rainfall data from 26 rainfall events (2009–2012). The vertical axis of the box plot represents the degree of data dispersion, and the center represents the typical distribution probability of EMC. Therefore, the typical value of EMC represents the location corresponding to the maximum distribution probability. In general, the typical EMC value is largest during light rain; the EMC during light rain (based on the median value) was almost four times higher than that during moderate rain, which was associated with the lowest EMC.

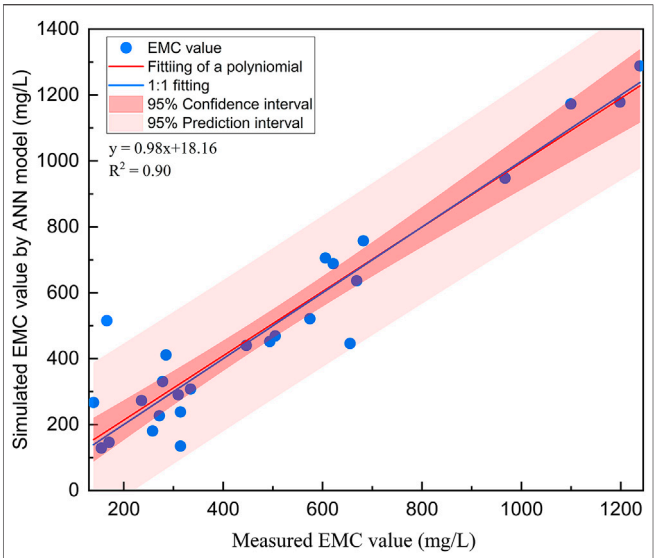

FIGURE 8 | Plot showing the ANN training performance.

Meanwhile, the EMC values corresponding to heavy rain and torrential rain were much lower than that for light rain.

Evaluating the effect of rainfall type on EMC requires analyzing the effects of different rainfall characteristics on EMC. In the case of light rain, the initial stage of rainfall will wash urban surface pollutants into the river, increasing the EMC. During moderate rain, rainfall runoff gradually increases, and the pollutants washed into the river channel change little, which reduces the EMC to a large degree. For heavy rain and torrential rain, the erosion of the river channel may wash pollutants from the deep layers of the ground into the river channel, resulting in a gradual increase in EMC.

Principal component analysis (PCA) was used to identify the correlations between rainfall characteristics and EMC. **Figure 4** shows the results of the PCA of rainfall characteristics and EMC. PC1 and PC2 explained 42% and 20.5% of the total variance of the data, respectively. The proportion contributed by each rainfall characteristic to PC1 and PC2 can be obtained from the directions and lengths of the blue arrows in **Figure 4**. Most of the scattered points in **Figure 4** are within the 95% confidence interval (shown by the red circle), which indicates that there were no obvious extreme values. A correlation matrix was used to calculate the correlation coefficients between EMC and the rainfall characteristics (**Figure 5**). In **Figure 5**, red and blue represent positive and negative correlations, respectively, and the intensity of the color indicates the strength of the correlation. Among the rainfall characteristics, dry period showed the strongest correlation with EMC (correlation coefficient = 0.5). Average rainfall intensity was negatively correlated with EMC (correlation coefficient = −0.13). The initial, average, and maximum runoff intensities were highly correlated. If the angle between the two rainfall eigenvalues in **Figure 4** was less than 30°, and the correlation coefficient was greater than 0.8 in **Figure 5**, we considered the correlation between two variables to be significant. Using these criteria, no significant correlations were observed between EMC and any single rainfall characteristic. Thus, it was necessary further analyze the data to reveal the relationships between multiple rainfall characteristics and EMC.

Using six rainfall characteristics (dry period, total amount of rainfall, average rainfall intensity, rainfall duration, maximum rainfall intensity in 10 min, and initial runoff intensity), we performed multiple linear regression fitting for EMC. **Figure 6** shows the relationships between EMC and various rainfall characteristics. Each black dot represents the EMC value of a rainfall event, and each figure contains 26 rainfall events. By constructing a linear fitting curve, we can observe the effects of different rainfall characteristics on EMC. In **Figure 6**, the dark orange range represents the 95% confidence interval between different rainfall characteristics and EMC, while the light orange range represents the 95% prediction interval between them. A positive correlation was observed between the dry period and EMC, while EMC gradually decreased as the initial runoff intensity increased. As the total amount of rainfall increased, EMC first decreased and then increased; a similar trend in EMC was observed for the maximum rainfall intensity. Thus, EMC showed different relationships with the various rainfall characteristics.

3.2 Analysis of the Relative Importance of Different Rainfall Characteristics in Determining Event Mean Concentration

Three widely used machine learning algorithms (RF, GBDT, and XGBoost) were used to analyze the relative importance of rainfall characteristics affecting runoff pollution (**Figure 7**). The most important rainfall characteristic affecting EMC was the dry period followed by the average rainfall intensity, the maximum rainfall in 10 min, the total amount of rainfall, and the initial runoff intensity. The high importance of the dry period may be

TABLE 2 | Effects of typical rainfall characteristics on EMC.

Rainfall characteristics	Light rain	Moderate rain	Heavy rain	Torrential rain
Dry period (h)	34.00	22.43	20.10	22.10
Rainfall depth (mm)	4.03	6.28	17.11	34.20
Maximum rainfall in 10 min (mm)	0.92	1.83	6.38	7.74
Rainfall intensity (mm/h)	0.70	1.03	1.53	2.03
Initial runoff (m^3/s)	0.76	0.94	2.07	1.40
Frequency	0.20	0.37	0.18	0.11
EMC (mg/L)	2612.20	1404.50	596.24	649.50

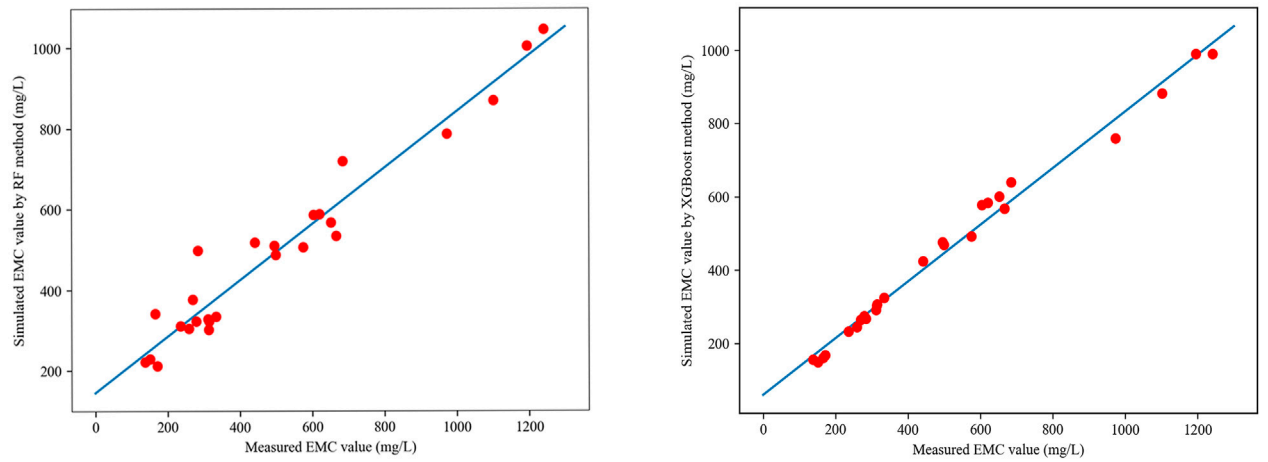

FIGURE 9 | Plot showing the training performance by RF and XGBoost.

related to the accumulation of surface pollutants during dry periods. During rainfall after an extended dry period, large quantities of pollutants are washed into the river, causing the EMC in the river to increase. However, due to the large differences in rainfall duration observed in the data, the effect of rainfall duration on EMC was relatively weak. The risk of runoff pollution was quantified by selecting the rainfall characteristics with the strongest effects on EMC based on the above analysis.

3.3 Construction and Analysis of the Prediction Model

Analyzing the input data improves the interpretability of the input data for neural network models. We established a model to predict runoff pollution from rainfall characteristics based on the relative importance of different rainfall characteristics and the availability of actual forecast data. The model considered the five rainfall characteristics with the strongest effects on EMC (i.e., dry period, average rainfall intensity, maximum rainfall in 10 min, total amount of rainfall, and initial runoff intensity), and the corresponding EMC values were used as the training targets. A total of 70% of the original data was used to train the ANN model, while the remaining 30% of the original data was used to verify the ANN model.

Figure 8 shows the training performance of the ANN model. The model training performance was 0.976, the test performance was 0.989, and the verification performance was 0.883. It also can be found that most of these scattered points are clustered near the fitted line from **Figure 8**, which show that the response results of this model are good; thus, the model can be used to predict EMC. The frequencies of rainstorms and extraordinary rainstorms were extremely low; thus, these rainfall types were ignored in the analysis of runoff pollution. Therefore, the typical EMC values for each rainfall characteristic under the other four rainfall types were used to predict EMC.

Under typical rainfall characteristics, the predicted EMC value was highest under the light rain scenario (2612.20 mg/L), and this EMC was approximately two times the predicted EMC under moderate rain (**Table 2**). The EMC prediction values for heavy rain and torrential rain were almost the same (both were one-fifth of the predicted EMC value for light rain). This may be explained by the fact that the dry period under the light rain scenario was typically longer than that under other rain types; thus, the dilution effect of pollutants washing into the river channel during light rain was weak. The dilution effect of heavy and moderate rain was more pronounced; under the torrential rain scenario, the predicted EMC value increased slowly because of the stronger effects of rainfall duration and runoff area. Rainfall events following long dry periods and light rain events require additional attention, and measures should be enacted in a timely manner to prevent water pollution.

The annual pollution load of non-point-source runoff for Shiyan River was estimated based on the predicted EMC values under typical rainfall characteristics (**Table 1**). EMC was used to approximate the annual runoff pollution load. Given that the traditional method of EMC value selection is relatively random, the predicted EMC values under typical rainfall events should be used. Hence, the estimation of rainfall-runoff pollution load considered the predicted values of EMC under typical rainfall events along with the probabilities of different rainfall patterns. The proportion of runoff events was 0.9, and the multi-year runoff depth of Shiyan River was 860 mm (average runoff depth is the product of the runoff coefficient and annual average rainfall). The EMC under different rainfall pattern was predicted based on the typical rainfall characteristics of the model, then the actual EMC value of this river can be obtained by weighted average of the probability values of different rainfall pattern, which was 1460 mg/L. Thus, according to the conversion of **Eq. 2**, the annual non-point-source COD pollution load was calculated to be 497.6 t. The annual non-point-source pollution load of COD in the built-up area of Shiyan Reservoir was previously reported to be 477 t (Yang et al., 2013), indicating an estimation accuracy for our model of 95.98%.

4 CONCLUSION AND DISCUSSION

Integrated learning methods were used to analyze the relationships between rainfall characteristics and EMC for Shiyan River. Rainfall characteristics were then used to predict the water quality by constructing an ANN model. The main findings are summarized below.

PCA of the rainfall characteristics revealed no significant correlations between rainfall characteristics. A positive correlation was observed between rainfall dry period and EMC, while EMC was negatively correlated with initial runoff intensity. Using mathematical statistical analysis and a variety of machine learning algorithms, we qualitatively described and ranked the effects of different rainfall characteristics on EMC. Among all rainfall characteristics, the dry period was the most important factor influencing EMC. This can be attributed to the build-up of surface pollutants as the dry period becomes longer. When rainfall occurs after a long dry period, large quantities of pollutants are washed into the river, causing EMC to increase. After dry period, the next most important rainfall characteristics were average rainfall intensity, maximum rainfall in 10 min, total amount of rainfall, and initial runoff intensity.

A model to predict EMC based on rainfall characteristics was constructed using the above five most influential rainfall characteristics as inputs, which greatly improved the interpretability of the neural network and the accuracy of the ANN model. The model training performance was 0.976, the test performance was 0.989, and the verification performance was 0.883. The prediction results under typical rainfall characteristics revealed that the runoff pollution caused by light rain is approximately two times that under moderate rain and five times that under heavy rain. Based on the predicted EMC values under typical rainfall characteristics, the annual non-point-source runoff pollution load of Shiyan River was estimated to be 497.6 t. The accuracy of the estimation method was 95.98%, indicating the robustness of the model.

We acknowledge that there are several limitations of this study. The relatively short time scale of the high-precision rainfall data in Shenzhen precludes a more in-depth study of future rainfall characteristics and trends under the influence of climate change. Because of the difficulty in monitoring rainfall-runoff pollution, the total number of samples used in this study was only 26 rainfall events. In order to prove the credibility of the results, we use RF and XGBoost methods to study this data. As can be seen in **Figure 9**, the simulation results of these two methods are good. The values of the coefficients of determination (r^2) obtained by RF and XGBoost methods are 0.879 and 0.914, which are similar to the results we predicted by ANN model (0.9). These results also prove that our findings are still reliable. Of course, subsequent studies should collect data over a longer time scale and consider the effects of land use and other factors on water quality/runoff pollution. The focus of this study was the relationships between rainfall characteristics and runoff pollution. Machine learning models can also be used to integrate rainfall and runoff data in future research.

The results of this study have implications for the utilization of urban rainwater and resources, engineering design, predicting rainfall-runoff pollution risk, and policy development.

DATA AVAILABILITY STATEMENT

The raw data supporting the conclusions of this article will be made available by the authors, without undue reservation.

AUTHOR CONTRIBUTIONS

ZT: Conceptualization, Discussion, Supervision, Writing (review and editing); ZY: Data curation, Planning, Writing (original draft); YL: Methodology, Data curation, Discussion; QK: Discussion, Writing (review and editing); JL: Conceptualization, Discussion, Supervision, Writing (review and editing); HL: Data provision, Discussion; YT: Data provision, Discussion. All authors read and approved the final manuscript.

FUNDING

This study was supported by the Science, Technology and Innovation Commision of Shenzhen Municipality (JCYJ20210324104004013). It was also supported by the National Key R&D Program of China (No. 2018YFE0206200).

ACKNOWLEDGMENTS

We acknowledge Aifang Chen, Wenfang Cao and Yanlong Guan of the iTOWER group for discussion and Pengfei Wang of the Southern University of Science and Technology for modifying graphs. We also acknowledge Xingxing Huang of the Shanghai Institute of Technology for his help.

REFERENCE

Adeyeri, O. E., Laux, P., Lawin, A. E., and Arnault, J. (2020). Assessing the Impact of Human Activities and Rainfall Variability on the River Discharge of Komadugu-Yobe Basin, Lake Chad Area. *Environ. Earth Sci.* 79 (6), 1–12. doi:10.1007/s12665-020-8875-y

Alias, N., Liu, A., Goonetilleke, A., and Egodawatta, P. (2014). Time as the Critical Factor in the Investigation of the Relationship between Pollutant Wash-Off and Rainfall Characteristics. *Ecol. Eng.* 64, 301–305. doi:10.1016/j.ecoleng.2014.01.008

Badrzadeh, H., Sarukkalige, R., and Jayawardena, A. W. (2015). Hourly Runoff Forecasting for Flood Risk Management: Application of Various Computational Intelligence Models. *J. Hydrology* 529, 1633–1643. doi:10.1016/j.jhydrol.2015.07.057

Bisht, D., Jain, S., and Raju, M. M. (2013). Prediction of Water Table Eevation Fluctuation through Fuzzy Logic & Artificial Neural Networks. *Int. J. Adv. Sci. Technol.* 51, 107–120.

Chau, K.-w. (2017). Use of Meta-Heuristic Techniques in Rainfall-Runoff Modelling. *Water* 9 (3), 186. doi:10.3390/w9030186

Chen, J., Theller, L., Gitau, M. W., Engel, B. A., and Harbor, J. M. (2017). Urbanization Impacts on Surface Runoff of the Contiguous United States. *J. Environ. Manag.* 187, 470–481. doi:10.1016/j.jenvman.2016.11.017

Feng, C., Mi, N., Wang, X., Cai, Z., and Di, W. (2015). Analysis of Road Runoff Pollution in Northern City Based on the Typical Rainfall. *Ecol. Environ. Sci.* 24 (3), 418–426. doi:10.16258/j.cnki.1674-5906.2015.03.008

Feng, Z., Cao, M., Mingming, C., Fan, K., Liu, Z., Muhua, F., et al. (2017). Analysis of Pollution Characteristics and First Flush Effect in Rainfall Runoff in Separate Storm Sewer System in Upstream of Tangxi River,Chaohu Catchment. *Hupo Kexue/Journal Lake Sci.* 29 (2), 285–296. doi:10.18307/2017.0204

Fernandes, A., Chaves, H., Lima, R., Neves, J., and Vicente, H. (2020). Draw on Artificial Neural Networks to Assess and Predict Water Quality. *IOP Conf. Ser. Earth Environ. Sci.* 612 (1), 012028. doi:10.1088/1755-1315/612/1/012028

Fotovatikhah, F., Herrera, M., Shamshirband, S., Chau, K.-w., Faizollahzadeh Ardabili, S., and Piran, M. J. (2018). Survey of Computational Intelligence as Basis to Big Flood Management: Challenges, Research Directions and Future Work. *Eng. Appl. Comput. Fluid Mech.* 12 (1), 411–437. doi:10.1080/19942060.2018.1448896

Gnecco, I., Berretta, C., Lanza, L. G., and La Barbera, P. (2005). Storm Water Pollution in the Urban Environment of Genoa, Italy. *Atmos. Res.* 77 (1–4), 60–73. doi:10.1016/j.atmosres.2004.10.017

Haghiabi, A. H., Nasrolahi, A. H., and Parsaie, A. (2018). Water Quality Prediction Using Machine Learning Methods. *Water Qual. Res. J.* 53 (1), 3–13. doi:10.2166/wqrj.2018.025

He, M., Zhang, J., Chen, C., Qi, X., and Chen, Q. (2018). Analysis of the Temporal and Spatial Characteristics of Rainfall-Runoff Pollution in Dianbei Basin of Shanghai. *Acta Sci. Circumstantiae* 38 (2), 536–545. doi:10.13671/j.hjkxxb.2017.0338

He, X., Bowers, S., Candela, J. Q., Pan, J., Jin, O., Xu, T., et al. (2014). "Practical Lessons from Predicting Clicks on Ads at Facebook," in Proceedings of the Eighth International Workshop on Data Mining for Online Advertising (ADKDD'14), Menlo Park, CA, August 24, 2014 (ADKDD'14), 1–9. doi:10.1145/2648584.2648589

Huan, J., Li, H., Li, M., and Chen, B. (2020). Prediction of Dissolved Oxygen in Aquaculture Based on Gradient Boosting Decision Tree and Long Short-Term Memory Network: A Study of Chang Zhou Fishery Demonstration Base, China. *Comput. Electron. Agric.* 175, 105530. doi:10.1016/j.compag.2020.105530

Huang, X., Li, Y., Tian, Z., Ye, Q., Ke, Q., Fan, D., et al. (2021). Evaluation of Short-Term Streamflow Prediction Methods in Urban River Basins. *Phys. Chem. Earth, Parts A/B/C* 123, 103027. doi:10.1016/j.pce.2021.103027

Jeung, M., Baek, S., Beom, J., Cho, K. H., Her, Y., and Yoon, K. (2019). Evaluation of Random Forest and Regression Tree Methods for Estimation of Mass First Flush Ratio in Urban Catchments. *J. Hydrology* 575, 1099–1110. doi:10.1016/j.jhydrol.2019.05.079

Joslyn, K. (2018). Water Quality Factor Prediction Using Supervised Machine Learning Citation Details. REU Final Report. AvaliableAt: https://archives.pdx.edu/ds/psu/26231 (Accessed November 20, 2021).

Kammen, D. M., and Sunter, D. A. (2016). City-integrated Renewable Energy for Urban Sustainability. *Science* 352 (6288), 922–928. doi:10.1126/science.aad9302

Kim, G., Chung, S., and Lee, C. (2007). Water Quality of Runoff from Agricultural-Forestry Watersheds in the Geum River Basin, Korea. *Environ. Monit. Assess.* 134 (1–3), 441–452. doi:10.1007/s10661-007-9635-0

Lee, J. Y., Kim, H., Kim, Y., and Han, M. Y. (2011). Characteristics of the Event Mean Concentration (EMC) from Rainfall Runoff on an Urban Highway. *Environ. Pollut.* 159 (4), 884–888. doi:10.1016/j.envpol.2010.12.022

Li, J., Li, Y., and Li, H. (2010). Study on the Calculation Method for Urban Surface Runoff Pollution Load. *J. Water Res. Water Eng.* 21 (2), 5–13.

Li, W., Chen, Y., and Chen, W. (2021). The Emergence of Anthropogenic Signal in Mean and Extreme Precipitation Trend over China by Using Two Large Ensembles. *Environ. Res. Lett.* 16 (1), 014052. doi:10.1088/1748-9326/abd26d

Li, Y. (2020). *Analysis of Rainfall Characteristics and Their Influence on Runoff and Water Quality in Maozhou River*. Master's Thesis. Harbin (China). Harbin Institute of Technology.

Liang, W., Luo, S., Zhao, G., and Wu, H. (2020). Predicting Hard Rock Pillar Stability Using GBDT, XGBoost, and LightGBM Algorithms. *Mathematics* 8 (5), 765. doi:10.3390/math8050765

Liu, A., Guan, Y., and Liu, L. (2014). Impact of Catchment and Rainfall Characteristics on Urban Runoff Quality. *J. Tsinghua Univ (Sci Technol)* 54 (7), 846–852. doi:10.16511/j.cnki.qhdxxb.2014.07.004

Palani, S., Liong, S.-Y., and Tkalich, P. (2008). An ANN Application for Water Quality Forecasting. *Mar. Pollut. Bull.* 56 (9), 1586–1597. doi:10.1016/j.marpolbul.2008.05.021

Pang, C., Wu, S., Zhou, J., and Lv, X. (2012). Nonpoint Source Pollution from Urban Runoff and Pollution Abatement in Urban Waterways. *Environ. Sci. Technol.* 35 (12), 2–6. doi:10.3969/j.issn.1003-6504.2012.12.037

Perera, T., McGree, J., Egodawatta, P., Jinadasa, K. B. S. N., and Goonetilleke, A. (2019). Taxonomy of Influential Factors for Predicting Pollutant First Flush in Urban Stormwater Runoff. *Water Res.* 166, 115075. doi:10.1016/j.watres.2019.115075

Qin, H., Tan, X., Fu, G., Zhang, Y., and Huang, Y. (2013). Frequency Analysis of Urban Runoff Quality in an Urbanizing Catchment of Shenzhen, China. *J. Hydrology* 496, 79–88. doi:10.1016/j.jhydrol.2013.04.053

Ran, Q., Su, D., Li, P., and He, Z. (2012). Experimental Study of the Impact of Rainfall Characteristics on Runoff Generation and Soil Erosion. *J. Hydrology* 424-425, 99–111. doi:10.1016/j.jhydrol.2011.12.035

Shi, B., Wang, P., Jiang, J., and Liu, R. (2018). Applying High-Frequency Surrogate Measurements and a Wavelet-ANN Model to Provide Early Warnings of Rapid Surface Water Quality Anomalies. *Sci. Total Environ.* 610-611, 1390–1399. doi:10.1016/j.scitotenv.2017.08.232

Wang, S., and Yao, X. (2013). Using Class Imbalance Learning for Software Defect Prediction. *IEEE Trans. Rel.* 62 (2), 434–443. doi:10.1109/TR.2013.2259203

Tian, H. (2016). *Research on Measurement and Evaluation Methods of Stormwater Runoff Pollution Load*. Master's Thesis. Beijing (China): Beijing University of Civil Engineering and Architecture.

Wang, H. (2015). *Pollution Characteristics Analysis and Pollution Load Estimation in Rainfall Runoff of Different Underlying Surface in Wuhan City*. Master's Thesis. Wuhan (China): Huazhong University of Science and Technology.

Wang, Z., Lai, C., Chen, X., Yang, B., Zhao, S., and Bai, X. (2015). Flood Hazard Risk Assessment Model Based on Random Forest. *J. Hydrology* 527, 1130–1141. doi:10.1016/j.jhydrol.2015.06.008

Wang, Z., Qi, F., Liu, L., Chen, M., Sun, D., and Nan, J. (2021). How Do Urban Rainfall-Runoff Pollution Control Technologies Develop in China? A Systematic Review Based on Bibliometric Analysis and Literature Summary. *Sci. Total Environ.* 789, 148045. doi:10.1016/j.scitotenv.2021.148045

Wu, Q., Ye, Y., Zhang, H., Ng, M. K., and Ho, S.-S. (2014). Forestexter: An Efficient Random Forest Algorithm for Imbalanced Text Categorization. *Knowledge-Based Syst.* 67, 105–116. doi:10.1016/j.knosys.2014.06.004

Yang, S., Liang, M., Qin, Z., Qian, Y., Li, M., and Cao, Y. (2021). A Novel Assessment Considering Spatial and Temporal Variations of Water Quality to Identify Pollution Sources in Urban Rivers. *Sci. Rep.* 11, 8714. doi:10.1038/s41598-021-87671-4

Yang, Y., Li, J., and Zhang, J. (2013). Study on Pollution Load of Watershed in Shiyan Reservoirs in Shenzhen. *Res. Conserv. Environ. Prot.* 8, 174. doi:10.16317/j.cnki.12-1377/x.2013.08.100

Ye, Z., Yang, J., Zhong, N., Tu, X., Jia, J., and Wang, J. (2020). Tackling Environmental Challenges in Pollution Controls Using Artificial Intelligence: A Review. *Sci. Total Environ.* 699, 134279. doi:10.1016/j.scitotenv.2019.134279

Zhang, W., Li, J., Sun, H., and Che, W. (2021). Pollutant First Flush Identification and its Implications for Urban Runoff Pollution Control: A Roof and Road Runoff Case Study in Beijing, China. *Water Sci. Technol.* 83 (11), 2829–2840. doi:10.2166/wst.2021.157

Zhang, Y. (2011). *Frequency Analysis of Rainfall Runoff Quality in Urbanizing Catchment: A Case Study of Shiyan River Catchment in Shenzhen*. Master's thesis. Beijing (China): Peking University.

Conflict of Interest: Author YT was employed by the company PowerChina Huadong Engineering Corporation Limited.

The remaining authors declare that the research was conducted in the absence of any commercial or financial relationships that could be construed as a potential conflict of interest.

Publisher's Note: All claims expressed in this article are solely those of the authors and do not necessarily represent those of their affiliated organizations, or those of the publisher, the editors and the reviewers. Any product that may be evaluated in this article, or claim that may be made by its manufacturer, is not guaranteed or endorsed by the publisher.

frontiers | Frontiers in Environmental Science

TYPE Review
PUBLISHED 07 February 2023
DOI 10.3389/fenvs.2023.1025665

OPEN ACCESS

EDITED BY
Xiaohong Chen,
Sun Yat-sen University, China

REVIEWED BY
Chidozie Charles Nnaji,
University of Nigeria, Nsukka, Nigeria
Yuan Li,
Hohai University, China
Peipeng Wu,
Zhengzhou University, China

*CORRESPONDENCE
Jiangyu Dai,
jydai@nhri.cn
Xiufeng Wu,
xfwu@nhri.cn
Shiqiang Wu,
sqwu@nhri.cn
Yu Zhang,
yuzhang@nhri.cn

SPECIALTY SECTION
This article was submitted to Water and Wastewater Management, a section of the journal Frontiers in Environmental Science

RECEIVED 23 August 2022
ACCEPTED 20 January 2023
PUBLISHED 07 February 2023

CITATION
Xu J, Dai J, Wu X, Wu S, Zhang Y, Wang F, Gao A and Tan Y (2023), Urban rainwater utilization: A review of management modes and harvesting systems. *Front. Environ. Sci.* 11:1025665. doi: 10.3389/fenvs.2023.1025665

Urban rainwater utilization: A review of management modes and harvesting systems

Jiayi Xu, Jiangyu Dai*, Xiufeng Wu*, Shiqiang Wu*, Yu Zhang*, Fangfang Wang, Ang Gao and Yanping Tan

State Key Laboratory of Hydrology-Water Resources and Hydraulic Engineering, Nanjing Hydraulic Research Institute, Nanjing, China

Due to the impact of climate change and rapid urbanization, issues around global urban flood control and water environment security have emerged as major global concerns. As a practical way to address these issues, exploitation of urban rainwater resources has become a worldwide hotspot for research and application. This paper 1) briefly examined the evolution of rainwater utilization management modes in advanced countries, 2) classified urban rainwater utilization measures from the utilization stages into three categories—source control, medium transmission, and terminal treatment, 3) summarized the advantages, disadvantages, and scope of the application of these measures, 4) reviewed the benefits, drawbacks, and application areas of these measures, and 5) conducted a quantitative analysis of their impact on rainwater pollution and flood control.

KEYWORDS

urban rainwater resources, management modes, utilization measures, pollution control, measure benefits

1 Introduction

According to the statistics from the United Nations, in 2018, 55.3% of the world's population resided in cities, and by 2030, 60% of all housing will be found in urban areas, with one in three people residing in a city with a population of at least 500,000. (UN, 2019). Rapid urbanization has given rise to an increase in impermeable urban surfaces, which has significantly altered the natural hydrological cycle in urban areas (Damien et al., 2016), making urban flooding a worldwide problem (Hussain et al., 2019). On the one hand, for instance, during the rainy season in China, cities like Beijing and Zhengzhou in the north and Guangzhou and Shenzhen in the south suffered from substantial storm water flooding issues, resulting in significant financial and human losses (Haghighatafshar et al., 2019; Liu et al., 2021; Zhao et al., 2021). On the other hand, as a joint result of population growth, low *per capita* water resources, and water quality contamination, more than 400 Chinese cities are currently struggling with acute shortages of water resources and water quality deterioration. Utilization of urban rainwater resources has become critical and urgent as it is an important means and method for alleviating urban waterlogging, reducing peak flow, and addressing urban water shortages.

The concept of urban rainwater resource utilization has been proposed for a long time. Initially focusing more on the safe management of urban rainwater flooding, it is now given new and different connotations by different countries based on their specific conditions (Fletcher et al., 2015).

Developed countries like the Netherlands and the United States are at the forefront regarding utilization of urban rainwater resources. In the United States, bills have been

passed by the Congress to assure the collection and storage of rainwater. Federal laws also mandate "*in situ* flood storage" for all new development zones (Cheng et al., 2007). In light of federal laws, each state has created "rainwater utilization regulations." For the same purposes, the United States has also provided economic incentives, such as general tax controls, issuance of obligation bonds, and federal and state loans (Steffen et al., 2013). In the Netherlands, people also have attached great importance to utilization of rainwater resources. Large buildings there have rainwater collection systems, and the country has very advanced real-time simulation technologies and utilization models for rainwater resources. Not only mechanical methods are used to purify rainwater, but also biochemical methods are applied to obtain high-quality rainwater treatment, allowing rainwater to be reused (Schets et al., 2010).

Concerning the issues of urban rainwater resource utilization, this article sets three objectives: 1) to summarize the histories of relevant modes adopted by different developed countries; 2) to outline, classify, and analyze various relevant methods; and 3) to provide a reference for the application and popularization of relevant measures in the future.

2 Urban rainwater management modes

The practice of rainwater management dates back to 3000 BC (Fletcher et al., 2015). Since the 1970s, developed countries have experienced 40 years of development and practice in urban rainwater and flood management and gradually formed a relatively complete and mature index system. The purpose of rainwater management in urban areas is to reduce the risk of urban flooding, alleviate the shortage of water, and ensure the safety of water resources. Urban rainwater management has recently developed quickly across the globe, and it now has an increasing number of modes and measures (Chen et al., 2016; Qi et al., 2020). Urban rainwater management requires the integrated management of the water cycle within a catchment area, combines the management of urban water supply, groundwater, wastewater, and rainwater (Eyni et al., 2021), and considers the various facilities and institutions involved in the urban water cycle roles and interactions involved in the urban water cycle (Fletcher and Deletic, 2007). It also plays an important role in legislation, concerning urban water management (Mitchell, 2006). Different rainwater utilization modes adopted by different countries are surveyed in the following sections.

2.1 America: Best management practices (BMPs), low impact development (LID), and green infrastructure (GI)

In the early 1970s, the United States realized that the traditional "drainage-based" approach was insufficient to address the problems of urban rainwater pollution and flooding (Haghighatafshar et al., 2019). In order to protect the water environment more actively, the term best management practices (BMPs) was first introduced in the Clean Water Act enacted in 1972. At first, the primary goal of BMPs was to control non-point source pollution. Now, BMPs are committed to taking comprehensive measures to solve the problems regarding water quality, water volume, and ecology, which significantly reduces peak flow by using centralized facilities (Ice, 2004). BMPs can generally be divided into two categories: structured measures and non-structural measures. Structured measures mainly include terminal treatment measures, such as rainwater pond, rainwater wetland, and infiltration facilities, while non-structural measures refer to various management measures (Che et al., 2014). From 1979 to 1983, the United States Environmental Protection Agency implemented the national urban runoff plan, which identified four types of urban rainwater BMPs: detention devices, recharge devices, housekeeping practices, and others (United States, 1972; United States, 1983). In the United States and Canada, BMPs were promoted in the cities through the national urban runoff plan in the early 1990s. Later, the concept of BMPs occurred in rainwater design manuals all over the United States, and the measures described in BMPs have been implemented and widely developed there.

The term low impact development (LID) was first coined in a land-use planning report in Vermont in 1977 (Liu et al., 2016; Mi et al., 2018). LID is a concept of urban rainwater management based on BMPs that serves as a supplement to macro-scale BMPs. LID aims to minimize the negative impact of urbanization or site development on the water environment from the very beginning, focusing on the use of small, decentralized eco-technical measures to maintain or restore the hydrological cycle before site development (Gregoire and Clausen, 2011; Rodak et al., 2019). LID minimizes the cost of rainwater management and solves the comprehensive problems of rainwater systems more efficiently and stably (Dietz et al., 2007; Xie et al., 2017). Specific measures include bio-retention facilities, green roofs, and grass ditches, which are near the source of runoff. The LID Research Center was established in 1998, which substantially promoted the development of the national urban runoff plan. The use of LID became mainstream in the early 21st century when it was incorporated into legislation throughout North America (TRCA, 2010).

The concept of green infrastructure (GI) was first introduced in the 1990s. GI originated from landscape design and landscape ecology, focusing on the ecological service function of urban greening. Since the 20th century, GI has been widely used by governments all over the world because of its rainwater management benefits and urban comfort improvements (Walmsley, 1995). GI is widely used in decentralized rainwater management networks to reduce rainwater runoff, improve water quality, and provide ecosystem sustainability (Fu et al., 2019). Compared with LID, GI involves some larger facilities, such as landscape water bodies, green corridors, and large wetlands (Koc et al., 2018), and emphasizes collaboration with urban planning, landscape design, ecology, and biological protection. GI is generally used in multi-scale regional planning or design to replace traditional drainage or gray regulation and storage facilities. It is more effective in achieving the dual objectives of rainwater control and protection or restoration of natural hydrological conditions and ecosystems.

2.2 Britain: Sustainable urban drainage systems (SUDS)

The drainage network in Britain that discharged sewage into the sea was built in the 18th century (Brown and Farrelly, 2009). Later, because the rainwater of the buildings and pavement areas on the catchment surface of the basin greatly exceeded the capacity of the drainage pipe network, floods caused by rainstorm and pollution problems caused by runoff became more and more salient, making it difficult to meet the national requirements for drainage and ecological

environment protection (Perales-Momparler, 2015). The concept of sustainable urban drainage systems (SUDS) was first proposed by Jim Conlin of Scottish Water in October 1997 (Butler and Parkinson, 1997). SUDS consist of a range of technologies and methods used for drainage, and the structural measures are essentially the same as that of LID. The concept of SUDS is based on simulating natural processes, such as infiltration, evaporation, and filtration, to deal with possible flood events (Perales-Momparler et al., 2015). At present, the development of SUDS focuses more on water quality management to mitigate the adverse effects of climate change (Gimenez-Maranges et al., 2020).

2.3 Australia: Water-sensitive urban design (WSUD)

The concept of water-sensitive urban design (WSUD) was first introduced in Australia in the 1990s (Cook et al., 2019). It was further refined in the early 21st century when the Australian Joint Committee on Urban Drainage established a WSUD task force in 2004 to promote the construction of an integrated water system design in the urban design process, which was an effort that involved many different industries. The early concept of WSUD centered around rainwater management, and afterwards it aimed to minimize the impact of urban development on the surrounding environment and covered the management of the integrated urban water cycle, including water supply, pollutant discharge reduction, water conservation, and rainwater management (Demuzere et al., 2014; Locatelli et al., 2020). WSUD has many subsets, and one of the most important subsets is rainwater management, aiming at flood prevention, flow management, water quality improvement, rainwater harvest, and non-potable water supplement (Fletcher et al., 2015).

2.4 China: Sponge city (SPC)

The concept of the sponge city (SPC) was first introduced in China in 2014. A sponge city has good "elasticity" in adapting to environmental changes and responding to natural disasters like a sponge. It absorbs, stores, seeps, and purifies water on rainy days and releases and uses the stored water when needed. A sponge city has the flexibility to deal with various disasters. It takes LID as the main design means and strives to keep the hydrological conditions untouched after the completion of the site development (Zhu et al., 2019; Yang et al., 2020). It satisfies the sustainable management idea of protecting the urban water source ecological environment. The sponge city requires all cities to establish a new urban rainwater treatment system that integrates infiltration, storage, stagnation, use, and drainage to retain about 80% of the rainwater, so as to conserve water and improve urban ecological benefits (Fletcher et al., 2015; Sang and Yang, 2017). China has selected 30 cities as pilot projects to promote sponge city construction (Hu et al., 2019; Eyni et al., 2021). However, the development of sponge cities in China is still in the preliminary stage, and there are still some problems, such as crude utilization methods, insufficient universality, lack of official standard for analyzing and assessing the benefits of rainwater utilization, blind construction of facilities, and lack of adequate planning.

2.5 New Zealand: Low impact urban design and development (LIUDD)

After about 30 years of research and practice, modern rainwater management in New Zealand has also formed a relatively complete system, which is at the forefront in the world and has achieved remarkable results. Based on BMPs and LID in the United States and WSUD in Australia, New Zealand puts a special emphasis on ecology and on respect for nature and coined the term "low impact urban design and development (LIUDD)" in "sustainable urban investment and development project" implemented by the New Zealand Foundation for Research, Science and Technology (FRST) in 2003. LIUDD combines national laws and plans and bases itself on the cultural heritage and legislative system. LIUDD emphasizes the application of local plant communities in urban low impact design to protect biodiversity, which uses interdisciplinary rainwater system design methods to simulate the process of natural ecosystems and highlights the combination of ecological functions and regional characteristics (Che et al., 2012).

2.6 Scope of application and features of the rainwater utilization modes

The modes of urban rainwater resource utilization and their histories in different countries are shown in Figure 1. Moreover, several typical rainwater utilization modes are compared and summarized in Table 1. As demonstrated in Table 1, current rainwater management modes are all improvements based on traditional drainage systems. BMPs, LID, and SUDS measures complement the existing drainage infrastructure. GI, WSUD, LIUDD, and SPC are more prominent in top-level design and integrated planning and cross-fertilizing and are widely used in urban planning, landscape design, and other multi-disciplines. Compared with the traditional rainwater measures, the methods and measures adopted in the new modes tend to be smaller, more decentralized, more integrated with the landscape, more protective of natural resources, and more cost-effective.

3 Construction of urban rainwater utilization measure systems

3.1 Classification of measures

Urban rainwater utilization measures can be classified along two dimensions: utilization ways and utilization stages. In terms of utilization ways, urban rainwater utilization measures can be divided into collection, transmission, infiltration, saving, and purification measures.

Collection measures are usually used to collect rainwater from roofs, roads, and green spaces, occupy small areas, and are easy to place. Collection measures include green roofs and rainwater tanks. Transmission measures can transfer the collected rainwater to other rainwater utilization facilities and municipal drainage systems and also have a certain collection capacity. Transmission measures mainly include grass ditches, permeation tubes, and permeation ditches. Infiltration measures infiltrate and supply groundwater, reduce surface runoff and the drainage pressure of the municipal pipe

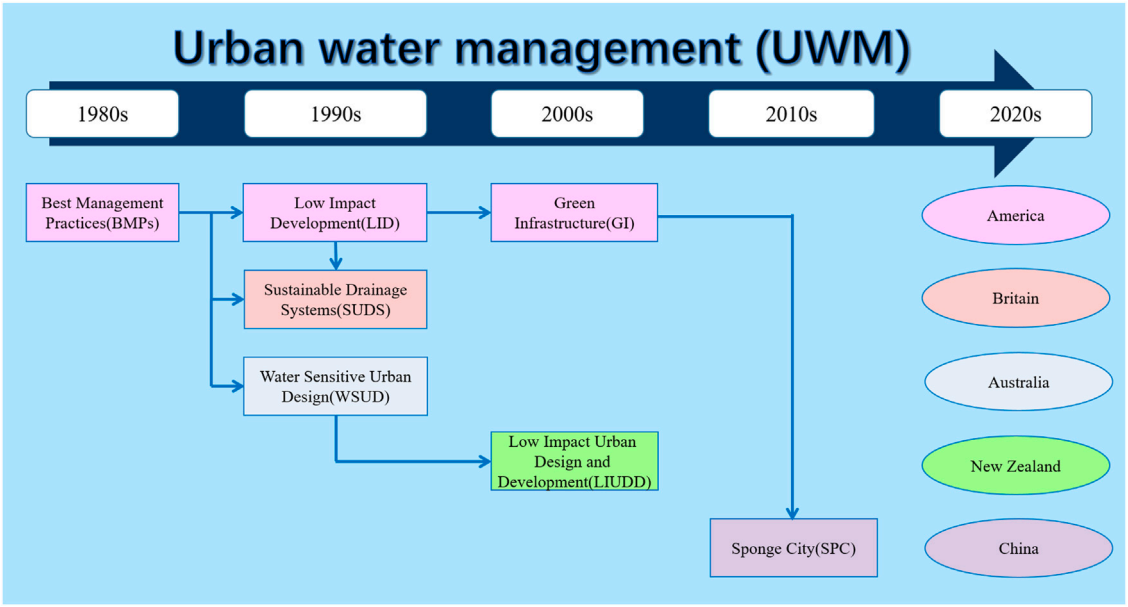

FIGURE 1
Rainwater utilization modes and developing course.

network, and alleviate urban waterlogging by direct rainwater infiltration. Infiltration measures mainly include permeable pavements, rainwater gardens, and infiltration wells. Saving measures use the naturally formed or artificially constructed water-storage space to retain or store rainwater and then slowly discharge it after the flood peak, so as to provide a basis for the reuse of rainwater resources in time and space, and achieve the role of peak cutting and peak shifting. The stored rainwater resources can be directly used for urban greening and irrigation. Saving measures mainly include impounding reservoirs and wet swales. Purification measures remove the polluted impurities in rainwater through the filtration of vegetation and the soil planted with vegetation and improve and control the water quality, so as to achieve water purification and environmental beautification. Purification measures mainly include vegetation buffer strands and bio-retention facilities.

With respect to the stages of rainwater utilization, such measures can be divided into source control, medium transmission, and terminal treatment measures. Source control measures are set before the rainwater enters the municipal pipe network, river ditches, and other drainage systems, with the purpose of controlling the water quantity and quality and increasing the infiltration and storage reuse. The main technical measures include green roofs, rainwater tanks, permeable pavements, and vegetation buffer strands. Medium transmission measures are generally set in the process of runoff confluence, and the overflowing rainwater is discharged into the municipal ditches and pipe networks after the rainwater exceeds the processing capacity of the source control measures. Medium transmission measures aim to intercept, regulate, and store rainwater, and the treated rainwater will be discharged or reused. The main technical measures include grass ditches, permeation tubes, permeation ditches, infiltration wells, and rainwater gardens. Terminal treatment measures are subjected to centralized physical, chemical, and biological treatments to remove pollutants in the rainwater and improve the rainwater quality and finally directly discharged into the receiving water body or reused after the rainwater is collected at the end of the drainage system. The main technical measures include impounding reservoirs, wet swales, and bio-retention facilities.

3.2 Application analysis of rainwater utilization measures

Current urban rainwater utilization measures include green roofs, rainwater tanks, grass ditches, permeation tubes/ditches, permeable pavements, rainwater gardens, infiltration wells, impounding reservoirs, wet swales, vegetation buffer strands, and bio-retention facilities (Li et al., 2014). A diagram of the distribution of the rainwater measures in cities is displayed in Figure 2.

3.2.1 Source control measures

3.2.1.1 Green roof

Green roofs as an important rainwater utilization measure have emerged in order to bring the inner urban cycle more harmonious with nature because modern urban rooftops account for approximately 20%–25% of the total urban area (Besir and Cuce, 2018). Green roofs, also known as vegetated roofs, eco-roofs, or natural roofs, are considered a new rainwater utilization technology integrating architectural art and greening technology, having the vegetation and the growth medium required for green vegetation (Vijayaraghavan, 2016). A green roof is composed of a vegetation, growth substrate, filter fabric, drainage element, protection layer, root barrier, insulation layer, water-proofing membrane, and roof deck from the top to bottom (He et al., 2016; Mao et al., 2021). A specific configuration of the green roofs is shown in Figure 3. Green roofs can fit in various types of buildings, such as office buildings, hotels,

10.3389/fenvs.2023.1025665

TABLE 1 Comparison of typical rainwater utilization modes.

Country	Utilization mode	Feature				Target function	Applicability						
		Small and medium rainfall control	Storm water control	Source measure	Top-level design		Facility feature	Required space	Interference with the site	Landscape integration degree	Natural resource conservation	Maintenance	Cost
—	Traditional drainage (1900s)		√			Relies on storm sewer systems to solve flooding problems	Integral	***	***			Professional	***
America	BMPs (1980s)	√	√	√		Peak flow reduction, end-of-pipe control, and water quality control	Centralized	**	**	*	**	Professional	**
	LID (1990s)	√		√		Maintains natural hydrology of the site	Distributed	*	—	***	***	Daily	*
	GI (2000s)	√	√	√	√	Replaces the utilization of more traditional gray storage facilities	Decentralized	*	—	***	***	Daily	*
Britain	SUDS (1990s)	√	√	√		Controls water quality and ecological landscape and end-of-pipe treatment	Penetration	*	—	***	***	Overall	*
Australia	WUSD (1990s)	√	√	√	√	Reduces the negative impact of natural water circulation	Integral	**	—	***	***	Overall	**
New Zealand	LIUDD (2000s)	√	√	√	√	Protects biodiversity and ecosystems and minimizes negative impact	Distributed	*	—	***	***	Daily	*

(Continued on following page)

TABLE 1 (*Continued*) Comparison of typical rainwater utilization modes.

Country	Utilization mode	Feature				Target function	Applicability						
		Small and medium rainfall control	Storm water control	Source measure	Top-level design		Facility feature	Required space	Interference with the site	Landscape integration degree	Natural resource conservation	Maintenance	Cost
China	SPC (2010s)	√	√	√	√	Improves the rainwater regulation and storage capacity of urban sub-base	Decentralized	*	—	***	***	Professional and overall	*

"√" indicates a very close association or a prominent role; more "*'s" indicate a higher degree; and "—" indicates none.

residences, schools, and gymnasiums (Shafique et al., 2018). Green roofs can reduce rainwater runoff, reduce greenhouse gas emissions to mitigate the urban heat island effect, reduce energy consumption, improve air and water quality, lower the pH of acid rainwater, provide better ecological urban living and wildlife habitat, and absorb noise (Coma et al., 2016; Tang and Qu, 2016; Abu-Zreig et al., 2019).

Wang et al. (2011) showed that the green roofs can effectively retain the roof rainwater runoff. The water retention rate is between 55%–88% during different seasons and different rainfalls, and the roof planted with different plants has the best reduction effect on storm runoff of 62%–80% under the same condition of the building substrate. Ayub et al. (2015) showed that planting suitable plants can reduce flood peak flow by 30.5%–67%. Simmons et al. (2008) showed that the green roofs can delay the peak runoff for 10 min, and when the rainfall is less than 10 mm, it will be absorbed by the green roofs. In addition, Wang et al. (2014) showed that the removal rates of TSS (total suspended solids), TP (total phosphorus), and TN (total nitrogen) pollution loads by green roofs can reach 40%, 31.6%, and 29.8%, respectively.

3.2.1.2 Permeable pavement

Permeable pavements are a form of pavement coverage that uses gravel and sand with good permeability and high porosity in the surface layer, subgrade, and lowest soil foundation, making rainwater enter the interior of the pavement structure smoothly and penetrate into the soil base through the drainage pipe inside the pavement, so as to reduce surface runoff and ground recharge (Qin, 2015). In terms of surface materials, permeable pavements can be classified into permeable bricks, permeable asphalt concrete, and permeable cement concrete pavements. An exact structure of permeable pavements is shown in Figure 4. The hydrological performance of permeable pavements depends on the water-storage capacity of the foundation and the saturated hydraulic conductivity of the foundation soil (Mullaney and Lucke, 2014; Kuruppu et al., 2019). The major advantages of permeable pavements lie in their abilities to purify water, restore natural hydrology, reduce runoff, mitigate urban heat island effects, and reduce road noise (Al-Rubaei et al., 2014; Yu et al., 2015; Gülbaz and Kazezyılmaz-Alhan, 2016).

Wang et al. (2019) showed that the total surface runoff of permeable pavements decreased by 1%–40%, and that the peak flow decreased by 7%–42%. Liu et al. (2020) found that, in the case of heavy rainfall, permeable pavements can effectively retain rainwater runoff, with an average runoff retention of 42.5%–52.5%. Regarding different materials of permeable pavements, Zhao et al. (2020) showed that the average peak delay time of structural permeable bricks and that of ordinary permeable bricks is 6.3 and 16.3 min, respectively. Li et al. (2018), summarizing several cases, concluded that the removal rates of TSS, TP, and TN pollution loads by permeable pavements can reach 56%–96%, 24%–63.4%, and 42%, respectively.

3.2.1.3 Bio-retention facility

Bio-retention facilities are similar to vegetated shallow trenches, planted in areas with a low terrain, making full utilization of the urban open space and improving rainwater quality through plant retention and soil infiltration. It is generally composed of a surface rainwater retention layer, vegetation planting layer, planting soil layer, sand-filter layer, and rainwater collection part (Nguyen et al., 2019).

Based on the KOSIM model, Tian et al. (2019) showed the environmental benefits of bio-retention facilities. The KOSIM

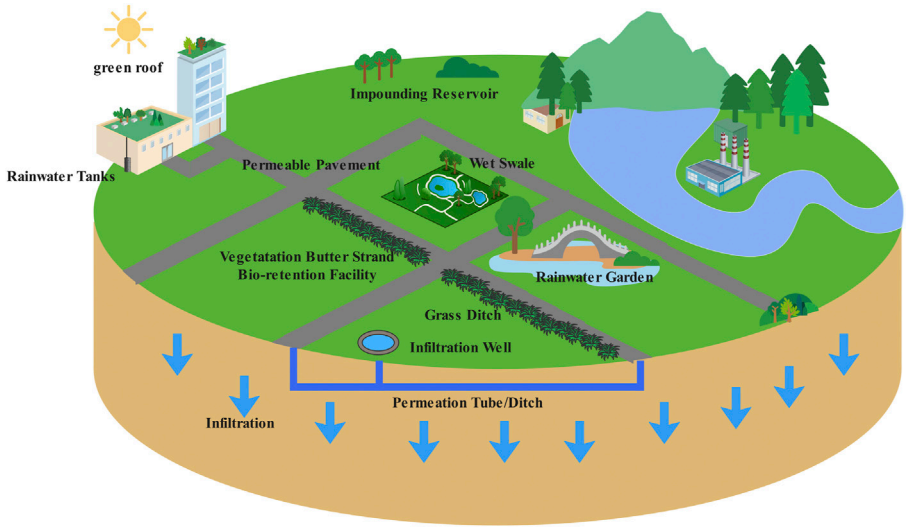

FIGURE 2
Distribution of rainwater measures in cities.

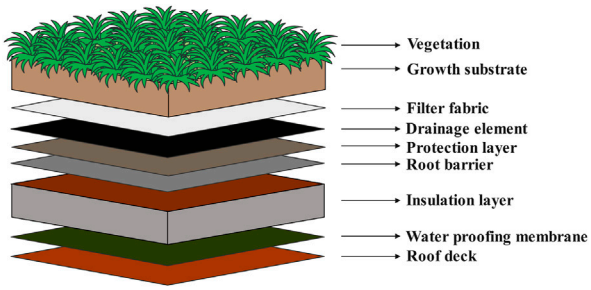

FIGURE 3
Specific structure of the green roof.

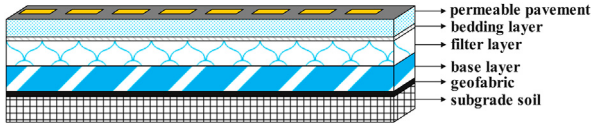

FIGURE 4
Specific structure of the permeable pavement.

model is a hydrological assessment model developed by Hanover Water Co., Ltd. As a Windows-based program for analyzing flood storage and detention areas of the urban drainage system, the KOSIM model can be used to calculate the performance of combined sewage overflow, sponge facilities, and rainwater storage tanks. In the case of large- and medium-sized rainstorms, the runoff retention rate of bio-retention facilities is 53%–79%. Pollutant removal is the main function of bio-retention facilities, while bio-retention facilities with different structures generally have different pollutant removal rates.

3.2.1.4 Vegetation buffer strand

A vegetation buffer strand, which consists of a horizontal water distributor and vegetation, uses surface plants and soil to intercept runoff pollutants. It disperses rainwater evenly across the vegetated area of the slope to promote infiltration and to diffuse runoff in the slope. Vegetation buffer strand plants are divided into two types: grass and woodland. The plants with better treatment effects are selected according to the specific situation. The infiltration and retention of vegetation are influenced by the slope, length, and plant species of the strip (Otto et al., 2008). Vegetation buffer strands are suitable for small areas, around impervious paved areas, parcel boundaries, and both sides of the roads (Gavrić et al., 2019). A specific structure of vegetation buffer strands is shown in Figure 5.

Zhang et al. (2022) showed that vegetation buffer strands can play an important role in preventing and controlling sedimentation, as their interception rate of sedimentation can reach more than 0.9 based on VFSMOD (vegetative filter strip modelling). At the same time, vegetation buffer strands also possess an important function of runoff regulation as they can completely intercept the runoff generated by small- and medium-sized rainfalls. Developed by Munoz-Carpena, VFSMOD estimated the flow and pollutant load in the runoff catchment area and the reduction of runoff flow and pollutant load in the buffer zone based on the model of storm and site conditions.

3.2.2 Medium transmission measures

3.2.2.1 Grass ditch

Grass ditches refer to surface ditches planted with vegetation that are used for collecting, transmitting, purifying rainwater, and connecting to other low-impact development facilities and municipal drainage systems. They can be generally divided into three types: transfer grass ditches, dry grass ditches, and wet grass ditches (Khadka et al., 2020). A specific configuration of grass ditches is shown in Figure 6.

Zhang et al. (2017) showed the control effect of different catchment methods of grass ditches on rainwater runoff flow. The experimental results showed that the rainwater runoff flow was reduced by 7.06%–9.51%, the peak reduction rate reached 2.67%–

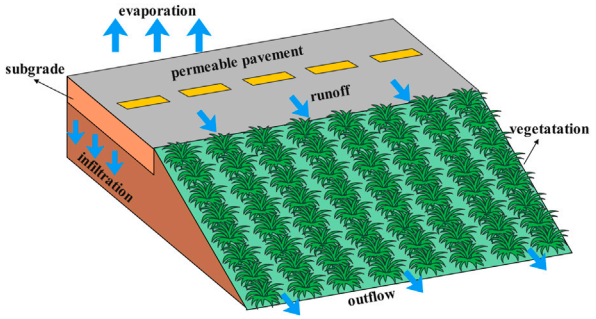

FIGURE 5
Specific structure of the vegetation buffer strand.

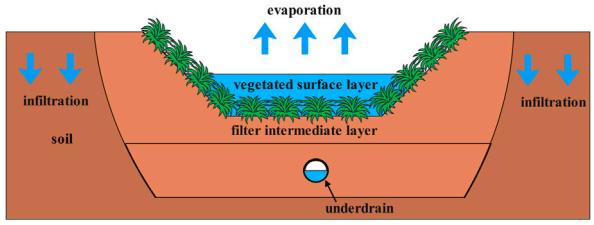

FIGURE 6
Specific structure of the grass ditch.

6.44%, and the peak appeared 9.6–12.2 min later. Wang et al. (2011) showed that the removal rates of TP and TN in grass ditches are generally 20%–40% and 20%–60%, respectively. Li et al. (2016) showed the removal ability of suspended solids and COD (chemical oxygen demand) in rainwater runoff by typical grass ditches. The experimental results showed that the removal rates of suspended solids and COD in rainwater runoff by grass ditches can reach 92.1%–99.3% and 51.72%–86.35%, respectively. Guo et al. (2015) showed that when the vegetation coverage of grass ditches reached about 60%, the removal rates of ammonia nitrogen and total phosphorus in rainwater runoff could be increased by about 10% and 20%, respectively.

3.2.2.2 Permeation tube/ditch

Permeation tubes/ditches refer to rainwater pipes/drains with an infiltration function, which can be made of a combination of perforated plastic pipes, sand-free concrete pipes/drains, and gravels (Bhagu et al., 2012). Permeation ditches, which are used to collect and store rainwater from a single area, can be set on the ground to intercept rainwater runoff or supply the phreatic layer underground as part of the rainwater pipeline. During the construction of permeation ditches, the influence of the soil infiltration rate and pollution on aquifers should be mainly considered.

3.2.2.3 Rainwater garden

Rainwater gardens are effective LID practices, usually constructed in green areas with low terrain. They supply groundwater through infiltration, remove pollutants before the rainwater enters the local rivers (Virginia Department of Forestry, 2019), and have landscape effects and ecological values. The advantages of rainwater gardens include purifying rainwater quality, delaying rainwater peaks, having low construction costs, having easy maintenance and management, and having high popularity (Amur et al., 2020). Although rainwater gardens retain a significant portion of rainwater and reduce the risk of flooding, the amount of water reduced during short periods of intense rainstorms is very small. Therefore, when designing rainwater gardens, it should be considered that the ability of rainwater gardens to reduce urban flood is limited (Martine et al., 2014; Guo et al., 2015). A specific structure of a rainwater garden is shown in Figure 7.

Tang et al. (2016) showed that the rainwater gardens with different fillers reduce the amount of rainfall by 9.8%–85.9% and the peak runoff by 11.2%–93.3%, and the flood peak delay time is 10–40 min. The urban storm flood process model built based on SWMM (storm water management model) has a runoff control rate of 50.9%–84.7% under different design rainfall return periods. SWMM is a rainstorm flood management model developed and studied by the United States Environmental Protection Agency (EPA) in 1971. It is applied to urban rainfall runoff simulation and is the most widely used urban rainstorm runoff model at present. For the removal of pollutants, Du et al. (2021) showed that the reduction rates of TSS, COD, TN, and TP are 20.8%–93.3%, 28.6%–92.6%, 11.6%–54.8%, and 9.8%–47.3%, respectively. The longer the recurrence period is, the lower the runoff control and pollutant reduction rates are.

3.2.2.4 Infiltration well

Infiltration wells are rainwater infiltration devices that can increase the infiltration effect through rainwater infiltration facilities on the well wall and on the bottom of the well. Infiltration wells are buried deeply under the ground, and horizontal infiltration drainage pipes are set around them to supplement the groundwater.

3.2.3 Terminal treatment measures

3.2.3.1 Rainwater tank

Rainwater tanks are normally connected to seepage places, such as rainwater gardens or gravel-filled dry wells, and installed in small rooms near buildings to collect rainwater flowing down from roof downpipes for non-potable water utilization, such as cleaning toilets.

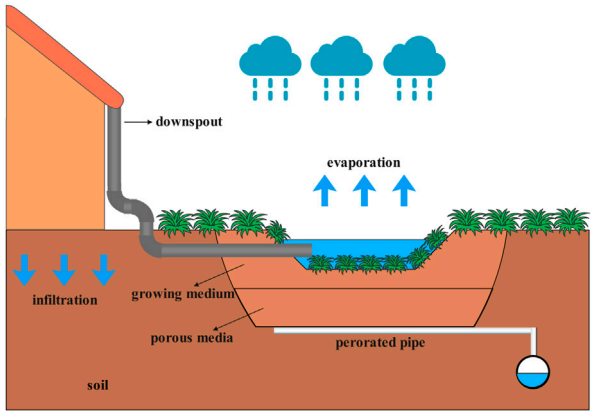

FIGURE 7
Specific structure of the rainwater garden.

The advantages of rainwater tanks include low-cost rainwater collection and use facilities, high water collection efficiency, simple setup, and easy maintenance management.

Rainwater tanks, with respect to the installation location, can be divided into above-ground rainwater tanks and underground rainwater tanks. A specific structure of rainwater tanks is shown in Figure 8. Rainwater tanks have a weak purification effect on rainwater quality, so it is necessary that they are cleaned regularly inside to avoid pollution, which affects their normal functional effects (Petrucci et al., 2012; Litofsky et al., 2014). The payback period of rainwater tank investment is influenced by a combination of tank size, water consumption, local water prices, location, and lifetime costs (Nachshon et al., 2016; Sharma and Gardner, 2020).

3.2.3.2 Impounding reservoir

Impounding reservoirs are commonly used facilities for collection and storage of rainwater. They are also a way to control the total amount of runoff and reduce the peak flow. Impounding reservoirs can be divided into reinforced concrete, masonry, and plastic module impounding reservoirs according to different materials. Urban areas with limited land utilization mostly use underground impounding reservoirs, which are built by reinforced concrete, masonry, or other materials, have good adaptability and save space but require a lot of excavation, and are more difficult to clean and maintain (Wu et al., 2020).

3.2.3.3 Wet swale

Most urban wet swales are artificial wet swales that simulate the structure and function of natural wet swales. Wet swales can efficiently control the pollution content of surface runoff, integrate ecological restoration and landscape aesthetic values, have low investment and simple operation and management, facilitate sedimentation, and have stable effects. In particular, they can operate reliably under unfavorable conditions, and their effects do not depend on soil properties.

Koon (1995) showed that the removal efficiency of TSS in the wet swales was between 67% and 81%, and the reduction range of TP was between 17% and 39%. Winston et al. (2012) showed that wet swales reduced TN in runoff by 40%.

3.3 Comparison of the technical measures of rainwater utilization

This article summarized the advantages, disadvantages, and application scope of the aforementioned technical measures, as shown in Table 2. In addition, this article also selected five typical measures and quantified their environmental benefits. The comparison results are shown in Table 3. Considering the control and reduction efficiency of the measures for runoff and rainfall runoff pollutants, eight indicators were selected to reflect the environmental benefits of the measures: the runoff reduction rate, peak reduction rate, rainwater retention rate, flood peak delay time, total suspended solids (TSS) reduction rate, total nitrogen (TN) reduction rate, total phosphorus (TP) reduction rate, and chemical oxygen demand (COD) reduction rate. The results showed that source control measures, including green roofs and permeable pavements, perform better regarding runoff reduction, peak reduction, rainwater retention, and flood peak delay, while medium transmission and terminal treatment measures, including grass ditches, rainwater gardens, and wet swales, perform better in pollutant removal. Green roofs can reduce runoff by 80%, reduce flood peak by 67%, retain rainwater by 88%, and delay flood peak time by 10 min. Permeable pavements can reduce runoff by 90%, reduce flood peak by 80%, retain rainwater by 52.5%, and delay flood peak time by 16.3 min. Grass ditches, rainwater gardens, and wet swales remove TSS by over 80%, TP by over 39%, and TN by over 40%.

For other benefits that are not easy to quantify, this article made a qualitative comparative analysis, and the comparison results are shown in Table 4. In terms of economic benefits, land areas of green roofs, permeable pavements, and infiltration wells are small, and construction costs of grass ditches, permeable pavements, and infiltration wells are low, and maintenance costs of grass ditches, permeable pavements, rainwater gardens, and vegetation buffer strands are low. With respect to the ecological benefits, pollution control, peak retardation, and total storage of rainwater gardens, wet swales, and bio-retention facilities show a relatively good performance. Regarding aesthetic benefits, green roofs stand out to some extent. Overall, different measures have different advantages and should be set in different locations in urban design planning, considering the specific local conditions.

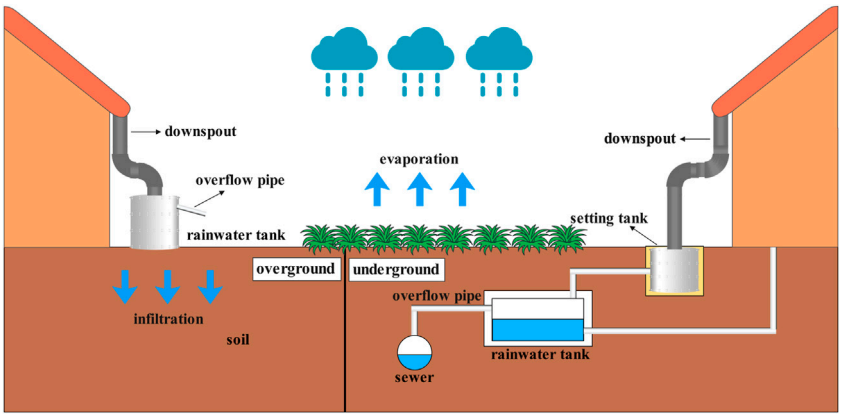

FIGURE 8
Specific structure of the rainwater tank.

TABLE 2 Advantages, disadvantages, and the scope of application for the technical measures of rainwater utilization.

Measure classification		Advantage	Disadvantage	Scope of application
Source control measures	Green roof	1) Reduces roof surface runoff and pollution load	Strict requirements for roof loading, waterproofing, slope, and space conditions	Suitable for flat roof buildings and sloped roof buildings with a slope of ≦15°
		2) Saves energy and reduces emission		
		3) Has a very good landscape benefit		
	Permeable pavement	1) Reduces the urban waterlogging area and heat island effect	High costs	Suitable for pavement, bicycle path, small garden path, and pedestrian street ground paving
		2) Improves the urban environment and water quality		
	Vegetation buffer strand	1) Reduces the consumption of energy and resources	High maintenance costs	Suitable for small areas, generally less than 2 ha, and constructed around impervious pavement areas
		2) Makes full utilization of the small urban space		
		3) Saves infrastructure costs and creates a good landscape effect		
Medium transmission measures	Grass ditch	1) Simple construction and low investment	Requires the shallow plant roots	Can be set on any permeable ground, such as squares in city parks, green areas, and around buildings
		2) Alleviates water on the road		
		3) Reduces rainwater to groundwater		
	Permeation tube/ ditch	1) Occupies a small area	Difficult inspection and repair	—
		2) Simple setup		
		3) Combines with the rainwater system to supply groundwater sources		
	Rainwater garden	1) Simple construction, low cost, and easy operation and management	1) Requires manual maintenance and high labor costs; 2) Temporary storage of rainwater	Set in the rainwater collection surface, such as roads, squares, and buildings in the park
		2) Has landscape benefits		
		3) Collects and reuses purified rainwater		
	Infiltration well	1) Occupies a small area	Low purification capacity of rainwater	Set in the park catchment area with less rainwater pollution
		2) Requires a centralized control and management		
Terminal treatment measures	Rainwater tank	1) High collection efficiency	Weak purification effect	Suitable for low-rise residential communities, commercial areas, and industrial plants
		2) Simple setup and easy installation, maintenance, and management		
		3) Collected rainwater can be used for non-potable water utilization		
	Impounding reservoir	1) Large storage volume and good adaptability	1) Cannot prevent frost and reduce evaporation; 2) requires extensive excavation	Should be integrated with overall planning and landscaping design
		2) Saves tap water usage and alleviates the urban water shortage		
		3) Improves ecological environment		

(Continued on following page)

TABLE 2 (*Continued*) Advantages, disadvantages, and the scope of application for the technical measures of rainwater utilization.

Measure classification		Advantage	Disadvantage	Scope of application
	Wet Swale	1) Low investment and simple operation and management	High costs and difficult maintenance	Suitable for minimum 5 ha and preferably more than 10 ha area
		2) Reliable operation under unfavorable conditions		
		3) Reduces suspension and has landscape and economic benefits		

"—" indicates none.

TABLE 3 Comparison of ecological benefits of urban rainwater utilization measures.

Environmental indicator		Source control measure		Medium transmission measure		Terminal treatment measure
		Green roof	Permeable pavement	Grass ditch	Rainwater garden	Wet swale
Runoff reduction rate (%)		62–80	40–90	7.1–9.5	9.8–85.9	—
Peak reduction rate (%)		30.5–67	20–80	2.7–6.4	11.2–93.3	—
Rainwater retention rate (%)		55–88	42.5–52.5	—	54.9–84.7	—
Flood peak delay time (min)		10	6.3–16.3	9.6–12.2	10–40	—
Pollutant removal rate	TSS (%)	40	56–96	92.1–99.3	20.8–93.3	67–81
	TP (%)	31.6	24–63.4	20–40	9.8–47.3	17–39
	TN (%)	29.8	42	20–60	11.6–54.8	40
	COD (%)	—	—	51.7–86.3	28.6–92.6	—

"—" indicates no data.

TABLE 4 Comparison of other benefits of urban rainwater utilization measures.

Measure classification		Economic benefit			Ecological benefit			Aesthetic benefit
		Land area	Construction cost	Maintenance cost	Pollution control	Peak retardation	Total storage	
Source control measures	Green roof	***	**	**	***	*	***	***
	Permeable pavement	***	*	*	*	*	***	**
	Bio-retention facility	**	***	**	***	***	***	**
	Vegetation buffer strand	**	*	*	**	**	**	*
Medium transmission measures	Grass ditch	**	*	*	*	*	***	**
	Permeation tube/ditch	**	**	**	*	**	*	—
	Rainwater garden	***	**	*	**	***	**	**
	Infiltration well	*	*	*	*	*	***	—
Terminal treatment measures	Rainwater tank	*	**	**	*	*	***	*
	Impounding reservoir	**	**	*	*	*	***	—
	Wet swale	***	***	**	***	***	***	**

More "*'s" indicate a higher degree; and "—" indicates none.

4 Prospects

The article provided an outlook on each of the two blocks: rainwater management modes and rainwater utilization measures.

4.1 Rainwater management modes

In the past few decades, the urban rainwater management model has undergone significant changes, from mainly relying on the traditional gray drainage system to reduce urban waterlogging to green facilities that combine environmental, health, social, and economic factors. Countries that have just started rainwater utilization can learn from rainwater management modes of leading countries as well as their experience and develop more rainwater utilization modes.

4.1.1 Establish and improve the relevant law and regulation system and incentive mechanism of rainwater management

The implementation of a system cannot be separated from the support of the legal force. The mature rainwater management mode has a sound system of laws and regulations related to rainwater management as well as an effective incentive mechanism. Countries should strengthen policy guidance, formulate appropriate discharge standards and charging systems, and ensure the acceleration of the city's rainwater management.

4.1.2 Popularize awareness of water conservation

While vigorously developing the economy, countries should also make people aware of the importance of environmental protection. Countries should vigorously publicize the importance of rainwater management and environmental protection. The public should understand and manifest the understanding in various activities, change public awareness through various channels, and actively participate in the construction of a new mode.

4.1.3 Strengthen interdisciplinary and multi-sectoral cooperation

Urban rainwater management is an extremely complex issue, involving architecture, planning, landscape, municipal engineering, environmental engineering, hydraulics, urban water supply and drainage, social resource management, and other disciplines. Although the importance of cooperation between various departments has been repeatedly emphasized when formulating relevant policies, more adjustments are needed in practice. Rainwater management personnel should have the basic knowledge of various disciplines involved in urban rainwater management and should be able to communicate and cooperate closely in the future design work, so as to make the drainage system design more scientific. When necessary, they can also collaborate with leading foreign design teams to learn advanced experience.

4.1.4 Adapt to national conditions

Each country has different geographical conditions and cultural customs. A mature rainwater utilization mode is often only suitable for certain specific conditions, such as abundant water or drought in the country. For example, the sponge cities in China have developed rapidly in recent years, and many rainwater management indicators have been set up, but most of them have not been implemented well because many indicators are simply copied from the technical indicators of developed countries in rainwater utilization, having the problem of lacking rationality. Therefore, each country should adjust its measures according to the local conditions, base its relevant works on national conditions, and establish a mode suitable for its own country.

4.1.5 Establish management systems with clear division of powers and responsibilities

To solve the urban storm flood problem, not only is it necessary to build drainage facilities, but also they should be maintained by relevant departments and developers in accordance with the rights and obligations specified in the relevant system. Establishing and improving the accountability system for rainwater management are helpful for finding ways to solve problems as soon as possible, which is beneficial to efficient working of the storm flood management facilities.

4.2 Rainwater utilization measures

There are many specific measures for rainwater utilization, which have ecological and sustainable characteristics and broad application prospects. In reality, rainwater utilization measures are basically sporadic, and comprehensive planning is needed to give full play to reap the maximum benefits. The government should carry out planning at different levels to form a rainwater management system with master planning, large watershed planning, small watershed planning, and environmental management planning and retain and reduce rainwater at all levels to achieve "zero growth" of regional development before and after runoff. At present, rainwater utilization measures and technologies are still in the exploratory stage, lacking extensive engineering applications, and their control and treatment effects on surface runoff are not stable. Countries should learn from each other's successful cases and choose appropriate rainwater utilization measures according to the local conditions.

Author contributions

All authors listed have made a substantial, direct, and intellectual contribution to the work and approved it for publication.

Funding

This research was jointly funded by the National Key R&D Program of China (2018YFE0206200), the Projects of National Natural Science Foundation of China (52179073), and the Natural Science Foundation of Jiangsu Province, China (Grant No. BK20200160).

Conflict of interest

The authors declare that the research was conducted in the absence of any commercial or financial relationships that could be construed as a potential conflict of interest.

Publisher's note

References

Abu-Zreig, M., Ababneh, F., and Abdullah, F. (2019). Assessment of rooftop rainwater harvesting in northern Jordan. *Phys. Chem. Earth* 114. doi:10.1016/j.pce.2019.08.002102794

Al-Rubaei, A. M., Viklander, M., and Blecken, G. T. (2014). Long-term hydraulic performance of stormwater infiltration systems. *Urban Water J.* 12 (8), 660–671. doi:10.1080/1573062x.2014.949796

Amur, A., Wadzuk, B. M., and Traver, R. (2020). Analyzing the performance of a rain garden over 15 Years: How predictable is the rain garden's response. Proceedings of the International Low Impact Development Conference, July 2020, Bethesda, Maryland.

Ayub, K. R., Ghani, A. A., and Zakaria, N. A., (2015). Green roof: Vegetation response towards lead and potassium. Proceedings of the 1st Young Scientist International 469 Conference of Water Resources Development and Environmental Protection, 5–7.

Besir, A. B., and Cuce, E. (2018). Green roofs and facades: A comprehensive review. *J. Renew. Sustain. Ener.* 82, 915–939. doi:10.1016/j.rser.2017.09.106

Brown, R. R., and Farrelly, M. A. (2009). Challenges ahead: Social and institutional factors influencing sustainable urban stormwater management in Australia. *Water Sci. Technol.* 59, 653–660. doi:10.2166/wst.2009.022

Butler, D., and Parkinson, J. (1997). Towards sustainable urban drainage. *Water Sci. Technol.* 35, 53–63. doi:10.2166/wst.1997.0330

Chahar, B., Graillot, D., and Gaur, S. (2012). Storm-water management through infiltration trenches. *J. Irrigation Drainage Eng.* 138 (3), 274–281. doi:10.1061/(asce)ir.1943-4774.0000408

Che, W., Frank, T., Li, J. Q., and Zhang, Y. J. (2012). Introduction to auckland modern stormwater management (I): Relevant legislation and plans. *Water and Wastewater Eng.* 38 (3), 28–32. (In Chinese).

Che, W., Yan, P., Zhao, Y., and Tian, F. (2014). Development and analysis of International updated stormwater management systems. *China Water and Wastewater* 30, 45–51.

Chen, Y., Samuelson, H. W., and Tong, Z. (2016). Integrated design workflow and a new tool for urban rainwater management. *J. Environ. Manage.* 180, 45–51. doi:10.1016/j.jenvman.2016.04.059

Cheng, J., Xu, Q. X., Yang, K., Liu, L. L., and Fan, Q. J. (2007). Comparison of foreign urban rainwater resource utilization management systemsand some inspirations. *China Water and Wastewater* 12, 68–72. (In Chinese).

Coma, J., Pérez, G., Solé, C., Castell, A., and Cabeza, L. F. (2016). Thermal assessment of extensive green roofs as passive tool for energy savings in buildings. *Renew. Energy* 85, 1106–1115. doi:10.1016/j.renene.2015.07.074

Cook, S., van Roon, M., Ehrenfried, L., LaGro, J., and Yu, Q. (2019). "WSUD 'best in class' - case studies from Australia, New Zealand, United States, europe, and asia," in *Approaches to water sensitive urban design* (Amsterdam, Netherlands: Elsevier), 561–585.

Damien, T., Ghassan, C., Daniel, P., Yves, K., and Marie-Christine, G. (2016). Impact of runoff infiltration on contaminant accumulation and transport in the soil/filter media of sustainable urban drainage systems: A literature review. *Sci. Total Environ.* 569, 904–926. doi:10.1016/j.scitotenv.2016.04.215

Demuzere, M., Orru, K., Heidrich, O., Olazabal, E., Geneletti, D., Orru, H., et al. (2014). Mitigating and adapting to climate change: Multi-functional and multi-scale assessment of green urban infrastructure. *J. Environ. Manage.* 146, 107–115. doi:10.1016/j.jenvman.2014.07.025

Du, Y. E., Hou, J. M., Ma, H. L., Liu, Q. C., Wang, X. H., Zhang, Z. A., et al. (2021). Spatial pattern optimization of LID facility based on SWMM. *China Water and Wastewater* 37 (19), 120–125. (In Chinese).

Eyni, A., Skardi, M. J. E., and Kerachian, R. (2021). A regret-based behavioral model for shared water resources management: Application of the correlated equilibrium concept. *Sci. Total Environ.* 759, 143892. doi:10.1016/j.scitotenv.2020.143892

Fletcher, T. D., and Deletic, A. (2007). *Data requirements for integrated urban water management*. Netherlands: Taylor and Francis.

Fletcher, T. D., Shuster, W., Hunt, W. F., Ashley, R., Butler, D., Arthur, S., et al. (2015). SUDS, LID, BMPs, WSUD and more - the evolution and application of terminology surrounding urban drainage. *Urban. Water J.* 12, 525–542. doi:10.1080/1573062x.2014.916314

Fu, X., Hopton, M. E., Wang, X. H., Goddard, H., and Liu, H. Q. (2019). A runoff trading system to meet watershed-level stormwater reduction goals with parcel-level green infrastructure installation. *Sci. Total Environ.* 689, 1149–1159. doi:10.1016/j.scitotenv.2019.06.439

Gavric, S., Leonhardt, G., Mar Sa Lek, J., and Viklander, M. (2019). Processes improving urban stormwater quality in grass swales and filter strips: A review of research findings. *Sci. Total Environ.* 669, 431–447. doi:10.1016/j.scitotenv.2019.03.072

Gimenez, M., Breuste, J., and Hof, A. (2020). Sustainable drainage systems for transitioning to sustainable urban flood management in the European union: A review. *J. Clean. Prod.* 255, 120191. doi:10.1016/j.jclepro.2020.120191

Gregoire, B. G., and Clausen, J. C. (2011). Effect of a modular extensive green roof on stormwater runoff and water quality. *Ecol. Eng.* 37, 963–969. doi:10.1016/j.ecoleng.2011.02.004

Gülbaz, S., and Kazezyılmaz-Alhan, C. M. (2016). Experimental investigation on hydrologic performance of lid with rainfall-watershed-bioretention system. *J. Hydrol. Eng.* 22, D4016003. doi:10.1061/(asce)he.1943-5584.0001450

Guo, F., Chen, J. G., Yang, J., Meng, Y. Y., and Gong, Y. A. (2015). Regulatory effect of grassed swales on road surface runoff in beijing city. *Bull. Soil Water Conservation* 35 (3), 176–181.

Guo, J. C. Y., and Lu, T. M. (2015). Operation of cap orifice in a rain garden. *J. Hydrol. Eng.* 20, 6015002. doi:10.1061/(asce)he.1943-5584.0001184

Haghighatafshar, S., Yamanee-Nolin, M., Klinting, A., Roldin, M., Gustafsson, L. G., Aspegren, H., et al. (2019). Hydroeconomic optimization of mesoscale blue-green stormwater systems at the city level. *J. Hydrol.* 578, 124125. doi:10.1016/j.jhydrol.2019.124125

He, Y., Yu, H., Dong, N. N., and Hang, Y. (2016). Thermal and energy performance assessment of extensive green roof in summer: A case study of a lightweight building in shanghai. *Energy Build.* 127, 762–773. doi:10.1016/j.enbuild.2016.06.016

Hu, M., Zhang, X. Q., Li, Y., Yang, H., and Tanaka, K. (2019). Flood mitigation performance of low impact development technologies under different storms for retrofitting an urbanized area. *J. Clean. Prod.* 222, 373–380. doi:10.1016/j.jclepro.2019.03.044

Hussain, F., Hussain, R., Wu, R. S., and Abbas, T. (2019). Rainwater harvesting potential and utilization for artificial recharge of groundwater using recharge wells. *Processes* 7, 623. doi:10.3390/pr7090623

Ice, G. (2004). History of innovative best management practice development and its role in addressing water quality limited waterbodies. *J. Environ. Eng.* 130 (6), 684–689. doi:10.1061/(asce)0733-9372(2004)130:6(684)

Khadka, A., Kokkonen, T., Niemi, T. J., Lhde, E., Sillanpää, N., and Koivusalo, H. (2020). Towards natural water cycle in urban areas: Modelling stormwater management designs. *Urban Water J.* 17, 587–597. doi:10.1080/1573062x.2019.1700285

Koc, C. B., Osmond, P., and Peters, A. (2018). Mapping and classifying green infrastructure typologies for climate-related studies based on remote sensing data. *Urban For. Urban Gree.* 37, 154–167.

Koon, J. (1995). *Evaluation of water quality ponds and swales in the issaquah/east lake sammamish basins*. Washington, D C, USA: King County Surface Water Management and Washington Department of Ecology.

Kuruppu, U., Rahman, A., and Rahman, M. A. (2019). Permeable pavement as a stormwater best management practice: A review and discussion. *Environ. Earth Sci.* 78, 327. doi:10.1007/s12665-019-8312-2

Li, H., Li, K., and Zhang, X. (2016). Performance evaluation of grassed swales for stormwater pollution control. *Procedia Eng.* 154, 898–910. doi:10.1016/j.proeng.2016.07.481

Li, M. Y., Zhang, S. H., Wang, Y. J., and Wang, Y. Q. (2018). Runoff management performances of permeable pavements: A review. *Environ. Sci. Technol.* 41 (12), 105–112.

Li, T., Zhang, W., and Huang, J. J. (2014). Integrated rainwater management planning, evaluation and implementation: Take Shanghai as an example. *J. Southeast Univ.* 30, 206–211.

Litofsky, A. L. E., and Jennings, A. J. (2014). Evaluating rain barrel storm water management effectiveness across climatography zones of the United States. *J. Environ. Eng.* 7, 1943–7870. doi:10.1061/(asce)ee.1943-7870.0000815

Liu, B. J., Li, N., and Xiong, K. Y. (2016). Study on construction of measures-system for low impact development and its effect. *Water Resour. Hydropower Eng.* 47 (8), 19–22.

Liu, S., Yin, Y., Xiao, H., Jiang, H., and Shi, R. (2021). The effects of ice nucleation on the microphysical processes and precipitation for a heavy rainfall event in Beijing. *Atmos. Res.* 253, 105476. doi:10.1016/j.atmosres.2021.105476

Liu, W., Feng, Q., Chen, W., and Deo, R. C. (2020). Stormwater runoff and pollution retention performances of permeable pavements and the effects of structural factors. *Environ. Sci. Pollut. Res.* 27, 30831–30843. doi:10.1007/s11356-020-09220-2

Locatelli, L., Guerrero, M., Russo, B., Martínez-Gomariz, E., Sunyer, D., and Martínez, M. (2020). Socio-economic assessment of green infrastructure for climate change

adaptation in the context of urban drainage planning. *Sustainability* 12, 3792. doi:10.3390/su12093792

Mao, J., Xia, B. Y., Zhou, Y., Bi, F., Zhang, X. D., Zhang, W., et al. (2021). Effect of roof materials and weather patterns on the quality of harvested rainwater in Shanghai, China. *J. Clean. Prod.* 279, 123419. doi:10.1016/j.jclepro.2020.123419

Martine, Galarneau, Michèle, Prévost, Laurène, Autixier, Madoux-Humery, A. S., Prevost, M., et al. (2014). Evaluating rain gardens as a method to reduce the impact of sewer overflows in sources of drinking water. *Sci. Total Environ.* 499, 238–247. doi:10.1016/j.scitotenv.2014.08.030

Mi, W. J., Zhang, A. J., and Ren, W. Y. (2018). Oversea utilization and development of urban rainwater resources with low impact and its implications for construction of sponge city in China. *Bull. Soil Water Conserv.* 3, 345–352.

Mitchell, V. G. (2006). Applying integrated urban water management concepts: A review of Australian experience. *Environ. Manage.* 37, 589–605. doi:10.1007/s00267-004-0252-1

Mullaney, J., and Lucke, T. (2014). Practical review of pervious pavement designs. *Clean-Soil Air Water* 42, 111–124. doi:10.1002/clen.201300118

Nachshon, U., Netzer, L., and Livshitz, Y. (2016). Land cover properties and rain water harvesting in urban environments. *Sustain. Cities Soc.* 27, 398–406. doi:10.1016/j.scs.2016.08.008

Nguyen, T. T., Ngo, H. H., Guo, W., Wang, X. C., Ren, N., Li, G., et al. (2019). Implementation of a specific urban water management-Sponge City. *Sci. Total Environ.* 652, 147–162. doi:10.1016/j.scitotenv.2018.10.168

Otto, S., Vianello, M., Infantino, A., Zanin, G., and Guardo, A. D. (2008). Effect of a full-grown vegetative filter strip on herbicide runoff: Maintaining of filter capacity over time. *Chemosphere* 71, 74–82. doi:10.1016/j.chemosphere.2007.10.029

Perales-Momparler, C. S. (2015). *A regenerative urban stormwater management methodology: The role of SUDS construction and monitoring in the transition of a mediterranean city*. Valencia, Spain: Universitat Politecnica de Valencia.

Perales-Momparler, S., Andres-Domenech, I., Andreu, J., and Escuder-Bueno, I. (2015). A regenerative urban stormwater management methodology: The journey of a mediterranean city. *J. Clean. Prod.* 109, 174–189. doi:10.1016/j.jclepro.2015.02.039

Petrucci, G., Deroubaix, J. F., Gouvello, B. D., Deutsch, J. C., Bompard, P., and Tassin, B. (2012). Rainwater harvesting to control stormwater runoff in suburban areas. An experimental case-study. *Urban Water J.* 9, 45–55. doi:10.1080/1573062x.2011.633610

Qi, Y., Chan, F. K. S., Thorne, C., O'Donnell, E., Quagliolo, C., Comino, E., et al. (2020). Addressing challenges of urban water management in Chinese sponge cities via nature-based solutions. *Water* 12 (10), 2788. doi:10.3390/w12102788

Qin, Y. H. (2015). A review on the development of cool pavements to mitigate urban heat island effect. *Renew. Sustain. Energy Rev.* 52, 445–459. doi:10.1016/j.rser.2015.07.177

Rodak, C. M., Moore, T. L., David, R., Jayakaran, A. D., and Vogel, J. R. (2019). Urban stormwater characterization, control, and treatment. *Water Environ. Res.* 91, 1034–1060. doi:10.1002/wer.1173

Sang, Y. F., and Yang, M. (2017). Urban waterlogs control in China: More effective strategies and actions are needed. *Nat. Hazards* 85, 1291–1294. doi:10.1007/s11069-016-2614-4

Schets, F. M., Italiaander, R., Van Den Berg, H. H. J. L., and de Roda Husman, A. M. (2010). Rainwater harvesting: Quality assessment and utilization in The Netherlands. *J. Water Health* 8 (2), 224–235. doi:10.2166/wh.2009.037

Shafique, M., Kim, R., and Rafiq, M. (2018). Green roof benefits, opportunities and challenges – a review. *Renew. Sustain. Energy Rev.* 90, 757–773. doi:10.1016/j.rser.2018.04.006

Sharma, A., and Gardner, T. (2020). Comprehensive assessment methodology for urban residential rainwater tank implementation. *Water* 12 (2), 315. doi:10.3390/w12020315

Simmons, M. T., Gardiner, B., Windhager, S., and Tinsley, J. (2008). Green roofs are not created equal: The hydrologic and thermal performance of six different extensive green roofs and reflective and non-reflective roofs in a sub-tropical climate. *Urban Ecosyst.* 11, 339–348. doi:10.1007/s11252-008-0069-4

Steffen, J., Jensen, M., Pomeroy, C. A., and Burian, S. J. (2013). Water supply and stormwater management benefits of residential rainwater harvesting in US cities. *J. Am. Water Resour. As.* 49 (4), 810–824. doi:10.1111/jawr.12038

Tang, S. C., Luo, W., Jia, Z. H., Li, S., Wu, Y., and Zhou, M. (2016). Effects of filler and rainfall characteristics on runoff reduction of rain garden and achieving the goal of sponge city construction. *J. Soil Water Conservation* 30 (01), 73–78. (In Chinese).

Tang, X., and Qu, M. (2016). Phase change and thermal performance analysis for green roofs in cold climates. *Energy Build.* 121, 165–175. doi:10.1016/j.enbuild.2016.03.069

Tian, Y., Zhang, Q. W., Li, D., Liu, G. H., Huang, L. L., Li, H. H., et al. (2019). Bio-retention effectiveness and parameter evaluation based on model simulation. *Environ. Eng.* 37 (7), 52–56. (In Chinese).

Toronto Region Conservation Authority (2010). *Low impact development stormwater management; plannign and desing guide*. Toronto, Canada: TRCA.

United Nations (2018). United nations population division world urbanization prospects: The 2018 revision. https://population.un.org/wup/.

United States of America (1972). Clean water Act (1972). *Texas Tech Law Review* 47, 585.

United States of America (1983). *Clean water Act (1983)*. Washington, DC, USA: United States Government.

Vijayaraghavan, K. (2016). Green roofs: A critical review on the role of components, benefits, limitations and trends. *Renew. Sustain. Energy Rev.* 57, 740–752. doi:10.1016/j.rser.2015.12.119

Virginia Department of Forestry Virginia Department of Forestry Rain gardens. http://www.dof.virginia.gov/manage/riparian/rain-gardens.html.

Walmsley, A. (1995). Greenways and the making of urban form. *Landsc. Urban Plan.* 33, 81–127. doi:10.1016/0169-2046(95)02015-l

Wang, H. Y., Wu, H., Ma, H. W., Wang, P., and Ling, L. (2019). Study on waterlogging reduction effect of three types of permeable pavements in sponge city construction. *China Water Wastewater* 35 (12), 44–48.

Wang, J., Yin, W., Ye, M., Lei, A. L., and Li, S. M. (2011). Advance on grassed swales technology in non-point source pollution control. *Environ. Sci. Technol.* 34 (5), 90–94.

Wang, S. M., Li, X. Y., Zhang, J. H., Yu, H., Hao, Y. Z., and Yang, W. Y. (2014). Influence of green roof application on water quantity and quality in urban region. *Chin. J. Appl. Ecol.* 25 (7), 2026–2032.

Wang, S. M., Yu, H., Zhang, B., and Shao, L. (2011). Review of green roof in controlling urban non point source pollution. *J. Chongqing Univ. Arts Sci. Nat. Sci. Ed.* 30 (04), 59–64.

Winston, R. J., Hunt, W. F., Kennedy, S. G., Wright, J. D., and Lauffer, M. S. (2012). Field evaluation of storm-water control measures for highway runoff treatment. *J. Environ. Eng.* 138 (1), 101–111. doi:10.1061/(asce)ee.1943-7870.0000454

Wu, H. T., Yan, A. P., Zeng, X. G., Wang, Z. X., and Yang, T. (2020). Design and optimization of combined initial rainwater storage tank in separate drainage system. *China Water Wastewater* 36 (12), 106–110.

Yang, M. Y., Liu, C. M., Pan, X. Y., and Liang, K. (2020). Analysis of sponge city system and research points from the perspective of urban water cycle. *Acta Geogr. Sin.* 75 (09), 1831–1844.

Yu, B., Jiao, L., Ni, F., and Yang, J. (2015). Long-term field performance of porous asphalt pavement in China. *Road. Mat. Pavement* 16, 214–226. doi:10.1080/14680629.2014.944205

Zhang, X. Y., Zhang, W., Shi, Z. N., and Li, S. M. (2017). Effect on grassed swales for hydrological regulation of urban stormwater runoff by different influent pattern. *Sci. Technol. Eng.* 17 (25), 290–294.

Zhang, Y. Y., Nie, S. H., Cai, G. Q., Sun, Z., and Zong, Q. L. (2022). Investigation and simulation on the effect of vegetative filter strip on surface runoff. *Res. Soil Water Conservation* 29 (02), 36–42. (In Chinese).

Zhao, D., Zha, J., and Wu, J. (2021). Changes in rainfall of different intensities due to urbanization-induced land-use changes in Shenzhen, China. *Clim. Dynam.* 56 (7-8), 2509–2530. doi:10.1007/s00382-020-05601-y

Zhao, Y. L., Wang, J. L., Li, L. H., et al. (2020). Effect of different types of permeable brick on the stormwater runoff quantity control. *Chin. J. Environ. Eng.* 14 (3), 835–841. (In Chinese).

Zhu, Z., Chen, Z., Chen, X., and Yu, G. (2019). An assessment of the hydrologic effectiveness of low impact development (LID) practices for managing runoff with different objectives. *Environ. Manage.* 231, 504–514. doi:10.1016/j.jenvman.2018.10.046

frontiers | Frontiers in Environmental Science

TYPE Original Research
PUBLISHED 13 April 2023
DOI 10.3389/fenvs.2023.1131954

OPEN ACCESS

EDITED BY
Huiyu Dong,
Chinese Academy of Sciences (CAS), China

REVIEWED BY
Konstantinos Nikolopoulos,
Durham University, United Kingdom
Jiabo Yin,
Wuhan University, China

*CORRESPONDENCE
Lili Yang,
yangll@sustech.edu.cn

RECEIVED 26 December 2022
ACCEPTED 03 April 2023
PUBLISHED 13 April 2023

CITATION
Zhang Z, Jian X, Chen Y, Huang Z, Liu J and Yang L (2023), Urban waterlogging prediction and risk analysis based on rainfall time series features: A case study of Shenzhen.
Front. Environ. Sci. 11:1131954.
doi: 10.3389/fenvs.2023.1131954

Urban waterlogging prediction and risk analysis based on rainfall time series features: A case study of Shenzhen

Zongjia Zhang[1,2], Xinyao Jian[2], Yiye Chen[2], Zhejun Huang[2], Junguo Liu[3,4] and Lili Yang[2]*

[1]School of Environment, Harbin Institute of Technology, Harbin, China, [2]Department of Statistics and Data Science, Southern University of Science and Technology, Shenzhen, China, [3]School of Environmental Science and Engineering, Southern University of Science and Technology, Shenzhen, China, [4]Henan Provincial Key Laboratory of Hydrosphere and Watershed Water Security, North China University of Water Resources and Electric Power, Zhengzhou, China

In recent years, the frequency of extreme weather has increased, and urban waterlogging caused by sudden rainfall has occurred from time to time. With the development of urbanization, a large amount of land has been developed and the proportion of impervious area has increased, intensifying the risk of urban waterlogging. How to use the available meteorological data for accurate prediction and early warning of waterlogging hazards has become a key issue in the field of disaster prevention and risk assessment. In this paper, based on historical meteorological data, we combine domain knowledge and model parameters to experimentally extract rainfall time series related features for future waterlogging depth prediction. A novel waterlogging depth prediction model that applies only rainfall data as input is proposed by machine learning algorithms. By analyzing a large amount of historical flooding monitoring data, a "rainfall-waterlogging amplification factor" based on the geographical features of monitoring stations is constructed to quantify the mapping relationship between rainfall and waterlogging depths at different locations. After the model is trained and corrected by the measured data, the prediction error for short-time rainfall basically reaches within 2 cm. This method improves prediction performance by a factor of 2.5–3 over featureless time series methods. It effectively overcomes the limitations of small coverage of monitoring stations and insufficient historical waterlogging data, and can achieve more accurate short-term waterlogging prediction. At the same time, it can provide reference suggestions for the government to conduct waterlogging risk analysis and add new sensor stations by counting the amplification factor of other locations.

KEYWORDS

urban waterlogging, time series, risk assessment, machine learning, rainfall, Shenzhen

1 Introduction

Influenced by global climate change, the frequency and scale of extreme weather events have been on the rise in recent years, and urban flooding disasters caused by extreme weather events such as typhoons and short-lived heavy rainstorms have been increasing (Ferreira et al., 2015; Zhang et al., 2017). The intensity of extreme precipitation in most regions of the world shows a trend towards intensification and a concentration of rainfall events (Yin et al.,

2022). Yin used simulations from a large climate–hydrology model ensemble of 111 members, their results provide crucial insights towards assessing and mitigating adverse effects of compound hazards on ecosystems and human wellbeing (Yin et al., 2023). Urbanization increases hardened area, reduces infiltration, increases runoff and triggers higher and faster peak water flow (Nayeb Yazdi et al., 2019; Sofia et al., 2019). It has reduced groundwater recharge from natural infiltration and has contributed to the high runoff (Nath et al., 2021). A large number of low-lying areas prone to flooding are incorporated into urban development plans, and the lack of drainage capacity further exacerbates the risk of flooding (Du et al., 2012). With increasing impervious cover in urban areas driving dramatic changes in rainfall infiltration and storage capacity, which lead that urban flood appear sudden and frequent (Mu et al., 2020).

Waterlogging events on a global scale may have a serious and direct impact on the economy and humanitarianism, as well as continue to adversely affect economic development (Arshad et al., 2019). Globally, the occurrence of urban floods has been unprecedented resulting in huge economic and social losses (Sundaram et al., 2021). In July 2021, the rainstorm in Zhengzhou, China caused 380 deaths and a direct economic loss of 120.06 billion yuan. Urban flood disaster has become a crucial problem restricting the healthy development of China's economy and society (Duan et al., 2022; Li et al., 2022). Urban floods can cause huge economic losses and casualties, and countries all over the world attach great importance to urban flood warning and mitigation. Therefore, obtaining timely and highly accurate waterlogging depth information with wide coverage is urgently needed for emergency response and risk mitigation, especially using an affordable, accurate, and widespread approach (Deo and Wen, 2016). Nowadays, more and more researchers have started to pay attention to urban waterlogging (Yin et al., 2015). Among them, accurate prediction of inland flooding is a hot research problem in the field. For accurate prediction and warning of the extent and depth of internal flooding, there are mainly numerical simulation methods, hydrological methods, and data-driven methods.

Numerical simulation method. Based on the principles of hydrodynamics, the model uses the underlying surface and elevation factors comprehensively in waterlogging process; it performs the whole process of city waterlogging formation in detail. Its simulation results are waterlogging distribution and waterlogging depth maps of a certain time step (Xue et al., 2016). Numerical simulation methods allow easy estimation of waterlogging under each recurrence period rainfall. It is interesting to note that under different urbanization and rainfall scenarios, the urban waterlogging susceptibility has a considerable variation (Explicit the urban waterlogging spatial variation and its driving factors: The stepwise cluster analysis model and hierarchical partitioning analysis approach). The hydrological and hydrodynamic model couples the distributed hydrological model and two-dimensional hydrodynamic model, which not only ensures the accuracy of the model but also has good calculation efficiency. It is a promising research direction for the flood model (Liu et al., 2022a). On the other hand, it also shortens waterlogging simulation time, and finally improves the applicability of waterlogging simulation (Zounemat-Kermani et al., 2020). But the disadvantage is that small number of data mining model parameters, such as the obscure physical implications of model parameters and the insufficient amount of simulation training, the simulation is prone to the problem of different arguments (Tang et al., 2021). Furthermore, the computational efficiency of numerical models is too low to meet the requirements of urban emergency management. Thus, many coupled methods of numerical simulation and other methods such as machine learning have emerged. A new method was established by combining a long short-term memory neural network model with a numerical model, which can quickly predict the waterlogging depth. The principle is to train the long and short-term memory neural network to predict and simulate the internal flooding process by using the numerical simulation results as training samples (Liu et al., 2022a). However, the disadvantage of this method is that the accuracy of LSTM results is extremely dependent on the results of previous numerical simulation. If the error of numerical simulation results is large, the results are difficult to guarantee.

In recent years, with the application of water sensor, many cities have established urban waterlogging monitoring and early warning system. But water level sensors are expensive and cannot be deployed all over the city (Loftis et al., 2018). Moreover, the simple monitoring data can only reflect the real-time depth of water accumulation, which does not have robust forecasting function (Liu et al., 2022b). As more and more water level sensors acquire large amounts of historical waterlogging data, some studies are beginning to train models based on historical real waterlogging data, or to use coupled models to improve the performance of prediction methods. The most representative of these is the data-driven method based on time series. Ding et al. proposed an explicable spatiotemporal attention long—short memory model (STA-LSTM) based on LSTM and attention mechanism, and established the model using dynamic attention mechanism and LSTM method to make explicable analysis of flood prediction (Ding et al., 2020). Yan et al. proposed a prediction model of the maximum water depth in time and space employing a neural network-numerical simulation model on the basis of coupling a two-dimensional hydrological and hydrodynamic model and a statistical analysis model. But due to data limitations, the actual rainfall and waterlogging data were not added to the database for training. Therefore, although the performance of the prediction model is satisfactory, its accuracy can be improved further after collecting enough data (Yan et al., 2021). Wu et al. established a real-time prediction model of flood depth based on waterlogging point by using GBDT algorithm based on multi-factor analysis and verified the validity and applicability of the model for real-time prediction of waterlogging process. However, the model that Wu used only be predicted when rainfall occurs, and cannot predict the flood depth after rainfall (Wu et al., 2020a).

However, some recent studies have shown that the prediction performance of a single method or model is always limited. Accounting for model structure, parameter and input forcing uncertainty in flood inundation modeling using Bayesian model averaging. The combination of multiple models can effectively improve the prediction performance. Multi-model combination methods to deal with model uncertainty and improve model performance (Yan and Hamid, 2016). Zhou et al. proposed an extreme flood information estimation method considering the uncertainty of distribution and model structure using the BMA

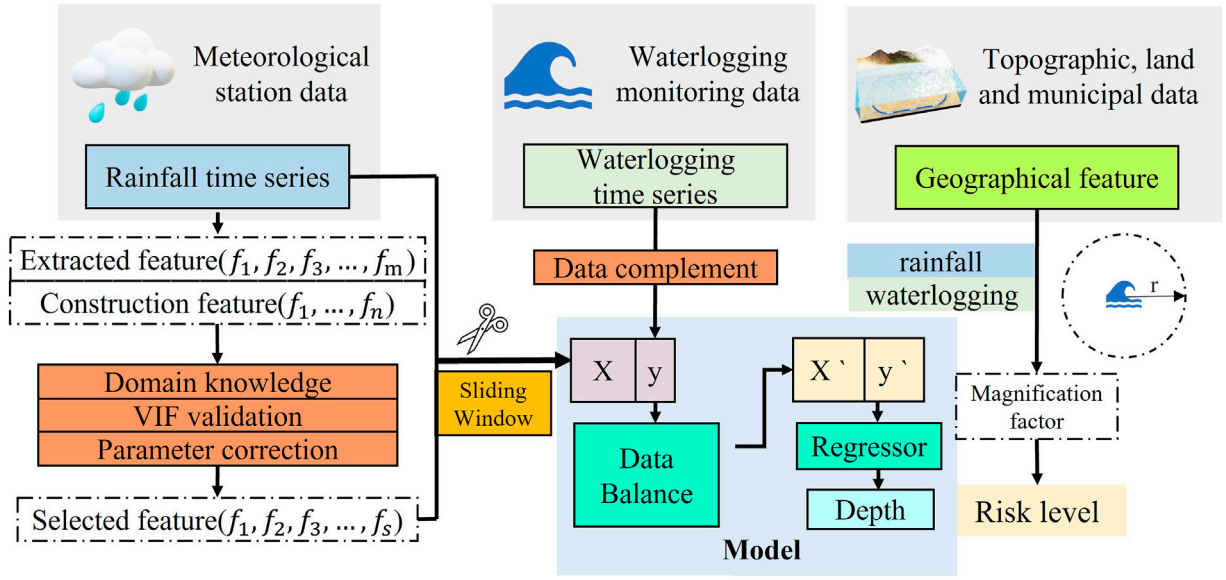

FIGURE 1
The framework of the method.

TABLE 1 Seasonal factor of the month to which the event belongs.

Indicators	MR	MT	MD
R_Mean	R_1	R_2	R_3
S	lg10	lg6	lg2

method. They construct a comprehensive prediction model by BMA and three machine learning methods (support vector machines (SVM), Back Propagation Neural Network (BPNN) and Adaptive Boosting (AdaBoost)) use rainfall forecast data to drive BMA model for fine early warning of urban flood. The analysis of early warning in two different urban flood events indicates that BMA is more suitable for the prediction of severe waterlogging and illustrates the great potential and prospects of BMA in urban flood early warning (Zhou et al., 2022). Naive Bayes (NB) and Random Forest (RF) algorithm were used to forecast the waterlogging point and the waterlogging process at the waterlogging point respectively to achieve the goal of predicting the whole process of urban waterlogging (Wang et al., 2021). Historical flooding events and the value of flood contributing factors are used as inputs for the model. These input data are converted to raster layers with help of GIS tools. Our dependent variable would be a one-hot encoded vector stating whether or not it was flooded with those conditions (Khatri et al., 2022). The stochastic forest (RF), Logistic model tree (LMT) and other bivariate models combined with data mining tools can be used to simulate flood susceptibility. The study found that the LMT has good predictive power, so the model can be used for future flood mitigation in specific areas (Shahabi et al., 2020). Data warehouse and deep learning algorithm were used to assess urban flood risk. The GBDT model shows 88.48% accuracy in the depth of water accumulation prediction (Wu et al., 2020b). An application of data-driven models using artificial neural network was presented, support vector regression and long-short term memory approaches and distributed forcing data for runoff predictions. The results showed that the long-short term memory and support vector regression models outperforms artificial neural network model for hourly runoff forecasting, and the predictive performance of the models was greater during the wet seasons compared to the dry seasons (Han and Morrison, 2021). Puttinaovarat and Horkaew proposed a novel flood forecasting system based on fusing meteorological, hydrological, geospatial, and crowdsource big data in an adaptive machine learning framework (Puttinaovarat and Horkaew, 2020).

Existing studies have not sufficiently analyzed rainfall time series. Combined with waterlogging sensor data, more accurate predictions of waterlogging depths can be obtained with an accuracy of centimeters or even millimeters. The input condition used in this paper is rainfall data, which is free from the limitation of waterlogging sensors. The transfer of the model prediction capability can be achieved at locations where the features are similar to the sensor points.

2 Methodology

2.1 Framework

This study follows this framework (Figure 1) by selecting features for training from the original rainfall time series using domain knowledge, VIF verification and parameter correction. After sliding window slicing and processing the data, the input-output matrix is constructed and the waterlogging prediction is performed by using machine learning regressors. Geographic features around the station are extracted from the geographic information, their

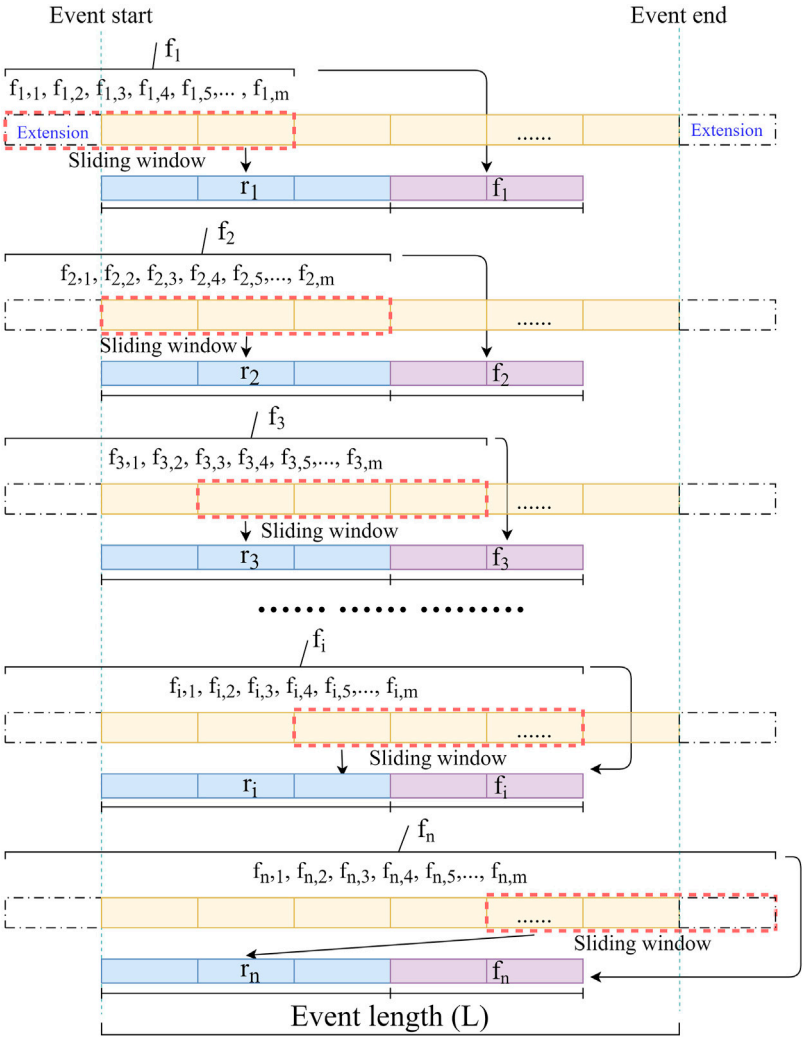

FIGURE 2
Schematic diagram of data slicing and integration.

influence on the amplification factor is analyzed, and this is used to regional waterlogging risk analysis.

2.2 Data processing

In this paper, the historical rainfall dataset and the waterlogging depth dataset are used to predict the future waterlogging depth. The amplification factor is established by characterization of geographic feature data. Data processing is divided into five main steps: 1) Data cleaning. Considering the possible sensor failure or low sensor sensitivity, the initial screening of valid stations is done according to the number of valid data in the cumulative flooding dataset. 2) Construction of uniform structured data. Uniform start and end time nodes, the different total working hours of different sensors lead to inconsistent start and end dates of collected data, here by truncating and artificially adding 0 nodes, so that the data sets of different stations can keep the same length. 3) Resampling. Considering the different working mechanisms of different sensors, their sampling intervals are not consistent, here the resampling function of Python is used to unify the sampling interval for subsequent model training. 4) Data interpolation. Use data interpolation to fill in the missing values in the data after resampling to make the time series continuous and in line with reality. 5) Sliding window slicing and data integration. According to the structural requirements of the training model and the prediction strategy, the time series are segmented by sliding windows, reconstructed with the extracted time series features, and the data are integrated into the model.

2.3 Model feature construction

2.3.1 Time series feature extraction and construction

In order to extract more valuable information for the model from the time series, this paper uses statistical methods and domain

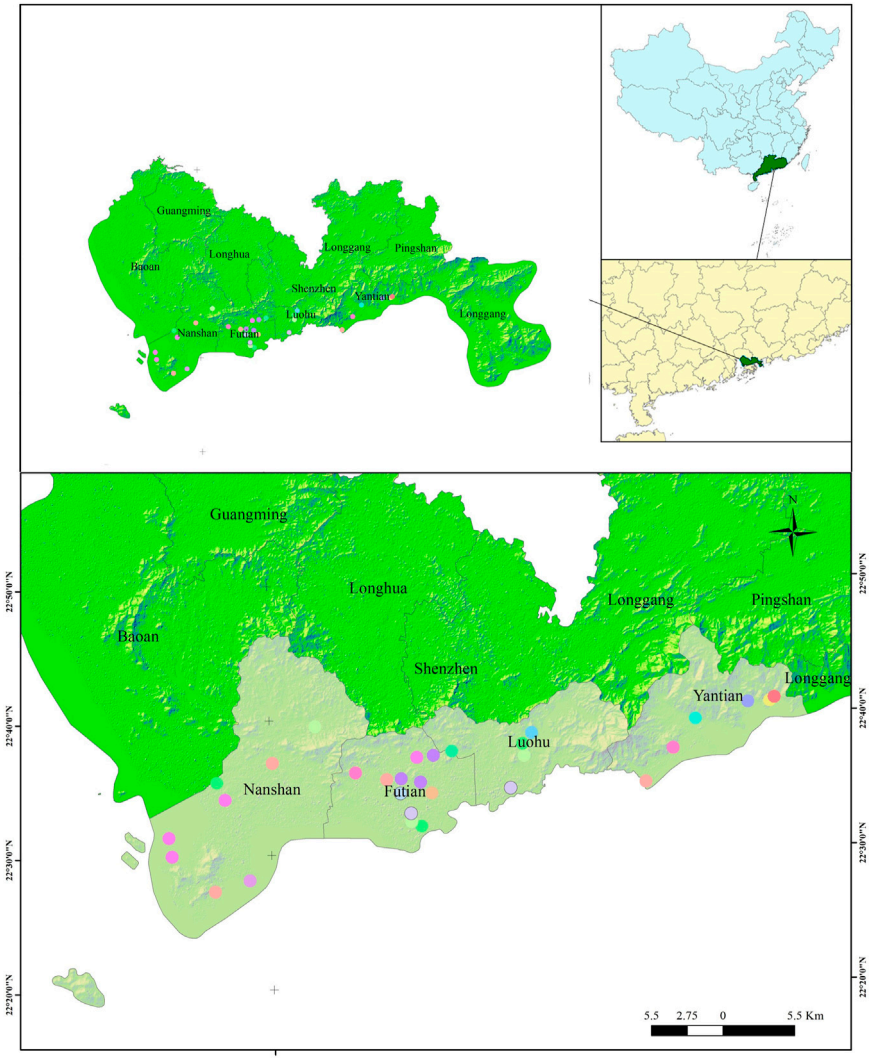

FIGURE 3
Study area of Shenzhen, China.

TABLE 2 Data description and sources.

Item	Data description	Data source	Resolution
Historical waterlogging sensor data	Waterlogging sensor monitoring data. (January 2019 to December 2020)	Water Bureau of Shenzhen Municipality (WBSM)	0.01 m
Historical meteorological station data	Meteorological basic observation data of rainfall, wind speed, visibility, temperature and humidity at all stations in the city. (January 2019 to December 2020)	Shenzhen Meteorological Bureau (SMB)	5 min
Digital elevation model (DEM)	Realize digital simulation of ground terrain through limited terrain elevation data	BIGEMAP	5m*5m
Land cover type	Current status of all land use in the city, including construction land, broad-leaved forest land, coniferous forest land, water bodies, wetlands, etc.	Global Fine Land cover product (GLC_FCS30-2019). Academy of Aerospace Information Innovation, Chinese Academy of Sciences	30*30 m
Drainage system	Rainwater outlet vector file, including location, orifice size, orifice shape	Water bureau of Shenzhen Municipality (WBSM)	0.001 m

TABLE 3 Comparison of machine learning algorithms.

Station	MSE of algorithm		
	Adaboost	GBDT	RF
A	0.006976	0.000409	**0.000089**
B	0.000071	0.000042	**0.000022**
C	0.000440	0.000302	**0.000254**
D	0.003706	**0.000190**	0.000238

The bold represents the result of the optimal algorithm for each station.

knowledge to extract and construct new feature vectors to improve the model prediction performance.

2.3.1.1 Unit rainfall

The rainfall data in this paper are sliding rainfall, which can reflect the total amount of rainfall in the previous period but lack direct description of the rainfall in the current period, which will lose the rainfall intensity information. The current rainfall intensity will largely affect the subsequent waterlogging. Therefore, an iterative algorithm is used here to calculate the unit rainfall (UR) from the sliding rainfall Eq. 1.

$$\begin{aligned} &\boldsymbol{R_t = R01H_t + R01H_{t-\tau} + R01H_{t-2\tau} + R01H_{t-3\tau} + , \ldots , + R01H_{t-p\tau} + \ldots} \\ &\boldsymbol{UR = R_{t_1} - R_{t_2}} \end{aligned} \tag{1}$$

where τ is 1 h, t is the current time, UR is the cumulated rainfall during time period $[t_1, t_2]$

2.3.1.2 Seasonality coefficient.

In addition to the amount of rainfall, the ability of the ground surface to form waterlogging is mainly influenced by the runoff coefficient. The runoff coefficient is mainly related to the type of land cover, slope, soil aridity and infiltration capacity. The process of runoff generation is also influenced by multiple factors such as latitude, climate zone, monsoon, and season (Tarasova et al., 2018). Differences in air humidity, air pressure, and temperature brought about by seasonal changes will directly affect the water content in the air and soil. During the dry season, the water content in the soil is low, rainfall is easily absorbed by the soil, and the intensity of rainfall is relatively low during the dry season, resulting in less occurrence of waterlogging (Burak et al., 2020). During the rainy season, the water content in the soil is high and even nearly saturated in some areas (e.g., seasonal wetlands). Rainfall is not easily absorbed by the soil, and the rainfall intensity is relatively high and transient during the rainy season, leading to relatively easy waterlogging (Zavala et al., 2008). Therefore, the seasonality coefficient S is defined and the dry months (MD), rainy months (MR) and transition months (MT) are determined based on the multi-year monthly average rainfall statistics (Table 1).

2.3.1.3 Correlation features related to rainfall interval.

The period between rainfall events affects the infiltration capacity and runoff coefficient. When two rainfall events are separated by a long interval, the water content in the soil or surface is already at a low level due to sufficient infiltration and evaporation. In contrast, when the water content between two rainfall events is high, surface runoff is more likely to form and thus converge to produce waterlogging when the rainfall occurs again (Ran et al., 2012). In this paper, we define the rainfall interval δ, which is the interval between the beginning of this rainfall period and the end of the previous rainfall period (h). We define the wetting coefficient C_w as Eq. 2 (Zhang et al., 2023), which is the ratio between the mean value of rainfall of this rainfall event and the rainfall interval δ, representing the wetting capacity of this rainfall on the land. Horton infiltration curves are commonly used in the field of hydrology to model the rate variation of fluid infiltration in different surfaces. The Horton infiltration equation (Yang et al., 2020) is $f = f_c + (f_0 - f_c)e^{-kt}$, where f is the infiltration rate, f_c is the stable infiltration rate, f_0 is the initial infiltration rate, t is the time, and k is an empirical constant related to soil properties. Considering that the surface differences of monitoring stations are not significant, the function e^{-t} is introduced as the basis function, and the integrated infiltration capacity C_i is fitted from the rainfall curve time series curve as Eq. 3.

$$\boldsymbol{C_w = \frac{R_{mean}}{\delta}} \tag{2}$$

$$\boldsymbol{C_i = e^{(-\lg \delta)} R_{max} \frac{\ln \sum |\alpha|}{L}} \tag{3}$$

where R_{mean} is the mean rainfall (mm), δ is the rainfall interval (h); R_{max} is the maximum value of rainfall in this segment (mm); α is the slope of each point of the rainfall event sequence curve; and L is the length of rainfall events.

2.3.1.4 Statistical features

The rainfall time series itself contains many features in its statistics. The mean value R_{mean} and the maximum value R_{max} reflect the scale of rainfall and are important indicators of the amount of rainfall. The standard deviation R_{std} reflects whether the rainfall is evenly distributed in time and is useful for identifying sudden and severe rainfall. The total rainfall is not large, but due to the high instantaneous intensity, it is also easy to trigger waterlogging (David et al., 2013). The kurtosis can determine

TABLE 4 Comparison of results of methods with and without features.

Station	With feature	Without feature	Performance improvement (%)
A	0.000089	0.000617	697.2
B	0.000022	0.000053	238.5
C	0.000254	0.000754	297.0
D	0.000238	0.000728	306.3

TABLE 5 Prediction model evaluation for four stations.

Station	MSE	MAE	R^2 score
A	0.00007	0.01083	0.95341
B	0.00001	0.00049	0.88907
C	0.00011	0.00091	0.92823
D	0.00006	0.00042	0.97167

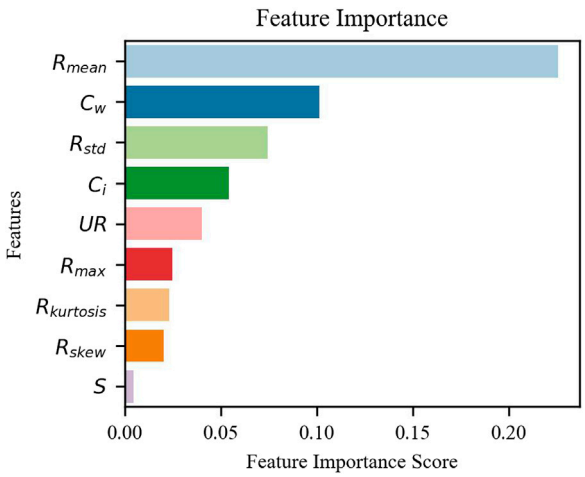

FIGURE 4
The weight value of 9 features in the model.

whether the rainfall curve is gentle or steep. Skewness can screen whether the peak intensity of rainfall comes from the first half or the second half of the rainfall curve. AUC is the area under the rainfall curve and can represent the total amount of rainfall.

2.3.2 Feature filtering

The statistical features extracted from the rainfall time series and the features constructed based on domain knowledge together form the feature set. However, sometimes some features may not correlate well with the model mechanism and do not have good predictive ability and may even negatively affect the model. By filtering the features through domain knowledge, model experiments and VIF validation, we can remove the insignificant features and thus improve the accuracy of the model. It can also reduce the computational cost and improve the interpretability of the model (Khalid et al., 2014).

2.4 Constructing model input and output matrices

A uniform rainfall slice length l is selected, and the number of slice bars within each rainfall event of irregular length (serial number k, total length L_k) can be denoted as n, n is calculated by Eq. 4. The rainfall events are iteratively sliced according to a fixed sliding window length (Figure 2).

$$n = L_k - l + 1 \tag{4}$$

The rainfall input vector r_i within each event can be expressed as Eq. 5

$$r_i = [r_{i1}\, r_{i2}\, r_{i3}\, r_{i4}, \cdots, r_{i(l-1)}\, r_{il}] \tag{5}$$

The rainfall time series feature vector f_i within each event can be expressed as Eq. 6, with each slice having a feature vector length of m. Unlike r_i, to characterize the cumulative effect of rainfall, each f_i is calculated from the data between the beginning of the rainfall event in that segment and the end of the slice in this segment.

$$f_i = [f_{i1} f_{i2} f_{i3} f_{i4}, \cdots, f_{i(m-1)} f_{im}] \tag{6}$$

The single input vector of the model can be expressed as Eq. 7.

$$x_i = [r_{i1}\, r_{i2}\, r_{i3}\, r_{i4}, \cdots, r_{il}, f_{i1} f_{i2} f_{i3} f_{i4}, \cdots, f_{im}] \tag{7}$$

The combined input matrix X can be expressed as Eq. 8, and the output matrix as Eq. 9. The input-output relationship in regression model can be expressed as Eq. 10.

$$X = \begin{bmatrix} r_1 & f_1 \\ r_2 & f_2 \\ \cdots & \cdots \\ r_i & f_i \end{bmatrix} \tag{8}$$

$$y = \begin{bmatrix} y_1 \\ y_2 \\ \vdots \\ \vdots \\ y_{i-1} \\ y_i \end{bmatrix} \tag{9}$$

$$y = \varphi(X) \tag{10}$$

2.5 Model training and validation

After processing the data, the model is trained and tested in the ratio of 70% and 30% of the training and test sets. The testing was carried out by random sampling method. Samples were imported into the regression model. The optimal parameters, including slice length, number of features, feature combination method and prediction strategy, are determined by testing. The performance of several machine learning algorithms is compared to obtain the optimal model configuration.

2.6 Geographical feature statistics and risk analysis

Through multi-source data analysis of meteorology, waterlogging, topography and municipality, the geographical features including topography terrain, land cover type and drainage network distribution within 500 m diameter of the station are integrated. The amplification factor (AF) between rainfall and waterlogging depth is calculated from historical data, and the risk of waterlogging in the area is also analyzed according to the amplification factor; the larger the AF, the higher the possibility of generating deeper waterlogging.

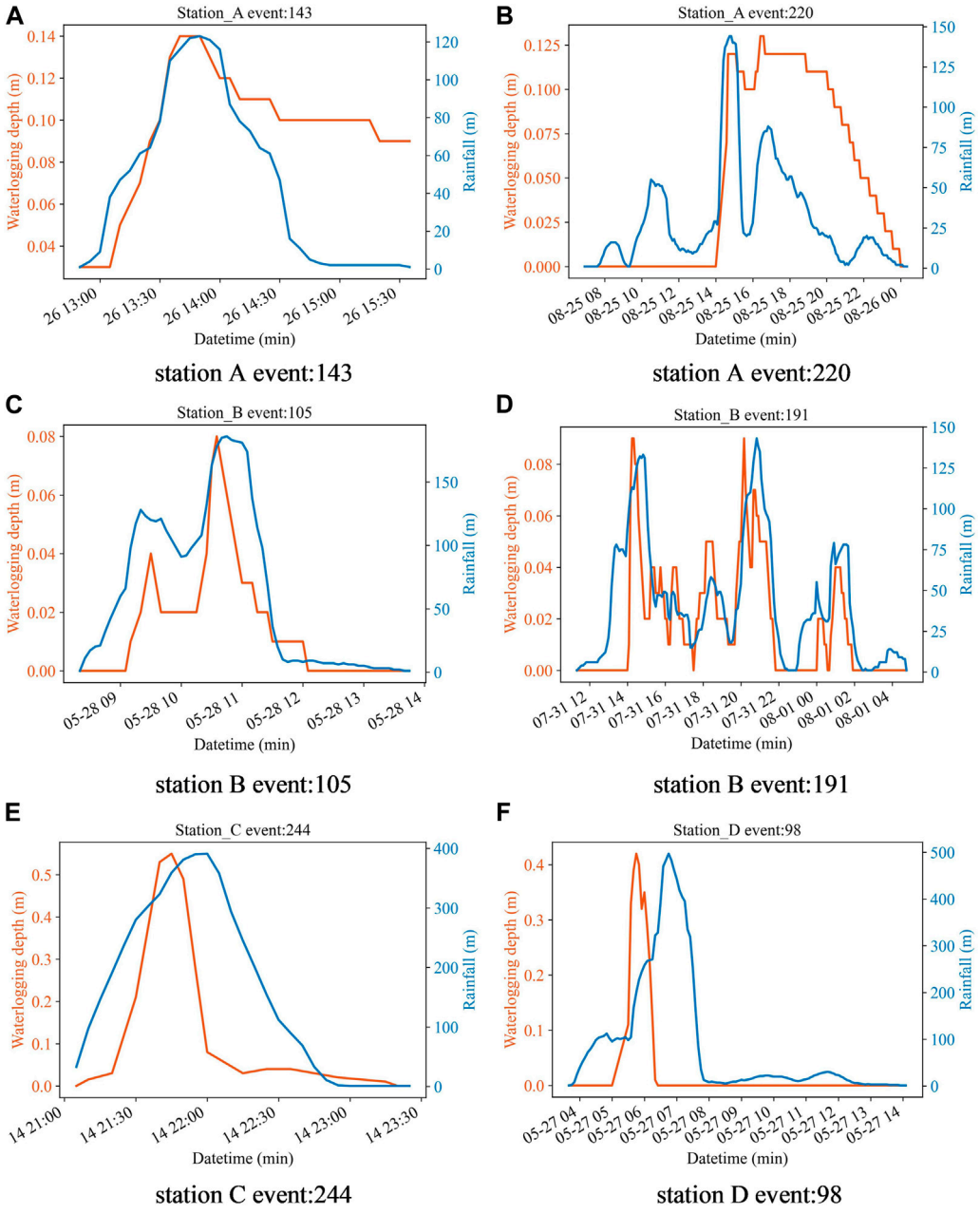

FIGURE 5
Rainfall and waterlogging curves for events in four stations. **(A)** station A event: 143; **(B)** station A event: 220; **(C)** station B event: 105; **(D)** station B event: 191; **(E)** station C event: 244; **(F)** station D event: 98.

3 Case study

3.1 Study area

Shenzhen is one of the core cities of the Guangdong-Hong Kong-Macao Greater Bay Area. Over the past 40 years, Shenzhen's GDP has grown rapidly from 270 million yuan in 1980 to 2,767.02 billion yuan in 2021. The annual average rainfall is 1935.8 mm, and the time distribution shows that the rainfall is mainly concentrated in April to September, with a spatial trend of decreasing rainfall from the southeast to the northwest. Typhoons and rainstorms are the most frequently occurring hazards in Shenzhen (Gong et al., 2022). Shenzhen is prone to frequent short-duration rainstorms, which often result in severe waterlogging in the city and, sometimes, can even cause casualties (Liu et al., 2020). Shenzhen City had an extreme rainstorm on 11 April 2019, resulting in an internal waterlogging event that killed 11 people in the city. Therefore, it is important to be able to predict and warn the occurrence of waterlogging disasters in advance to protect the safety of citizens as well as to improve the disaster prevention and mitigation capacity of the city. Figure 3 shows the location of Shenzhen and the area involved in the study, and Table 2 shows the data used for the case.

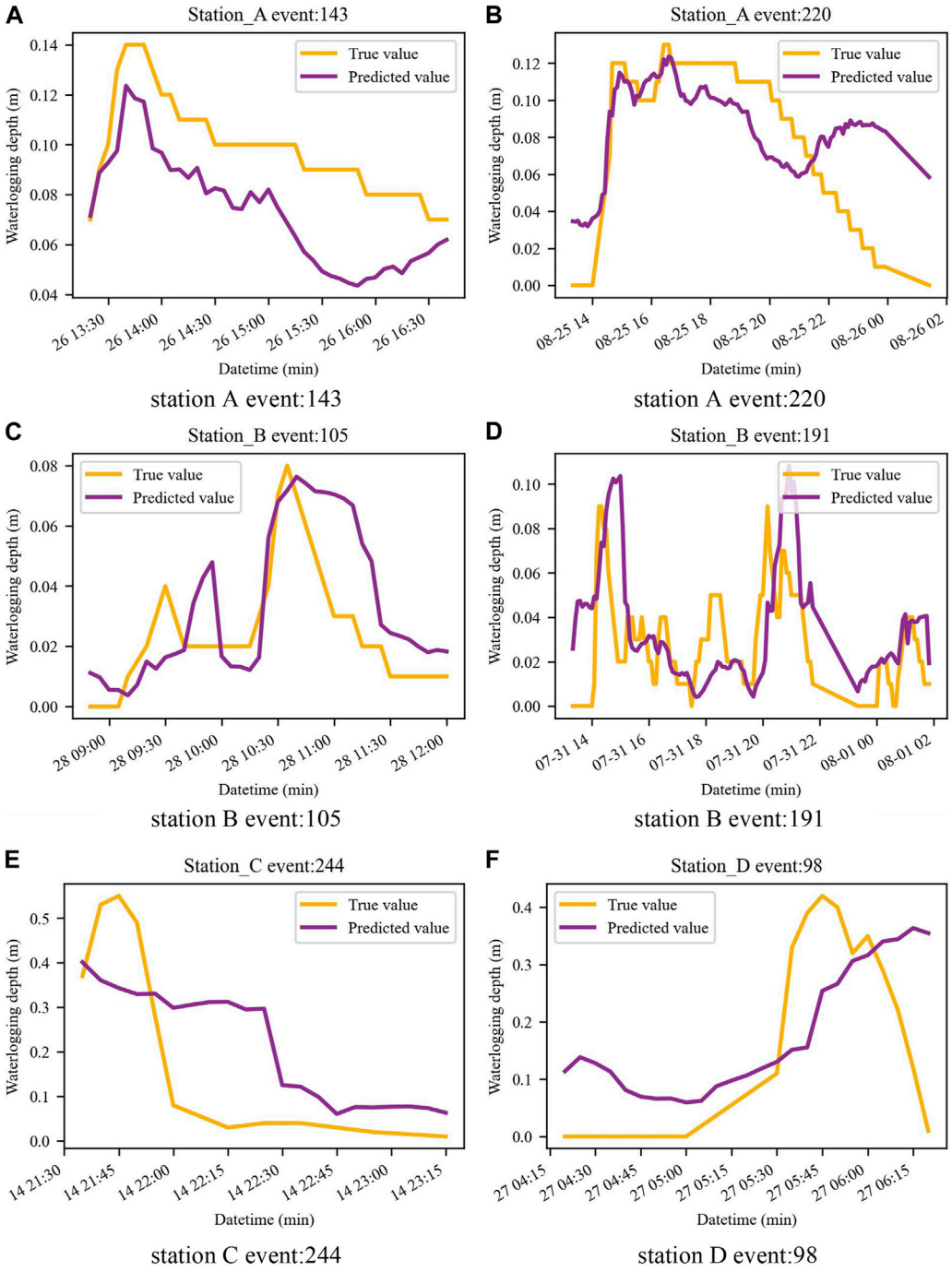

FIGURE 6
Predicted depth of waterlogging at four stations. **(A)** station A event: 143; **(B)** station A event: 220; **(C)** station B event: 105; **(D)** station B event: 191; **(E)** station C event: 244; **(F)** station D event: 98.

4 Results

The paper conducted experiments on four monitoring stations. As shown in Table 3, in the comparison of the three algorithms, Random Forest (RF) has the smallest MSE except at station D, where RF has a slightly larger MSE than Gradient Boosting Decision Tree (GBDT), indicating that RF is better adapted to this prediction task.

Compared to direct prediction using the original time series, the method of adding extracted features achieves a larger improvement at all four stations (Table 4). It indicates that using features for training can improve the prediction ability of the model to a greater extent.

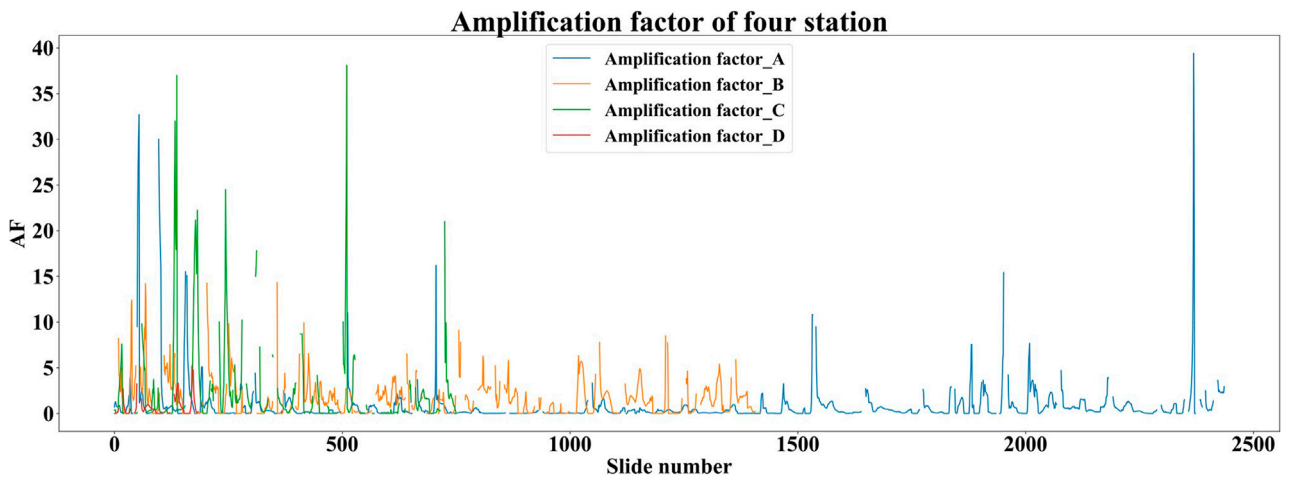

FIGURE 7
Results of amplification factors for the four stations.

TABLE 6 Statistical results of geographical characteristics of the four stations.

Station	DEM (m)	D_min (m)	D_max (m)	D_std	Land cover	Sum_flow	Dra_A (m^2)	Dra_V (m^3)	Number of waterlogging slices
A	33	21	43	***3.91***	IS	**2151063**	***145.46***	***7,210.38***	**2,437**
B	18	−3	90	13.71	IS	4,047.50	236.93	9,448.44	1419
C	***5***	−8	72	13.33	IS	***1192.20***	198.45	**14,863.07**	751
D	11	−15	41	8.28	IS	10,600.46	**335.14**	11,961.56	***185***

IS, Impermeable surface; Dra_A, Drainage area; Dra_V, Drainage volume.
*Bold represents larger values, italic represents smaller values.

As shown in Figure 4, the constructed and extracted features possess different weights, and with the algorithmic feature visualization function, we conclude. The R_{mean}, C_w and R_{std} of rainfall are the three most important features. In fact, these three features correspond to the magnitude, variability and temporal characteristics of rainfall, respectively.

After the configuration combination experiments, the configuration with the best results was finally selected as follows: when selecting the original rainfall data, it is better to use the 1-h sliding rainfall, which can enhance the fine waterlogging prediction. Of the total number of features constructed and extracted, 9 feature combinations were determined to balance computational efficiency and prediction accuracy (*rain dry, rain month, rain min, rain AUC* and *rain cum* were removed). Nine features did not overfit on 4 stations, proving that our feature construction makes sense. The experimental results of the three algorithms were compared, and the RF algorithm had superior robustness.

In Figure 5, the blue curve is the rainfall and the orange curve is the waterlogging depth, and it can be seen that there is a strong correlation between the two. Figure 6 shows the predicted and true values of the waterlogging depth, and it can be seen that the model can predict the change trend well, with an average error within 2 cm. Prediction model evaluation for four stations can be seen in Table 5.

5 Discussion

1) The method in this paper has a smaller MSE and more accurate prediction results than the results obtained by directly using the original rainfall event series. The model enhances the performance and robustness by time series feature extraction. Better prediction results are achieved by adjusting the feature parameters when the model is not over-fitted.
2) Figure 7 shows the ratio of rainfall (m) to waterlogging depth (m) for each of the four stations in each slice of the waterlogging event, which we define here as the Amplification factor. Because the number of waterlogging events at each station is different from the length of time, the amount of data at station A is much larger than that at stations C and D. The curves reflect the vulnerability of each station to rainfall mitigation capacity in terms of waterlogging events. The AF of station A is generally larger, indicating that station A is more likely to form deeper water under the same rainfall event. The AF of station D is generally smaller, indicating its better ability to withstand waterlogging hazards. As seen in Table 6. Statistical results of geographical characteristics of the four stations., station A has the least drainage outlet area in the area and the drainage volume is at a lower level. As seen in Figure 8, the topography of station A

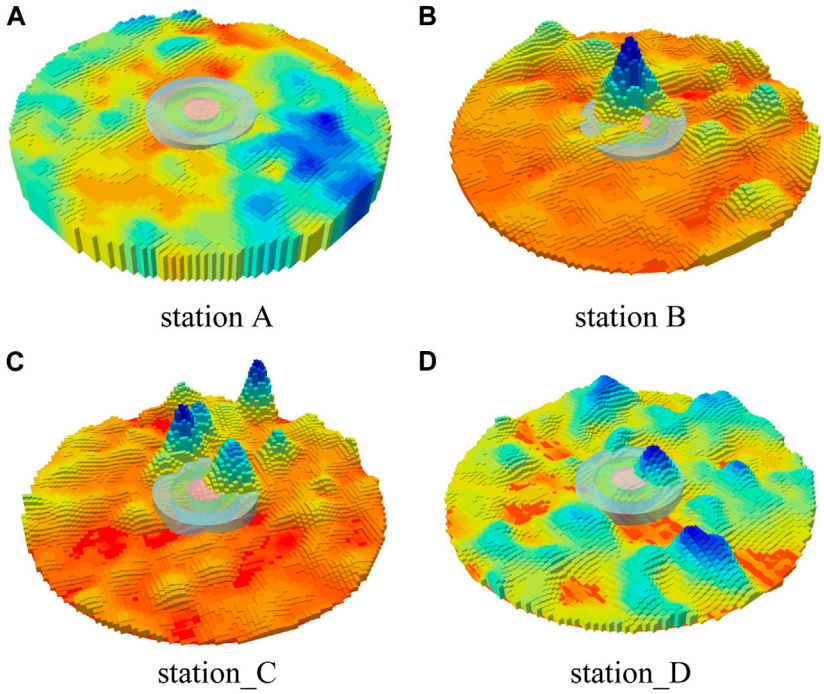

FIGURE 8
Topography within a 500 m radius of stations. **(A)** Station A; **(B)** station B; **(C)** station C; **(D)** station **(D)**. Blue represents higher elevation values and red represents lower elevation values. The middle circles represent the zones of 50, 100, 150 m from the station. (The terrain is stretched, with a stretch factor of 3).

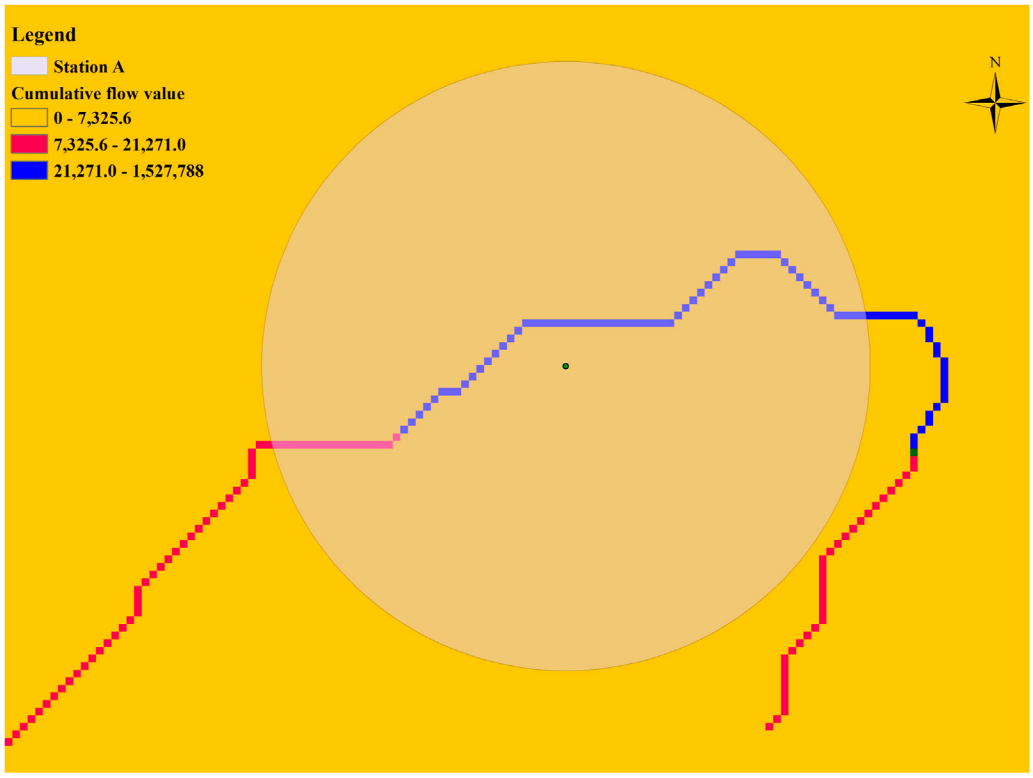

FIGURE 9
Cumulative value of flow in the area of station A.

is the flattest among the four stations (Table 6, variance of DEM is only 3.91), and the central terrain of the area is in a significant depression, so its is more likely to form standing water. In terms of the number of waterlogging events, station A also has the most, reaching 13.7 times that of station D.

3) The results of flow cumulative values extracted from the topographic data can reflect the runoff direction and flow results. From Table 6, the combined regional flow cumulative value of station A reaches 2,151,063, and it can be seen from Figure 9 that the area of station A contains a flow vector with a larger cumulative value. The combined factors mentioned in 1) constitute the result of a larger AF at station A.
4) Station D has the best comprehensive drainage capacity among the four stations. With other geographical features similar to B, the total waterlogging time at station D is only 24.63% of that at station B. This indicates that the better the regional drainage facilities, the lower the risk of waterlogging.
5) It can be seen from Figure 8 that all four waterlogging monitoring stations are set up in the more low-lying areas of the region. It indicates that the setting of monitoring stations is generally oriented to the occurrence of waterlogging hazards, and the priority of construction is higher in places with high frequency of occurrence. The results of this study on geographic features can be used to find areas with similar geographic features and thus provide reference for the additional waterlogging monitoring stations.
6) The four selected waterlogging monitoring stations are all in urban built-up areas, and the land cover type is impervious surface. This type of land surface possesses a runoff coefficient of about 0.95–1, so the infiltration capacity of rainfall is weak. If the percentage of impervious surface on the surrounding ground is high, it will further increase the risk of waterlogging formation.
7) The proportion of waterlogging events in the total events is low, which can affect the prediction effect of the model. By selecting a sample of waterlogging events in advance, the positive sample weights are enhanced through stratified sampling and data balancing, which can improve the model prediction ability and reduce errors.

6 Conclusion

Short-term prediction of waterlogging has been a hot issue for research, because earlier warning can reduce casualties and property damage from disasters. Due to the Markovian character of itself, future waterlogging can be predicted using the waterlogging of previous periods. However, how to use rainfall data to predict waterlogging where there are no sensors becomes an urgent problem. In this study, a time-series machine learning model using feature extraction for rainfall events significantly improves the prediction with an average error of less than 2 cm. The nine features extracted are validated and proved to be really beneficial and reasonable for model capability improvement. Combined with future rainfall forecast information, it is possible to calculate whether waterlogging will form at a point in the short-term future time period. Based on the prediction results, the government can dispatch rescue forces or block the relevant roads in advance. It provides a reliable basis for government emergency decision-making and risk analysis.

Data availability statement

The original contributions presented in the study are included in the article/supplementary materials, further inquiries can be directed to the corresponding author.

Author contributions

ZZ and LY contributed to conception and design of the study. ZZ and YC organized the database. ZZ, XJ, and YC performed the statistical analysis. ZZ and XJ completed the code compilation and method. ZH and JL revised the manuscript. LY and JL managed the implementation of the research activities and reviewed the manuscript All authors contributed to manuscript revision, read, and approved the submitted version.

Funding

This research was funded by National Key R&D Program of China (2018YFC0807000), Natural Science Foundation of China (71771113), National Key R&D Program of China (2019YFC0810705), Shenzhen Scientific Research Funding (Grant No. K22627501), and Shenzhen Science and Technology Plan platform and carrier special (Grant So. ZDSYS20210623092007023). It was also partly supported by the Shenzhen Science and Technology Program (KCXFZ20201221173601003) and the Henan Provincial Key Laboratory of Hydrosphere and Watershed Water Security.

Conflict of interest

The authors declare that the research was conducted in the absence of any commercial or financial relationships that could be construed as a potential conflict of interest.

Publisher's note

References

Arshad, B., Ogie, R., Barthelemy, J., Pradhan, B., Verstaevel, N., and Perez, P. (2019). Computer vision and IoT-based sensors in flood monitoring and mapping: A systematic review. *Sensors (Basel)* 19 (22), 5012. doi:10.3390/s19225012

Burak, S., Bilge, A., and Ülker, D. (2020). Computation of monthly runoff coefficients for Istanbul. *Therm. Sci.* 25, 1561–1572. doi:10.2298/TSCI191102147B

David, N., Alpert, P., and Messer, H. (2013). The potential of cellular network infrastructures for sudden rainfall monitoring in dry climate regions. *Atmos. Res.* 131, 13–21. doi:10.1016/j.atmosres.2013.01.004

Deo, R., Wen, X., and Qi, F. (2016). A wavelet-coupled support vector machine model for forecasting global incident solar radiation using limited meteorological dataset. *Appl. Energy* 168, 568–593. doi:10.1016/j.apenergy.2016.01.130

Ding, Y., Zhu, Y., Feng, J., Zhang, P., and Cheng, Z. (2020). Interpretable spatio-temporal attention LSTM model for flood forecasting. *Neurocomputing* 403, 348–359. doi:10.1016/j.neucom.2020.04.110

Du, J., Fang, J., Xu, W., and Shi, P. (2012). Analysis of dry/wet conditions using the standardized precipitation index and its potential usefulness for drought/flood monitoring in Hunan Province, China. *Stoch. Environ. Res. Risk Assess.* 27, 377–387. doi:10.1007/s00477-012-0589-6

Duan, Y., Gao, Y., Zhang, Y., Huawei, L., Li, Z., Zhou, Z., et al. (2022). The 20 july 2021 major flood event" in greater Zhengzhou, China: A case study of flooding severity and landscape characteristics. *Land* 11, 1921. doi:10.3390/land11111921

Ferreira, C., Walsh, R. P. D., Shakesby, R., Keizer, J. J., Soares, D., gonzalez-pelayo, O., et al. (2015). Differences in overland flow, hydrophobicity and soil moisture dynamics between Mediterranean woodland types in a peri-urban catchment in Portugal. *J. Hydrology* 533, 473–485. doi:10.1016/j.jhydrol.2015.12.040

Gong, W., Jiang, J., and Yang, L. (2022). Dynamic risk assessment of compound hazards based on VFS–IEM–IDM: A case study of typhoon–rainstorm hazards in shenzhen, China. *Nat. Hazards Earth Syst. Sci.* 22, 3271–3283. doi:10.5194/nhess-22-3271-2022

Han, H., and Morrison, R. (2021). Data-driven approaches for runoff prediction using distributed data. *Stoch. Environ. Res. Risk Assess.* 36, 2153–2171. doi:10.1007/s00477-021-01993-3

Khalid, S., Shehryar, T., and Nasreen, S. (2014). "A survey of feature selection and feature extraction techniques in machine learning," in Proceedings of the 2014 science and information conference, London, UK, August 2014.

Khatri, S., Kokane, P., Kumar, V., and Pawar, S. (2022). Prediction of waterlogged zones under heavy rainfall conditions using machine learning and GIS tools: A case study of Mumbai. *GeoJournal* 87, 1–15. doi:10.1007/s10708-022-10731-3

Li, X., Li, M., Cui, K., Lu, T., Xie, Y., and Liu, D. (2022). Evaluation of comprehensive emergency capacity to urban flood disaster: An example from Zhengzhou city in henan province, China. *Sustainability* 14, 13710. doi:10.3390/su142113710

Liu, Y., Li, L., Liu, Y., Chan, P. W., and Zhang, W. (2020). Dynamic spatial-temporal precipitation distribution models for short-duration rainstorms in Shenzhen, China based on machine learning. *Atmos. Res.* 237, 104861. doi:10.1016/j.atmosres.2020.104861

Liu, Y., Yesen, L., Zheng, J., Chai, F., and Ren, H. (2022a). Intelligent prediction method for waterlogging risk based on AI and numerical model. *Water* 14, 2282. doi:10.3390/w14152282

Liu, Y., Zhang, W., Yan, Y., Li, Z., Xia, Y., and Song, S. (2022b). An effective rainfall–ponding multi-step prediction model based on LSTM for urban waterlogging points. *Appl. Sci.* 12, 12334. doi:10.3390/app122312334

Loftis, J., Forrest, D., Katragadda, S., Spencer, K., Organski, T., Nguyen, C., et al. (2018). StormSense: A new integrated network of IoT water level sensors in the smart cities of hampton roads, va. *Mar. Technol. Soc. J.* 52, 56–67. doi:10.4031/MTSJ.52.2.7

Mu, D., Luo, P., Lyu, J., Zhou, M., Huo, A., Duan, W., et al. (2020). Impact of temporal rainfall patterns on flash floods in Hue City, Vietnam. *J. Flood Risk Manag.* 14. doi:10.1111/jfr3.12668

Nath, B., Ni-Meister, W., and Choudhury, R. (2021). Impact of urbanization on land use and land cover change in Guwahati city, India and its implication on declining groundwater level. *Groundw. Sustain. Dev.* 12, 100500. doi:10.1016/j.gsd.2020.100500

Nayeb Yazdi, M., Ketabchy, M., Sample, D., Scott, D., and Liao, H. (2019). An evaluation of HSPF and SWMM for simulating streamflow regimes in an urban watershed. *Environ. Model. Softw.* 118, 211–225. doi:10.1016/j.envsoft.2019.05.008

Puttinaovarat, S., and Horkaew, P. (2020). Flood forecasting system based on integrated big and crowdsource data by using machine learning techniques. *IEEE Access* 8, 5885–5905. doi:10.1109/access.2019.2963819

Ran, Q., Su, D., Li, P., and He, Z. (2012). Experimental study of the impact of rainfall characteristics on runoff generation and soil erosion. *J. Hydrology* 424, 99–111. doi:10.1016/j.jhydrol.2011.12.035

Shahabi, H., Shirzadi, A., Ghaderi, K., Omidvar, E., Al-Ansari, N., Clague, J. J., et al. (2020). Flood detection and susceptibility mapping using sentinel-1 remote sensing data and a machine learning approach: Hybrid intelligence of bagging ensemble based on K-nearest neighbor classifier. *Remote Sens.* 12 (2), 266. doi:10.3390/rs12020266

Sofia, G., Ragazzi, F., Giandon, P., Dalla Fontana, G., and Tarolli, P. (2019). On the linkage between runoff generation, land drainage, soil properties, and temporal patterns of precipitation in agricultural floodplains. *Adv. Water Resour.* 124, 120–138. doi:10.1016/j.advwatres.2018.12.003

Sundaram, S., Devaraj, S., and Yarrakula, K. (2021). Modeling, mapping and analysis of urban floods in India-a review on geospatial methodologies. *Environ. Sci. Pollut. Res.* 28, 67940–67956. doi:10.1007/s11356-021-16747-5

Tang, X., Li, J., Li, L., Yu, H., and Wang, F. (2021). A method to increase the number of positive samples for machine learning-based urban waterlogging susceptibility assessments. *Stoch. Environ. Res. Risk Assess.* 36, 1–18. doi:10.1007/s00477-021-02035-8

Tarasova, L., Basso, S., Zink, M., and Merz, R. (2018). Exploring controls on rainfall-runoff events: 1. Time series-based event separation and temporal dynamics of event runoff response in Germany. *Water Resour. Res.* 54 (10), 7711–7732. doi:10.1029/2018WR022587

Wang, H., Zhao, Y., Zhu, Y., and Wang, H. (2021). Prediction of urban water accumulation points and water accumulation process based on machine learning. *Earth Sci. Inf.* 14, 2317–2328. doi:10.1007/s12145-021-00700-8

Wu, Z., Zhou, Y., Wang, H., and Jiang, Z. (2020b). Depth prediction of urban flood under different rainfall return periods based on deep learning and data warehouse. *Sci. Total Environ.* 716, 137077. doi:10.1016/j.scitotenv.2020.137077

Wu, Z., Zhou, Y., and Wang, H. (2020a). Real-time prediction of the water accumulation process of urban stormy accumulation points based on deep learning. *IEEE Access* 8, 1. doi:10.1109/ACCESS.2020.3017277

Xue, F., Huang, M., Wang, W., and Zou, L. (2016). Numerical simulation of urban waterlogging based on FloodArea model. *Adv. Meteorology* 2016, 1–9. doi:10.1155/2016/3940707

Yan, H., and Hamid, M. (2016). Toward more robust extreme flood prediction by bayesian hierarchical and multimodeling. *Nat. Hazards* 81, 203–225. doi:10.1007/s11069-015-2070-6

Yan, X., Xu, K., Feng, W., and Chen, J. (2021). A rapid prediction model of urban flood inundation in a high-risk area coupling machine learning and numerical simulation approaches. *Int. J. Disaster Risk Sci.* 12, 903–918. doi:10.1007/s13753-021-00384-0

Yang, M., Zhang, Y., and Pan, X. (2020). Improving the Horton infiltration equation by considering soil moisture variation. *J. Hydrology* 586, 124864. doi:10.1016/j.jhydrol.2020.124864

Yin, J., Gentine, P., Slater, L., Gu, L., Pokhrel, Y., Hanasaki, N., et al. (2023). Future socio-ecosystem productivity threatened by compound drought–heatwave events. *Nat. Sustain.* 6, 259–272. doi:10.1038/s41893-022-01024-1

Yin, J., Guo, S., Wang, J., Chen, J., Zhang, Q., Gu, L., et al. (2022). Thermodynamic driving mechanisms for the formation of global precipitation extremes and ecohydrological effects. *Sci. China Earth Sci.* 66, 92–110. doi:10.1007/s11430-022-9987-0

Yin, J., Ye, M., Yin, Z., and Xu, S. (2015). A review of advances in urban flood risk analysis over China. *Stoch. Environ. Res. Risk Assess.* 29, 1063–1070. doi:10.1007/s00477-014-0939-7

Zavala, L., Jordán, A., and Bellinfante, N. (2008). Seasonal variability of runoff and soil loss on forest road backslopes under simulated rainfall. *Catena* 74, 73–79. doi:10.1016/j.catena.2008.03.006

Zhang, H., Wu, C., Chen, W., and Huang, G. (2017). Assessing the impact of climate change on the waterlogging risk in coastal cities: A case study of guangzhou, south China. *J. Hydrometeorol.* 18, 1549–1562. doi:10.1175/JHM-D-16-0157.1

Zhang, Z., Zeng, Y., Huang, Z., Liu, J., and Yang, L. (2023). Multi-source data fusion and hydrodynamics for urban waterlogging risk identification. *Int. J. Environ. Res. Public Health* 20 (3), 2528. doi:10.3390/ijerph20032528

Zhou, Y., Wu, Z., Xu, H., and Wang, H. (2022). Prediction and early warning method of inundation process at waterlogging points based on Bayesian model average and data-driven. *J. Hydrology Regional Stud.* 44, 101248. doi:10.1016/j.ejrh.2022.101248

Zounemat-Kermani, M., Matta, E., Cominola, A., Xia, X., Liang, Q., Hinkelmann, R., et al. (2020). Neurocomputing in surface water hydrology and hydraulics: A review of two decades retrospective, current status and future prospects. *J. Hydrology* 588, 125085. doi:10.1016/j.jhydrol.2020.125085

Frontiers in Environmental Science

Explores the anthropogenic impact on our natural world

An innovative journal that advances knowledge of the natural world and its intersections with human society. It supports the formulation of policies that lead to a more inhabitable and sustainable world.

Discover the latest Research Topics

See more →

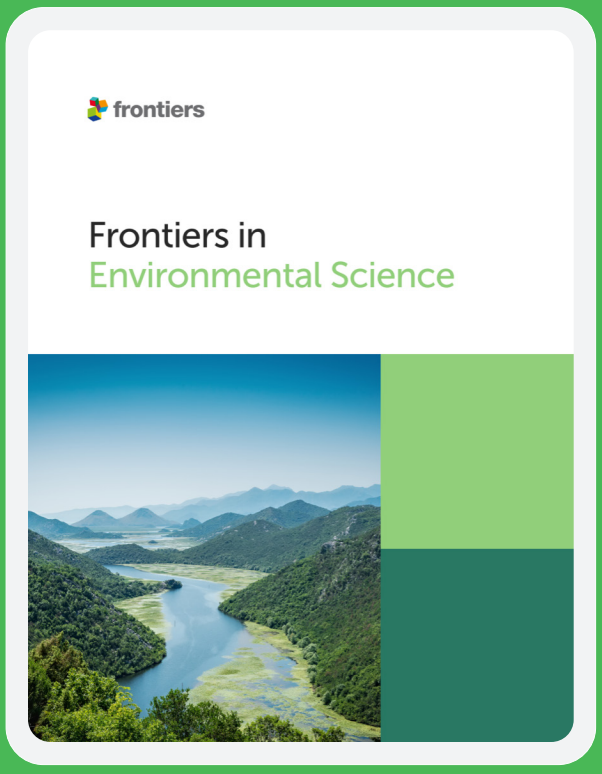

Frontiers

Avenue du Tribunal-Fédéral 34
1005 Lausanne, Switzerland
frontiersin.org

Contact us

+41 (0)21 510 17 00
frontiersin.org/about/contact